MODULATION OF SOUTH AFRICAN SUMMER RAINFALL BY GLOBAL CLIMATIC PROCESSES

by

BEENAY M. R. PATHACK

A Thesis submitted to the University of Cape Town
in fulfillment of the requirements for the
degree of Doctor of Philosophy

August 1993

ABSTRACT

Global climatic processes which control the interannual variability of summer rainfall over South Africa are studied. Monthly and seasonal rainfall variations are analysed with respect to fluctuations in sea surface temperature (SST), outgoing longwave radiation (OLR) and tropospheric winds. OLR is used as a proxy for convective intensity and for the identification of areas of sympathy and opposition to convection over South Africa. Wind data (and derived parameters) are employed to explore large-scale tropical dynamical structures. Plausible explanations are offered for the observed associations.

A change in sign of the correlation structure from the October/November rainfall regime to the December through March regime is indicative of a shift from downstream advective processes (Atlantic side) to a teleconnection-type of behaviour (Indian Ocean side). Rainfall variations during the late summer months show significant (and negative) links with SST fluctuations within the equatorial/tropical Pacific and Indian Ocean areas and are consistent with results obtained in analyses with respect to OLR fluctuations.

December OLR in the Western Equatorial Indian Ocean is associated with a large portion of the variance in late summer rainfall, and points to a possible relation with the evolution of the Indian monsoon. The positive association implies that reduced cloudiness off the eastern coast of equatorial Africa in the spring precedes above normal mid- and late- summer rainfall over South Africa.

Vertical mass overturnings are investigated through the velocity potential and derived parameters (the Zonal Circulation and Meridional Circulation Indices). The results suggest that the vertical tropospheric cells are among the important associated components which modulate climate across southern Africa, and that broad scale flows

have an impact upon regional circulation cells. Evaluation of the vertical circulations with respect to wet and dry composites reveals that the Walker-type cell which connects a branch over the Indian Ocean gradually forms after November and reaches peak development in February. A slight increase of SST in the Central Equatorial Indian Ocean (CEI) modifies the Walker cell anomaly leading to below normal summer rainfall over South Africa. Additional thermodynamic inputs in the CEI region are conducive to deeper convection, hence elevated outflow signatures are observed in the velocity potential and related fields. It is conjectured that the teleconnections between South Africa, the CEI and the remote Pacific Ocean regulate the depth of moisture influx and convergence over South Africa.

Based on the results of this study, it is believed that empirical models could be designed for long-range prediction of summer rainfall anomalies over the central interior of South Africa.

CONTENTS

LIST OF FIGURES

LIST OF TABLES.

CHAPTER 1

SOUTH AFRICAN SUMMER RAINFALL PREDICTION:

MOTIVATION AND METHODOLOGY

1.1. INTRODUCTION

Prediction of rainfall could be of considerable economic value to various sectors, such as agriculture, water resources, hydropower, industries, and to the community at large. However, the benefit that these sectors derive from such predictions depends essentially on the temporal and spatial scales of the predictions. Hence forecasts are desired on a large spectrum of time and space scales.

Given the complex nature of the interactions among the diverse fields which form weather and climate, different methods are employed to monitor, analyse and forecast the required variables. Forecasts on time scales of days to weeks have significantly improved during the last two decades with the implementation and success of numerical global weather forecasting models; whereas predictions on longer time scales have generally been limited and they are virtually all based on empirical formulations. This is largely due to the complexities and uncertainties involved in the interactions among the atmosphere, hydrosphere and cryosphere. In addition, the highly diverse time and space scales involved in weather-producing systems make the development of models which incorporate sound physics quite difficult. In these cases, solutions are often sought through parameterization schemes which essentially involve the representation of small scale processes in terms of large scale parameters. Output from a model can be much dependent upon the particular parameterization scheme or schemes used. Parameterizations of varying complexities have been developed, mostly in connection with the evolution of tropical moist convection and

the representation of the boundaries (Shukla, 1986; Molinari and Durek, 1992). Another factor is that long-term integrations in physical models may produce results which are strongly region- and model-dependent; forecasts are better for certain regions than for others depending on the region and the particular model used. Still, it is believed that long-term (monthly to seasonal) forecasts can best be made through the use of realistic physical models. However, since such Coupled General Circulation Models (CGCMs) tailored for use in the prediction of South African rainfall are yet to come, an alternative avenue is to investigate the possibility of developing empirical models through statistical associations. Results from statistical studies are also of value in testing the performance of numerical models; a sound empirical understanding is believed to be a prerequisite for the design of realistic numerical models (Hastenrath, 1986).

Due to their statistical nature, empirical models are often liable to severe criticism. They are almost always region dependent. Statistical relationships are often used in predictions even when the underlying physics are not well understood. High correlations may be observed among various climatic variables, but these may not be stable in time (for example, Lindesay, 1988). But, through judicious and cautious formulations, empirical models can be potentially useful tools in predictions as long as their limitations are defined and respected.

Numerous studies have investigated the relationships between rainfall and various meteorological and oceanic parameters. The observational studies generally concentrate on statistical correlations while the numerical studies are based on atmospheric general circulation models of varying complexities. Whatever technique is followed, the goal is always towards the understanding of the mechanisms which influence weather patterns and climate, and ultimately towards the prediction of weather and climate.

Rainfall is one of the most important parameters reflecting climate variability and obviously one of the most useful to forecast. The main bulk of summer rain over tropical and near-tropical regions of Africa, including South Africa, precipitates from convective systems. An understanding of the factors that control deep convection is essential to many aspects of ocean-atmosphere interaction research. Two principal factors are necessary for the generation and sustenance of organized deep convection in the tropics. First the atmosphere must be thermodynamically unstable with respect to deep convection. Second, dynamical forcing must be present to provide the large-scale vertical motion needed to realise the instability in the atmospheric profile. The stratification of the atmosphere helps determine the initiation and development of convection as well as its vertical extent. Slowly varying factors may determine the thermodynamic stability of the atmosphere.

Many investigators have identified 'key' parameters in 'key' areas which appear to have direct or indirect influence on rainfall distribution and variability across diverse regions; significant simultaneous or lagged correlations have been established. In this study, the various relevant parameters which explain significant portions of summer rainfall variance over South Africa are investigated. This should help in the formulation of empirical models for long-term rainfall prediction across the summer rainfall area of South Africa. A location map with the topography of the region is shown in Figure 1.1.

Section 1.2 describes an observational background of relevant works with particular emphasis on the more recent ones. Notes on tropical circulation features are given in Section 1.3 followed (in Section 1.4) by a general discussion on numerical/theoretical approaches. Section 1.5 outlines the general objectives of the study. Details on the datasets utilized (rainfall, sea surface temperature, tropospheric wind, and Outgoing Longwave Radiation) are given in Section 1.6, while Section 1.7 presents the analysis procedures.

1.2. OBSERVATIONAL BACKGROUND

Mainly in the form of literature review, this section presents a background of results and circulation features of importance in the present context. As it is not feasible to give a detailed review of all the works done in the field, brief mention will be made to those believed more pertinent. However, emphasis will be placed on the studies of Walker (1989), Lindesay (1988) and Harrison (1986) as they are the most recent, comprehensive and of direct concern to South African rainfall distribution and variability. Of particular interest in these works are investigations related to large-scale circulation features. In addition to an earlier review by Namias (1968), details on recent developments in long-range forecasting can be found in Nicholls (1980), Barnett and Somerville (1983), Harrison et al. (1985), and Hastenrath (1985, 1986, 1990).

1.2.1. OBSERVATIONAL BACKGROUND: SOUTH AFRICA

Walker (1989) investigated the link between the variability of rainfall over the summer rainfall region of South Africa with respect to SST. The rainfall data set, which was compiled by Lindesay (1988), was obtained from the Climatology Research Group, University of the Witwatersrand. The SST data mainly incorporated information from merchant ships collated at the United Kingdom Meteorological Office. The SST domain considered extended over a limited area, from equator to 40°S, 20°W to 70°E, with a grid format of 5° latitude by 5° longitude. The rainfall series were grouped into 2 areas for which indices (standardized anomalies) were derived for early (October, November, December) and late (January, February, March) summer seasons. The analysis procedure essentially followed correlative techniques applied to data (SST and rainfall) covering the period 1949 to 1984.

Figure 1.2, from Walker (1989), shows a sample of the results of simultaneous correlation between SST and late summer rainfall. Since the Southern Oscillation Index (SOI) is significantly related to South African rainfall (see later in this section for details), the correlations were re-computed excluding data for those years when SOI was relatively high or relatively low; this led to the exclusion of about 10 of the 36 years of data. The new results (Figure 1.3) show that the correlation values generally increased, especially within the adjacent ocean areas. A point to be noted here is that, since the number of degrees of freedom decreased due to the exclusion of high and low SOI years, the statistical significance remained essentially the same.

Figure 1.4 displays the results of lagged correlation with SST leading rainfall by 3 months. From this diagram it may be inferred that October-November-December SST variations within the Agulhas/Mozambique Current can explain 15 to 25 per cent of January-February-March rainfall variance in the absence of Southern Oscillation influence on rainfall. Thus SST in this area appears to be a useful indicator of late summer rainfall. But, as will be found later (Chapter 2), a more complex correlation pattern is obtained when the time resolution of the parameters is changed to a monthly time scale, primarily when lagged correlations are considered. The work of Walker (1989) thus provides a basis for further research given the plausible mechanistic links detailed therein.

Low level easterly wind anomalies across the tropical south-west Indian Ocean and source regions of the Agulhas Current were found to accompany and precede the local oceanic 'warm events' which were simultaneously positively correlated with wetter conditions across the summer rainfall areas of South Africa. The thermodynamic implication is that the easterly wind forcing across a warmer than normal sea surface should produce enhanced moisture flux, low-level convergence and convection over the subcontinent. To the south of the subcontinent, positive SST anomalies generate surface heat flux anomalies,

thus increasing atmospheric instability and moisture levels within the boundary layer. At the same time, horizontal heat flux gradients are strengthened across the Agulhas/Subtropical Convergence SST front and the Agulhas Retroflection zone in addition to the optimization of conditions necessary for subtropical cyclogenesis and westerly wave amplification (Jury and Walker, 1988; Mey et al., 1989). Through the intensification of tropical and temperate weather systems, positive SST anomalies are also believed to increase the likelihood of formation of tropical-temperate troughs which account for the major part of rainfall in the summer rainfall area of South Africa (Harrison, 1984, 1986; Tyson, 1984a).

The thermodynamic components of the mechanisms suggested above receive support from the studies of Sanders and Gyakum (1980), Höflich (1984), James and Anderson (1984), Reed and Albright (1986), and Nuss and Anthes (1987). As far as rainfall prediction is concerned, however, there does not seem to be strong enough lagged correlations of rainfall with adjacent ocean temperatures. However, the equatorial regions show consistent lagged association. It is conjectured that SSTs within such areas may prove useful in empirical prediction models. Since upper layer ocean water advection is relatively strong in regions increasingly poleward of the tropics, SSTs at higher latitudes are generally not as persistent as across equatorial areas. On the other hand, SSTs at higher latitudes do show significant concurrent correlations with rainfall and other meteorological variables at certain preferred places and times (see, for example, Namias, 1973; Yarnal, 1985; Yarnal and Kiladis, 1985; and Cane, 1986)

The Southern Oscillation phenomenon has been the subject of a vast number of studies. It is reported (Montgomery, 1940; Lindesay, 1988) to have been first identified at the turn of the century (Hildebrandsson, 1897; Lockyer and Lockyer, 1902) and followed by extensive investigations by Walker (1923, 1924, 1928) and Walker and Bliss (1930, 1932, 1937) in

the search for precursors of the Indian monsoon. Later, Berlage (1957, 1966) provided a global correlation map of surface pressure and defined the centers of action of the Southern Oscillation. The correlation in surface pressure showed a maximum of -0.8 between two major centers, one around the Indonesian region and the other over the Eastern South Pacific. In the simplest term, the Southern Oscillation can be described as the swaying of pressure (and mass) between areas surrounding these two major centers. It is believed that fluctuations within the centers tend towards two preferred modes. One mode, the high phase, occurs when surface pressure is relatively high over the Eastern Pacific where there is subsidence accompanied by suppressed convection and lower than average SSTs, while pressure is relatively low over the Indonesian region where there is increased cloudiness and high rainfall. During the opposite mode, the low phase, the anomalies show a reversal. Although the phenomenon is regarded as an oscillation, the change from one phase to the other is far from periodic, with periods ranging from 2 to 10 years (Trenberth, 1976).

The Southern Oscillation is intricately linked with the El Niño phenomenon which manifests through a warming of the waters across the eastern equatorial Pacific and the coastal waters of western South America. This composite ocean-atmosphere feature has been termed ENSO (El Niño-Southern Oscillation) (Philander, 1983; Yarnal, 1985; Yarnal and Kiladis, 1985). A common measure of the Southern Oscillation Index (SOI) is the surface pressure difference between Tahiti (in the eastern South Pacific) and Darwin (on north Australian coast); thus high phase Southern Oscillation coincides with higher than normal pressure at Tahiti and vice versa.

Lindesay (1988) has made a detailed study of several meteorological parameters in connection with SOI and its relationships to the rainfall variability across South Africa. The association between variations in SOI and atmospheric circulation variables over Southern Africa within the period 1957 to 1983 was examined after first establishing the

nature of the correlation between the Southern Oscillation and South African rainfall. During the early summer months of October and November, both positive and negative correlations were found over South Africa, but the links were poor and the distribution of oppositely correlated areas lacked spatial coherence. For December, January and February, the correlations were characterized by spatially coherent areas of positive values over the central parts of the country, especially in December when correlations exceeded +0.45 (significant at better than the 99 per cent level) at some stations. An inverse relationship was found over the south-west Cape Province. A north-west to south-east oriented zone of relatively high positive correlation is present in the fields for the months of December to March, a feature probably related to the effects of tropical-temperate troughs on South African summer rainfall. A plausible physical explanation proposed for the observed simultaneous relationships between Southern Oscillation and rainfall across South Africa was that the Southern Oscillation modulated variations in the frequency and preference in location of major cloud bands which contribute to a large proportion of the summer rainfall over the country (Harrison, 1984, 1986).

Simultaneous variations of SOI and rainfall account for, at most, 20 per cent of rainfall variance over central South Africa. The relationships in this area are such that higher rainfall tends to coincide with the high phase of the Southern Oscillation, and vice versa; the links are, however, not stable in time. Lagged correlations, including spectral analyses were also considered by Lindesay (1988); the time scales involved were of the order of years. The rather aperiodic nature of the Oscillation limits its use as a predictor on such time scales. However, the close relationships between summer area rainfall and SOI spectra at both quasi-biennial and Southern Oscillation periods support the physical mechanism linking phase changes of the oscillation with zonal and meridional circulation

adjustments over Southern Africa, and thence with rainfall variations over central parts of South Africa (Lindesay, 1988).

Harrison (1986) has made an extensive study of the synoptic climatology of South African rainfall variations. The central hypothesis was that monthly rainfall totals over the central interior of South Africa increase with enhanced poleward momentum fluxes across the Southern African subcontinent. Of the eight major types of synoptic systems identified by Harrison (1986), tropical-temperate troughs were found to account for 35 per cent of the annual rainfall over the central interior, and for about 50 per cent in January. Rainfall from these troughs decreases in December compared to that in November and in January. Tropical-temperate troughs form at times of interaction between the tropical and temperate circulations and mark channels for the poleward export by the mean meridional circulation of momentum and energy generated along the Inter Tropical Convergence Zone (ITCZ). The troughs develop most frequently when the ITCZ is furthest south in January. Momentum and energy generation over Africa in the vicinity of 20°S appears to be a necessary condition for the formation of tropical-temperate troughs.

Circulation variations over the equatorial Pacific Ocean related to the Southern Oscillation prove to be an important remote control on energy release across tropical Africa. The signal from the Pacific is transmitted to Africa partly via the zonal vertical Walker circulation across the tropical Indian Ocean. Control on African energy release is strongest in summer as a result of circulation changes on the semi-annual scale.

van Heerden et al. (1988) also investigated the relationship between the summer rainfall over South Africa and the Southern Oscillation. They suggest two modes of circulation during summer, baroclinic and quasi-barotropic. During January and February, when the SOI-rainfall relationship is fairly weak, rainfall develops in a predominantly quasi-

barotropic circulation. On the other hand, during December and March the more significant SOI- rainfall correlation coincides with a shift towards baroclinic systems.

Statistical techniques have been applied to Southern African rainfall data in search of periodic fluctuations (Tyson et al., 1975; Rodhe and Virji, 1976; Tyson, 1980; Harrison, 1986; Tyson, 1986). A summary of the results as well as confirmation of the existence of certain quasi-regular fluctuations is found in Tyson (1986) where it is reported that rainfall spectra show variance peaks in the region of 18 to 22 years. Other peaks also occurred at around 10 to 12 years, at 3.5 years, and at 2.3 years. The 2.3-year cycle reflects the Quasi-biennial Oscillation (QBO). The 18-year oscillation was found to be common throughout Southern Africa (Tyson, 1986). About thirty per cent of the variance of the annual rainfall totals over South Africa may be explained by quasi-periodicities, a proportion that is believed sufficient to act as a basis for providing estimates of future rainfall tendencies over the interior of the country (Tyson and Dyer, 1975 and 1978). But, given the long time scales of these fluctuations as well as the irregularity in the periods, they can perhaps be used as a background over which forecasts on relatively shorter time scales should be superimposed.

1.2.2. OBSERVATIONAL BACKGROUND: OTHER COUNTRIES

Abundant literature exists on the search for long-range prediction in other parts of the world. Namias (1968) reviewed preliminary attempts to provide seasonal forecasts. More recent developments in long-range forecasting have been reviewed by Nicholls (1980), Barnett and Somerville (1983), Harrison et al. (1985) and Hastenrath (1985, 1986).

Various techniques of seasonal climate prediction have been developed, but those employing teleconnections between atmospheric circulation patterns and tropical SST

anomalies bear the greatest promise (Nicholls 1980). With regard to the ENSO evolution, Nicholls (1984) presented a model in which it was postulated that wind-induced mixing of the upper ocean is an important mechanism affecting SST in the Indonesian region, although other processes (e.g. heating and advection) also affect the SST. Markham and McLain (1977) correlated rainfall in Ceara, north-eastern Brazil, with SST in the south Atlantic Ocean. Hypothesizing that the SST affects the height of the trade wind inversion and thus the height of the moist layer, they suggest that knowledge of SST makes possible a useful rainfall forecast.

Barnett (1983, 1984a,b, 1985) and Wright et al. (1988) have shown that warm episodes in the equatorial Pacific are also accompanied by wind and pressure fluctuations over the tropical Indian Ocean. In general, they suggest that perturbations associated with the Southern Oscillation signal originate in the tropical Indian Ocean and propagate eastward.

Through the use of empirical orthogonal functions and spectral analyses, Nicholson and Nyenzi (1990) investigated the temporal and spatial patterns of SST variability in the Atlantic and Indian Oceans. A major finding was that SSTs vary coherently throughout most of the tropical regions of the two oceans considered within a dominant time scale of 5-6 years which is also the case for the Southern Oscillation. The greatest coherence was evident from 10°N to 30°S in the Atlantic and 20°N to 35°S in the Indian Ocean. SST variations were found to be roughly in phase within each ocean. The SST anomalies appeared to propagate eastward from north-east Brazil; the eastern Atlantic lagged the western by two to six months and the Indian Ocean lagged the western Atlantic SST by four to eight months.

Angell (1981) found a correlation of 0.72 between the SST over the equatorial eastern Pacific and the zonally averaged tropical troposphere temperature two seasons later. Low,

but significant at nearly the 99 per cent level, was the negative correlation (about -0.3) between the SST and rainfall in eastern Australia.

Streten (1983) analysed the extreme distributions of Australian annual rainfall in relation to SST variations. Years of extensive drought were found to be associated with a predominantly low SST persisting throughout the year over the eastern Indian Ocean; very wet years over the continent were associated with a persistently warm SST extending from the equator to the mid latitudes within the same longitude. Although the extremes tended to be related to the periods when the Southern Oscillation Index peaked (high or low), this was not always the case.

Cloud bands identified in satellite imagery are often observed to be associated with troughs connecting the tropical and temperate zones. The possible relation of these cloud bands (associated with tropical-temperate troughs) to the hemispheric long-wave pattern has been discussed by Streten (1973); annual and seasonal frequencies of location of maximum brightness (cloudiness) bands appearing on southern hemisphere five-day-averaged satellite data were analysed. It was found that, on average, the location of high band frequency was largely stable in the Pacific and Atlantic Oceans, but that the bands in the Indian Ocean displayed higher frequencies to the west (towards Africa) in summer and to the east (towards Australia) in winter. The location of the tropical to temperate connection was, in general, related to that of the long-wave hemispheric pattern. Since the three low-latitude positions of high band frequency were located over Africa, South America, and in particular, over the eastern tip of New Guinea (the eastern extremity of the maritime continent), it was suggested (Streten, 1973; Harrison, 1986; Tyson, 1986) that the bands might visually represent the mean channels wherein energy flow occurs into the mid-latitude westerlies from these tropical-continental areas of most active convection.

Kung and Sharif (1982) used multi-regression techniques for the long-range prediction of the Indian monsoon (the onset date and the rainfall over India). Predictors included the upper air parameters at 100, 200 and 700 hPa over India and Australia and the SST in the Indian region. Their forecast experiments for the period 1958-77 show the predicted onset dates and seasonal rainfall to be very close to the recorded dates and rainfall. Similar models could be developed for the prediction of South African rainfall, but stable relationships among relevant parameters should first be identified.

1.3. TROPICAL CIRCULATION FEATURES

The tropical belt, defined as the area between the mean latitudinal axes of the surface subtropical high pressure systems of the northern and southern hemispheres, occupies half of the global surface. The atmosphere overlying this belt receives excess angular momentum from the earth's surface and heat energy. The heating process is indirect, that is, a portion of the shortwave solar radiation is first absorbed by the earth's surface (land and water). The energy is then released to the overlying atmosphere. In this way, the tropical region receives energy in excess of what is lost through outgoing radiation to space. On the other hand, on average, there is a general loss of momentum and energy from the air overlying the extratropical zones. In order to create a balance, heat energy and momentum must be imported into the extratropics from the tropics. The exact mechanisms responsible for the exchange between the two regions are indeed very complex. Strictly speaking, therefore, dynamics and thermodynamics of the tropical and higher latitude circulations cannot be treated as isolated from each other. In fact, the ocean current systems, which contribute substantially towards the transfer, should also be incorporated in longer-term models. The circulation systems involved in the transfer assume a large continuous spectrum of time and space scales, all of which are interdependent. The

temporal scale ranges from hours to decades, while the spatial scale varies from one kilometre to over a thousand kilometres. One convenient way of handling the problem is to treat the spectra within discrete scales (micro-, convective-, meso-, synoptic-, planetary- etc.) within which weather-producing systems are distinguished by their scales and characteristic features.

It is recognized that knowledge of the structural characteristics of tropical convection is important in order to understand the organization of individual convective cells and their interactions with large-scale circulations; this may also help improve parameterization schemes in general circulation models (Machado et al., 1992). Sui and Lau (1992) have demonstrated examples of multiscale interactions in the tropical atmosphere-ocean-land system over the western Pacific Ocean during the northern winter of the First Global GARP (Global Atmospheric Research Program) Experiment (FGGE) year. The results showed diverse variabilities in equatorial convection and the associated low-level winds ranging from intraseasonal to synoptic to diurnal time scales. It was found that the diurnal cycle was most dominant over the maritime continent (southeast Asia-Indonesia region) and northern Australia; synoptic-scale waves were active over the equatorial Indian and western Pacific Oceans. It was thus concluded that the spatial distributions were indicative of the importance of diurnal heating in the boundary layer over the maritime continent as a forcing mechanism that controlled the life cycle of cloud clusters in the absence of low-frequency disturbances. On the other hand, intraseasonal oscillations provided favourable large-scale conditions for the development of synoptic-scale wave activities over the warm ocean where diurnal forcing was weaker.

Although the diverse scales interact, it is believed that gross features of the circulation patterns may be captured through certain filtering processes, such as averaging. Depending on the aim of the particular study, the filtering/smoothing processes suppress features

within specified frequency bands while accentuating those within the bandwidth of interest. The smaller scales (possessing higher frequencies than those being studied) are usually referred to as 'noise', while those in the opposite range are usually believed not to significantly affect conclusions drawn from the selected bandwidth.

The manner in which a given small scale convective system evolves depends a lot on the large-scale environmental set-up within which the system is embedded. For instance, a cumulus cell will be encouraged to grow, and eventually precipitate, only if it is evolving within an environment characteristic of, say, low-level moisture convergence, among other factors. On the other hand, the cloud would dry out and decay if it happens to be, or move to, within an environment where low-level divergence is predominant. This simple concept is, however, complicated by the fact that the cumulus motion also, in turn, affects the large-scale circulation; the interactions then become highly non-linear and almost impossible to model mathematically.

Through analytical scaling arguments, it has been suggested (Holton, 1979) that, to a large extent, the structure of tropical synoptic disturbances is determined by the field of heating provided by latent heat release in areas of active precipitation. The CISK (Conditional Instability of the Second Kind) mechanism (Holton, 1979), which implies that large scale convergence provides moisture for the smaller scale convective systems (cumulus cells), and these act cooperatively to provide a large scale heat source. The CISK mechanism has, however, been questioned. For instance, for the area over the Western Pacific, Xu and Emanuel (1989) suggest that tropical disturbances result from a redistribution of preexisting kinetic energy (as in barotropic instability) or feedback mechanisms that increase the entropy of the subcloud layer and possibly the tropical intraseasonal oscillations. Danard (1986) investigated the influences of surface fluxes and convective precipitation for two 36-hour periods of cyclogenesis over the northeastern Pacific through an 8-level

primitive equation model; it was observed that predicted cyclogenesis was very sensitive to sea temperature. As the low moved over warmer water, the effect of sensible heating was found to increase the moisture convergence in the atmospheric boundary layer, thus increasing precipitation rates and accelerating the deepening of the system.

Although much work remains to be done in order to further understand the dynamics of tropical climate and weather, theoretical and numerical approaches have been encouraging.

1.4. THEORETICAL/NUMERICAL APPROACHES

The two approaches possible in the use of large-scale numerical models of the atmospheric general circulation in long-term prediction are the boundary value sensitivity approach and the initial value approach. An example of the former case is that, given the deviations from normal of the SST field for the coming month (or season) as boundary conditions, the numerical model determines how the atmospheric behaviour will differ from normal. Whereas in the initial value approach, given sufficiently accurate atmospheric and oceanic data fields for a specified day (time) as initial conditions, the model should integrate from the initial conditions out to a month or season ahead.

Rowntree (1972, 1976) studied the response of a numerical model to tropical SST anomalies and found that warmer SSTs generally caused the model's tropical atmospheric sea level pressure to decrease and the air temperature and rainfall to increase; extratropical effects were also observed after several days. Shukla (1975) found that a cold SST anomaly near the Somali coast drastically reduced the model rainfall in the Indian monsoon region. These results, as well as the models used, have been criticized as unrealistic by Ramage (1977). But the fact that the model atmosphere reacts to SST changes, although not strictly correct, is promising because, with improved models and accurately predicted

SSTs a month or season ahead, the model's results might provide guidance for long-range predictions (Nicholls, 1980).

Webster (1981) used a linear baroclinic spherical primitive equation model to study the mechanisms which control the local and remote (teleconnection) response of the atmosphere to the thermal forcing from SST anomalies at various latitudes. He recognized two basic limits of response to forcing by SST anomalies. These are a diabatic limit and an advective limit. The diabatic limit occurs where the anomaly interacts with the atmosphere in regions of relatively small magnitude of the Coriolis parameter so that advective terms play little part in the determination of vertical velocity, that is equatorward of approximately 20° latitude. The advective limit occurs where vertical velocity is a function of both diabatic and thermal advective processes. The advective terms are more significant in middle and high latitudes where zonal winds are strong. Through such theoretical reasoning, Webster (1981) explained the more vigorous development of vertical velocity within tropical latitudes than at higher latitudes upon the imposition of a heating anomaly.

Large changes in the tropical latent heat release patterns might perturb and shift major Hadley (vertical-meridional) and Walker (vertical-zonal) circulations which would result in global-scale circulation changes (Chelliah et al., 1988). An example of this type of circulation change occurred during the 1982-83 El Niño (Quiroz, 1983).

The association of rainfall in the tropical Atlantic sector with anomalous circulations (and, by inference, rainfall) has been studied empirically and numerically. Namias (1972) found correlations of rainfall in the north-east of Brazil with the subtropical anticyclones and higher latitude cyclones in empirical studies on time scales as short as five days. Moura and Shukla (1981) investigated these correlations in extended integrations of a general circulation model initialized with idealized data. Buchmann et al. (1986, 1989) performed

numerical forecast experiments designed to study the impact of tropical Pacific heating anomalies upon South American rainfall; similarly, Paegle et al. (1987) investigated the influence of such anomalies on North American weather. Their results suggest that a relatively cool eastern tropical Pacific Ocean causes reduced rainfall over the subtropical portions of eastern South America and reduced cyclonic activity over North America.

Buchmann et al. (1990) studied the effect of tropical Atlantic heating anomalies upon general circulation model rain forecasts across the Americas. They found that the location of the heating anomaly was crucial to the model results. The South American response was more sensitive to the location of the anomaly. When the anomaly was situated just to the north of the equator, drying occurred over north-east Brazil, but this region received increased rainfall when the anomaly was placed just to the south of the equator. Both experiments displayed a region of reduced rainfall over the Andes mountains (significant at the 95% level of confidence), and over the southern parts of Brazil (not significant). The model drying-out effects was explained only partly by enhanced local subsidence; much of the rainfall reduction appeared to be related to a re-orientation of the synoptic scale wave pattern in which the lower tropospheric circulation was unfavourable for water vapour inflow from source regions over the tropical Atlantic and Amazon Basin. Time-averaged circulation statistics suggest that subsidence and reduced water vapour flux both contribute to the rainfall suppression.

According to Buchmann et al. (1990), the most important circulation response to the heating anomalies are probably the enhanced equatorward flows predicted at low levels around the eastern section of both North and South America. These modifications would allow relatively less moisture to penetrate the United States and east-central South America from the main sources located over the Gulf of Mexico and the Amazon Basin, respectively.

1.5. OBJECTIVES

In the foregoing literature review it is seen that relationships have been found to exist between the variations of summer rainfall and SSTs over limited areas of the oceans in the South African context. Simultaneous associations found between rainfall and SSTs within the boundary current systems were significant, but lagged correlations were generally not significant. Newly available high-resolution gridded data sets will enable a further exploration of such relationships with SSTs over a larger spatial domain. The ocean-atmosphere interaction should be evident in the circulation and convection patterns. These may be examined with the gridded wind and OLR fields.

The main hypothesis explored is that, to a large extent, SST anomalies in the equatorial belt govern the overlying east-west tropical circulation variability, thereby altering the convective pattern over Southern Africa. The interaction between the SST and the zonal circulation anomalies may, in turn, be linked to the Southern Oscillation. It is conjectured that fluctuations in SST, OLR, and/or tropospheric winds within 'key' boxes could explain a significant fraction of the summer rainfall variance over South Africa. The relevant parameters could thus be utilized in formulating predictive models.

The principal goal is therefore to provide an objective and statistical basis for the prediction of South African summer rainfall anomalies on monthly to seasonal time scales. South African rainfall variations are analysed statistically with respect to the fluctuations of SST and OLR. Gridded tropospheric wind data are utilized in analyses of circulation dynamics in view of confirming and complementing observed relationships.

1.6. DATA

This section describes the datasets used throughout the analyses in the present study. The parameters considered are rainfall, SST, tropospheric winds, and OLR.

1.6.1. RAINFALL

The data bank at the Computing Center for Water Research (CCWR), in Pietermaritzburg (South Africa), includes rainfall data from thousands of stations scattered throughout South Africa. Many of the records start from the late 1800s. The original data were compiled by the Department of Agricultural Engineering, University of Natal (South Africa), from a set of primary data obtained from the following sources which are acknowledged:

South African Weather Bureau.
Department of Agriculture and Water Supply.
South African Forestry Research Institute of the Department of Environment Affairs.
South African Sugar Association Experiment Station.
Provincial parks boards, organized agriculture.
Municipalities and mines, and private individuals.

After downloading the data from the CCWR (Gorven, 1988; Gorven and Dent, 1988), various procedures were followed in order to establish a representative sample. Considerable screening, based on spatial and temporal homogeneity, was done before selecting suitable stations. Assuming nearby stations experience precipitation from similar processes, monthly long-term averages were produced for each of the series. The correlation matrix involving all the long-term records was carefully evaluated whereby six homogeneous rainfall zones were apparent: four in the north-eastern parts of the country (the summer rainfall area), one in the south-western Cape Province (the winter rainfall area) and one along the southern coastal and near-coastal regions (which experience rain throughout the year). A few stations did not fall within any of these six categories and were rejected. Each of the selected series was also subjectively checked for obvious errors. Finally, six correlation matrices were formed, one for each homogeneous rainfall zone (the

term 'zone' will be used hereafter). Obvious outliers were rejected at this stage. The correlations among the series were generally superior to +0.5, significant at better than the 95 per cent level of confidence.

Figures 1.5 and 1.6 show the locations of the 77 selected stations and the six rainfall zones, respectively. The data for the selected stations have been compiled for the period 1950 to 1986. Zone 1 falls within the Transvaal Province situated in the northeastern parts of South Africa. Among the 13 rainfall stations of this zone are Pretoria, De Hoek and Sterkfontein. Zone 2 consists of 17 rainfall stations. It covers mostly the Orange Free State and includes stations like Barkly West, Klipfontein, Potchestroom and Heritage. Zone 3 which consists of 15 stations is located mainly within the eastern regions of the Cape Province and covers areas to the south and west of Lesotho. It includes stations like Adelaide, Philadelphia, Colesberg and Mount Fletcher. Zone 4, in the northern regions of the Cape, forms part of the Greater Karoo which is a relatively dry area. Among the 14 stations of zone 4 are Sandpan, Geelkop and Rietfontein. Unlike the other areas identified, Zone 5 experiences rain almost exclusively during the winter months; it is situated in the south-west extremes of South Africa. The zone contains 10 rainfall stations among which are Tokai, Montagu, and Saldanha Bay. Along the southern extremes of the subcontinent is zone 6 which experiences rain throughout the year. Stilbaai, Humansdorp, and Concordia are three of the 8 rainfall stations included in this area.

Figure 1.7 shows the areal average long-term monthly rainfall totals for the six zones. Zones 1 through 4 show rather similar patterns as opposed to the winter (zone 5) and all-year (zone 6) rainfall areas. It should be noted that station rainfall data series are usually 'noisy', so a simple arithmetic averaging of total precipitation amounts from several stations does not necessarily produce a representative sample for an area. An efficient technique of combining data from diverse stations, as used by Kraus (1977) and

described in Section 1.6 (normalization), has been used to develop rainfall indices for the different zones. Since the main objective is to study summer rainfall variations across South Africa, attention will be focussed on zones 1 to 4; zones 5 and 6 have been presented for comparison and completeness. The latter zones will not be considered in the investigations. Rainfall index series are derived for each of the 4 zones (see Section 1.6 for the procedure followed). An index, called the 'All-Area' index, is also formed by considering an ensemble of all the individual station indices within the 4 summer zones. Figure 1.8 shows the All-Area rainfall index time series for October to March.

It should be noted that, as expected, the resulting zones are similar to those in other studies (for example, Nicholson, 1986a,b; Lindesay, 1988; Walker 1989) although the grouping procedures were not the same. In particular, rainfall area 1 of Walker (1989) corresponds to the total of zones 1 to 3 as defined in this study. The Climatology Research Group of the University of the Witwatersrand (South Africa) also used a similar data set (Lindesay, 1988). Consistency among the records should augment confidence in the rainfall data set.

Statistical analyses sometimes rely on the degree of normality of the population from which the samples originate. Sample variables like pressure and temperature can usually be assumed as being drawn from populations which are normally distributed. Rainfall data may follow Gamma distributions (Panofsky and Brier, 1968) in which case the data must be transformed to, say, a normal distribution, depending on the tests to be applied. Log-normal plots are sometimes used to display the degree of normality of certain distributions. It should, however, be noted that satisfaction of the condition leading to normality does not guarantee normality of the series in question. What may perhaps be concluded is that the particular distribution deviates from normal. January rainfall series generally show significant deviation from Gaussian, whereas series for the other months are fairly normal.

Other test methods could be pursued, but again, they also do not necessarily guarantee that the particular sample has been drawn from a normally distributed population. An alternative is to use non-parametric methods of analyses and tests. Non-parametric statistics do not rely on any pre-assumed probability distribution of the variables. In the present study, the test required is for the significance of linear correlations. In order to reduce ambiguity and to augment confidence, it has been decided to compute both the Pearson product-moment correlation coefficient as well as the Spearman rank correlation. Tests of results from the former rely on normality whereas the latter do not.

1.6.2. SEA SURFACE TEMPERATURE (SST)

The Comprehensive Ocean Atmosphere Data Set (COADS) is one of the most extensive compilation of marine data. The compilation project was initiated in the United States at the University of Colorado/NOAA (National Oceanic and Atmospheric Administration) Cooperative Institute for Research in Environmental Sciences (CIRES) in Boulder, Colorado (Fletcher et al., 1985). The final COADS compilation was the result of a joint project between CIRES, the National Climatic Data Center at Asheville, North Carolina, and the National Center for Atmospheric Research in Boulder. The COADS contains most of the archived historical marine data. These were assembled from various international archives, carefully checked for duplication errors, and then summarized by month on a two-degree latitude by two-degree longitude spatial grid. Release 1 of the set contained data for the years 1854 to 1979 on three magnetic tapes, while a fourth tape supplemented the data until 1988. The initial input consisted of about 100 million ship reports which, after elimination of duplicates, resulted in about 70 million (for the period 1854-1979). For the present study, mean SST data have been extracted from the "Monthly Summaries Trimmed Group" in the COADS. In these trimmed summaries only those basic

observations were kept that were within 3.5 standard deviations of the long-term mean value. Further details on COADS are described in Fletcher et al. (1985). The quality of the results depends not only on the amount of data, but also on their temporal and spatial distributions. Figures 1.9 a, b, and c show the temporal distribution of the number of reports. The number of observations has monotonically increased since 1950. The data density is generally biased by major shipping routes.

Several investigators have addressed the question of SST data quality (e.g., Barnett, 1984c; Ramage, 1984; Mobley and Preisendorfer, 1985, Wright, 1986; Oort et al., 1987). Details on the quality and quantity of the observations will not be discussed here. It should, however, be mentioned that the data usually suffer from problems such as uneven temporal and spatial sampling, systematic errors due to instrumentation changes over time, as well as random errors caused by both human and instrument inaccuracies (Mobley and Preisendorfer, 1985). Since the frequency of observations has generally increased after World War II, the data period selected extends from 1950 through 1986. SST data within this period are believed to be accurate enough for purposes of the present study. The spatial domain extends from 20°N to 40°S and encompasses the globe. Strong SST gradients may exist near coastal areas due to ocean currents. Since the present study concentrates on rather large scale features, any box which had a contribution of SST data from coastal areas were excluded (these boxes are indicated with a '*' in Fletcher et al., 1985). In order to reduce the magnitude of probable errors, the field was smoothed in the zonal direction. Thus the SST for a central 2° by 2°-box was added to four adjacent-box SSTs, two to the west and two to the east of the central box. The SST of the central box was then obtained by averaging the values within the 5 boxes involved. Before addition, each monthly SST value within a box was first weighted by its associated number of observations. So a SST value within a particular box was, at least slightly, influenced by

SSTs observed at up to about 800 km away. It should be noted that no inverse distance weighting was applied. The method is justified due to the generally weak zonal (compared to meridional) temperature gradient on the scale considered.

Most studies dealing with COADS have considered SST data up to the 1979 period. This is probably mainly due to the change in quality and quantity since the start of the blending of observations by conventional and satellite methods. For purposes of this study, the period extends from 1950 to 1986. Computations based on different time windows are found to be comparable and consistent.

Figure 1.10 shows the 37-year monthly mean SST distribution throughout the domain considered for the months of January and July. As expected the patterns are similar to those in earlier publications (Halpert and Ropelewski, 1989; Nicholson and Nyenzi, 1990). Although near-coastal SSTs have been excluded from the analysis, the major regions of upwelling are clearly apparent, especially the Humbolt/Peru Current (off western South American coast), the Benguela Current (south-eastern Atlantic), and the Canary Current (off the north-western coast of Africa). Another interesting feature in the SST distribution is the extension of a cold tongue of equatorial surface waters in the Atlantic and Pacific Oceans, but not in the Indian Ocean. Equatorial upwelling in the Atlantic and Pacific are due to the persistence of easterly surface winds throughout the year; whereas along the equatorial Indian Ocean the surface winds are easterly only during the southern hemisphere winter months.

1.6.3. TROPOSPHERIC WIND

The zonal (U ms^{-1}) and meridional (V ms^{-1}) components of the total horizontal wind were available on magnetic tape from the Climate Analysis Center, NOAA, U.S.A. The components were digitized on a monthly mean basis for six standard vertical pressure levels: 1000, 850, 700, 500, 300 and 200 hPa. The data covered the period March 1968 to February 1987 for 700, 500, 300 and 200 hPa, December 1974 to February 1987 for 850 hPa, and December 1975 to February 1987 for 1000 hPa.

The raw wind data originated from pilot balloon and radar wind observations scattered throughout the globe. Such observations are not homogeneous in space and time; there is a bias toward continental areas where wind sounding stations are much denser compared to large oceanic regions with little or no observations. Furthermore, observations from certain continental regions, such as equatorial Africa, are less frequent than from European or North American areas. Also used in the analyses are aircraft wind data as a supplement to conventional observations. Aircraft wind observations, primarily above 500 hPa, have generally increased since the seventies. All the observations go through quality control procedures while being subjected to objective analyses. The resultant gridded data should enable analyses of large scale circulation features which are of importance to the present study.

The winds were derived from twice daily (0000 UT and 1200 UT) observations. Roughly 8 per cent of the days were missing except for September 1972, which had 70 per cent missing, and October/November 1972, which were entirely missing (Arkin, 1982). No attempt has been made to replace missing data. The winds were extracted from analyses performed by the operational centre of the National Meteorological Center (NMC), in the United States. The analyses produced U and V components of the wind on a Mercator grid projection with a longitudinal spacing of 5 degrees around the globe. The latitudinal circles

were symmetrical about the equator and were placed North and South at 48.1°, 44.6°, 41.0°, 37.1°, 33.0°, 28.7°, 24.2°, 19.6°, 14.8°, 10.0°, 5.0° and the equator. So a 72-point (zonal) by 23-point (meridional) grid format was obtained.

Significant changes in the analysis procedures occurred during the data period. The general procedure used is to modify a first guess climatology field by interpolating observations to the grid points. Changes occurred in both the interpolation technique and the method employed to obtain the first guess field. Four different interpolation techniques were used during the period. From March 1968 to August 1974, a successive correction scheme, called Cressman Analysis (Bedient et al., 1967), was used and changed to the Hough analysis from September 1974 to August 1978 (Rosen and Salstein, 1980). From September 1978 through February 1979, the operational analysis employed the optimum interpolation technique (Gandin, 1963), which used three-dimensional correlation functions to make observation-generated corrections to the first guess field (Bergman, 1979).

A major switch to a spectral model and the use of non linear normal mode initialization occurred in March 1979; details may be found in Kistler and Parrish (1982). Rosen and Salstein (1985) have described the effect of this procedure as being in the nature of smoothing, which, however, does not appear to be of major importance.

Chiu and Lo (1979), Rosen and Salstein (1980), Lau and Oort (1981), and Arkin (1982) have all addressed questions regarding the quality of the wind analyses and concluded that they were generally of sufficiently good quality for circulation studies. Of course, the products should be used judiciously and with great caution, depending on the particular investigation.

In this study, wind data derived from the Hough analysis procedure (i.e., from September 1974 through August 1978) have been excluded in the computation of the velocity potential

field and derived parameters. This is because the technique imposes the constraint of non-divergence which in turn has a large effect on the data, particularly in the tropics where the divergent circulation is known to be important (Krishnamurti et al., 1973; Kanamitsu and Krishnamurti, 1978). Earlier data have however been retained. Computations based on the earlier part of the data and the more recent part were found to yield comparable results.

1.6.4. OUTGOING LONGWAVE RADIATION (OLR)

The OLR data (Wm^{-2}) were also obtained from the Climate Analysis Center, USA, together with the tropospheric wind data (see above) on the same tape and grid format as for the winds. They were derived from AVHRR (Advanced Very High Resolution Radiometer) window channel radiances. The data covered the period from June 1974 through February 1987, with March 1978 to December 1978 missing. Being largely modulated by cloudiness, OLR has proved to be useful for studies of the large-scale circulation over the tropics. The sensitivity of OLR at the top of the atmosphere to small changes in convective cloudiness provides a good estimate of relative changes in the distribution of energy sinks and sources, especially in the tropical latitudes.

Low OLR values (assumed to be associated with low cloud-top temperatures) indicate the major convective systems that extend upward through the troposphere. OLR in these systems is often of the order of 225 Wm^{-2} or less. In contrast, the tropical land or sea surface and the trade wind cumulus regime, extending upward about a kilometre or so above sea level, appear relatively warm and emits higher radiation, of the order of 275 Wm^{-2} or more. As long as caution is exercised, OLR distributions may be useful as a proxy for convective activity as in other studies (see, for example, Winston and Krueger, 1977; Heddinghaus and Krueger, 1981; Liebmann and Hartmann, 1982; and Lau

and Chan, 1983a, b). Such proxy is particularly justified in the summer months when the background temperature is uniform.

In tropical oceans, OLR has proved to be useful for studies of large scale circulation and in estimating relative changes in the distribution of energy sources and sinks (Lau and Chan, 1983; Winston and Krueger, 1977). It should be noted that, in cloudless oceanic areas, OLR is basically a measure of SST. Moreover, across certain tropical oceans, low OLR values do not always mean strong convection. This is particularly true in the eastern subtropical North Pacific where high-level (cold) cirrus clouds prevail in association with the subtropical jet stream.

Due to limitations in the number of independent events, the results may not meet rigorous statistical significance tests. However, *a priori* knowledge of association patterns should increase confidence in the results. As far as possible, only those features are highlighted which are consistent with the present knowledge of the dynamics of the systems concerned.

Gadgil et al. (1992) investigated variations of the mean July-August OLR against the rainfall across the Indian region. They observed a systematic bias in the NOAA OLR dataset. In particular, the OLR fluxes derived from NOAA-SR (1974-1978) were found to be consistently higher than those from NOAA 7 (1982 onward) over a large portion of the tropical belt. They suggested that the lower values of OLR in the latter period might be a manifestation of a systematic bias arising from various factors such as changes in instruments, satellite equatorial crossing time, etc. Steps have been taken (see Chapter 3) to confirm and remove the bias from the OLR dataset before its use in the investigations.

1.7. PROCEDURES

1.7.1. NORMALIZATION

The normalization process is most useful in situations where it is required to produce indices which are representative of ensembles of observations from stations with diverse characteristics. For example, rainfall data from stations in regions which receive water mainly from convective systems are 'noisy'; a few isolated perturbations can produce transient excess precipitation locally at some stations, while nearby areas remain relatively dry. Simple arithmetic averaging of data from stations in such areas may not be representative of the larger scale phenomena involved. One way of combining data from various locations within a given region is through normalization (Kraus, 1977), a method which provides a useful 'index' (e.g, standardized rainfall index) for the particular area. Indices developed in this manner have the properties of zero mean and unit variance.

If the time series of monthly data over N years for a station is written X(i), i=1,2,3,...,N, then the index series for that station, Y(i), is given by

$$Y(i) = (X(i)-m) / s,$$

where m and s are, respectively, the mean and the standard deviation for the particular month considered. Areal indices are formed by averaging over all the individual station indices within the area concerned. In addition to the property of unit variance and zero mean, indices computed on monthly basis will have seasonal biases suppressed.

1.7.2. CORRELATION AND SIGNIFICANCE TESTS

Linear correlation analyses have been widely used in climatology as a tool for assessing the strength of relationships among variables (Weare, 1979; Horel and Wallace, 1981; Hirst and Hastenrath, 1983; Parthasarathy and Pant, 1984; Tyson, 1984a, b; Harrison, 1986; Lindesay, 1988; van Heerden et al., 1988; Walker, 1989; and many more). The tool should, however, be used only with caution, as it may lead to erroneous conclusions. The technique does not have any built-in ability to distinguish between cause and effect.

The ratio of the explained variation to the total variation is called the coefficient of determination, denoted by R^2. If there is zero explained variation, that is, the total variation is all unexplained, the ratio is zero. And if the total variation is all explained, the ratio is one. The quantity R, called the correlation coefficient, varies from -1 to +1.

Suppose two time series, each of N elements, are denoted by X and Y. Then,

$$R = \Sigma(xy) / \sqrt{[(\Sigma x^2)(\Sigma y^2)]},$$

where,
x = deviation of X from the mean of the X series,
y = deviation of Y from the mean of the Y series.
The coefficient (R) is known as the Pearson's product moment correlation.

Another type of measurement of the strength of association between two series is the Spearman's rank correlation, R_s. The data in the two given series (X and Y, each of N elements) are first ranked in order of size using the numbers 1, 2, 3,...N. Then,

$$R_s = 1 - 6\Sigma D^2 / [N(N^2-1)],$$

where, D = difference between ranks of corresponding values of X and Y.

Tests of significance for the more common statistic (Pearson's correlation coefficient) relies on the degree of normality of the frequency distributions of the data sets involved, while Spearman's rank correlation is non-parametric, that is, it does not depend on the underlying frequency distributions of the series. It has been observed (Section 1.4.1) that rainfall data for certain months deviate from normal; hence, for purposes of this study, both statistics will be referred to wherever necessary.

Results of correlative analyses are tested against randomness by the Student's T-test. In cases where the serial correlation within series are significant, the actual number of observations do not represent independent observations. A method commonly used to estimate the effective number of degrees of freedom is due to Quenouille (1952). If the serial correlation coefficients in two series, both of N terms, are r_1, r_2, r_3, ... and r_1', r_2', r_3', ..., then the effective number of independent observations (N_{eff}) is estimated from

$$N_{eff} = N / (1 + 2r_1r_1' + 2r_2r_2' + \ldots\ldots \text{ until negligible}).$$

The formula provides an approximate correction for serial correlation provided the number of observations in each of the series is large. The results of analyses obtained from using the shorter period time series should be interpreted with reservation.

In order to ascertain the patterns of correlation between series, field (global) significance tests should normally be applied. Global significance tests include the use Monte Carlo simulation techniques. The method follows that of Livezey and Chen (1983) and Hastenrath (1990). Suppose that, of the total number N_T of individual correlations, N reach local significance at the 95% confidence level; then the field significance at the 95% level is exceeded when N surpasses N_*, where N_* is the 95 percentile of the number of locally significant correlations in a field correlated with random series with statistical properties similar to those of the original respective series. The procedure consists

essentially of two steps. First, assuming no spatial interdependence, N_* is equal to the 95 percentile of a binomial distribution with N trials and success probability p = 0.05 (Livezey and Chen, 1983). If N does not exceed N_*, the pattern does not possess field significance at the 95% level of confidence, and the process is terminated. Otherwise the second step is followed, in which the spatial interdependence within the field is accounted for. The original series (rainfall index, for example) is first randomly scrambled and then correlated with the other series (SST index, for example). The Monte Carlo experiment is repeated 400 times, say. This results in 400 values of the number N_{mc} of locally significant correlations. When N exceeds the 95 percentile of empirically determined N_{mc}'s, then the pattern is considered to possess field significance at the 95% level of confidence.

Due to computation time constraints, limited application is made of such tests. However, full application is made where seasonal South African rainfall series is correlated with gridded SST.

1.7.3. VELOCITY POTENTIAL AND CIRCULATION INDICES

East-west and north-south mass overturning are important features of large-scale atmospheric circulations. The most commonly known are the Walker (zonal-vertical) and Hadley (meridional-vertical) circulations. Studies of the characteristic patterns and intensities of such features do help in the understanding of climate variability from a dynamic point of view. One way of analysing the zonal and meridional circulations is through the examination the velocity potential field. Computational procedures are described next. Definitions and procedures closely follow those of Holton (1973), Krishnamurti et al, (1973), Krishnamurti and Kanamitsu (1978), Chiu and Lo (1979), and Chu and Park (1984).

Using Helmholtz theorem, the total two-dimensional wind vector (V) can be decomposed into the sum of the divergent (V_χ) and the rotational part (V_ψ). Thus,

$$V = V_\chi + V_\psi$$

$$= \nabla\chi + K \times \nabla\psi$$

where χ denotes the velocity potential, ψ the streamfunction,
and K is the vertical component of the unit vector.

The two components are defined as

$$\nabla . V = \nabla^2\chi$$

$$K . \nabla \times V = \nabla^2\psi$$

where, ∇^2 is the Laplacian operator.

Due to the nature of tropical dynamics, the velocity potential field will be emphasized in this study. The field is solved through mathematical relaxation processes using the computed divergence; there are no east or west boundaries (round the globe data) and the values at the south (48.1°S) and north (48.1°N) boundaries are set to zero.

In order to analyse the east-west and north-south mass overturnings, the velocity potential field is transformed into two parameters, the Zonal (east-west) Circulation Index (ZCI), and the Meridional (north-south) Circulation Index (MCI). These are defined as

$$ZCI = \frac{1}{L_y} \int_{y_1}^{y_1 + L_y} U_x \, dy$$

$$MCI = \frac{1}{L_x} \int_{x_1}^{x_1 + L_x} V_x \, dx$$

where,
Y_1 is the starting latitude, L_y is the length of a meridional extension.
X_1 is the starting longitude, L_x is the length of a zonal extension.

$$U_x = \frac{\partial\chi}{\partial x}$$

$$V_x = \frac{\partial\chi}{\partial y}$$

The geometry of the distribution patterns may be interpreted as follows: If the isopleths of the velocity potential are parallel to the latitude lines, then there is no east-west circulation; similarly, if the isopleths are parallel to the longitude meridians, north-south overturnings are absent. Regions of large divergence may be interpreted as having an analogous relation to the curvature and shear of velocity potential isopleths just as regions of large vorticity have to the curvature and shear of the streamfunction isopleths.

Computation of the velocity potential field was done through a program provided by Professor Krishnamurti and co-workers, Florida State University, USA. Proper alterations were made to the program before processing the data.

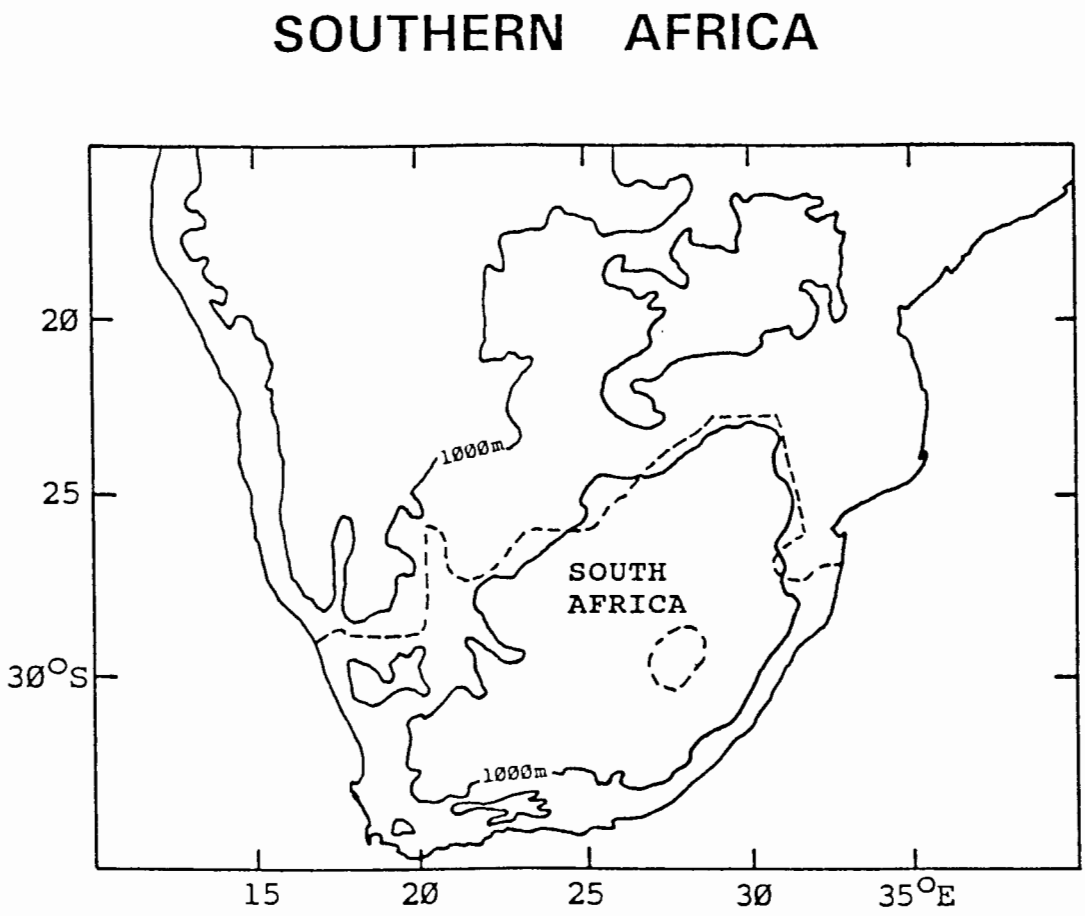

Figure 1.1. Location map.
1000 m contours are outlined (solid line).
The dashed line indicates the borders of South Africa.

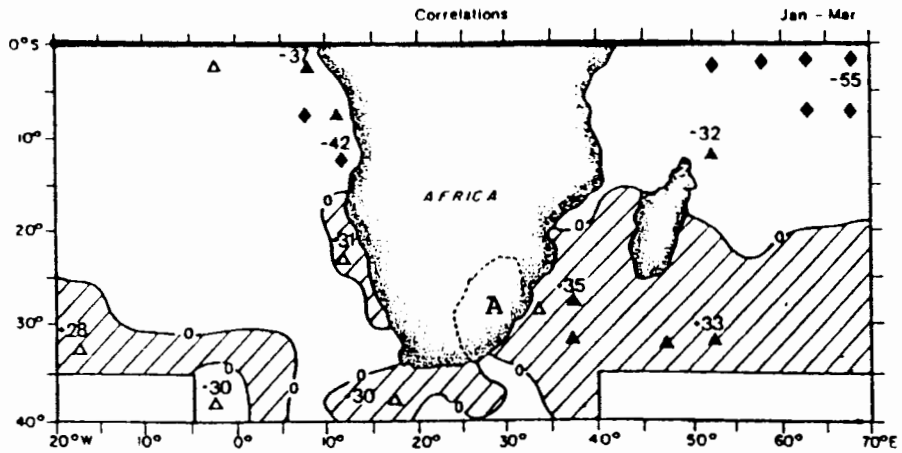

Figure 1.2. Simultaneous correlation (x100) between area-averaged rainfall in region A and grid-square (5°x5°) SST departures in late summer (January, February, March). N=36.
Significance: ♦ 99%; ▲ 95%; △ 90%. Area of positive correlations hatched. (From Walker, 1989).

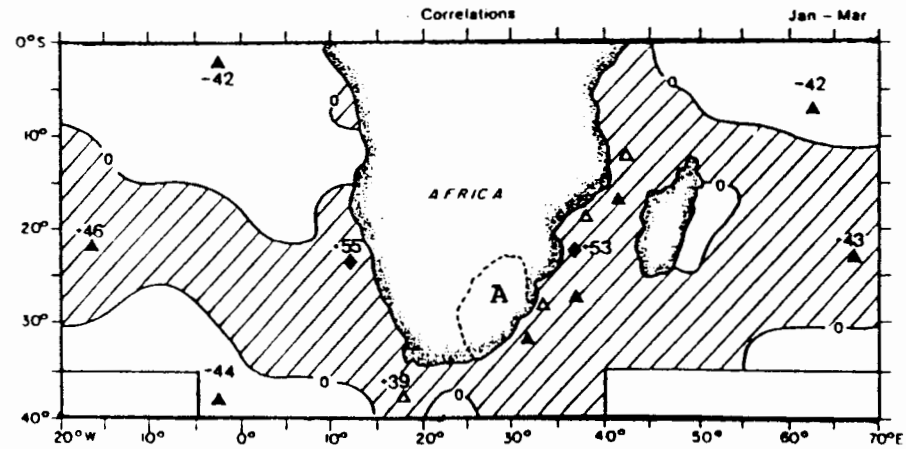

Figure 1.3. Simultaneous correlation (x100) between area-averaged rainfall in region A and grid-square (5°x5°) SST departures in late summer (January, February, March). Southern Oscillation influence on rainfall excluded. N=22.
Significance: As in Figure 1.2. Area of positive correlations hatched. (From Walker, 1989).

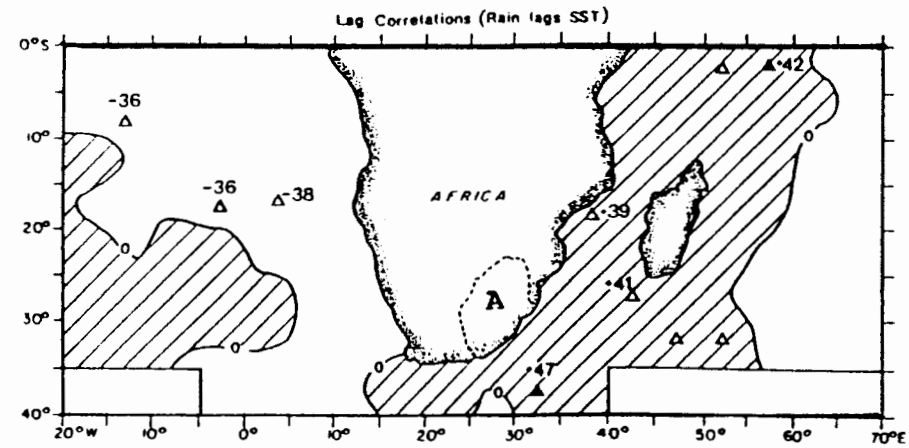

Figure 1.4. Lagged correlation (x100) between area-averaged rainfall in region A in late summer (January, February, March) and grid-square (5°x5°) SST departures in early summer (October, November, December). Southern Oscillation influence on rainfall excluded. N=22.
Significance: As in Figure 1.2. Area of positive correlations hatched. (From Walker, 1989).

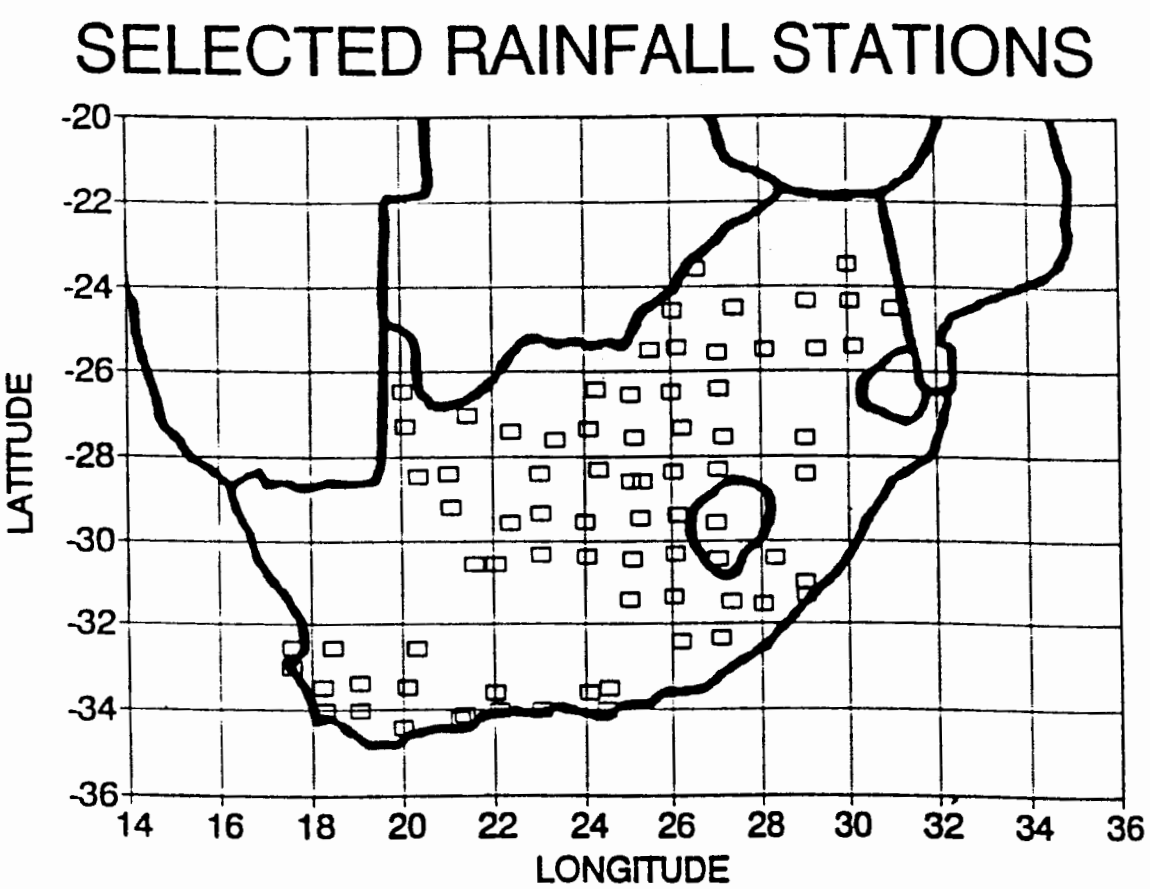

Figure 1.5. Locations of the selected rainfall stations.

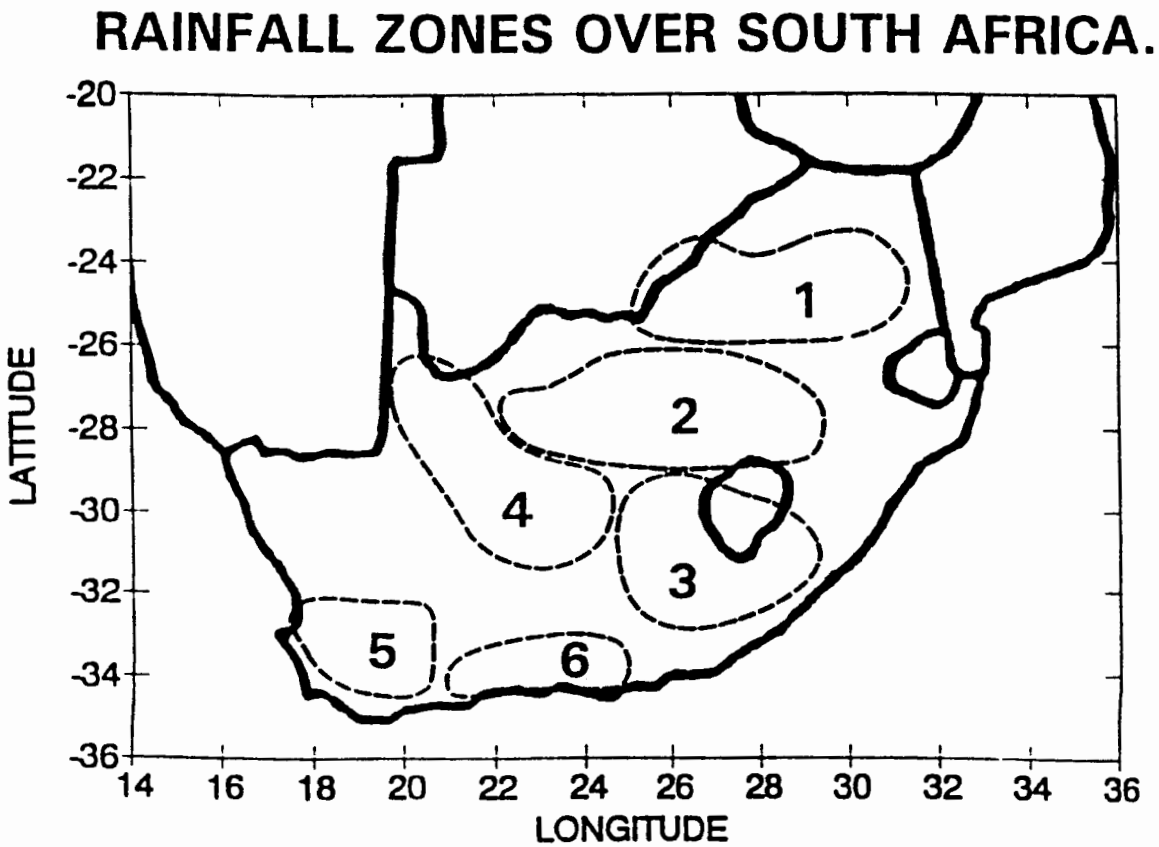

Figure 1.6. Six homogeneous rainfall zones.

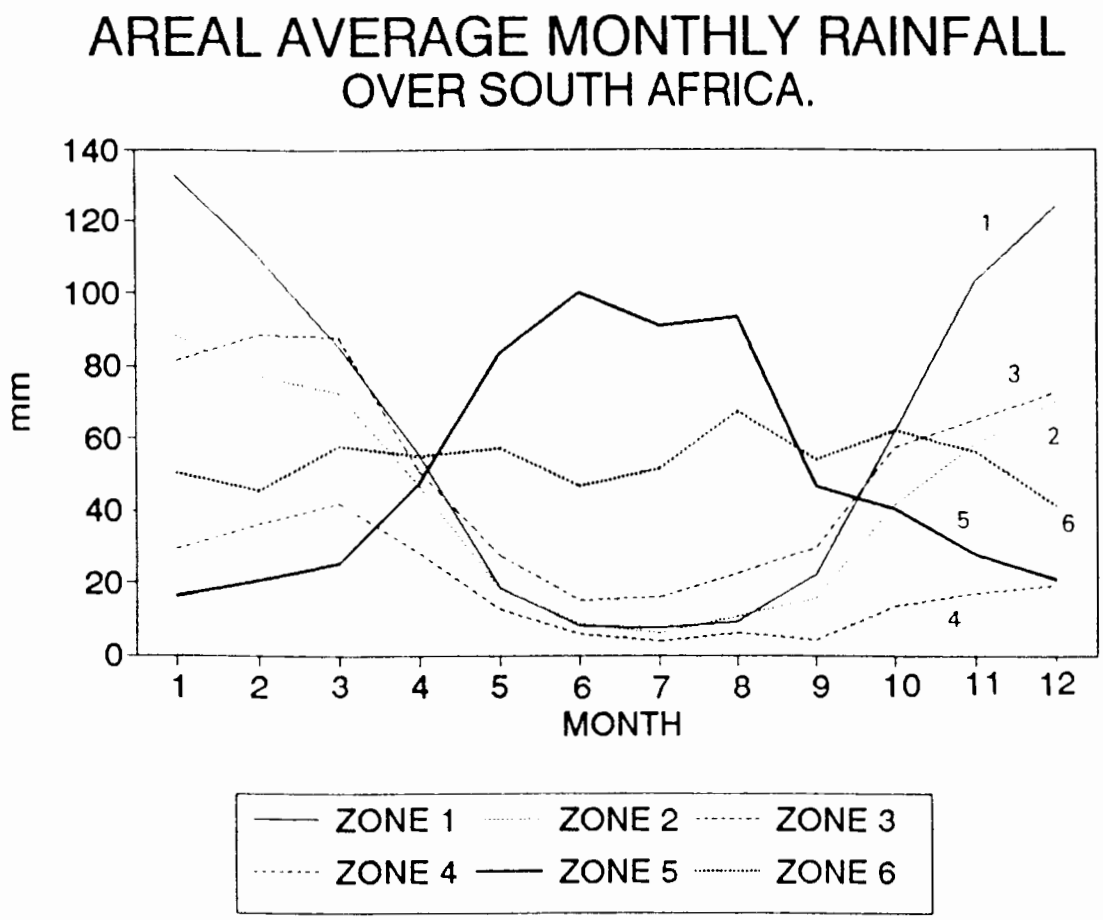

Figure 1.7. Average monthly rainfall totals for the six zones. Based on years 1950 to 1986.
(See Figure 1.6 for locations of the zones.)

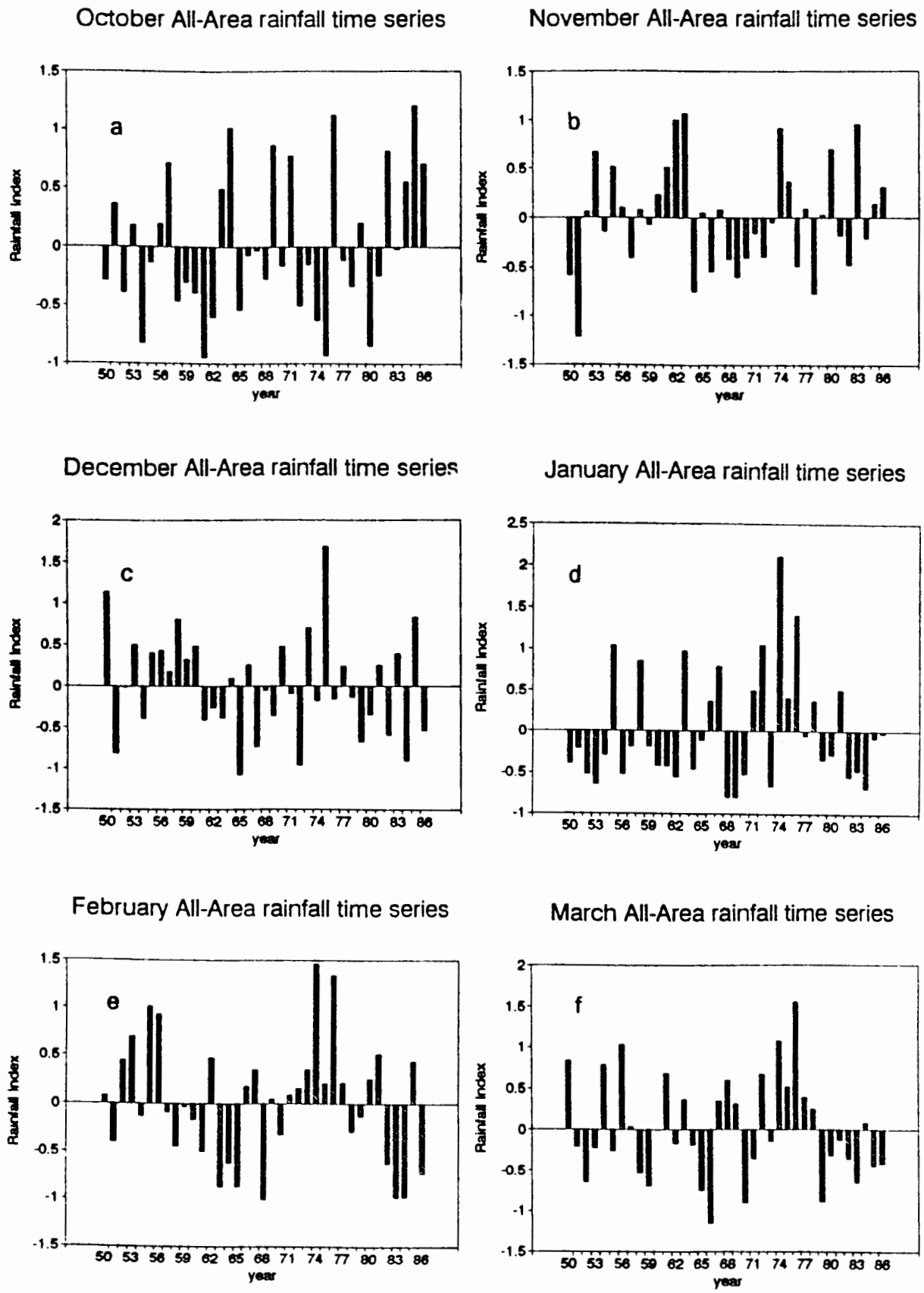

Figure 1.8. All-Area rainfall index time series (standardized departures).
a. October; **b.** November; **c.** December;
d. January; **e.** February; **f.** March.

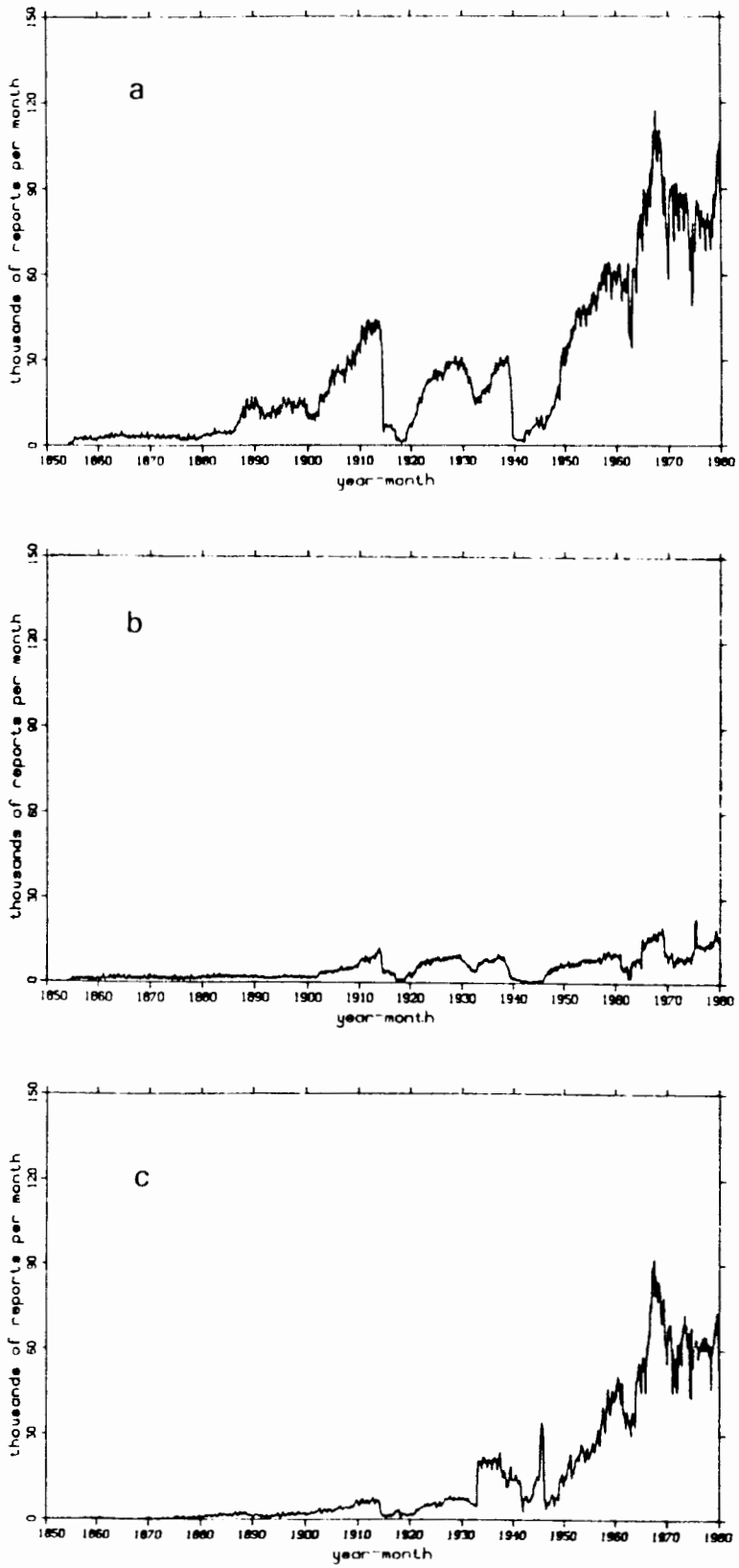

Figure 1.9. Number of marine reports after duplicate elimination. (COADS, Fletcher et al. 1985).
a. Atlantic, b. Indian Ocean, and c. Pacific basins

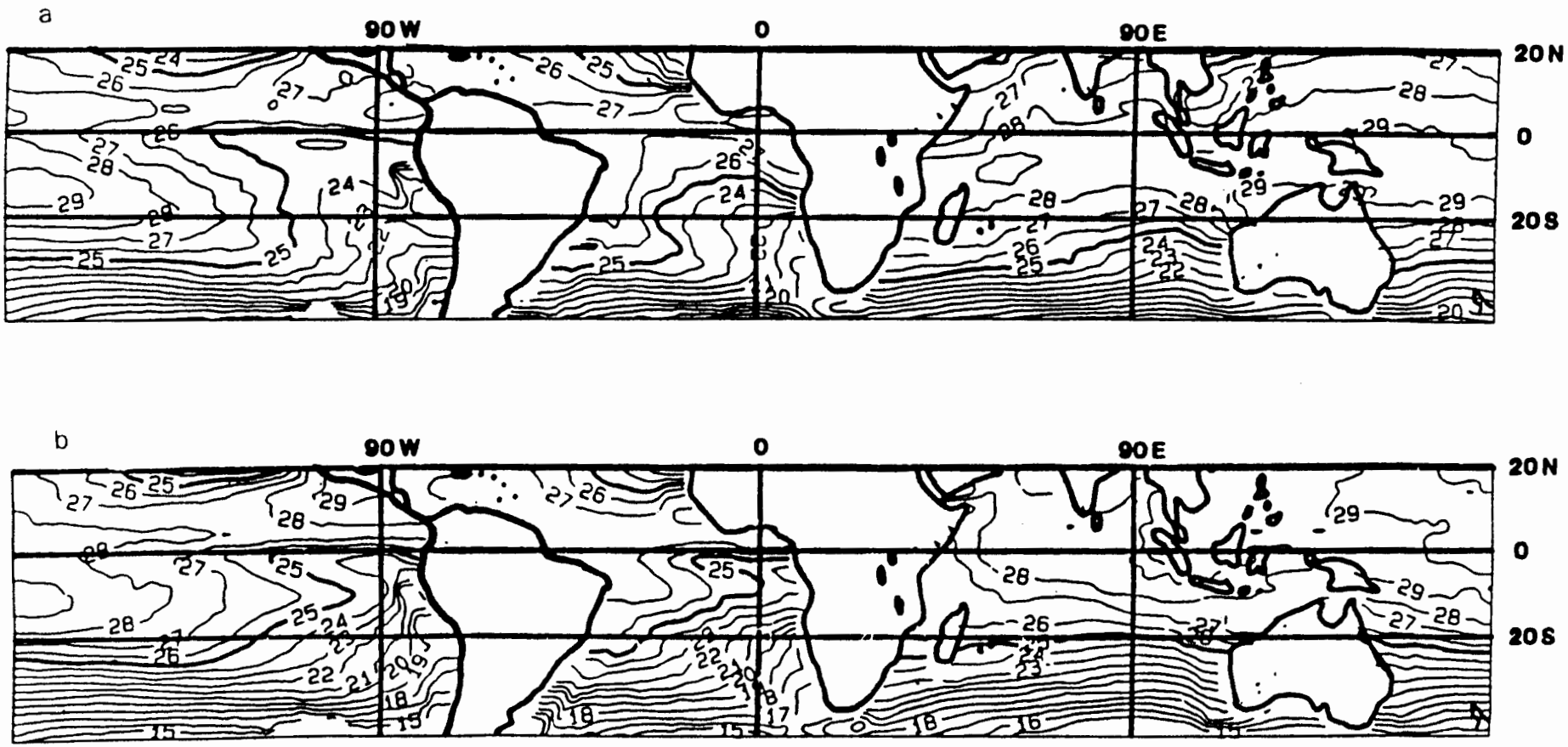

Figure 1.10. Mean SST (°C), based on years 1950-1986.
a. January; b. July.

CHAPTER 2

VARIATION OF SOUTH AFRICAN SUMMER RAINFALL WITH SEA SURFACE TEMPERATURE

2.1. INTRODUCTION

There has been an increasing interest in the study of large-scale air-sea interactions, with particular emphasis on the spatial and temporal relationships between the variations of sea surface temperature (SST) anomalies and atmospheric circulation anomalies. The primary motivation for this type of research is the eventual prediction of the state of one medium given that of the other. The interpretation of the results usually leads to forecasts of, say, mean precipitation amount and distribution, mean temperature, and other fields, within the framework of physically sound links. Statistical associations have been observed in many cases, but cause and effect could often not be determined even though the issue of causality has important implications for the application of oceanic and atmospheric parameters to relatively long-range (monthly to seasonal) climate predictions.

Experiments utilizing SSTs as extended weather indicators have been encouraging, but these indicators are not entirely straightforward to apply, mainly due to the seasonal and regional variations in their relationships with the atmosphere and the imperfect nature of the resulting statistics (Namias and Cayan, 1981). The physical reasons for expecting a linkage between mean SST pattern and mean atmospheric circulation are that the SST anomaly patterns often have much spatial coherence, cover large areas (10^6 km^2), persist for several months, and can be responsible for significant sensible and latent heat fluxes from the sea to the atmosphere, Namias and Born (1974), and Sawyer (1965).

The persistent features of SST anomalies are mostly due to the great thermal inertia of the oceans. The question of cause and effect between SST and atmospheric anomaly patterns is still a matter of debate. But, with a vast literature in the background, one of the safest ways to condense the circular argument of causality is to view the two media (the ocean and the atmosphere) as being more or less coupled with seasonally varying feedback mechanisms operating.

The problem of particular importance to be addressed in this chapter is the relationship between rainfall variation across the summer rainfall area of South Africa and the variation of SST, with the view towards monthly and seasonal rainfall anomaly prediction. Walker (1989) analysed the correlation between rainfall over South Africa and SST over the south-east Atlantic Ocean and south-west Indian Ocean. A brief summary of that part of her work which is of relevance here is given. The rainfall data was grouped into 2 areas within the summer rainfall region. Both the rainfall and SST data sets were stratified with a temporal resolution of 3 months. Significant positive simultaneous correlations between rainfall and the SST over the surrounding seas, especially in the Agulhas Current zone and the narrow Benguela Current area were found.

The calculations of Walker (1989) were repeated to produce lagged (with SST leading) correlations, using the same data sets, but including all the years, even those when the SOI was high or low. An important result was apparent in the 3-month lag correlation with SST leading rainfall. Insignificant relationship was noted between rainfall and SST over most of the surrounding areas, but the negative correlations with equatorial Indian Ocean SST remained significant, a factor which could be useful in empirical models for long term rainfall predictions.

The following section provides a summary of the data used. In Section 2.3, under the heading 'Key-Box Selection', preliminary correlations between rainfall and grid

point SST around the globe within the belt 20°N to 40°S are discussed followed by the selection of key boxes. Section 2.4 presents the results of correlation between the variations of summer rainfall within the four zones defined in Chapter 1 and SST within boxes selected in Section 2.3. The four summer rainfall zones are reproduced in Figure 2.1. An 'All-Area' rainfall index is computed; this area index includes all the rainfall station indices involved in zones 1 through 4. Section 2.5 presents the results of correlations between the variations of the 'All-Area' rainfall index and the SST within the selected boxes. Results of investigations utilizing seasonal data are discussed in Section 2.6. Section 2.7 summarizes and concludes this chapter.

2.2. DATA

Normalized monthly anomalies were computed for each selected station within the summer rainfall area of South Africa. The anomalies were then grouped into 4 homogeneous rainfall zones (Figure 2.1). An 'All-Area' rainfall index series was formed which comprised all the station rainfall indices of zones 1 through 4. The data period considered in the following sections extends from 1950 to 1986 for both sets. Details on procedures and data (quality, quantity, and processing) are given in Chapter 1.

2.3. KEY-BOX SELECTION

This section is concerned with the selection of key areas which will form the basis of the bulk of the analyses to be performed. The key-box selection procedure biases towards SST variation because it is believed that SST, especially over the tropical latitudes, represents a relatively strong potential in rainfall prediction across South Africa.

A linear correlation map was produced between the monthly mean rainfall index for one rainfall zone and the standardized SST anomaly at each of the grid points throughout the SST domain, that is, 20°N to 40°S and around the globe. This procedure was repeated for each of the four summer rainfall zones and for each of the six summer months (October to March). Apart from simultaneous correlation maps, lagged correlation maps were also produced, beginning with SST leading rainfall by up to six months and ending with SST lagging rainfall by up to six months. This resulted in more than 300 teleconnectivity maps which, for practical reasons, cannot be presented here, but samples of simultaneous and lagged point-correlation maps are displayed in Figures 2.2 and 2.3. Although computation was performed for a large domain, the samples shown cover only a limited area. Absolute correlation values of greater than about 0.31 are significant at better than the 95% level of confidence.

One of the salient features observed is coherence in the patterns of the correlation distributions across the tropical Indian and Pacific Oceans (Pacific sector not shown here); the correlations remain negative up to lags of the order of -4 months (Figure 2.3). Simultaneous correlations are generally weak over the Atlantic sector, but a change in the sign of the lagged correlations is notable. Across the extratropical regions the correlations are generally positive at zero lag. The values in the region off the south-west coast of South Africa remain negative from zero up to several lags. However, in the region affected by the Agulhas Current waters, the

relationship is positive at zero lag, but lagged correlations (with SST leading) become negative. In order to reduce noise in the data, teleconnectivity maps were also prepared using seasonal All-Area rainfall index series against 1-month, 2-month, and 3-month SSTs at various lags. Figure 2.4 shows the distribution of lagged correlation between mean SST (June + July) and seasonal (October to March) All-Area rainfall. The results are generally consistent with the previous ones. Negative links with the tropical belt as well as positive links with southern extratropical areas are more marked across the Pacific compared to monthly analyses. Field significance tests were applied in order to ascertain the correlation patterns against randomness. The procedure (described in Chapter 1) is similar to that explained in Livezey and Chen (1983) and Hastenrath (1990). Results of over 400 Monte Carlo simulations confirmed that the patterns attained field significance at better than the 95% level of confidence.

All the SST-rainfall correlation results were scanned in order to identify key areas with the most coherent and significant response. While this procedure assumes apriori assumptions, the statistical results should be regarded with reservation until properly justified. More emphasis was placed on the spatial extent and coherence of the values rather than only on the values. Another statistical feature to be considered in this type of analysis is the degree of closeness to normality of the frequency distributions of the time series in question. While the SSTs may be assumed to be nearly Gaussian, the rainfall series for the months treated are not all near normal, an example being January rainfall which deviates significantly from normal (as discussed in Chapter 1). Emphasis was put on the data density distribution and coherence of the results while selecting the boxes. Evaluation of the rainfall-SST teleconnectivity maps led to the selection of the 12 key boxes listed in Table 2.1; their locations are shown in Figure 2.5.

TABLE 2.1
List of selected Key Boxes.
1. CSA Central South Atlantic Ocean: 14°S-24°S, 20°W-4°E.
2. BCR Benguela Current Region: 22°S-34°S, 10°E-16°E.
3. ARR Agulhas Retroflection Region: 34°S-38°S, 10°E-20°E.
4. ACR Agulhas Current Region: 28°S-36°S, 32°E-40°E.
5. SEI South East Indian Ocean: 20°S-30°S, 80°E-100°E.
6. WEI Western Equatorial Indian Ocean: 0°S-10°S, 40°E-60E.
7. CEI Central Equatorial Indian Ocean: 0°S-10°S, 60°E-80°E.
8. EEI Eastern Equatorial Indian Ocean: 0°S-10°S, 80°E-100°E.
9. ASA Arabian Sea Area: 10°N-0°N, 50°E-70°E.
10. WEP Western Equatorial Pacific Ocean: 4°N-6°S, 160°E-160°W.
11. EEP Eastern Equatorial Pacific Ocean: 4°N-6°S, 140°W-100°W.
12. SWP South West Pacific Ocean: 20°S-30°S, 180°W-160°W.

SEI, which is in the far South-East Indian Ocean, is included because wind stress in this area is likely to affect the SST within equatorial Indian Ocean areas which in turn is significantly related to South African rainfall variability. The Western Equatorial Indian Ocean (WEI) region and the Arabian Sea Area (ASA) lie in regions where the Indian monsoon wind circulation shows a remarkable reversal from winter to summer (Halpert and Ropelewski, 1989), a feature which could have an effect on South African rainfall distribution. Winter dryness over much of the Southern African subcontinent is either directly or indirectly related to the Asian monsoon circulation, and so is the summer rainfall regime of Southern Africa. These form part of a complex interrelated circulation system. The dynamics may be studied through analyses of the divergent flow in the tropical troposphere and will be dealt with in a later chapter in connection with the analysis of the velocity potential and related fields.

Selection of the Western and the Eastern Equatorial Pacific (WEP and EEP) are obvious because SST variations in these areas are related to the well-known ENSO phenomenon (Julian and Chervin, 1978; Rasmusson and Carpenter, 1982; Philander, 1983; Yarnal and Kiladis, 1985, Cane, 1986, Ropelewski and Halpert, 1987 and Wright et. al., 1988). Of particular interest in the context of South African rainfall variation are the studies of Harrison (1983), Harrison (1986), Lindesay (1988) and van Heerden et al (1988), (see Chapter 1 for review). While

delineating the two Equatorial Pacific boxes, consideration was given to the boundaries of the Nino 4 and Nino 3 areas; these areas are defined in the United States Climate Diagnostic Bulletin which is published regularly. So, WEP and EEP were made as close as possible to Nino 4 and Nino 3 areas, respectively. This should make comparisons easier.

Box 12 (SWP) lies in the South West Pacific. Several studies have indicated the response of atmospheric parameters at extra-tropical latitudes to the variation of equatorial SST (Bjerknes, 1966, 1969; Webster, 1982; Philander, 1983; Rowntree, 1972; Chiu and Lo, 1979). So, indirect feedback can be gained from selecting an area off the East Australian coast.

Several studies have identified various SST areas, similar to most of those selected here, which display spatially coherent behaviour and which have links with southern African rainfall anomalies (see, for example, Hirst and Hastenrath (1983), Hastenrath (1984), Nicholson and Entekhabi (1987); Janowiak (1988), Walker (1989, 1990); Nicholson and Nyenzi, 1990; and Jury and Pathack (1991). These investigations have used Principal Component Analysis, correlation-type of analysis, or the like, but the results are comparable.

Nicholson and Entekhabi (1987) analysed fluctuations of SST in the upwelling region along the Benguela Coast and its relationship to rainfall variability both along the coast and throughout equatorial and Southern Africa. The results of Walker (1989) also show the importance of SST within limited regions of the Indian and Atlantic Oceans in summer rainfall modulation across South Africa. Whereas all previous studies in connection with rainfall variability of South Africa have considered limited ocean areas, the SST domain in this study extends throughout the entire tropical region.

2.4. RESULTS - RAINFALL VS BOX SST CORRELATIONS

The main objective of this section is to identify SST precursors which may be useful in the prediction of monthly rainfall across the summer rainfall area of South Africa. Linear correlation coefficients (both Pearson's product-moment and Spearman's rank) were computed between the monthly rainfall index for a particular zone and SST anomalies within each of the 12 key boxes identified in Section 2.3. Computation extended over a series of lags: SST leading rainfall by 18 months through to SST lagging rainfall by 6 months. The procedure was repeated for each of the 4 rainfall zones within the summer rainfall area of South Africa and for each of the six summer months, October through March. Tests of significance are all based on the number of degrees of freedom adjusted for serial correlation by the method suggested in Quenouille (1952) and described in Chapter 1. The number of degrees of freedom generally varies from case to case, depending on the number of missing values. Where statistical significance is not specifically indicated, the following critical limits do provide a safe guideline in the discussions: for 35 independent degrees of freedom, minimum absolute values of correlation of 0.27, 0.32 and 0.42 for 90%, 95% and 99% confidence limits.

The correlation matrices produced in the manner described in the beginning of this section were all examined, but are not all presented here; rather, samples which are believed important for the present purposes are reproduced. Correlation patterns for each of the rainfall zones are described in the following sub-sections. Negative lags, for example -5-month lag, should be interpreted to mean that SST is leading the rainfall month by 5 months, +3-month lag means that SST follows rainfall by 3 months and, of course, lag zero refers to simultaneous correlation.

2.4.1. ZONE 1 RAINFALL VS BOX SST

The 13 stations of zone 1 include Pretoria, De Hoek, and Sterkfontein.

No significant relationship is found between the variations of October zone 1 rainfall and SST. The only notable feature is the generally positive values of the correlations with SSTs in the Central Equatorial Indian Ocean (CEI), Eastern Equatorial Indian Ocean (EEI), Arabian Sea Area (ASA), Western Equatorial Pacific (WEP) and Eastern Equatorial Pacific (EEP) boxes. It will be noted later that these regions show negative links with rainfall for other months. Even with the Agulhas Current Region (ACR) SST there seems to be no association at zero lag.

Like October, November rainfall in zone 1 appears unrelated to SST in the 12 boxes selected in this study. Perhaps the +0.32 simultaneous correlation with respect to the Agulhas Current Region (ACR) SST is worth noting.

December rainfall of zone 1 shows significant relationships with SST. The correlations against SST within 6 of the important boxes are displayed in Table 2.2. The largest value (-0.64) occurs in the Central Equatorial Indian Ocean (CEI) at a lag of -1 month. Arabian Sea Area (ASA), Western and Eastern Pacific (WEP and EEP) show similar patterns with large magnitudes, significant at better than the 99% level at lags of up to at least -4 months. The most useful SST from rainfall prediction point of view appears to be that of the EEP box.

TABLE 2.2
Correlation (x100) between December zone 1 rainfall and SST within the specified boxes. Correlations significant at better than the 95% level are in bold.

Lag	SST Month	WEI	CEI	ASA	WEP	EEP	SWP
-5	Jly	-20	-20	-26	**-40**	**-46**	+24
-4	Aug	**-37**	-19	**-42**	**-42**	**-40**	+27
-3	Sep	**-40**	-19	**-54**	**-49**	**-50**	**+37**
-2	Oct	**-48**	**-40**	**-54**	**-48**	**-58**	**+45**
-1	Nov	**-41**	**-64**	**-55**	**-59**	**-55**	**+36**
0	Dec	-25	**-51**	**-52**	**-44**	**-62**	+23

WEI, CEI: Western and Central Equatorial Indian Ocean.
WEP, EEP: Western and Eastern Equatorial Pacific.
ASA: Arabian Sea Area. SWP: South West Pacific.

January rainfall in zone 1 shows no association with the SST, with the exception of the +0.38 simultaneous correlation and +0.40 at a lag of -1 month with the Agulhas Current Region (ACR) SST.

February zone 1 rainfall variations are significantly linked to SST variations within several of the boxes as shown in Table 2.3. The Central Equatorial Indian Ocean box (CEI) shows the most consistent and significant correlations, with strongest signals at lags of from -4 to -7 (Table 2.3). Values of -0.36 and +0.30 are observed in simultaneous correlations of February zone 1 rainfall with the Benguela and Agulhas Current Region (BCR and ACR) SSTs, respectively, but no lagged associations are found.

TABLE 2.3
Correlation (x100) between February zone 1 rainfall and SST within the specified boxes. Correlations significant at better than the 95% level are in bold.

Lag	SST Month	SEI	WEI	CEI	EEI	ASA
-10	Apr	-28	**-40**	**-39**	**-49**	-27
-9	May	**-50**	-16	**-47**	**-46**	-29
-8	Jun	**-42**	**-31**	**-47**	**-40**	-24
-7	Jly	**-43**	**-42**	**-59**	**-34**	-18
-6	Aug	**-40**	**-37**	**-58**	**-50**	-30
-5	Sep	**-33**	-12	**-59**	-05	-18
-4	Oct	**-35**	**-40**	**-60**	-23	**-47**
-3	Nov	**-30**	**-34**	**-38**	**-31**	-29
-2	Dec	**-36**	-29	**-42**	**-45**	-23
-1	Jan	-09	-26	-20	-08	**-39**
0	Feb	-10	-20	**-40**	**-33**	**-33**

WEI, CEI, EEI: Western, Central and Eastern Equatorial Indian Ocean.
SEI: South-East Indian Ocean. ASA: Arabian Sea Area.

March rainfall of zone 1 does not seem to show a strong link with SST in 11 of the 12 boxes. Although not very significant, Central Equatorial Indian Ocean (CEI) SST shows some indication of its use as a predictor. In this region correlations of -0.34, -0.36 and -0.28 are observed at respective monthly lags of -3, -2 and -1. The consistently negative values may justify the use of CEI SSTs in empirical estimation of March zone 1 rainfall.

2.4.2. ZONE 2 RAINFALL VS BOX SST

Zone 2 consists of 17 rainfall stations. It covers mostly the Orange Free State and includes stations like Barkly West, Klipfontein, Potchefstroom and Heritage. Zone 2 is to the south of zone 1, as shown in Figure 2.1.

October rainfall shows no significant link with SST. Perhaps one should note correlations of +0.26, +0.26, +0.33 and +0.31 at respective monthly lags of -3, -2, -1 and 0 with Eastern Equatorial Pacific (EEP) SST.

With respect to November rain in zone 2, only the Central South Atlantic (CSA), Benguela and Agulhas Current Region (BCR and ACR) SSTs are worth mentioning. Figure 2.6 shows a plot of the correlation distributions for these regions. Of interest are the large positive values at higher lags with CSA and the sign stays positive up to zero lag. With ACR SST, the positive associations are at lags from -8 through 0.

December zone 2 rainfall displays relatively strong links with SST, especially in those areas which are located further away from the sub-continent. The responses are quite similar to those of December zone 1 rainfall with SST. A summary of the results is given in Table 2.4 where it is seen that the Arabian Sea Area (ASA) and Western Equatorial Pacific (WEP) SSTs are best related to December zone 2 rainfall. The correlation with Agulhas Current Region SST is only -0.12 at zero lag.

TABLE 2.4
Correlation (x100) between December zone 2 rainfall and SST within the specified boxes. Correlations significant at better than the 95% level are in bold.

Lag	SST Month	WEI	CEI	ASA	WEP	EEP	SWP
-7	May	-03	+06	-24	**-42**	**-47**	-10
-6	Jun	-14	**-32**	-29	**-46**	**-36**	-01
-5	Jly	-13	-08	-25	**-41**	**-40**	-27
-4	Aug	-29	-19	**-45**	**-55**	**-43**	**+34**
-3	Sep	**-39**	-19	**-50**	**-57**	**-47**	**+43**
-2	Oct	**-44**	**-35**	**-59**	**-47**	**-48**	+27
-1	Nov	**-42**	**-53**	**-57**	**-43**	**-51**	**+33**
0	Dec	**-45**	**-55**	**-57**	**-43**	**-51**	**+36**

WEI, CEI: Western and Central Equatorial Indian Ocean.
WEP, EEP: Western and Eastern Equatorial Pacific.
ASA: Arabian Sea Area. SWP: South West Pacific.

For January zone 2 rainfall, at short SST lags of up to about -3 months, only Central Equatorial Indian (CEI) and Western Equatorial Pacific (WEP) boxes appear useful from a prediction point of view (see Figure 2.7). Correlations of -0.42, -0.37, -0.53 and -0.41 are found with CEI at lags of -3, -2, -1 and 0, respectively, whereas with WEP SST the values are -0.34, -0.35, -0.27, -0.42 and -0.37 at respective lags of -4, -3, -2, -1 and 0. Alike several other zones, January zone 2 rainfall shows a positive peak in correlations with Central South Atlantic (CSA) at high lags (Figure 2.7), for example in the range of -6 to -9 months.

Figure 2.8 displays plots of lagged correlation between February rainfall in zone 2 and SST in the Central and Eastern Equatorial Indian Ocean (CEI and EEI) boxes. The variation of SST for October in CEI explains over 20% of the variance in rainfall during the following February rainfall in zone 2; it should be noted that the corresponding variance explained is over 35% for zone 1 rainfall. EEI SST also shows a strong relationship with zone 2 February rain, but spurious values occur at lags of -4 and -5 months. A correlation of +0.32 is observed with the ACR SST at zero lag, but is not consistent with the lagged correlations.

Out of the 12 SST boxes selected, 6 of them are worthy of mention with respect to March rainfall variation within zone 2. From Table 2.5 it is noted that the Central and Eastern Equatorial Indian Ocean (CEI and EEI), and Western and Eastern Equatorial Pacific (WEP and EEP) SST variations show consistently high and negative values through lags of several months. Again the consistent nature of the positive association in the case of SWP should be noted.

TABLE 2.5
Correlation (x100) between March zone 2 rainfall and SST within the specified boxes. Correlations significant at better than the 95% level are in bold.

Lag	SST Month	CEI	EEI	ASA	WEP	EEP	SWP
-5	Oct	-17	-22	**-33**	**-51**	**-47**	+24
-4	Nov	-23	-24	-24	**-54**	**-44**	**+42**
-3	Dec	**-45**	**-61**	-25	**-48**	**-56**	**+47**
-2	Jan	**-59**	**-52**	**-41**	**-54**	**-44**	+17
-1	Feb	**-44**	**-50**	**-44**	**-36**	**-45**	+21
0	Mar	**-43**	**-37**	-27	**-52**	**-43**	+09
+1	Apr	**-39**	**-41**	-22	**-33**	**-41**	-15

CEI, EEI: Central and Eastern Equatorial Indian Ocean.
WEP, EEP: Western and Eastern Equatorial Pacific.
ASA: Arabian Sea Area. SWP: South West Pacific.

2.4.3. ZONE 3 RAINFALL VS BOX SST

Zone 3 which consists of 15 stations is located within the northeastern regions of the Cape Province and covers areas to the south and west of Lesotho. It includes stations like Adelaide, Philadelphia, Colesberg and Mount Fletcher.

October zone 3 rainfall also shows generally no link with SST, except in the remote regions like the Western and Eastern Equatorial Pacific (WEP and EEP), and South West Pacific (SWP) where significant correlations occur at lags of up to -3 months.

November zone 3 rainfall is significantly correlated with Central South Atlantic (CSA) SST at lags of from -18 to -13 months. This behaviour is similar to the CSA relationship with zone 2 November rainfall and, to a slightly lesser extents, with zone 4 and zone 1 November rainfall at comparative lags. It will be seen later that these contribute towards a strong link between the variations of CSA SST and November All-Area rainfall variations. Most interesting, however, is the general consistency in the sign (positive) of the correlations through most lags up to zero lag. Figure 2.9 displays the plots of correlation between the variations of November zone 3 rainfall and SST within the Central South Atlantic (CSA) and the Agulhas Current Region (ACR). Zone 3 rainfall during November correlates positively with

ACR SST at lags of up to -5 months. SSTs within other boxes do not show any notable link in this case.

December rainfall of zone 3 is most closely linked to SSTs within the Arabian Sea Area (ASA), Western and Eastern Equatorial Pacific (WEP and EEP). The results are given in Table 2.6. The correlation with Agulhas Current Region (ACR) SST is near zero at zero lag and at almost all other lags. Unlike zone 2 for December rainfall, zone 3 December rainfall variation is not strongly linked with Central and Eastern Equatorial Indian Ocean (CEI and EEI) SSTs. On the other hand, the behaviour of WEP and EEP SST variations with respect to zone 3 December rainfall variations is more or less alike the corresponding case concerning zone 2 rainfall (compare Tables 2.4 and 2.6); however, the links are stronger with zone 2 rainfall variations. SWP is included for comparison, as it shows links which are opposite to others.

TABLE 2.6
Correlation (x100) between December zone 3 rainfall and SST within the specified boxes. Correlations significant at better than the 95% level are in bold.

Lag	SST Month	ASA	WEP	EEP	SWP
-7	May	-19	**-43**	**-32**	-03
-6	Jun	-20	**-49**	-26	-06
-5	Jly	-04	**-31**	**-34**	+30
-4	Aug	-26	**-42**	**-39**	**+37**
-3	Sep	**-34**	**-49**	**-40**	**+42**
-2	Oct	**-42**	**-41**	**-43**	+14
-1	Nov	**-42**	**-49**	**-45**	+15
0	Dec	**-51**	**-39**	**-48**	**+35**

ASA: Arabian Sea Area. WEP: Western Equatorial Pacific.
EEP: Eastern Equatorial Pacific. SWP: South West Pacific.

CSA (Central South Atlantic) SST fluctuations shows significant association with January zone 3 rainfall (Figure 2.10); Benguela Current Region (BCR) also displays a similar pattern, but the relationship is less marked. Weak positive links are observed with the Agulhas Current Region (ACR) SST; the correlations are +0.26, +0.28 and +0.28 at the respective lags of -2, -1 and 0 (Figure 2.10).

Unlike February rainfall of zones 1 and 2 which strongly relate to the Central and Eastern Equatorial Indian (CEI and EEI) SST boxes at various lags, the coupling between the corresponding variables in the case of zone 3, located further west, is weaker (see Table 2.3 and Figure 2.8). The correlations at respective lags of -4, -3, -2, -1 and 0 are -0.36, -0.28, -0.40, -0.19 and -0.34. A high correlation of -0.63 occurs at lag -2 between February zone 3 rainfall and EEI SST (the corresponding correlations being -0.65 for zone 2, -0.59 for zone 4 and -0.45 for zone 1). This could be a coincidence, but the consistency cannot be ignored. If the relationship is assumed to be true, then December SST variation in the EEI box could explain over 35% of February rainfall variance in zones 2, 3 and 4, and about 20% in zone 1. Western and Eastern Equatorial Pacific (WEP and EEP) SSTs are weakly associated with February zone 3 rainfall, but in both cases the sign is consistently negative and most of which are significant at at least the 90% level. This is in general agreement with February rainfall of zones 1, 2 and 4. With the Agulhas Current Region (ACR), February zone 3 rainfall shows a strong simultaneous correlation of +0.51, but the variables are uncorrelated at other lags, the sign of the correlation reverses even at short lags of -2 to -3 months.

March zone 3 rainfall behaves in a similar manner to those of zones 1, 2 and 4. Table 2.7 displays the results. Central Equatorial Indian Ocean (CEI) SST shows a maximum correlation of -0.53 at a lag of -2 months, but statistically significant values are equally found at higher lags of up to about -6 months with the Western and Eastern Equatorial Pacific (WEP and EEP). Compared to the other boxes shown in Table 2.7, the Arabian Sea (ASA) box is of secondary importance. March zone 3 rainfall correlations with the Central South Atlantic (CSA) box at lags of -2, -1 and 0 are, respectively, +0.27, +0.27 and +0.30, all significant at better than the 90% level.

TABLE 2.7
Correlation (x100) between March zone 3 rainfall and SST within the specified boxes. Correlations significant at better than the 95% level are in bold.

Lag	SST Month	CEI	EEI	ASA	WEP	EEP	SWP
-7	Aug	+06	00	-11	**-36**	-29	+30
-6	Sep	+02	+12	-16	**-35**	**-44**	**+33**
-5	Oct	-21	-11	**-33**	**-45**	**-47**	+26
-4	Nov	-17	-11	-29	**-42**	**-41**	+27
-3	Dec	**-38**	**-50**	**-35**	**-47**	**-46**	**+39**
-2	Jan	**-53**	**-43**	**-44**	**-40**	**-48**	+26
-1	Feb	**-41**	**-47**	**-36**	**-36**	**-44**	+11
0	Mar	**-42**	**-45**	-28	**-33**	**-40**	+17
+1	Apr	**-32**	**-41**	-23	**-34**	**-33**	-12

CEI, EEI: Central and Eastern Equatorial Indian Ocean.
WEP, EEP: Western and Eastern Equatorial Pacific.
ASA: Arabian Sea Area. SWP: South West Pacific.

2.4.4. ZONE 4 RAINFALL VS BOX SST

Zone 4 is in the northern regions of the Cape Province and forms part of the Greater Karoo which is a dry area. Among the 14 stations of zone 4 are Sandpan, Geelkop and Rietfontein.

As with rainfall variations within zones 1, 2 and 3, generally low and insignificant correlations are found between zone 4 October rainfall and box SSTs, with correlations of both signs occurring inconsistently. What should probably be noted are the positive values at zero and short lags with the Western and Eastern Equatorial Pacific (WEP and EEP) SSTs, a maximum of +0.29 occurs with WEP at zero lag followed by +0.27 with EEP at a lag of -1 month. No association is observed with SSTs fluctuations within the surrounding oceans, including the Agulhas Current Region.

For November rainfall of zone 4, the Agulhas Current Region (ACR) stands out compared to all the other boxes which show no notable relationships. The highest correlation (+0.50) occurs at zero lag with ACR and equally significant values are found at lags of -5 to -3 months (see Figure 2.11). It should be mentioned that,

while December to March rainfall are negatively related to CEI SST, the correlations with November zone 4 rainfall are mostly positive.

With respect to December rainfall of zone 4, only SSTs in the Central South Atlantic (CSA), Western and Eastern Equatorial Pacific (WEP and EEP) are notable (Figure 2.12). WEP SST shows correlations of -0.29, -0.30, -0.39 and -0.39 at respective monthly lags of -3, -2, -1 and 0. Central South Atlantic (CSA) SST indicates an interesting link with December rainfall (see Figure 2.12), with relatively strong positive correlations at high lags.

TABLE 2.8
Correlation (x100) between January zone 4 rainfall and SST within the specified boxes. Correlations significant at better than the 95% level are in bold.

Lag	SST Month	ACR	CEI	WEP	EEP
-7	Jun	-03	-12	**-34**	**-34**
-6	Jly	-17	+03	-29	-25
-5	Aug	-04	-05	**-33**	-26
-4	Sep	+13	-17	**-34**	-28
-3	Oct	00	**-39**	**-40**	**-33**
-2	Nov	+06	**-33**	**-32**	**-31**
-1	Dec	+09	**-53**	**-44**	**-34**
0	Jan	**+35**	**-44**	**-38**	**-35**

ACR: Agulhas Current Region. CEI: Central Equatorial Indian Ocean; WEP, EEP: Western and Eastern Equatorial Pacific

Several of the SST boxes show significant association with January rainfall of zone 4. Among the most useful are the Central Equatorial Indian Ocean (CEI) and Western and Eastern Equatorial Pacific (WEP and EEP). The results are displayed in Table 2.8. CEI and WEP show stronger correlations especially at lags with SST leading. It is noticed that ACR SST correlates simultaneously at better than the 95% level with January zone 4 rainfall, but drops sharply at short lags. As with other zones, Central South Atlantic (CSA) shows consistent, positive association with January zone 4 rainfall at high lags of about -18 to -5 months (Figure 2.13). The significant peaks at lags of -7 to -8 months are notable, although the magnitudes are generally low.

Simultaneous correlation of February rainfall of zone 4 with the Agulhas Current Region (ACR) SST is +0.26, significant at better than the 90% level, but the lagged values do not justify the use of ACR in predictive models; in fact the correlation changes sign at a lag of -2 months. Important SST regions, as far as February zone 4 rainfall variations are concerned, are the Eastern and Central Indian Ocean (EEI and CEI) and the Western Equatorial Pacific (WEP). The results are listed in Table 2.9 where SWP is again included for comparison.

TABLE 2.9
Correlation (x100) between February zone 4 rainfall and SST within the specified boxes. Correlations significant at better than the 95% level are in bold.

Lag	SST Month	CEI	EEI	WEP	SWP
-4	Oct	-29	+03	**-37**	**+35**
-3	Nov	-28	-21	**-31**	**+38**
-2	Dec	**-50**	**-59**	**-40**	**+32**
-1	Jan	**-42**	**-45**	**-34**	+30
0	Feb	**-38**	**-35**	-29	+30

CEI, EEI: Central and Eastern Equatorial Indian Ocean.
WEP, SWP: Western Equatorial and South-Western Pacific.

March rainfall variation in zone 4 is associated with SST variations in several of the boxes, including Central and Eastern Equatorial Indian Ocean (CEI and EEI), Arabian Sea Area (ASA), Western and Eastern Equatorial Pacific (WEP and EEP) and South West Pacific (SWP) (see Table 2.10). As for zones 1, 2 and 3, zone 4 rainfall variations during March show strong negative links with the SST of the previous January within the CEI box (correlation = -0.58). Also notable are the correlations of -0.40 and -0.50 at respective lags of -4 and -3 months with WEP SST. Alike several other cases discussed, SWP SST shows generally positive association.

TABLE 2.10
Correlation (x100) between March zone 4 rainfall and SST within the specified boxes. Correlations significant at better than the 95% level are in bold.

Lag	SST Month	CEI	EEI	ASA	WEP	EEP	SWP
-7	Aug	-12	-04	-28	**-41**	-23	+20
-6	Sep	-10	-05	-28	**-31**	-30	+26
-5	Oct	-26	-06	**-38**	**-37**	**-37**	**+39**
-4	Nov	-24	-23	**-37**	**-40**	**-32**	+28
-3	Dec	-28	**-32**	**-34**	**-50**	**-42**	**+35**
-2	Jan	**-58**	**-43**	**-47**	**-36**	**-39**	**+35**
-1	Feb	**-43**	**-48**	**-37**	**-32**	**-42**	-11
0	Mar	**-45**	**-37**	**-39**	**-34**	**-37**	+12

CEI, EEI: Central and Eastern Equatorial Indian Ocean.
WEP, EEP: Western and Eastern Equatorial Pacific.
ASA: Arabian Sea Area. SWP: South West Pacific.

2.5 ALL-AREA RAINFALL ASSOCIATION WITH BOX SST

All-Area refers to a region which comprises all the individual stations included within the zones 1, 2, 3 and 4 (Figure 2.1). In general, it is found that summer rainfall anomalies over the central and eastern interior of South Africa (equivalent to the 'All-Area' defined in this study) are more coherent in space than in time, a fact which indicates that different physical mechanisms operate during different months (or seasons). The spatial coherence implied here is in agreement with Nicholson (1986a,b), Janowiak (1988) and Nicholson and Entekhabi (1987), among others. The 'large-scale' mechanisms involved are, however, far from simple to explain and interpret.

The analyses and arguments presented do provide justification for combining all the station indices involved in zones 1, 2, 3 and 4. In the following, details are given of the degree of association between the variations of All-Area standardized rainfall and SST. Results of investigations utilizing data on seasonal time scale are considered in Section 2.6.

It can be gathered from the details of results presented in the previous sections that there is not much in common between the variations of October rainfall and SST. This is also evident from the results of All-Area index against SST correlations.

Even the Agulhas Current Region SST does not show significant link, with +0.16 correlation at zero lag, and becoming negative, but still weak, at antecedent lags. Of interest probably is the overall sign distribution. The correlation between the variations of October rainfall and SSTs within Central and Eastern Indian Ocean (CEI and EEI), Arabian Sea Area (ASA) and Western and Eastern Equatorial Pacific (WEP and EEP) at lags from -12 to +6 months are almost all positive, being stronger in the case of WEP and EEP and at shorter lags. But the corresponding correlations when the other summer months are concerned, especially December, February and March, are significantly negative. This behaviour confirms that the links are strongly dependent on the month and that different physical mechanisms become important at different times of the year.

October and November rainfall variations show little similarity with respect to variations of SST. The most notable feature is the link between the November All-Area rainfall index and the Central South Atlantic (CSA) SST fluctuations. The significantly positive correlations of +0.36, +0.55, +0.56 and +0.37 at respective lags of from -18 to -15 months (Figure 2.14) are due to consistent contributions from all the 4 individual zones. The sign remains positive up to zero lag. In addition, SST variations within the nearby major ocean current systems, namely the Agulhas and Benguela Current Regions (ACR and BCR), show positive links with the variation of the All-Area rainfall index (Figure 2.14). Apart from the spurious low value at -2-month lag, ACR SST indicates a relatively strong link with November All-Area rainfall at lags of up to -5 months.

Moving from November to December there appears to be a shift in the correlation patterns. Whereas October and November rainfall show generally positive links with SSTs to the west, from December onwards the correlations change sign and become more significant, particularly with those SST boxes located further away from the subcontinent. A change in the importance of large-scale rainfall producing

mechanisms is implied here. This behaviour is indicative of teleconnection type of associations of South African rainfall with remote SST forcing. The teleconnections are found to be stronger for rainfall during the months of December, February and March and weaker for the other summer months (including January).

TABLE 2.11
Correlation (x100) between December All-Area rainfall and SST within the specified boxes. Correlations significant at better than the 95% level are in bold.

Lag	SST Month	CSA	WEI	CEI	ASA	WEP	EEP	SWP
-6	Jun	+01	-10	-30	-24	**-43**	**-33**	-01
-5	Jly	+12	-04	-10	-09	**-35**	**-40**	+29
-4	Aug	-25	-20	-14	**-34**	**-48**	**-43**	**+37**
-3	Sep	-26	-30	-13	**-42**	**-54**	**-47**	**+40**
-2	Oct	-22	**-44**	**-33**	**-54**	**-48**	**-53**	+28
-1	Nov	-09	**-38**	**-52**	**-49**	**-60**	**-52**	+24
0	Dec	-21	**-37**	**-52**	**-57**	**-48**	**-54**	**+33**
+1	Jan	-26	**-37**	**-56**	**-48**	**-42**	**-44**	+09

WEI, CEI: Western and Central Equatorial Indian Ocean.
WEP, EEP: Western and Eastern Equatorial Pacific.
CSA: Central South Atlantic. ASA: Arabian Sea Area. SWP: South West Pacific.

December all-Area rainfall is negatively linked with SST variations within the Western and Eastern Equatorial Pacific (WEP and EEP), the Arabian Sea Area (ASA) and the Central Equatorial Indian Ocean (CEI), but positively, though less strongly, with SST variations within the South West Pacific (SWP) (see Table 2.11). Results with CSA are included in Table 2.11 for comparison purposes. The three most important regions are WEP, EEP, and ASA where negative correlations are among the strongest at lags of up to at least -4 months. SSTs within these boxes could be considered in empirical formulations of prediction models for December rainfall of the central and north-eastern interiors of South Africa.

January All-Area rainfall exhibits generally weak association with SST, particularly in comparison with December, February and March rainfall variations. This feature has already been noted in analyses with respect to the individual zones 1 to 4. Thus the weak correlation cannot be attributed to a cancellation effect. Somewhat like the November rainfall case, Central South Atlantic (CSA) temperatures at lags of -7 to

-9 months are indicative of positive links with January All-Area rainfall (see Figure 2.15 and Table 2.12).

TABLE 2.12
Correlation (x100) between January All-Area rainfall and SST within the specified boxes. Correlations significant at better than the 95% level are in bold.

Lag	SST Month	CSA	BCR	CEI	ASA	WEP	EEP
-8	May	**+40**	**+32**	-02	+01	-10	-27
-7	Jun	**+42**	+27	+02	-24	**-32**	**-32**
-6	Jly	+28	+18	+10	-02	-16	-20
-5	Aug	+25	+11	-01	-22	-24	-29
-4	Sep	+02	-12	-17	-12	-30	-26
-3	Oct	-03	-14	**-37**	-24	**-33**	-27
-2	Nov	-04	+04	-28	-20	-24	-27
-1	Dec	-09	-05	**-50**	**-39**	**-39**	**-33**
0	Jan	-12	-10	**-42**	**-43**	**-37**	**-35**

CSA: Central South Atlantic. BCR: Benguela Current Region.
CEI: Central Equatorial Indian Ocean. ASA: Arabian Sea Area.
WEP, EEP: Western and Eastern Equatorial Pacific.

Since the frequency distribution of January rainfall generally deviates from normal, Spearman's rank correlations were also evaluated, but the conclusions remain the same as with Pearson's product-moment coefficients. Note that December Central Equatorial Indian Ocean (CEI) SST, at a lag of -1 month, correlates with the following January rainfall at better than the 99% level (coefficient = -0.50); the amount of variance explained is only 25%, but it can still be used in a subjective way to confirm forecasts made with other predictors. Long-term prediction of January rainfall can perhaps be made with Central South Atlantic (CSA) box SST which shows consistently positive link (Figure 2.15). Although the Agulhas Current Region (ACR) SST correlates significantly (correlation = +0.34) at zero lag with January rainfall, antecedent correlations are insignificant.

February All-Area rainfall shows strong links with SSTs within the equatorial boxes. Figure 2.16 displays plots of correlations between February All-Area rainfall index and SST indices within four of the equatorial boxes (CEI, EEI, WEP and EEP). The correlations are virtually all negative. The very high value of -0.69 with EEI at a lag of -2 months should be noted. It means that December SST fluctuations

within EEI can explain nearly 50% of the variance in rainfall during the following February. However, the link with CEI SST appears more consistent than with EEI SST; variations of CEI SST during October (-4-month lag) explain about 25% of the All-Area rainfall variance during the following February. Like in January, All-Area precipitation variation during the month of February relates significantly with Agulhas Current Region (ACR) SST variations at zero lag (coefficient = +0.41), but antecedent correlations are insignificant and even the sign is reversed. SSTs within the Western and Eastern Equatorial Pacific (WEP and EEP) show significant (negative) links with February All-Area rainfall variations.

TABLE 2.13
Correlation (x100) between March All-Area rainfall and SST within the specified boxes. Correlations significant at better than the 95% level are in bold.

Lag	SST Month	CEI	EEI	ASA	WEP	EEP	SWP
-7	Aug	-04	-05	-18	**-41**	-25	+22
-6	Sep	-02	+06	-22	**-38**	**-40**	**+37**
-5	Oct	-25	-14	**-39**	**-46**	**-46**	**+33**
-4	Nov	-25	-21	**-32**	**-49**	**-41**	**+39**
-3	Dec	**-44**	**-54**	**-32**	**-49**	**-48**	**+48**
-2	Jan	**-63**	**-48**	**-48**	**-45**	**-46**	+30
-1	Feb	**-47**	**-52**	**-43**	**-45**	**-45**	+19
0	Mar	**-43**	**-39**	**-31**	**-35**	**-40**	+13
+1	Apr	**-39**	**-34**	-23	**-42**	**-38**	-19

CEI, EEI: Central and Eastern Equatorial Indian Ocean.
WEP, EEP: Western and Eastern Equatorial Pacific.
ASA: Arabian Sea Area. SWP: South West Pacific.

Results of analyses between March All-Area rainfall and SST are displayed in Table 2.13. Central and Eastern Equatorial Indian Ocean (CEI and EEI) SST variations show significant correlations at lags of up to -3 months, while the Western and Eastern Pacific (WEP and EEP) relate more significantly up to longer lags (about -6 months). Fluctuations of SST within the Arabian Sea Area (ASA) and the South West Pacific show significant, but opposite, links with March rainfall. Agulhas Current Region (ACR) SST against March All-Area rainfall gives a simultaneous correlation of +0.29 and antecedent correlations become very weak, so ACR SST is comparatively of no significance as far as prediction is concerned,

although SST changes there act to coincidentally modify rainfall distribution across South Africa.

2.6. SEASONAL RAINFALL ASSOCIATION WITH SST

In order to further reduce noise, an All-Area seasonal rainfall index is developed. This series combines data from all the individual stations within the four zones (see Figure 2.1) for the six summer months (October through the following March), thus filtering out smaller scale features. Analyses utilizing such data could reveal larger scale patterns of association. It should be noted that inclusion or exclusion of October rainfall data does not change the results significantly. Correlations were computed using the seasonal rainfall series against 2-month and 3-month SST indices. Only the results with 2-month SST series are presented here. Table 2.14 summarises the relationship between seasonal rainfall and SST. The results confirm the consistency in the patterns of association and the effects of smoothing are readily observed.

Agulhas Current Region (ACR) and South West Pacific (SWP) SST fluctuations show generally positive links with South African summer rainfall. It is interesting to note that the correlation with SWP (remote) is stronger than with ACR. A correlation of +0.30 between ACR SST and summer rainfall is in agreement with the results of Walker (1989) who used different data sets. Links with variations of SST within BCR, ARR, and SEI are poor while those with WEI and EEI are significant mostly at positive lags (SST lagging rainfall). The connection of seasonal rainfall with CSA SST shows up again mainly at long lags of the order of -15 months.

TABLE 2.14
Correlation (x100) between seasonal All-Area rainfall and SST within the specified boxes. Correlations significant at better than the 95% level are in bold.

SST Months	ACR	CEI	ASA	WEP	EEP	SWP
Apr/May	-19	-15	-14	**-31**	-28	+05
May/Jun	-03	-27	-18	**-40**	**-36**	+14
Jun/Jly	+09	-19	-08	**-40**	**-38**	+14
Jly/Aug	+09	-09	-12	**-37**	**-37**	+28
Aug/Sep	+02	-14	-27	**-44**	**-41**	**+35**
Sep/Oct	+01	**-32**	**-41**	**-50**	**-48**	**+36**
Oct/Nov	+08	**-46**	**-44**	**-52**	**-49**	**+41**
Nov/Dec	+07	**-55**	**-42**	**-56**	**-51**	**+44**
Dec/Jan	+16	**-68**	**-55**	**-56**	**-55**	**+38**
Jan/Feb	+30	**-65**	**-58**	**-46**	**-53**	+17
Feb/Mar	+25	**-61**	**-51**	**-40**	**-46**	+11
Mar/Apr	+15	**-53**	**-39**	**-40**	**-42**	-03
Apr/May	+07	**-42**	**-37**	**-37**	-28	-25

ACR: Agulhas Current Region. CEI: Central Equatorial Indian Ocean.
ASA: Arabian Sea Area. SWP: South West Pacific.
WEP, EEP: Western and Eastern Equatorial Pacific.
The 'SST Months' column refers to mean SST for the two consecutive months. Top row corresponds to SST leading rainfall and bottom row to SST lagging rainfall. Thus the values along the Jun/Jly row are correlations between variations of June/July SST index versus rainfall index for the following October through March season.

SST variations within the other boxes, namely, CEI, ASA, WEP, and EEP, are negatively correlated to the rainfall series (Table 2.14). The most significant values occur within the 'quasi-simultaneous' range, that is, between summer rainfall and 2-month SSTs within the October to March period. At negative lags (SST leading), the Pacific areas show generally stronger relationships with South African summer rainfall than the Indian Ocean SSTs. The results demonstrate the potential use of SST in rainfall prediction models.

2.7. SUMMARY AND SYNTHESIS

The primary objective here is to identify variables which may be used in empirical models to predict summer rainfall across South Africa on monthly to seasonal time scales. Given the fact that the oceans represent enormous thermal inertia, a logical step is to examine the association between rainfall and SST. Results of the investigations have been presented in this chapter.

The rainfall and SST data sets were first stratified on a monthly basis and their standardized departures from their respective long-term monthly means were computed for the period from 1950 to 1986. Rainfall indices for the 4 homogeneous zones, defined in Chapter 1, were cross-correlated with grid point SST indices. Twelve key boxes were identified from the SST domain which encompassed the globe within the belt from 20°N to 40°S (see Table 2.1 and Figure 2.5). The correlation distributions of seasonal rainfall with SST have also been examined; the patterns attained field significance at better than the 95% level. Standardized box SST indices were in turn lag-cross-correlated with the rainfall indices of the 4 zones in order to determine their inter-relationships. The 'All-Area' standardized rainfall index time series was also lag-cross-correlated with the key-box SST series. Table 2.15 provides a summarized list of key boxes which appear to be of relevance in the development of predictive models. The boxes are listed in order of importance from a rainfall prediction perspective.

October rainfall variations do not show much relationship with SST variations. Lagged and simultaneous correlations are insignificant even with SSTs across the surrounding ocean areas. It should be mentioned that the transition month of October is the driest of the 6 summer months considered; the areal average of 'All-Area' long-term monthly mean total of rainfall for October is 44 mm, whereas the corresponding averages generally exceed 60 mm for the other summer months.

TABLE 2.15
Summary of key boxes where SST variations show significant relationships with rainfall variations within the specified zones The SST boxes are listed in order of importance from a rainfall prediction perspective.

Rainfall	Nov	Dec	Jan	Feb	Mar
Zone 1		ASA	ACR	CEI	CEI
		EEP		WEP	
		WEP			
		CEI			
Zone 2	ACR	WEP	CEI	CEI	EEI
	CSA	ASA	WEP	WEP	WEP
		EEP	CSA		EEP
		CEI			CEI
Zone 3	ACR	WEP	CSA	EEI	EEP
	CSA	EEP		WEP	WEP
					CEI
					EEI
Zone 4	ACR	WEP	CEI	EEI	WEP
	CEI	EEP	WEP	CEI	ASA
		CEI	EEP	WEP	CEI
					EEP
All-Area	ACR	WEP	CEI	CEI	CEI
	CSA	EEP	WEP	WEP	EEI
		ASA	CSA	EEP	WEP
		CEI			EEP
					ASA

For Seasonal All-Area rainfall: WEP, EEP,CEI,ASA.

Figure 2.17 displays the distributions of lagged correlations between November rainfall indices of the 4 zones and All-Area with SST index series of the Central South Atlantic (CSA) box. The highly significant correlations (exceeding +0.5) at lags of -16 to -17 months are particularly notable in the cases of zones 2 and 3 and All-Area rainfall fluctuations. At comparable lags, zones 1 and 4 also show positive links, but the associations are relatively weak. Significantly positive correlations are apparent at a lag of -6 months, and to a lesser degree at closer to zero lags. SST in the CSA area may give a statistical indication of the nature of November rainfall 16 to 17 months in advance. However, since no physical explanation can be given for such behaviour, the statistics may only be used with great caution. November

rainfall is positively correlated with Agulhas Current (ACR) SST, but the magnitudes are generally low.

A shift in the correlation patterns has been noted when moving from November to December rainfall regimes. Whereas October and November rainfall variations show generally positive, albeit weak, links with SST variations over most ocean areas, in December the correlations abruptly change sign and at the same time become more significant, particularly with those SST boxes which are situated further away from the subcontinent; the sign of the correlations are then generally maintained until at least the following March. This behaviour, as mentioned earlier, is indicative of teleconnection type of associations of South African rainfall with remote SST forcing. The teleconnections are strongest for rainfall variations during the months of December, February and March, and are relatively weaker in the case of January rainfall. This is in agreement with the recent study of van Heerden et al. (1988). (Details in this regard are discussed towards the end of this part).

Among the SST regions which represent potential for prediction of December rainfall include the Western and Eastern Equatorial Pacific Ocean (WEP and EEP), the Central Equatorial Indian Ocean (CEI), and the Arabian Sea Area (ASA). The SST variations within these regions (especially the Pacific areas) are associated with a significant portion of December rainfall variance across almost the entire summer rainfall area of South Africa. The Pacific SST fluctuations, which are known to be closely related to the evolution of the ENSO seesaw, may be used in tentative empirical models for December rainfall prediction. However, the inter-relationships among the variables should first be determined in order to confirm the degree of their independence and their relative contributions towards rainfall variance.

There is a general drop in the degree of association between January rainfall and SST in comparison with the neighbouring months, December and February. The

coastal SST boxes show little link. Although zone 1 January rainfall indicates correlations of +0.38 and +0.40 with Agulhas Current SST at zero and -1 month lag, respectively, the links at larger lags and with the other rainfall zones are negligible. Central Equatorial Indian Ocean (CEI), Western and Eastern Equatorial Pacific (WEP and EEP), which all show negative correlations with January rainfall, appear to be the regions of relative importance with regard to the aims of this study.

A significant positive peak at -7 to -8 months lag in the correlation between the fluctuations of January rainfall of all the individual zones (except zone 1) and Central South Atlantic (CSA) SST is evident in Figure 2.18. Another positive peak, but less significant, shows up at lags of around -17 months. While these results may serve in the speculation of January rainfall well in advance, the empiricism implied should be viewed with skepticism until valid physical explanations are provided. One possibility is that sea temperatures during the cold months of May and June carry most of the signals which are associated with the variations in the following January rainfall.

February and March rainfall modulations are observed to be strongly associated with variations in SST. The ocean areas showing significant correlations are mostly within the Equatorial belt. The notable areas are the Western and Eastern Equatorial Pacific (WEP and EEP) and the Central Equatorial Indian Ocean (CEI). An example is shown in Figure 2.19 where correlation distributions of February rainfall against CEI SST are plotted.

Rainfall variability across the central and eastern interiors of South Africa are spatially coherent, in agreement with Nicholson (1986a,b), Janowiak (1988) and Nicholson and Entekhabi (1987). Statistical analyses have shown that there is an abrupt change (from November to December) in the behaviour of the simultaneous,

as well as lagged, associations between rainfall and SST variations, with a general change in sign distribution of the correlations.

A weaker relationship is observed between January rainfall and Pacific SSTs compared to the neighbouring December and February months. In particular, there is a stronger link between Pacific box SSTs and South African rainfall during the months of December and March than during the intermediate January and February months. van Heerden et al. (1988) found that rainfall during December and March correlates significantly with the previous winter's Southern Oscillation Index (SOI) (Troup, 1965), but rainfall variations during the mid-summer months of January and February show much weaker correlations. A significant relationship was detected between summer rainfall and mean geopotential heights as well as the 850-500 hPa thermal wind at Bloemfontein (20° 07'S, 26° 11'E, elevation 1351 m) which was taken as representative of the central parts of South Africa. They concluded that during January and February when the Southern Oscillation/rainfall relationship is fairly weak, rainfall develops in a predominantly quasi-barotropic circulation. Whereas during December and March the most significant Southern Oscillation/rainfall correlation coincides with a shift towards baroclinic systems. The results of this study are in agreement with the findings of van Heerden et al. (1988) and Lindesay (1988) with respect to temporal dependence of the variables.

There are physical grounds to justify the negative association between the variations of South African summer rainfall and equatorial Indian Ocean SST. The following mechanism is proposed: when the SST over the equatorial South Indian Ocean is above average, there is a tendency for intense tropical cyclones in the area to be more frequent during southern summer (see Figure 2.20). During such situations, moisture convergence and convective activity become anomalously intense over these oceanic areas, thus depriving the southern African subcontinent of moisture

influx. In a preliminary analysis (Figure 2.20), it has been found that there is a statistically significant positive association between the September to November SST within the major tropical cyclogenesis zone of the South-West Indian Ocean and the total number of intense tropical cyclones forming in the following summer months (December to March). Intense tropical cyclones in the South-West Indian Ocean may also cause large-scale atmospheric subsidence and drying-out at their remote outskirts including the Southern African subcontinent.

A recent study (Jury and Pathack 1991) has documented a dipole-like behaviour in the climate variations between Southern Africa and the Southwest Indian Ocean. In addition, Hofmeyer and Gouws (1964) have long noted the tendency towards below normal sea-level pressure east of Madagascar to be accompanied by unfavourable conditions for rain over South Africa, particularly over the Transvaal. The Central and Eastern Equatorial Indian Ocean (CEI and EEI) boxes are located near an area of major cyclogenesis (Padya, 1989). It should be noted that, although most cyclones originate at lower latitudes, they acquire considerable intensity only when they move away beyond the 10°S to 15° S latitude, largely because of Coriolis effects. CEI and EEI, which are confined within the Equator to 10°S area, are seldom directly affected by tropical cyclones, so the SSTs in these areas are more representative of unperturbed conditions. However, CEI appears to be a better predictor than EEI. This may be related to the effect of 'throughflow' between the Pacific and Indian Oceans via the Indonesian region (Godfrey and Golding, 1981), a feature linked with the strength of the trade winds, which are in turn associated with the ENSO (Philander, 1983) phenomena. The 'throughflow' probably superimposes 'noisy' signals on the EEI SST distribution.

The general pattern of the associations between the fluctuations of rainfall and SST (especially over the equatorial regions) confirm the temporal dependence and the

diverse mechanisms which operate in the modulation of large-scale circulation and hence precipitation.

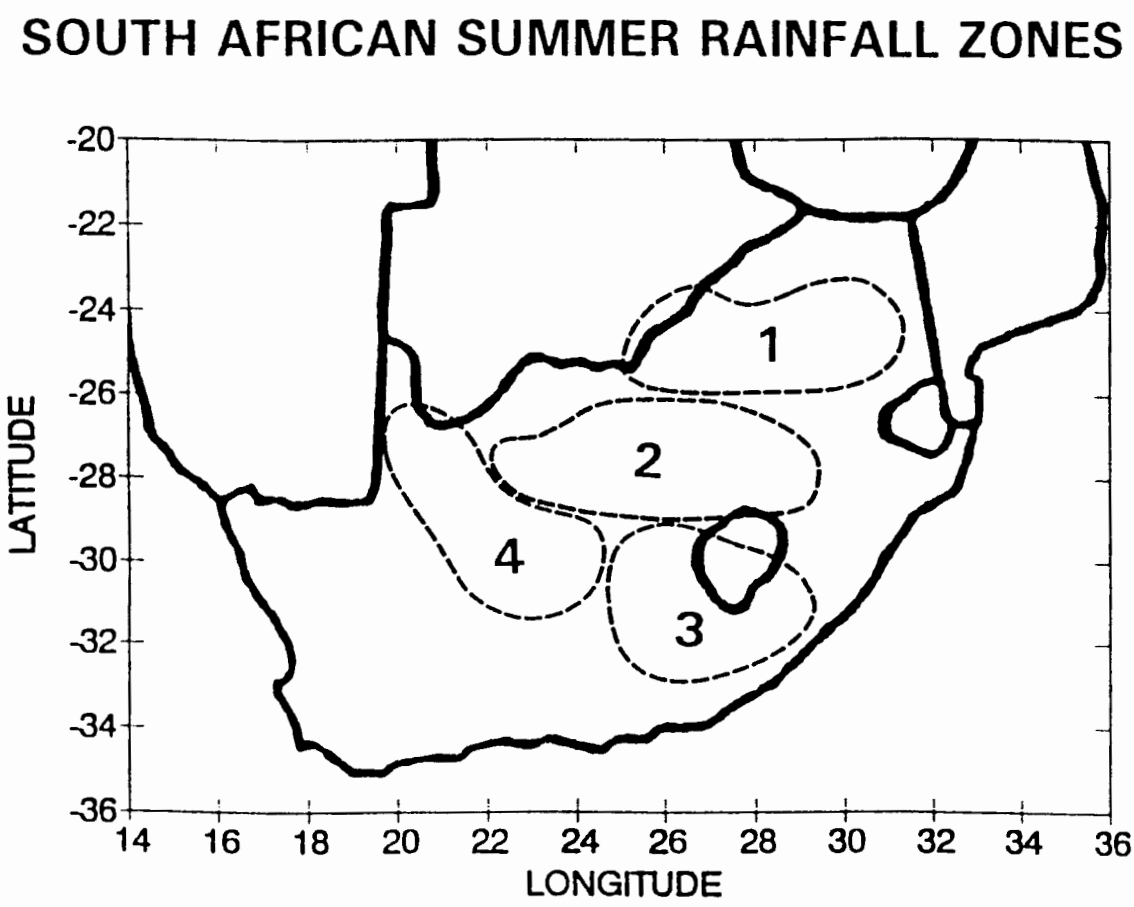

Figure 2.1.
Four zones representing the summer rainfall area of South Africa.

Figure 2.2. Simultaneous correlation (x100) between February gridded SST and February All-Area rainfall.
Dotted region represents approximate location of rainfall area.
Data years: 1950 to 1986. Domain: 12°N-34°S, 0°E-100°E. (°S negative).
Grid spacing: 2° latitude x 2° longitude.

Latitude --->

Long.	-33	-31	-29	-27	-25	-23	-21	-19	-17	-15	-13	-11	-09	-07	-05	-03	-01	+01	+03	+05	+07	+09	+11	+13	Long.
1	11	-24	-26	-14	-11	-19	-32	-40	-31	-30	-26	-20	-25	-18	-24	-22	-40	-21	13	-10					1
3	14	-24	-24	-8	-23	-33	-43	-38	-28	-30	-26	-23	-20	-12	-19	-21	-24	-22	3	-4					3
5	14	-23	-23	-16	-34	-41	-41	-34	-26	-31	-26	-11	-2	-25	-26	-36	-29	-30	-10	-2					5
7	4	-21	-22	-33	-39	-37	-37	6	-11	-34	-9	9	12	-23	-33	-36	-32	-14	-16						7
9	-8	-18	-28	-35	-17	0	13	8	-6	-17	-7	-8	-13	-38	-38	-36	-32	-10	-23						9
11	-14	-27	-15	-8	-15	0	13	16	-7	-17	5	-4	-22	-47	-22										11
13	-32	-24	-16	-7	-13	2	14					-4	-26												13
15	-29	-25	-17	-4																					15
17	-28	-28																							17
19																									19
21			::::::::::																						21
23			::::::::::::::																						23
25			::::::::::::::::																						25
27			::::::::::::::::										AFRICA												27
29	10		::::::::::::::																						29
31	11	13	::::::::::																						31
33	11	19	31	17																					33
35	22	19	37	20	20																				35
37	10	15	40	21	22	19	27	2																	37
39	13	26	47	26	22	17	26	3																	39
41	16	32	53	25	27	17	26	3	15	1	-19	-13	-18	-15	12	19	-2								41
43	19	13	53	26	31	42	37	2	15	1	-16	-13	-20	-24	11	5	-14							-6	43
45	33	31	46	23						1	-18	-15	-21	-25	9	5	-14	-12					-13		45
47	34	38	35	18	MADAGASCAR					6	-13	-12	-24	-30	2	-5	-13	-11	-24				-17	-2	47
49	32	37	31	20	-2	-5	-29				-9	-4	-22	-29	-5	-3	-23	-15	-25	-11			-18	-2	49
51	21	36	36	43	-1	-3	-29	-28	-17	-18	-17	-14	-25	-27	-3	1	-19	-22	-30	-14	-9	-11	-16	-5	51
53	-12	35	30	45	-1	-3	-34	-29	-16	-19	-26	-19	-29	-14	-15	-6	-23	-31	-29	-9	-14	-14	-18	-4	53
55	6	34	33	22	7	-3	-31	-36	-14	-25	-33	-20	-30	-25	-23	-13	11	-23	-26	-18	-27	-16	-21	-7	55
57	16	35	36	35	3	0	-29	-37	-38	-27	-26	-32	-30	-22	-21	-25	-12	-7	-3	-42	-22	-16	-23	-1	57
59	13	41	33	23	11	2	-28	-34	-49	-31	-20	-31	-24	-30	-4	-24	-18	8	-13	-33	-21	-20	-24	-16	59
61	14	44	33	23	12	21	-12	-38	-47	-33	-24	14	-37	-25	-19	-24	-28	-16	-30	-31	-18	-30	-15	-8	61
63	18	42	36	22	13	16	-6	-37	-52	-43	-38	25	-32	-31	-19	-26	-19	-21	-34	-37	-13	-40	-26	-12	63
65	16	44	47	24	12	31	-1	-35	-52	-39	-35	-20	-32	-34	-11	-25	-33	-28	-31	-37	15	-16	-20	-16	65
67	23	40	51	22	10	25	0	-16	-37	-41	-38	-13	-32	-29	-16	-37	-36	-29	-27	-18	-6	-24	-25	-15	67
69	23	47	52	29	7	12	0	-35	-22	-36	-35	-12	-26	-29	-24	-41	-37	-26	-31	-3	-16	-23	-30	-19	69
71	23	37	58	33	2	-14	16	-24	-22	-35	-25	-14	-22	-28	-39	-47	-40	-32	-29	-22	-30	-25	-23	-21	71
73	22	27	59	25	6	-9	-9	-20	-11	-12	-18	-14	-24	-34	-40	-49	-45	-27	-36	-37	-33	-25	-23	-22	73
75	12	15	30	21	1	-13	-14	4	-24	-23	-13	-14	-31	-39	-51	-49	-39	-30	-41	-40	-34	-32	-21		75
77	-2	15	27	13	2	-10	-24	-19	-19	-14	-12	-31	-37	-38	-47	-41	-41	-30	-42	-41	-35				77
79	1	8	20	1	-1	-11	-14	-8	-18	-37	-14	-25	-34	-42	-46	-42	-39	-34	-46	-41	-34	-23			79
81	11	2	17	0	-7	-20	-12	-10	-10	-10	-26	-19	-34	-39	-44	-40	-41	-31	-44	-39		-35	-14	-31	81
83	16	-6	23	8	-20	-5	-19	-13	-13	1	-36	-28	-29	-41	-37	-39	-39	-37	-43	-39	-38	-36	-15	-26	83
85	16	7	27	2	-10	-18	-23	-16	-14	-16	-30	-39	-36	-29	-25	-37	-43	-42	-40	-37	-33	-36	-15	-24	85
87	16	11	15	9	-9	-2	-22	-15	-21	-20	-32	-33	-36	-19	-28	-38	-43	-41	-47	-39	-33	-37	-17	-28	87
89	11	4	8	11	-23	-2	-20	-16	-30	-23	-30	-31	-30	-20	-25	-30	-44	-38	-43	-39	-36	-36	-13	-25	89
91	4	6	-4	-1	-24	4	-27	-27	-37	-30	-16	-22	-24	-21	-24	-33	-32	-41	-52	-40	-31	-37	-23	1	91
93	-13	-10	-4	0	-24	-6	-32	-38	-29	-26	4	-21	-22	-10	-18	-32	-34	-36	-45	-36	-25	-28	-17	4	93
95	-16	-17	-12	-10	-8	-8	-38	-34	-15	-9	3	-23	-25	-11	-11	-19	-24	-14	-43	-29	-23	-26	-25	8	95
97	-22	-21	-7	-1	-10	-24	-33	-33	-21	-14	0	-22	-20	-14	-7	-14	-20	-4	-18	-27	-15	-11	-5	2	97
99	-24	-13	-7	4	-16	-31	-37	-24	-24	-18	8	-15	-22	-21	-17	-16	-4		-16	-24	3	-12	-7	-27	99

Figure 2.3. Lagged correlation (x100) between October gridded SST and the following February All-Area rainfall.
Dotted region represents approximate location of rainfall area.
Data years: 1950 to 1986. Domain: 12°N-34°S, 0°E-100°E. (°S negative).
Grid spacing: 2° latitude x 2° longitude.

Latitude --->

Long.	-33	-31	-29	-27	-25	-23	-21	-19	-17	-15	-13	-11	-09	-07	-05	-03	-01	+01	+03	+05	+07	+09	+11	+13	Long.
1	7	9	-16	-15	19	6	1	-7	-4	4	-2	-6	14	9	4	3	15	10	25	31					1
3	-9	13	-11	-3	2	10	-20	-9	8	2	-2	-8	8	19	8	15	12	2	7	17					3
5	1	-7	-7	-5	-5	-13	-20	-4	15	4	-4	5	15	22	16	21	20	12	7	8					5
7	-4	-19	-7	-11	-13	-17	-18	10	25	-4	10	17	15	35	27	23	5	5	8						7
9	-12	-27	-17	-15	-9	-2	-6	14	22	11	11	17	13	37	29	23	9	13	3						9
11	-20	-23	-16	-14	-8	3	-4	5	18	22	34	21	18	35	30										11
13	-30	-26	-18	-17	-2	2	-17					31	11												13
15	-29	-24	-19	-12																					15
17	-29	-22																							17
19																									19
21			::::::::::::																						21
23			::::::::::::::																						23
25			::::::::::::::::																						25
27			::::::::::::::::											AFRICA											27
29	-17		::::::::::::::																						29
31	-19	-23		::::::::::::																					31
33	-19	-21	-32	9																					33
35	-41	-20	-26	1	-26																				35
37	-27	-29	-24	-2	-25	-16	-18	-4																	37
39	-17	-19	-14	-7	-28	-15	-19	-4																	39
41	-4	-6	-4	-17	-31	-15	-19	-4	-4	-19	-6	-6	-6	-2	-11	-15	-19								41
43	4	9	11	-11	-42	-15	-14	-12	-4	-20	-11	-5	-7	-1	-12	-21	-17							-8	43
45	-1	16	15	-4						-20	-12	-9	-7	-1	-15	-20	-15	-22					-18		45
47	-10	20	20	1	MADAGASCAR					-17	-28	-15	-13	-11	-16	-26	-16	-18	-16				-20	-15	47
49	2	27	28	15	6	12	-13				-35	-23	-15	-20	-18	-21	-22	-21	-19	-11			-24	-22	49
51	-7	9	29	26	6	13	-1	-3	24	-21	-46	-28	-26	-21	-27	-20	-27	-20	-19	-12	1	-17	-31	-26	51
53	-8	-2	30	25	6	10	-7	-10	-13	-14	-48	-31	-21	-50	-50	-32	-26	-20	-19	-10	-3	-19	-31	-31	53
55	-18	-3	21	13	13	13	-6	-13	-13	-26	-32	-45	-21	-18	-50	-40	-20	-9	-22	-15	-12	-20	-30	-27	55
57	-20	5	19	7	19	23	-7	-7	-22	-15	-38	-54	-14	-12	-41	-40	-22	-40	-25	-27	-11	-22	-28	-40	57
59	-18	0	15	-4	26	30	-5	-4	-23	-21	-43	-57	-15	-12	-31	-38	-38	-33	-36	-37	-7	-22	-30	-37	59
61	-8	0	17	-10	29	29	8	-7	-27	-21	-38	-51	-19	-15	-22	-45	-44	-39	-35	-37	-14	-25	-20	-28	61
63	7	4	17	-34	30	20	7	-9	-30	-24	-27	-36	-28	-24	-21	-41	-44	-49	-28	-41	-12	-31	-21	-28	63
65	-18	2	17	-29	22	11	3	-5	-26	-19	-24	-39	-20	-30	-34	-39	-53	-50	-32	-40	-16	-30	-29	-41	65
67	-8	12	19	-21	13	14	19	-18	-18	-18	-23	-33	-34	-35	-41	-37	-55	-39	-27	-30	-23	-33	-40	-34	67
69	-8	10	23	-18	-1	4	25	-32	-8	-13	-24	-35	-55	-41	-41	-38	-56	-37	-23	-44	-35	-35	-41	-35	69
71	-6	5	20	0	2	1	9	-25	-49	-9	-22	-39	-56	-46	-47	-38	-53	-45	-18	-32	-39	-35	-35	-35	71
73	-4	11	19	7	-12	3	10	-9	-30	4	-22	-42	-57	-44	-52	-36	-42	-35	-24	-17	-40	-35	-33	-33	73
75	-2	9	11	8	-5	8	9	7	-23	0	-26	-42	-55	-45	-48	-35	-30	-33	-28	-26	-34	-36	-33		75
77	8	19	2	28	-7	12	2	5	-1	-6	-27	-42	-56	-43	-47	-34	-16	-41	-33	-24	-34				77
79	3	19	5	15	-10	16	0	0	9	-15	-13	-38	-47	-40	-45	-41	-21	-42	-32	-28	-33	-36			79
81	8	21	0	2	-8	30	15	-5	7	-34	2	-25	-40	-38	-39	-41	-27	-39	-41	-32		-39	-35	-31	81
83	13	15	5	-16	-10	16	14	-9	-8	-10	-4	-25	-21	-28	-37	-42	-29	-31	-41	-34	-26	-35	-30	-26	83
85	6	4	2	0	-19	8	12	-23	-12	-11	-4	-14	-20	3	-27	-37	-28	-21	-23	-34	-23	-22	-32	-29	85
87	1	1	-11	-1	-15	-8	-1	-28	-22	-10	-13	-18	-3	5	-6	-32	-34	-14	-7	-37	-26	-10	-37	-23	87
89	4	8	-12	15	-13	6	0	-4	-26	-2	-25	-1	3	6	1	-11	-30	-12	-11	-35	-27	-8	-29	-21	89
91	1	-3	-34	4	-7	0	-13	10	-37	-4	-7	18	5	11	-9	4	-21	-11	-3	-31	-25	-2	-23	-15	91
93	4	2	-36	3	-2	-6	-18	6	-37	3	4	16	13	15	2	-25	-19	-4	-8	-28	-26	-16	-18	-25	93
95	7	3	-11	-15	4	-2	-20	-12	-30	8	7	22	27	17	3	-32	-15	-2	-27	-27	-27	-22	-16	-5	95
97	5	5	23	-4	-1	-18	-24	-23	-5	12	6	29	14	27	-17	-19	-7	-13	1	-25	-24	-23	-15	-2	97
99	9	7	-14	-13	-27	-16	-31	-23	6	17	14	28	6	9	-11	-22	4		6	-19	-10	-13	-12	-8	99

Figure 2.4. Lagged correlation (x100).
Mean June + July gridded SST versus seasonal (October to March) All-Area rainfall.
Dotted region represents approximate location of rainfall area.
Data years: 1950 to 1986. Domain: 12°N-34°S, 0°E-100°E. (°S negative).
Grid spacing: 2° latitude x 2° longitude.

Latitude --->

Long.	-33	-31	-29	-27	-25	-23	-21	-19	-17	-15	-13	-11	-09	-07	-05	-03	-01	+01	+03	+05	+07	+09	+11	+13	Long.
1	14	-12	5	21	22	20	28	27	25	25	25	31	24	18	7	8	5	37	25	19					1
3	16	-9	13	24	19	18	17	25	24	24	25	27	18	17	14	11	13	34	28	23					3
5	25	-8	16	17	20	15	17	22	22	25	27	17	5	17	7	11	40	36	34	21					5
7	13	1	13	16	15	17	10	26	42	34	25	9	18	20	7	14	48	37	33						7
9	10	5	4	13	17	12	19	27	35	31	17	15	17	19	25	13	60	35	35						9
11	6	2	15	21	15	6	18	25	25	20	26	14	17	23	19										11
13	-2	11	13	22	13	5	9					15	9												13
15	-2	10	14	21																					15
17	-2	10																							17
19																									19
21			::::::::::::																						21
23			::::::::::::::																						23
25			::::::::::::::::																						25
27			::::::::::::::::											AFRICA											27
29	18		::::::::::::::																						29
31	16	11	::::::::::::																						31
33	17	11	19	12																					33
35	7	12	19	15	18																				35
37	10	8	19	15	17	4	15	17																	37
39	12	6	17	13	16	4	15	18																	39
41	13	3	19	11	10	4	15	18	22	24	17	9	12	10	15	-9	-10								41
43	26	1	21	11	-1	8	17	18	22	22	15	10	12	1	8	6	-9							-14	43
45	19	6	15	9						22	16	11	11	1	7	8	4	-1					10		45
47	15	7	18	7	MADAGASCAR					10	16	12	10	-2	6	9	7	2	20				42	-15	47
49	16	4	13	10	13	4	3				5	5	12	3	2	13	2	2	18	22			27	-32	49
51	18	1	4	6	12	7	4	-8	11	0	9	8	2	5	-2	13	4	0	12	15	13	5	19	-39	51
53	14	-1	-5	-6	11	7	11	-2	9	2	10	8	0	8	-8	15	4	-7	0	9	9	2	14	-35	53
55	7	-4	-6	-15	12	4	8	-3	9	1	4	9	1	13	-10	20	8	-3	-12	-6	5	2	0	-30	55
57	2	-11	-10	-21	-3	6	8	1	8	13	11	-5	-1	15	-6	9	-5	-3	-17	-10	0	-2	-19	-23	57
59	1	-17	-6	-17	-1	10	8	3	5	5	5	-14	-1	6	4	-12	-9	-6	-12	-4	-9	0	-20	-19	59
61	-4	-21	-6	0	-2	-2	9	4	1	4	4	-10	-2	-8	-13	-3	-4	-13	-15	-5	-10	-1	-7	-6	61
63	-4	-23	-1	-5	9	-1	-7	4	6	4	-11	-14	-4	-27	-17	-10	-3	-15	-12	-2	-20	-10	-9	0	63
65	-6	-17	1	-7	21	2	-8	-2	6	4	-20	-28	-14	-12	-18	-21	-1	-13	0	-11	-32	-14	-13	-2	65
67	-8	-8	-4	-10	19	4	-18	-12	7	-6	-22	-24	-24	-8	-29	-24	-10	-10	-6	-15	-29	-20	-7	-14	67
69	-7	-12	1	-14	27	5	-12	-16	3	-7	-19	-20	-24	-8	-32	-25	-14	1	-6	-20	-29	-15	-12	-12	69
71	-9	-5	8	-13	19	6	2	-11	4	1	-15	-16	-27	-14	-24	-31	-13	0	-7	-29	-20	-8	-19	-12	71
73	-4	-3	2	-10	17	13	7	-11	-5	-4	-17	-17	-26	-25	-25	-30	-12	-5	-9	-25	-8	-6	-17	-8	73
75	-2	-12	-2	-18	11	15	4	-14	-17	-4	0	-13	-24	-21	-20	-24	-16	-10	-11	-12	-7	-5	-16		75
77	1	-4	1	3	13	22	1	-11	-15	-23	7	2	-19	-22	-17	-4	-11	-10	-1	3	-6				77
79	10	-7	7	7	-10	7	-3	-11	-12	-22	-13	38	-16	-24	-6	0	-12	-15	1	3	-7	-19			79
81	7	-7	-9	14	-13	3	-11	-14	-17	-22	0	16	17	-20	-7	0	-2	-16	1	1		-28	-22	-27	81
83	0	-5	-9	26	-10	-8	-24	-12	-17	-18	-9	32	11	5	-11	-2	6	-11	1	0	-6	-28	-24	-21	83
85	-5	5	-11	27	-2	7	-15	-3	-5	-16	-14	11	3	-14	-21	-7	8	-9	6	1	-1	-31	-20	-22	85
87	-5	8	-11	10	-5	7	-20	-1	-7	-11	-9	1	-28	-15	-15	-2	11	-6	4	-2	-3	-20	-27	-22	87
89	-8	6	-17	14	8	1	-1	-2	-6	1	-14	-18	-33	-15	-14	-9	16	-3	1	-6	4	-11	-21	-10	89
91	-2	12	-25	6	3	-21	-1	14	-3	-11	-18	-22	-37	-12	-15	4	21	-1	-1	-10	2	-18	-15	5	91
93	7	17	-28	-4	-18	-24	-4	6	-1	-31	-28	-24	-31	-13	-16	9	-3	-3	-3	-14	0	-18	-12	-10	93
95	9	14	-14	-9	-13	-12	-6	0	-11	-46	-24	-27	-10	-6	-5	14	-16	12	-11	-11	-5	-9	0	-10	95
97	11	9	-22	-22	-9	3	0	-6	-12	-38	-25	-21	-2	21	2	8	-4	-18	-13	-14	-4	-8	7	2	97
99	9	-8	-17	-18	-20	-2	-4	-10	-12	-37	-18	-13	11	21	-1	9	-3		-7	-16	-10	5	9	5	99

Figure 2.5. Location map. 12 key boxes.

CSA: Central South Atlantic.
BCR: Benguela Current Region.
ARR: Agulhas Retroflection Region.
ACR: Agulhas Current Region.
WEI: West Equatorial Indian Ocean.
CEI: Central Equatorial Indian Ocean.
EEI: East Equatorial Indian Ocean.
SEI: South-East Indian Ocean.
ASA: Arabian Sea Area.
WEP: West Equatorial Pacific Ocean.
EEP: East Equatorial Pacific Ocean.
SWP: South-West Pacific Ocean.

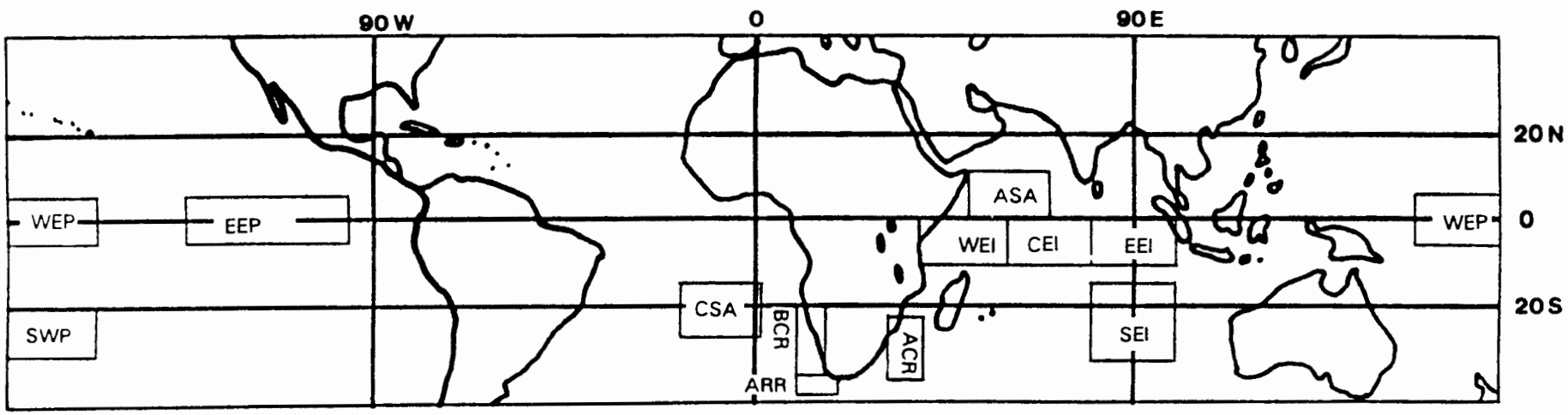

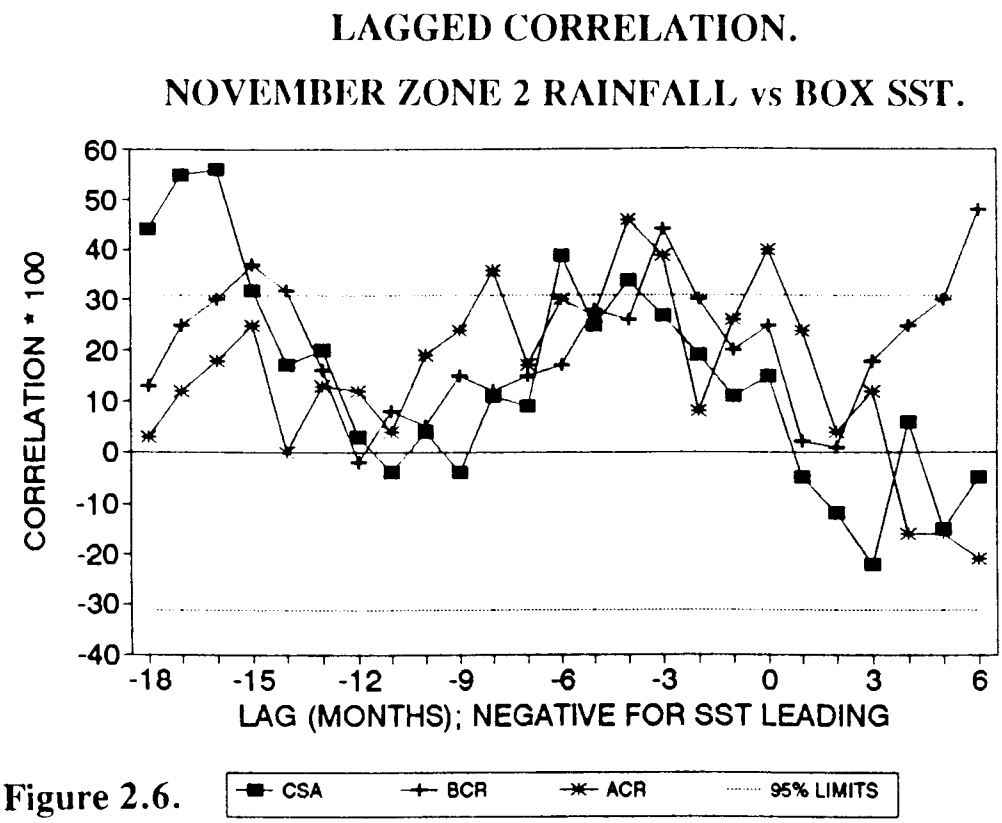

Figure 2.6.

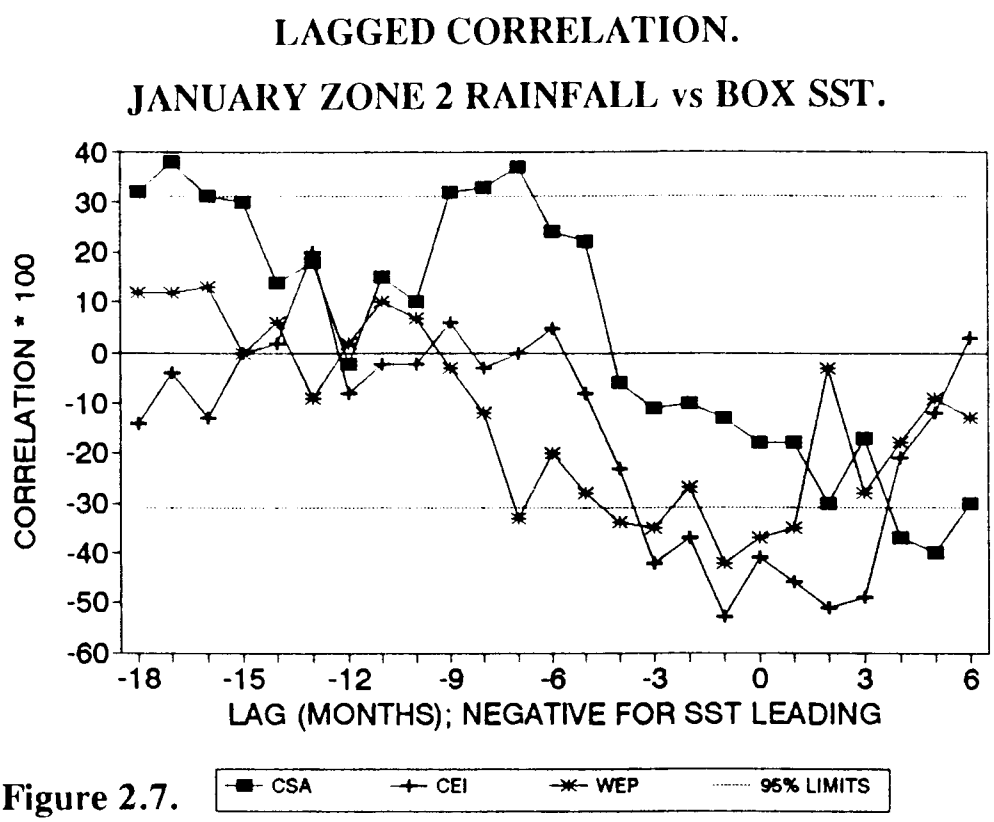

Figure 2.7.

LAGGED CORRELATION.

FEBRUARY ZONE 2 RAINFALL vs BOX SST.

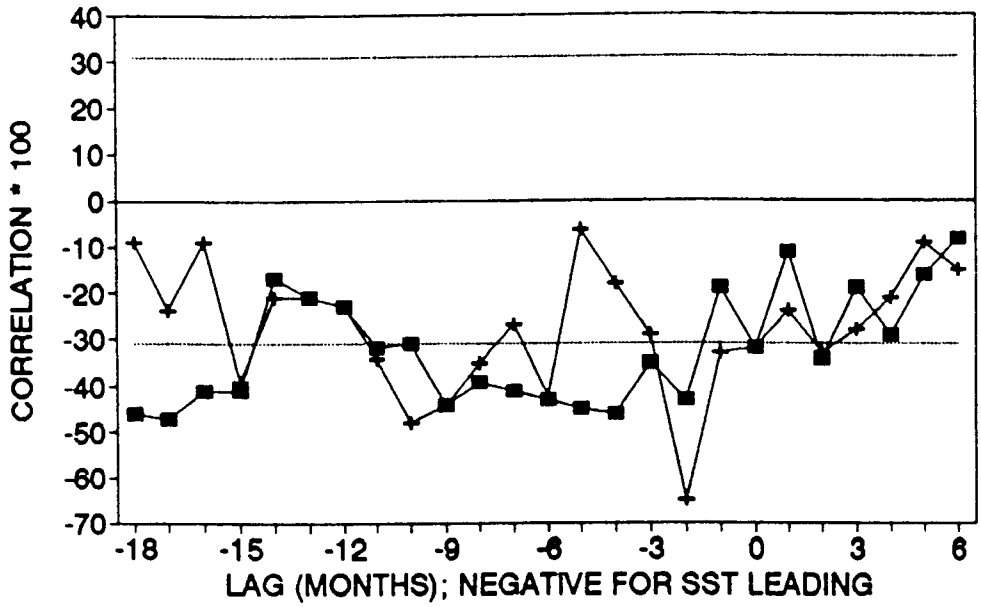

Figure 2.8.

LAGGED CORRELATION.

NOVEMBER ZONE 3 RAINFALL vs BOX SST.

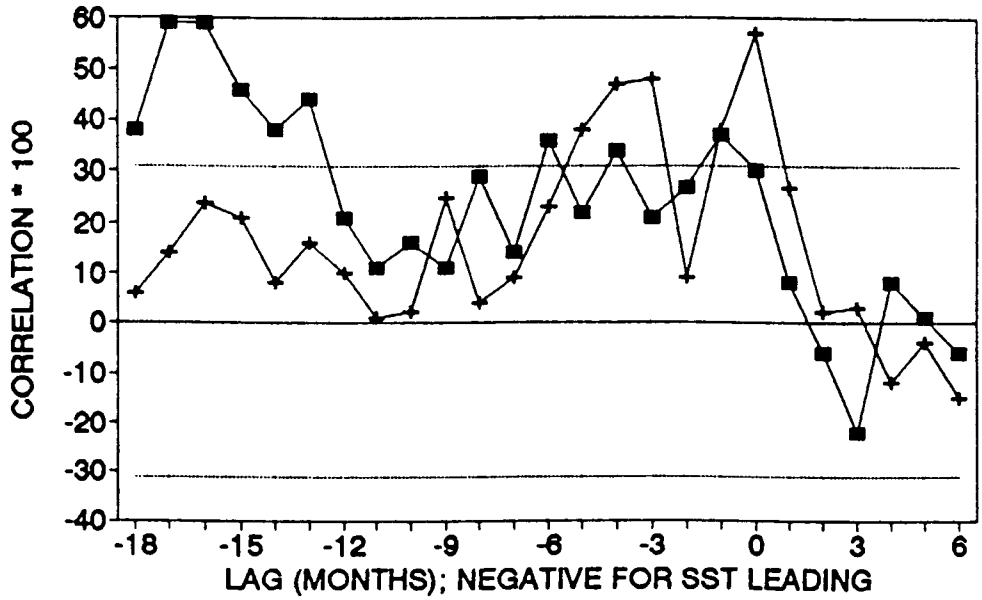

Figure 2.9.

LAGGED CORRELATION.

JANUARY ZONE 3 RAINFALL vs BOX SST.

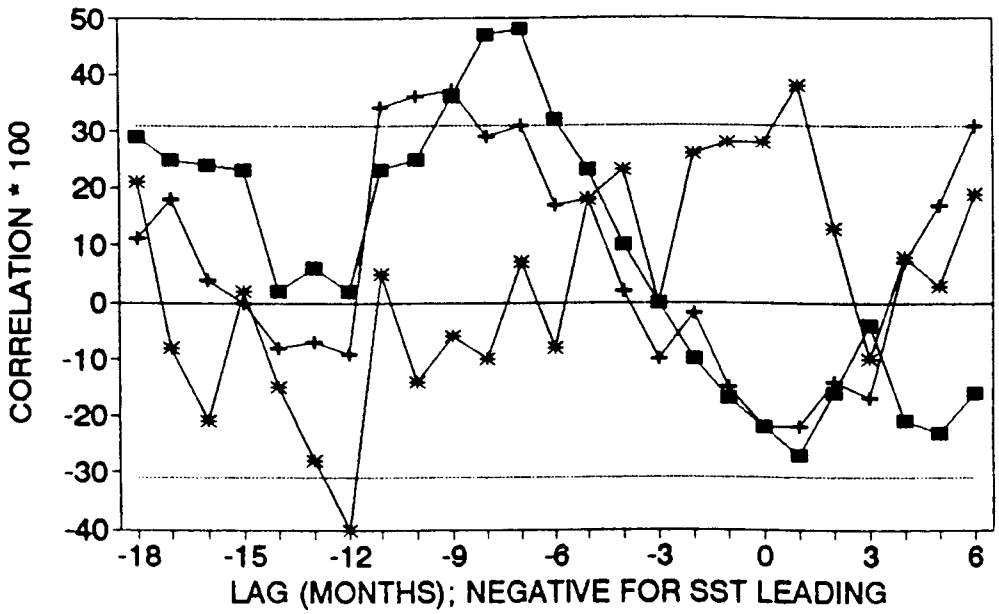

Figure 2.10.

LAGGED CORRELATION.

NOVEMBER ZONE 4 RAINFALL vs BOX SST.

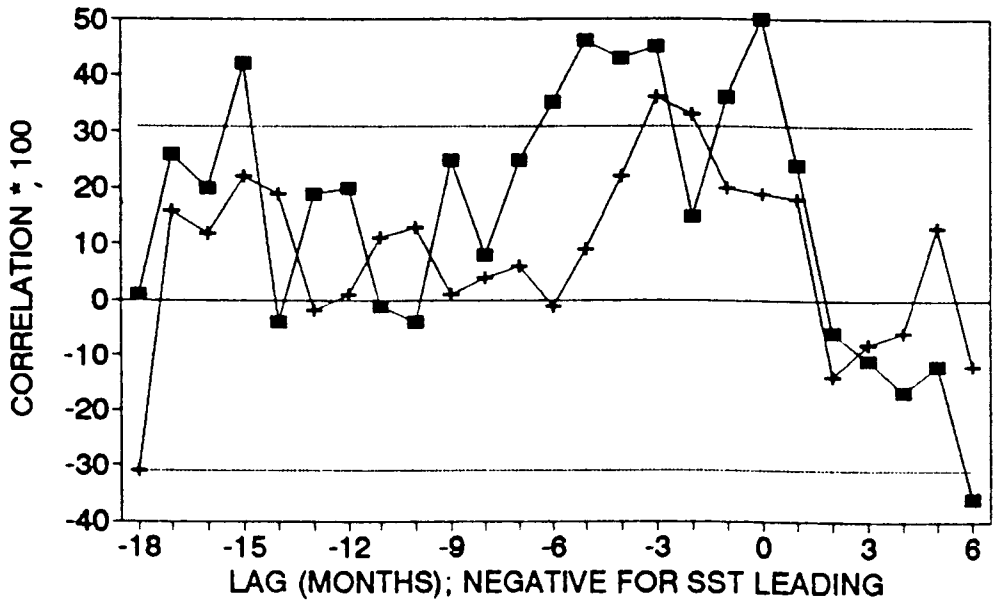

Figure 2.11.

LAGGED CORRELATION.

DECEMBER ZONE 4 RAINFALL vs BOX SST.

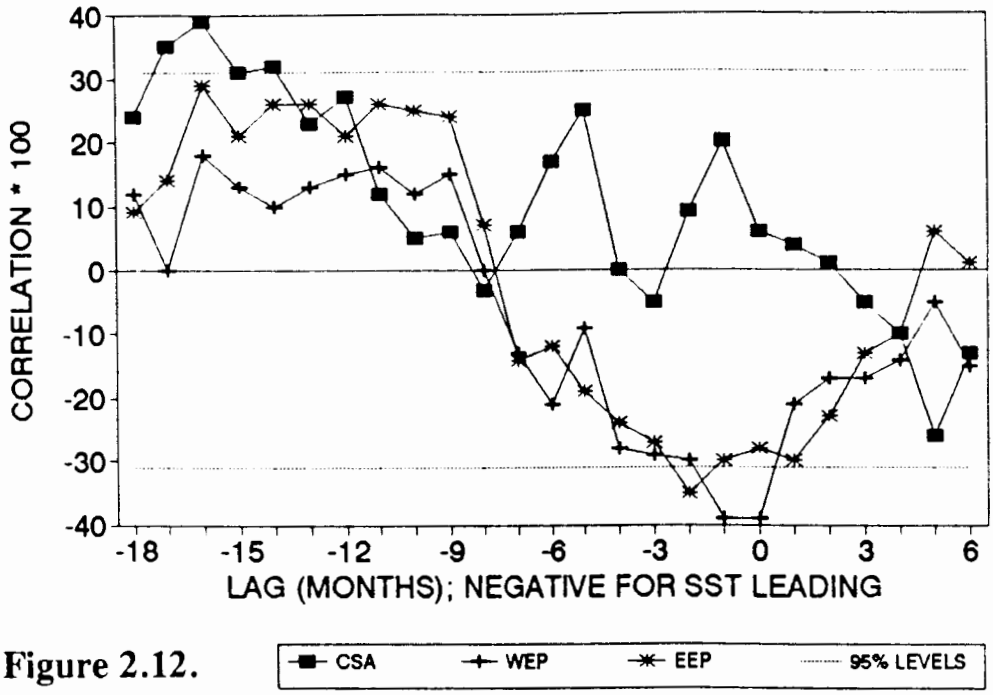

Figure 2.12.

LAGGED CORRELATION.

JANUARY ZONE 4 RAINFALL vs BOX SST.

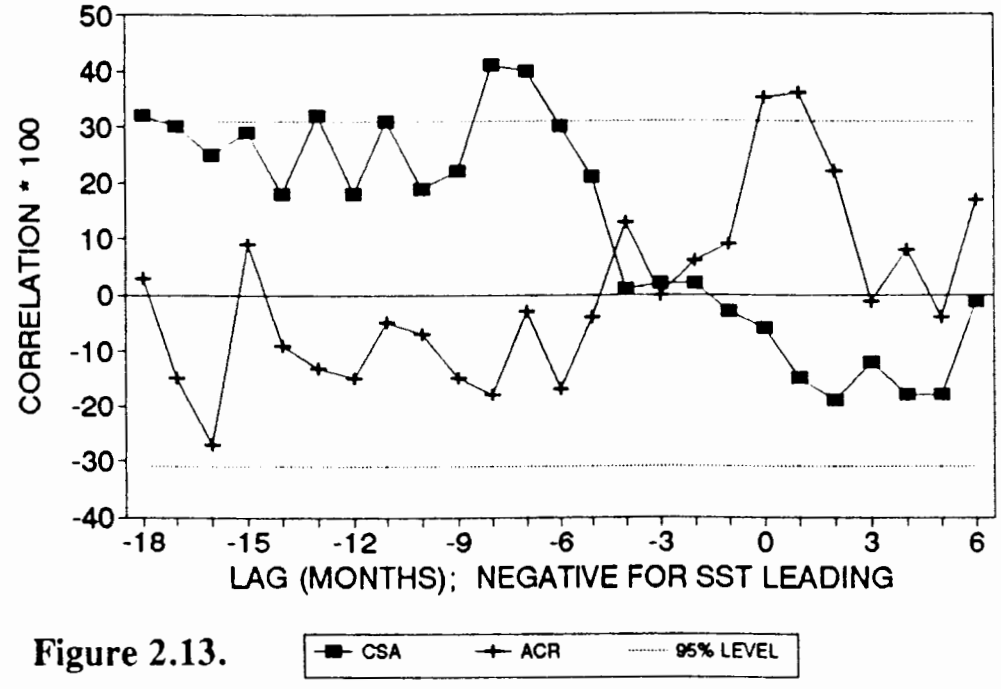

Figure 2.13.

LAGGED CORRELATION.

NOVEMBER ALL-AREA RAINFALL vs BOX SST.

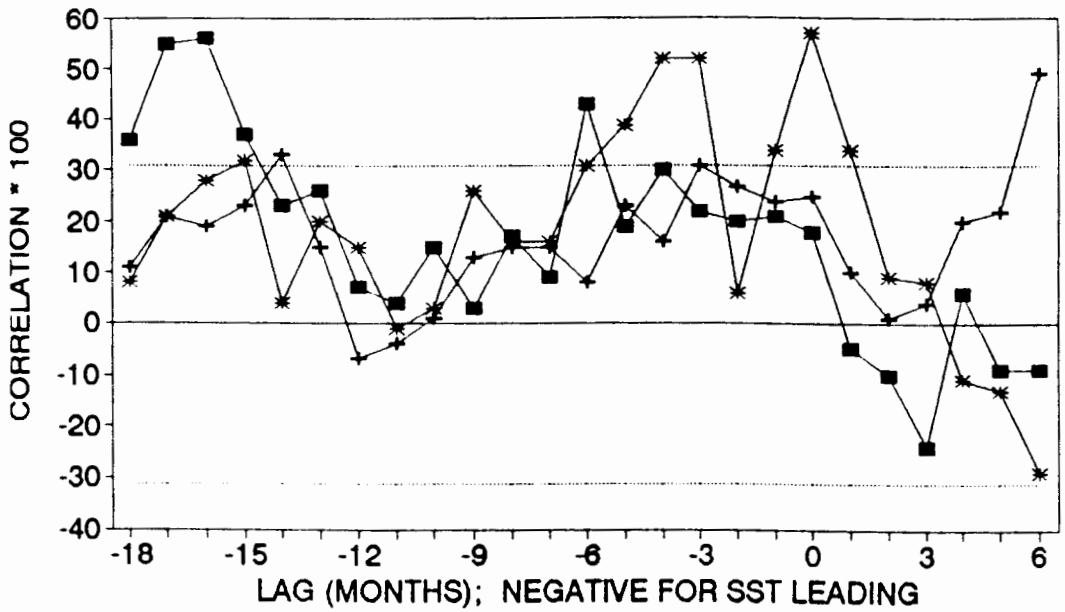

Figure 2.14. CSA BCR ACR 95% LEVELS

LAGGED CORRELATION.

JANUARY ALL-AREA RAINFALL vs BOX SST.

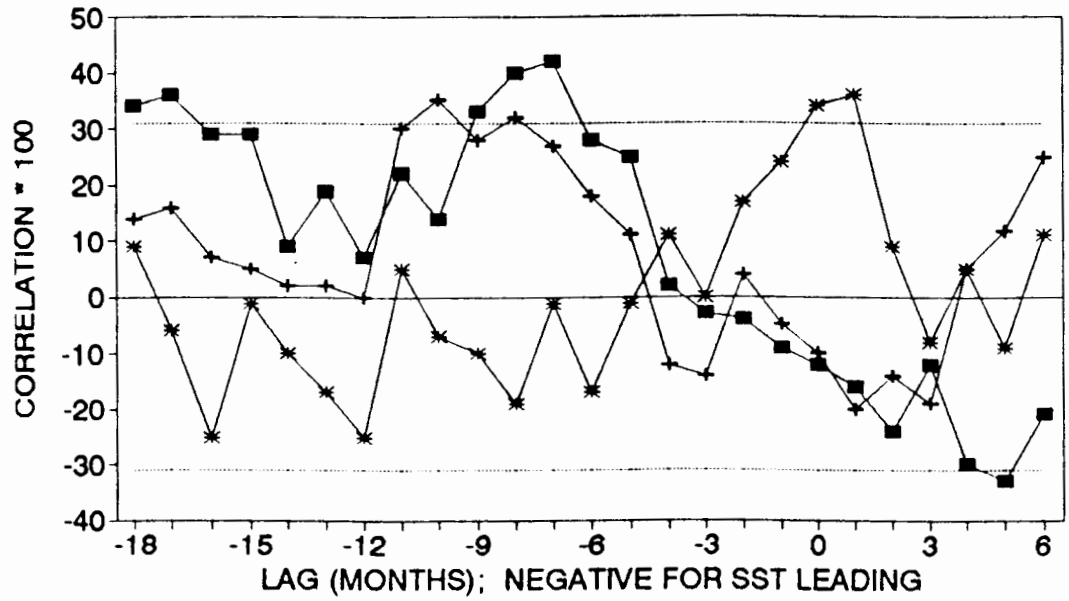

Figure 2.15. CSA BCR ACR 95% LEVELS

LAGGED CORRELATION.

FEBRUARY ALL-AREA RAINFALL vs BOX SST.

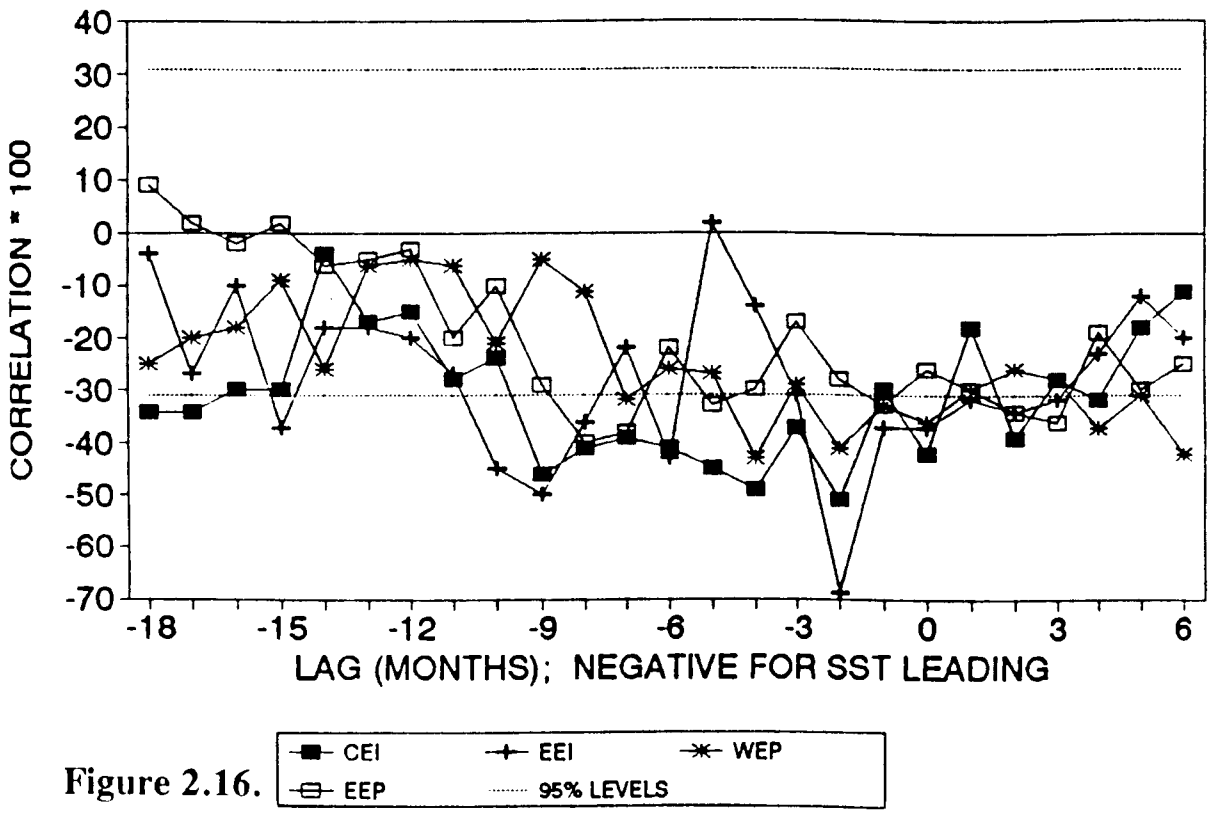

Figure 2.16.

LAGGED CORRELATION.

NOVEMBER RAINFALL vs CSA BOX SST.

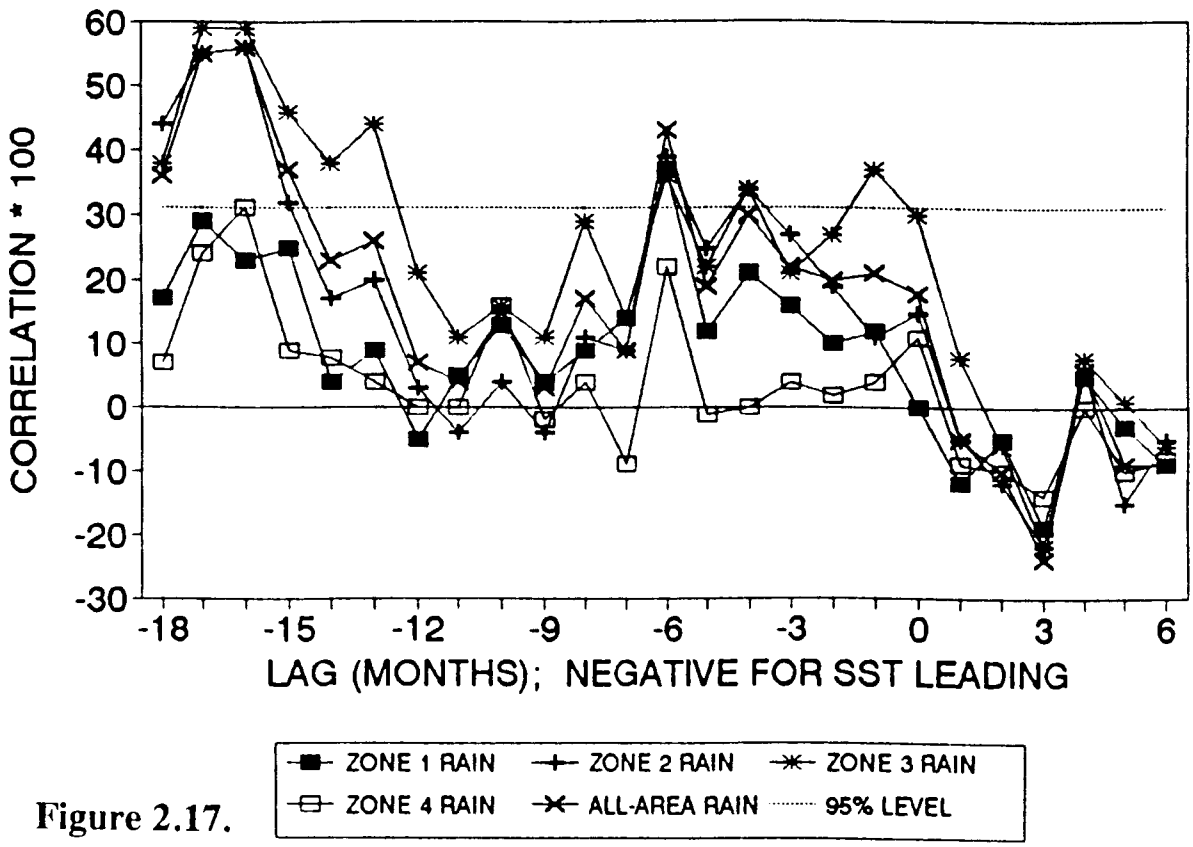

Figure 2.17.

LAGGED CORRELATION.

JANUARY RAINFALL vs CSA BOX SST.

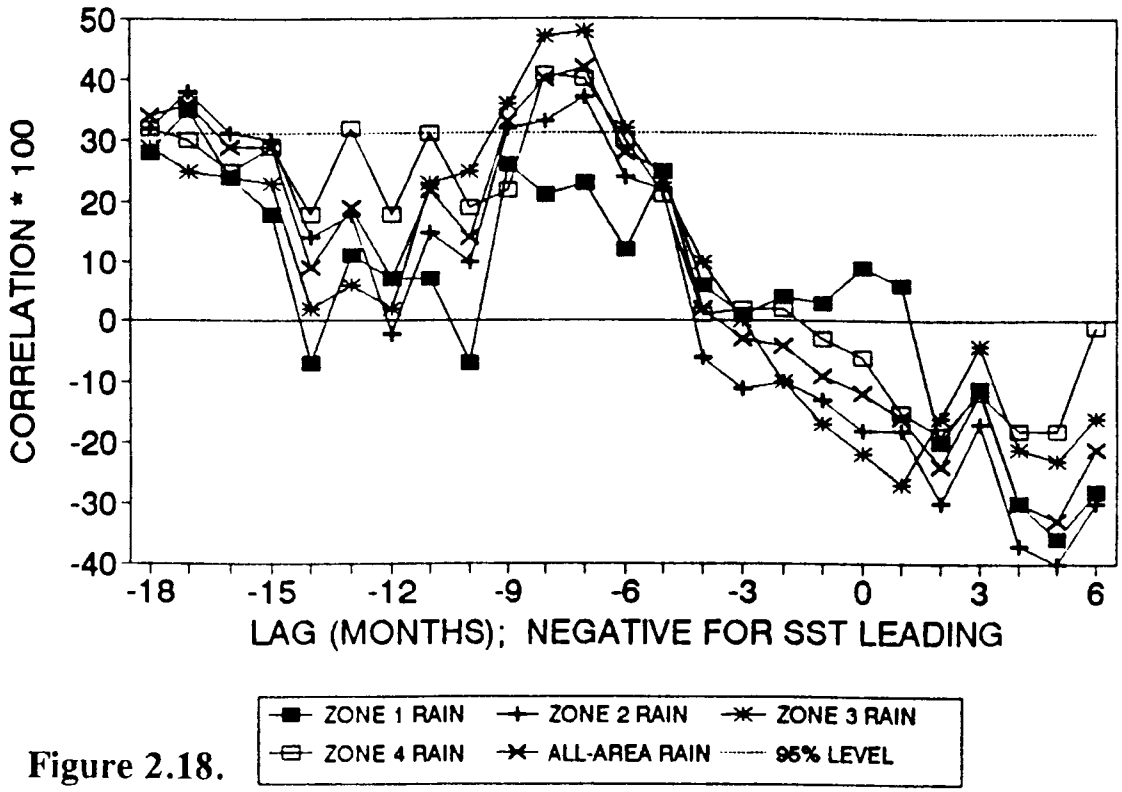

Figure 2.18.

LAGGED CORRELATION.

FEBRUARY RAINFALL vs CEI BOX SST.

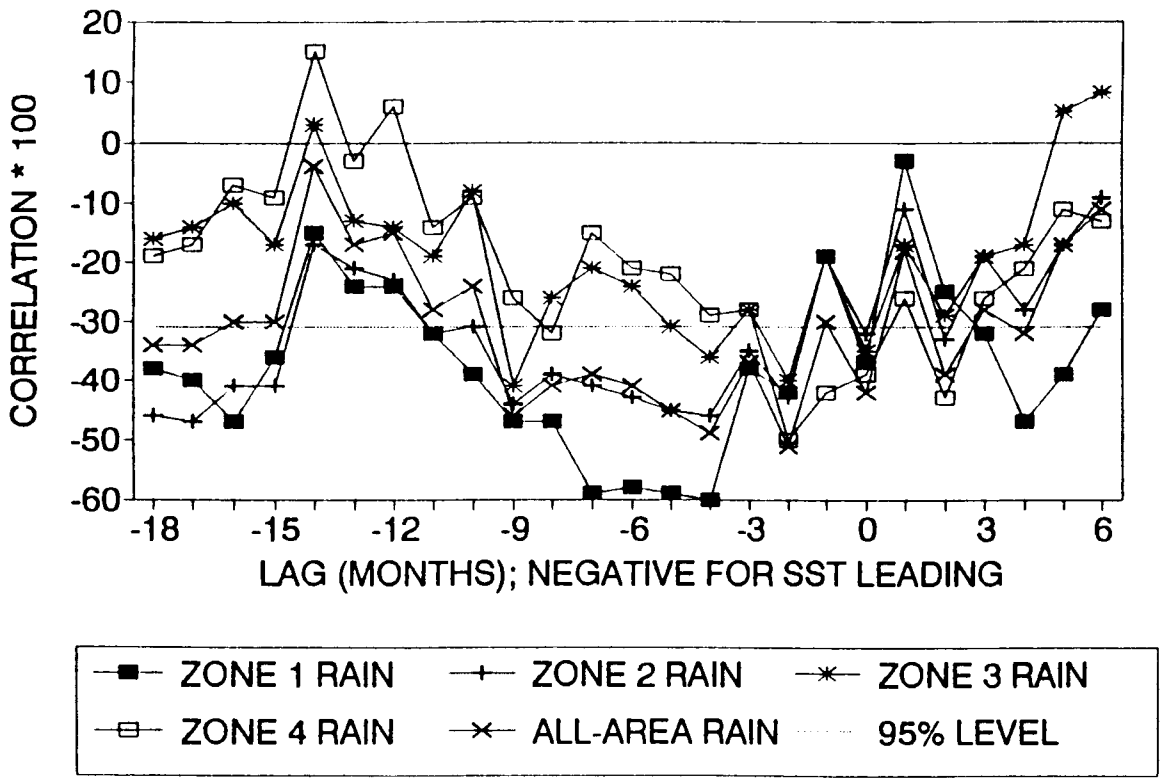

Figure 2.19.

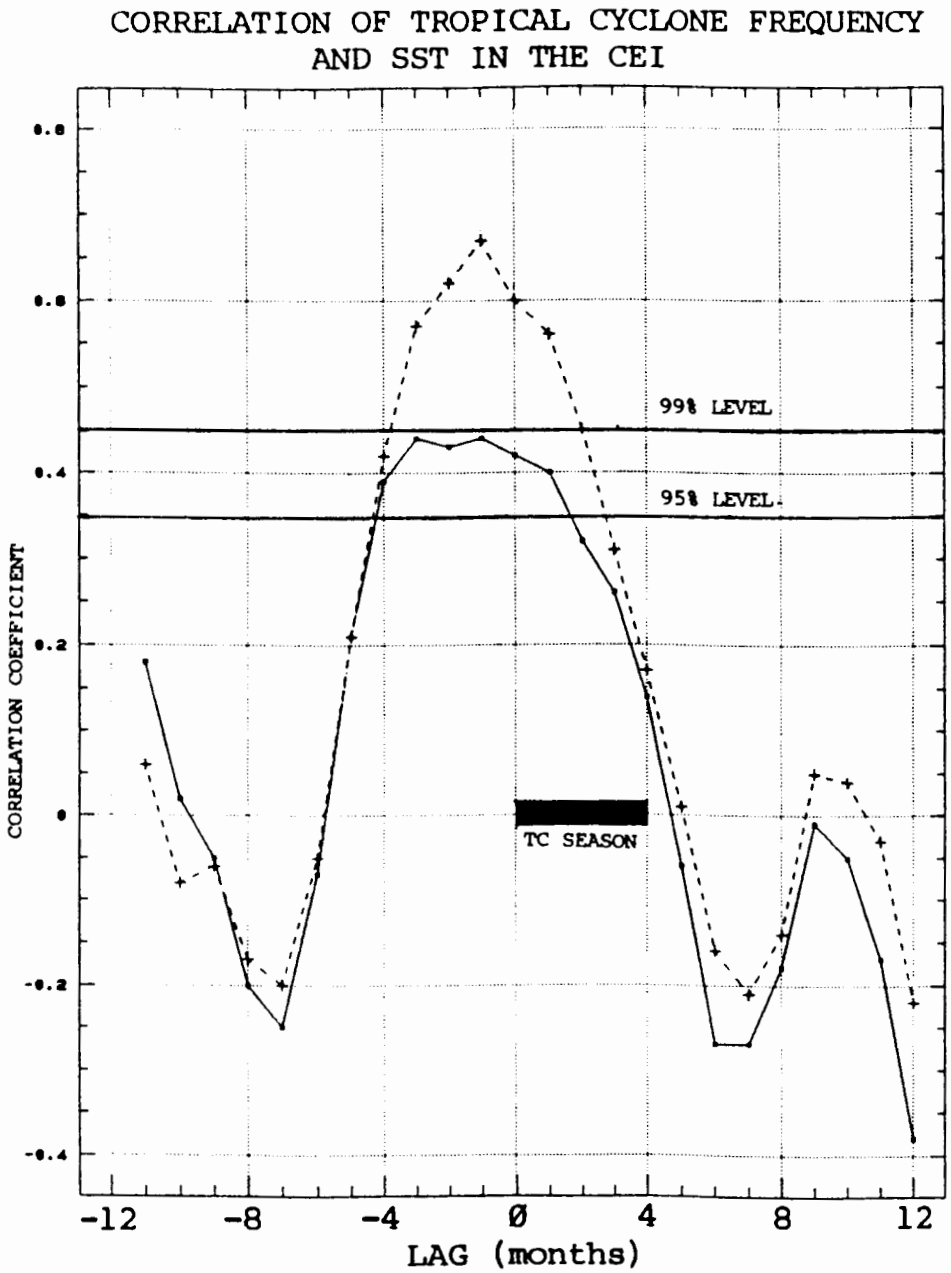

Figure 2.20. Correlation between Central Equatorial Indian Ocean SST and the frequency of intense tropical cyclones in the south-west Indian Ocean.
Dotted line: Distribution of correlation between SST and January to March cyclone season.
Continuous line: Distribution of correlation between SST and December to April cyclone season.
Data period: 1950 to 1986.
The horizontal axis refers to 3-month mean SST; for example, -4 lag corresponds to the mean SST for the months of September, October, and November, -2 lag corresponds to SST for November, December, and January, zero lag corresponds to mean SST for January, February, and March, etc.

CHAPTER 3

SOUTH AFRICAN SUMMER RAINFALL AND OUTGOING LONGWAVE RADIATION

3.1. INTRODUCTION

Knowledge of the large-scale distributions and variations of latent heating, especially within the tropics, both in space and time, are important for understanding and modeling the general circulation. The latent heat fluctuations are difficult to measure directly, but reasonable approximations of their horizontal distribution may be inferred from rainfall amounts recorded at the earth's surface. However, quantitative in-situ measurements of precipitation are unavailable from much of the globe, particularly over the ocean areas. One practical way to deduce large-scale atmospheric latent heat variation is by estimating it from satellite-observed Outgoing Longwave Radiation (OLR). However, cautious application is recommended, especially when used over continental and higher latitude areas where relatively large OLR fluctuations occur due to surface temperature changes which are not correlated with variations in convective cloudiness.

Satellite-derived earth radiation budgets have been widely used to study large-scale circulation changes in the tropical atmosphere. Winston and Krueger (1977) used such data to study tropical radiative heat source and sink distributions during the northern summer monsoon. Through Empirical Orthogonal Function analysis, Heddinghaus and Krueger (1981) showed that annual and interannual changes in OLR are related to variations of the same time scale in the large-scale tropical circulation. Liebmann and Hartmann (1982) demonstrated the link between OLR and SST anomalies associated with the Southern Oscillation.

Lau and Chan (1983a, b) performed detailed analyses on seven years of monthly OLR data through simultaneous and lagged correlation techniques. Positive associations were found with equatorial central Pacific, equatorial East Africa, western North Atlantic, and Siberia, and negative associations with the Indonesian regions, Australia, Southern Africa, Northeast Brazil, Hawaii, and the South Pacific dry zone. The relationships or teleconnections were shown to possess preferred temporal and spatial distributions. Minor variations in the time-scale of two to three months were associated with quasi-stationary fluctuations in the Walker (zonal-vertical) circulation, while a major shift in the mean level of fluctuation was attributed to the 1975-1976 El Niño, the only one observed within that data period. The generally long time and large spatial scales in the variations of these teleconnections suggest the possibility of prediction of time-averaged atmospheric conditions over a given region from events occurring in a remote, but correlated, region (Lau and Chan, 1983b)

Before utilizing satellite-derived OLR data for long-range (monthly to seasonal) prediction, coherent relationships of OLR variations over key regions have to be determined. Furthermore, in order to use atmospheric teleconnectivity in practical models, the target region (predictand) must be given first, then source regions (predictors) identified, and finally the lag times over which the relationships are strongest must be investigated. Simultaneous as well as lagged correlations are analysed in this study in order to identify possible predictors for South African summer rainfall. Due to the large spatial scales of the variations discussed, only the All-Area rainfall series (see Chapter 1) will be considered in the following investigations.

Lau and Chan (1983a) have supported the idea that OLR may be representative of rainfall rate over tropical regions. However, cautious application is recommended when continental areas are involved, because of the relatively large OLR fluctuations due to,

for example, moisture and surface temperature changes not associated with convective cloudiness fluctuations. For example, the low values over the north Asian continent in January cannot be discussed in the context of convection. Likewise, OLR distributions over large areas within the Southern African region are not representative of convective cloudiness during the southern winter. With the exception of areas in the southwestern and southern extremes of South Africa which experience winter or all-year-round rainfall, most of the southern subcontinent of Africa is very dry in winter (see Figure 1.7).

It has been found (Jury et al., 1991) that, during the southern hemisphere summer months, precipitation and OLR across the interior of Southern Africa are significantly negatively correlated. Absolute correlation values superior to 0.8 have been observed between the variables; although the number of independent data points (of the order of 13) were not large, *a priori* expectations augment the significance of the relationship. So the use of OLR as a proxy for rainfall over this region during summer months is justified.

In addition, a large number of studies have utilized OLR as representative of cloudiness, convection, and precipitation, particularly over the tropical oceans (for example, Winston and Krueger, 1977; Heddinghaus and Krueger, 1981; Liebmann and Hartmann, 1982; Lau and Chan, 1983 a, b; Ferranti et al., 1990; Gutzler and Wood, 1990; and Janowiak, 1992, among others). A summary of pioneering research in the field of climate time-scale precipitation estimation is provided in Arkin and Ardunay (1989).

Data and analysis procedures have been described in Chapter 1, but a summary of the OLR data source and limitations are provided in Section 3.2 where steps taken to

remove bias in the dataset are included. As a background, Section 3.3 compares OLR distributions during the peak months, January and July. Results of correlations between the variations (monthly) of South African summer rainfall and OLR are presented in Section 3.4, while variations on a seasonal time scale are dealt with in Section 3.5. Section 3.6 provides a discussion and synthesis.

3.2. OLR DATA

Due to limitations in the number of independent events, the results of investigations utilizing OLR data may not meet rigorous statistical significance tests. However, *a priori* knowledge of association patterns should augment confidence in the results.

In investigations of variations of the mean July-August OLR against rainfall across the Indian region, Gadgil et al. (1992) observed a systematic bias in the NOAA OLR dataset. Over a large portion of the tropical belt, OLR fluxes derived from NOAA-SR for the period 1974 to 1978 were found to be consistently higher compared to those from the NOAA 7 satellite for the period 1982 onward. They suggested that the lower values of OLR in the latter period might be a manifestation of a systematic bias arising from various factors such as changes in instruments, equatorial crossing time of the satellite, etc. If such bias is present, the data should be adjusted.

The present OLR dataset was subjected to statistical tests in order to substantiate the results of Gadgil et al. (1992). Means and standard deviations based on different periods were computed for the whole domain as well as for various limited belts (tropical and higher latitude). Statistical tests, particularly for verifying difference between means (Spiegel, 1961; Mitchell et al., 1966), were then applied to the relevant samples. The results confirmed that the OLR values for the post 1980s period were

generally lower than those for the pre-1980s. Although the actual magnitude of the difference was small, the data was adjusted. The bias was filtered out by subtracting a computed fraction (0.64%) from the raw values corresponding to the period from 1974 to 1979. Adjusted OLR values are used where fluctuations in the variables are involved, whereas long-term means are computed from the original dataset.

3.3. LONG-TERM MEAN OLR DISTRIBUTIONS

As a background, the long-term mean OLR distributions for the months of January and July are interesting and worth examining. Figure 3.1 shows the average OLR distributions for these months based on the years 1974 to 1987; data for January 1974, July 1978, and July 1987 are missing. The major and more persistent features of the tropical atmosphere are delineated. Lower values of OLR (Wm^{-2}) indicate higher convective activity, and vice versa. The large-scale global circulation is dominated by three major areas of intense convective activity where the OLR values are generally less than 250 Wm^{-2}. These are (1) the maritime regions around Indonesia-Borneo, (2) the Central Americas, and (3) Central Africa. The areas of intense convection inferred from the OLR distributions follow the annual cycle in solar declination, with longitudinal and hemispheric asymmetries associated with differing distributions of continents and oceans. The three-wave pattern takes a more southeasterly location during January and is displaced to a northwesterly position in July. This interesting feature will be discussed in detail in Section 3.4. The evolution of the Asian monsoon during the peak northern summer month of July is clear with OLR contours generally below 225 Wm^{-2}.

Another distinctive pattern is observed over the oceans. As discussed earlier, there is less problem inferring convective activity from OLR distributions across the oceans (equatorward of 30° latitude) due to the more uniform background temperature in such areas. But again, OLR fluxes over areas where cirrus clouds prevail are not representative of convection. From Figure 3.1, it is seen that the trade wind regions are superposed by large values of long wave radiation over the three tropical oceans, more intense in the South Pacific and South Atlantic, and in July because of the more vigorous Hadley (north-south) overturning during northern hemisphere summer. These large values indicate the suppression of cloudiness through widespread subsidence and are associated with strong and steady trade wind flow (Heddinghaus and Krueger, 1981; Barnett, 1977).

Although the aim here is to investigate relationships with respect to South African summer rainfall, it is instructive to examine large scale features during winter as a comparison. In addition, the early part of the summer season, like October and November, often exhibit features characteristic of winter months. In July, the South Pacific and South Atlantic dry zones show OLR values of over 275 Wm^{-2}, whereas the whole of the South Indian Ocean area is covered by OLR values of the order of 250-275 Wm^{-2}. Most of the Southern African subcontinent is dry during the southern winter months. As noted earlier in the introduction section, OLR distributions in such cases are not representative of convective activity, because of the reduced background radiation from the surface.

Among the possible causes of winter dryness across most of Southern Africa are: subsidence of dry air outflowing from the northern African ITCZ, return flow from the monsoon of Southeast Asia, and advection of dry air from the Atlantic sector. There is no general consensus about the most effective process; it is likely that all three factors

contribute to a certain extent towards the drying out over Southern Africa. Cressman and Helmick (1989) provide support to the view that the air in the westerlies departing from the western South Atlantic region undergoes subsidence while crossing the South Atlantic Ocean; subsequently, orographically-induced low-level anticyclonic circulation over Southern Africa serves to mix and circulate the subsiding air around in the lower troposphere. However, a preliminary examination of the velocity potential field (which represents the divergent part of the horizontal wind flow, see Chapter 4) indicates that the circulation over the Asian monsoon areas appears to have more influence on the Southern African climate system. This is in agreement with the influence of the ENSO event over the area.

3.4. RESULTS: ALL-AREA RAINFALL VERSUS OLR RELATIONSHIPS

Lagged correlations have been computed between the variations of South African All-Area summer rainfall and OLR. The method employed is the same as for rainfall-SST correlation computations described in Chapter 2. For each rainfall series the monthly OLR lagged from -18 to +6 months relative to the rainfall reference month. Negative lags refer to cases where OLR leads rainfall.

It should be noted that the numbers of degrees of freedom (numbers of independent data points) have significantly decreased due to the temporal limitation of the OLR dataset compared to the rainfall (and SST) records. Therefore, only the main features which appear consistent with known atmospheric dynamics should be interpreted. Certain patterns may not satisfy rigorous statistical significance tests, but are, however, expected from independent observations or predicted by dynamical models.

Results are presented for relationships of rainfall with OLR within six boxes, namely, Benguela and Agulhas Current Regions (BCR and ACR), Western and Central Equatorial Indian Ocean (WEI and CEI), and Western and Eastern Equatorial Pacific (WEP and EEP). Analyses of South African summer rainfall variations with respect to SST (Chapter 2) show that the equatorial areas just mentioned are among the most important as far as rainfall prediction is concerned. The areas adjacent to the subcontinent are included for further exploration of the importance of advective processes. Also observed in Chapter 2 was that rainfall variations across the summer rainfall area of the country were spatially homogeneous. The All-Area rainfall index series will be used as representative of the region's rainfall distribution. For more accurate analyses, however, the four zones forming the All-Area should be treated individually. The results of simultaneous and lagged correlations between variations of South African summer rainfall and OLR are discussed in the following sections. Correlation maps are also presented in some cases. The intention here is to further explore the structure of South African summer rainfall variations and confirm the results obtained in earlier investigations, such as the implied dipole-like circulation pattern between South Africa and the Indian Ocean areas. The correlation structures indicate the importance of advective and teleconnective processes in the temporal domain. Tropical dynamics will be examined in the next chapter through the use of observed gridded tropospheric wind data. Negative correlations in the following sections refer to a sympathetic response between rainfall over South Africa and convection in the specified area.

3.4.1. OCTOBER ALL-AREA RAINFALL AND OLR

Lagged relationships between October All-Area rainfall and OLR are rather incoherent (see Table 3.1). Strong negative simultaneous correlation with the Benguela and Agulhas Current Regions (BCR and ACR) highlight a sympathetic response over South Africa and confirm the importance of advective forcing. Advection seems to be more likely from the east than from the west. Associations with the Western and Eastern Equatorial Pacific (WEP and EEP) are weak but consistently negative up to a lag of -4 months. The high negative correlations with BCR OLR of July and August are not representative since OLR variations during winter months do not reflect convective activity over the area.

TABLE 3.1
Correlation (x100) between October All-Area rainfall and OLR within the specified boxes. Correlations significant at better than the 95% level are in bold.
OLR data corrected for bias.

Lag	Month	BCR	ACR	WEI	CEI	WEP	EEP
-8	Feb	+11	+46	-44	**-58**	+32	+16
-7	Mar	-25	-12	-19	+07	+08	+23
-6	Apr	+05	+26	-17	-21	+27	+13
-5	May	+49	+03	+02	-04	+16	+08
-4	Jun	+40	+17	-19	+01	-25	-05
-3	Jly	**+77**	+36	+46	+28	-33	-40
-2	Aug	**+56**	+28	-13	-40	-39	-20
-1	Sep	+22	+26	+20	+37	**-63**	-48
0	Oct	-47	**-68**	**-57**	-41	**-59**	-44

BCR, ACR: Agulhas and Benguela Current Regions.
WEI, CEI: Western and Central Equatorial Indian Ocean.
WEP, EEP: Western and Eastern Equatorial Pacific Ocean.

3.4.2. NOVEMBER ALL-AREA RAINFALL AND OLR

Table 3.2 displays the correlation between November All-Area rainfall and OLR within the six boxes. Again, as observed with October rainfall variations, the relatively high simultaneous correlations with the adjacent BCR and ACR (Benguela and Agulhas Current Regions) indicate the importance of advective processes, more from the east than from the west, on the production of precipitation. The slightly weaker correlations in this case are interpreted to mean that advective processes tend to decrease in November compared to October.

In contrast to the October case, correlations with the Western and Eastern Equatorial Pacific (WEP and EEP) are positive up to a lag of about -3 months. This remarkable change in the sign of the correlations from October to November (compare Tables 3.1 and 3.2) is indicative of an abrupt shift in the control mechanism of the large-scale environment (most probably related to monsoon development) within which the synoptic-scale weather systems are embedded. Also notable is the change in sign of simultaneous correlations in the October case (in comparison to November) in the WEI and CEI regions.

TABLE 3.2
Correlation (x100) between November All-Area rainfall and OLR within the specified boxes. Correlations significant at better than the 95% level are in bold. OLR data corrected for bias.

Lag	Month	BCR	ACR	WEI	CEI	WEP	EEP
-8	Mar	**+53**	+43	00	-29	+05	**-53**
-7	Apr	-15	+04	-22	-36	+16	**-57**
-6	May	+06	+41	-07	-01	-47	**-55**
-5	Jun	-15	-23	+31	-07	-04	-32
-4	Jly	-36	-47	-46	-22	+09	+00
-3	Aug	-13	+02	00	+33	+31	-08
-2	Sep	-27	-03	-48	-29	+49	+32
-1	Oct	+26	**+62**	**+55**	+03	**+58**	+50
0	Nov	-41	**-63**	+41	**+58**	+43	**+58**

BCR, ACR: Agulhas and Benguela Current Regions.
WEI, CEI: Western and Central Equatorial Indian Ocean.
WEP, EEP: Western and Eastern Equatorial Pacific Ocean.

3.4.3. DECEMBER ALL-AREA RAINFALL AND OLR

Simultaneous correlations between the variations of December rainfall and OLR within the Benguela and Agulhas Current Regions (BCR and ACR) are weak (Table 3.3). However, there appears to be a strong teleconnection between the rainfall and OLR variations within the Western Equatorial Pacific (WEP), but not with the Eastern Equatorial Pacific. OLR fluctuations over WEP during October, for instance, can explain over 40 per cent of the variance in rainfall of the following December. The significant positive associations with OLR variations within the Western and Central Equatorial Indian Ocean (WEI and CEI) boxes at -1-month lag are notable.

TABLE 3.3
Correlation (x100) between December All-Area rainfall and OLR within the specified boxes. Correlations significant at better than the 95% level are in bold. OLR data corrected for bias.

Lag	Month	BCR	ACR	WEI	CEI	WEP	EEP
-8	Apr	**-53**	-10	+32	+07	+06	+07
-7	May	-22	-14	+32	+08	+45	-02
-6	Jun	-08	+02	+28	+45	+36	-03
-5	Jly	-47	-16	-47	+14	+48	+26
-4	Aug	+14	+40	-51	-41	+52	+02
-3	Sep	+02	+28	-48	-29	**+60**	+02
-2	Oct	-01	+12	+31	+14	**+65**	+13
-1	Nov	-37	-17	**+60**	+46	**+60**	+33
0	Dec	-31	-50	+25	+19	**+55**	+25

BCR, ACR: Agulhas and Benguela Current Regions.
WEI, CEI: Western and Central Equatorial Indian Ocean.
WEP, EEP: Western and Eastern Equatorial Pacific Ocean.

3.4.4. JANUARY ALL-AREA RAINFALL AND OLR

Table 3.4 displays results of correlation between January All-Area rainfall and OLR. The high significance of the simultaneous link with BCR (correlation = -0.71) indicates that, during January, convective activity varies generally in phase across the central interior of South Africa and the Benguela Current area. Relationship with ACR OLR variations is rather insignificant.

Mostly positive associations are observed with OLR fluctuations across the equatorial areas. The link with the Western Equatorial Pacific (WEP) remains consistently positive, especially at higher lags, similar to variations with respect to December rainfall series. On the other hand, there is a slightly better link with the Central Equatorial Indian Ocean (CEI) and the Eastern Equatorial Pacific (EEP), especially at negative lags. A peak correlation of +0.67 is observed with WEI OLR variations at a lag of -1 month; therefore December OLR fluctuations in WEI can explain about 45 per cent in rainfall variance of the following January. It is probable that this indicates a connection with outflow from the northern winter monsoon circulation.

TABLE 3.4
Correlation (x100) between January All-Area rainfall and OLR within the specified boxes. Correlations significant at better than the 95% level are in bold.
OLR data corrected for bias.

Lag	Month	BCR	ACR	WEI	CEI	WEP	EEP
-8	May	-13	+14	+41	+24	+47	+39
-7	Jun	+13	+35	-06	+19	+52	+46
-6	Jly	-46	-19	-35	-01	**+64**	**+64**
-5	Aug	-38	+15	+23	+29	+40	**+61**
-4	Sep	-30	-38	+20	+33	**+71**	+26
-3	Oct	-19	-03	+46	**+61**	**+57**	+22
-2	Nov	-30	+11	+14	+52	+52	+20
-1	Dec	-51	-39	**+67**	+50	+36	+24
0	Jan	**-71**	-40	+37	+30	+04	+13

BCR, ACR: Agulhas and Benguela Current Regions.
WEI, CEI: Western and Central Equatorial Indian Ocean.
WEP, EEP: Western and Eastern Equatorial Pacific Ocean.

An interesting trend in the pattern of association is observed in Table 3.4; the maximum value of the correlation is at a lag of -1 month with WEI, -3 months with CEI, -4 months with WEP, and -6 months with EEP. This feature is probably indicative of a westward propagating large-scale wave.

In general January rainfall shows more of a teleconnection type of behaviour compared to October and November. Correlation maps have been produced by considering

January All-Area rainfall variations with respect to OLR variations at each grid point. Figure 3.2 displays the simultaneous correlation map, while Figures 3.3 to 3.5 display lagged correlations. To preserve the readability of the correlation values, only approximate land mass boundaries are superposed.

High correlation values (about -0.8) over the central interior of South Africa confirm that OLR can be taken as a proxy for rainfall of the region. The north-west south-east orientation of the correlation pattern (Figure 3.2) is probably linked to the effect of tropical-temperate troughs on rainfall distribution. Similar patterns have been observed by Lindesay (1988) who examined fluctuations of South African rainfall with respect to the Southern Oscillation Index. Coherent positive correlations across the central and equatorial parts of the south Indian Ocean are in agreement with a dipole-like relationship with the South African Area. Highly significant negative correlations occur in the tropical south east Pacific where El Niño signals are usually observed (off the west coast of tropical South America). The representativeness of this feature requires further detailed investigations using more and better data. Examination of the correlation maps (Figures 3.2 to 3.5) reveals that the area of maximum positive values displaces from the equatorial parts of the Indian Ocean at a lag of -3 months to the southern regions at zero lag.

There appears to be a simultaneous link between the implied rising motion over South Africa in January and descending motion over the western part of the south Atlantic (Figure 3.2), but this link becomes less marked at negative lags and changes in sign at -3-month lag (Figures 3.3 to 3.5).

3.4.5. FEBRUARY ALL-AREA RAINFALL AND OLR

Table 3.5 summarises the main results of correlation between the variations of February All-Area rainfall and OLR. Statistical links with the Benguela and Agulhas Current Regions (BCR and ACR) are generally negative and mainly weak, although they are significant at -1-month lag.

December or January OLR variations within the Western Equatorial Indian Ocean (WEI) can explain over 40 per cent of the variance in rainfall of the following February. Similar patterns of associations were found with December and January rainfall series.

TABLE 3.5
Correlation (x100) between February All-Area rainfall and OLR within the specified boxes. Correlations significant at better than the 95% level are in bold. OLR data corrected for bias.

Lag	Month	BCR	ACR	WEI	CEI	WEP	EEP
-8	Jun	+25	+48	-44	-20	+43	+40
-7	Jly	-32	-30	-14	-07	**+68**	**+64**
-6	Aug	-44	-12	**+62**	+42	+39	**+75**
-5	Sep	-33	**-65**	+41	+38	**+64**	+45
-4	Oct	-22	-04	**+59**	**+90**	+46	+36
-3	Nov	-41	+16	+14	+48	**+55**	+22
-2	Dec	-49	-43	**+78**	**+76**	+38	+37
-1	Jan	**-55**	**-57**	**+65**	+45	+14	+32
0	Feb	-44	-32	-17	+16	+13	+37

BCR, ACR: Agulhas and Benguela Current Regions.
WEI, CEI: Western and Central Equatorial Indian Ocean.
WEP, EEP: Western and Eastern Equatorial Pacific Ocean.

February rainfall shows strong positive links with OLR fluctuations across the equatorial belts of the Indian and Pacific Oceans, especially at negative lags (OLR leading rainfall). Figure 3.6 shows the simultaneous correlation distribution between February All-Area rainfall and gridded OLR, while Figures 3.7 and 3.8 show correlations at lags of -2 and -4 months, respectively. Over the Atlantic Ocean, the African continent and the Indian Ocean sectors, the simultaneous and lagged

correlations display patterns which are similar to those observed in the case of January rainfall; namely, high simultaneous correlations in the rainfall area, the northwest-southeast orientation across the southern African subcontinent, the Indian Ocean-South African dipole, and the northward shift in the maximum value of correlation in the Indian Ocean region. The associations of OLR in the equatorial Indian Ocean are slightly stronger with February rainfall than with January rainfall; whereas the negative links with OLR fluctuations in the tropical areas off the coast of South America are much less marked at zero and -2-month lags.

3.4.6. MARCH ALL-AREA RAINFALL AND OLR

Significant association is observed between the variations of March All-Area rainfall and the Benguela Current Region (BCR) OLR up to a lag of -4 months (Table 3.6), whereas relationship with the Agulhas Current Region (ACR) OLR is poor. Similar to January and February rainfall variations, fluctuations of OLR within the Western Equatorial Indian Ocean (WEI) during the month of December can explain nearly 50 per cent of rainfall variance of the following March. Relationships with the Western and Central Equatorial Indian Ocean (WEI and CEI) remain mostly significant and coherently positive up to a lag of -5 months.

The links between variations of March All-Area rainfall and the Eastern Equatorial Pacific (EEP) OLR are coherently positive, but they are very weak, especially when compared to the results concerning January and February rainfall variations. However, correlations with the Western Equatorial Pacific (WEP) are positive throughout and are strong up to lags of -4 to -6 months.

TABLE 3.6
Correlation (x100) between March All-Area rainfall and OLR within the specified boxes. Correlations significant at better than the 95% level are in bold.
OLR data corrected for bias.

Lag	Month	BCR	ACR	WEI	CEI	WEP	EEP
-8	Jly	**-71**	-23	**-61**	-05	+48	+27
-7	Aug	-27	+04	+09	+12	+52	+25
-6	Sep	-44	-24	-24	-02	**+72**	+03
-5	Oct	-08	+13	**+63**	**+59**	**+68**	+24
-4	Nov	**-70**	-25	**+53**	**+74**	**+74**	+21
-3	Dec	**-77**	-29	**+69**	+44	+47	+31
-2	Jan	**-58**	-04	+16	+26	+29	+12
-1	Feb	-47	-30	+25	+46	+39	+09
0	Mar	**-66**	-20	**+57**	**+61**	+21	+15

BCR, ACR: Agulhas and Benguela Current Regions.
WEI, CEI: Western and Central Equatorial Indian Ocean.
WEP, EEP: Western and Eastern Equatorial Pacific Ocean.

3.5. SEASONAL ALL-AREA RAINFALL AND OLR VARIATIONS

The aim in this section is to examine the results of association between variations of rainfall and OLR at seasonal time scales. The summer season indices are obtained by averaging the parameter over the months from October through March. Figure 3.9 displays the simultaneous correlation between the seasonal rainfall and OLR. In spite of temporal smoothing, the larger scale coherent features are apparent. The high negative values across the summer rainfall area of South Africa (shaded on the map) reflect the representativeness of OLR as an index for convective activity (for the area and the season). The south Indian Ocean-Southern African dipole is readily observed, with significant correlations of opposite signs.

South African summer rainfall shows significant negative correlations with OLR variations off the west coast of tropical South America; but the values are generally positive over the land areas of tropical South America and tropical south-west Atlantic Ocean. Somewhat less marked, but coherent positive links are noted over most of the central and western equatorial Pacific Ocean. On the whole, a wave number three type

of structure is apparent across the southern hemisphere, with coherent features oriented in a north west-south east direction.

Lagged cross-correlations have also been computed between 2-monthly OLR variations and summer (October to March) South African rainfall. The results are presented in Table 3.7. 'Quasi-simultaneous' link with BCR (Benguela Current Region) OLR is relatively high, while the link with ACR (Agulhas Current Region) OLR is weak. The dipole type of relation with respect to the equatorial Indian Ocean is apparent. Correlations of seasonal rainfall variations with EEP OLR are insignificant, but those with WEP OLR are relatively strong, mainly at lags with OLR leading rainfall by a few months.

TABLE 3.7
Correlation (x100) between seasonal All-Area rainfall and OLR within the specified boxes. Correlations significant at better than the 95% level are in bold.
OLR data corrected for bias.

OLR MONTHS	BCR	ACR	WEI	CEI	WEP	EEP
Feb/Mar	+19	+23	+14	+14	**+64**	+06
Mar/Apr	-18	-02	**+61**	+29	+50	+11
Apr/May	-06	-06	**+60**	+43	**+59**	+12
May/Jun	+13	+23	+44	**+53**	+48	+13
Jun/Jly	-18	-02	-45	+20	**+60**	+33
Jly/Aug	-32	00	-27	+08	**+63**	+44
Aug/Sep	-28	+04	-04	+12	**+69**	+31
Sep/Oct	-37	-16	+35	+48	**+76**	+22
Oct/Nov	**-58**	**-55**	**-55**	**+73**	**+73**	+29
Nov/Dec	**-60**	-26	**+64**	**+67**	**+70**	+36
Dec/Jan	**-74**	-30	+46	+36	+48	+28
Jan/Feb	**-58**	-24	+39	+49	+41	+25

BCR, ACR: Agulhas and Benguela Current Regions.
WEI, CEI: Western and Central Equatorial Indian Ocean.
WEP, EEP: Western and Eastern Equatorial Pacific Ocean.
The 'OLR MONTHS' column refers to mean OLR for the two consecutive months. Top row corresponds to OLR leading rainfall and bottom row to OLR lagging rainfall.
Thus the values along the Jun/Jly row are correlations between the variations of June/July OLR index vs rainfall index for the following October to March season.

3.6. DISCUSSION AND SYNTHESIS

With the aim identifying predictors for South African summer rainfall, OLR variations within key boxes have been analysed. Due to the relatively limited length of the OLR data series, only the major features which are believed consistent with known atmospheric dynamics have been emphasized. Some of the patterns may not satisfy rigorous statistical tests, but they may be expected either from independent observations or predicted by numerical/dynamical models. These observations or model results need not necessarily involve OLR directly, but some comparable variables (see, for example, Webster, 1972; Liebmann and Hartmann, 1982; Lau and Chan, 1983a, b; Stone and Chervin, 1984; Lindesay, 1988; Walker, 1989; Jury et al., 1991). Results of lagged and simultaneous correlations between fluctuations of monthly All-Area rainfall and OLR within six boxes (BCR, ACR, WEI, CEI, WEP, and EEP) have been examined. Due to data limitations, field significance tests have not been applied.

Precursors of October and November All-Area rainfall are not evident in the OLR field. With respect to these months, the only significant links identified are the simultaneous ones with the Benguela and Agulhas Current Regions (BCR and ACR). Of particular note is the change in sign of association when October and November rainfall series are correlated with Equatorial Pacific OLR distributions. This feature is indicative of an abrupt shift in the manner of association.

December rainfall shows consistent positive correlations with the Western and Eastern Equatorial Pacific (WEP and EEP) OLR variations up to lags of several months; the associations are stronger with the former area where peak values of +0.55, +0.60, +0.65, and +0.60 occur at lags of 0, -1, -2, and -3 months, respectively. Moreover, the Western and Central Equatorial Indian Ocean (WEI and CEI) OLR fluctuations show respective correlations of +0.60 and +0.46 at a lag of -1 month.

January, February, and March All-Area rainfall variations tend to behave rather similarly with respect to OLR fluctuations within the four equatorial boxes (WEI, CEI, WEP, and EEP). December OLR in WEI can explain a large portion (about 50 per cent) of the variance in rainfall of the following January, February, and March. This observation points to a possible link with an atmospheric response within the WEI region as regards outflow from the Indian monsoon. The positive association implies that reduced cloudiness off the eastern coast of equatorial Africa in the November-December period is usually followed by above normal mid- and late- summer rainfall across South Africa. The positive associations of rainfall during the late summer months with WEP and EEP OLR are generally strong at lags of about -4 to -6 months.

It has been noticed that the All-Area rainfall variations during the months of December to March are mainly positively correlated with OLR variations over the equatorial areas of the Indian and Pacific Oceans . The rainfall relationships with convection across the equatorial Indian Ocean confirm, and are consistent with, results obtained in analyses with respect to SST (Chapter 2). The connection with the WEP may seem contradictory when compared to links found in connection with the evolution of El Niño-type of situations; it should, however, be noted that the WEP box extends eastwards well into the Pacific past the dateline (from 160°E eastward to 160°W). Thus the variables within WEP are not considered as indices of the Southern Oscillation/El Niño (ENSO) seesaw (Philander, 1983; Yarnal and Kiladis, 1985; Wright et al., 1988).

It appears that local advective processes (from the west) are mainly responsible for the winter climate of Southern Africa, whereas the mid-summer climate has a general tendency to be more influenced by remote teleconnections, especially with circulations to the east of the region. It should also be recognized that low-level moisture influx is mostly provided through advection from the Indian Ocean side of the subcontinent; the

mean climate is then determined by the large-scale environmental features. These large-scale features interact with the small-scale systems in such a way that either teleconnection type or advective type of behaviour ensues. Teleconnection here implies sympathetic response with remote areas, an example being the connection found in Walker type of circulation. From the analyses presented so far, it appears that, in general, teleconnections are important to the mean weather during the months from December to March (January to a lesser extent), advective processes seem to govern winter climate.

The three-wave pattern in the distribution of mean OLR (Figure 3.1) shows a zonal oscillation from January to July; convective hot spots take a more southeasterly location during January and displace to a northwesterly position in July. This large-scale feature reflects the three major land mass distributions which show a general north-west to south-east orientation, particularly within the tropical belt. From such a point of view, the sympathetic January to July shift in the mean zonal OLR distributions (large-scale wave number 3) should not be surprising due to the seasonal march of solar declination and the contrasting heat capacities of land and water. So the thermodynamic interpretation is consistent with the large scale behaviour of the systems involved.

Stone and Chervin (1984) performed a series of numerical experiments which were designed to determine the relative importance of continentality, topography, and SST gradients in driving the tropical circulation. The changes in the circulation patterns found in the experiments showed that continentality and SST gradients were the major factors in the asymmetric forcing, with the former appearing to be dominant. This result was anticipated by Ramage (1968) and Webster (1972). Statistical verification of the model results (Stone and Chervin, 1984) showed that the atmospheric forcing correlated with the continentality rather than the SST gradients. Furthermore, it was

shown that continentality was the most important asymmetric forcing even affecting the meridional mass overturning, with the mean Hadley circulation redistributing momentum and energy.

Considering the relative importance of the continentality factor (that is, vertical sensible heat fluxes and associated convergence), it can be hypothesized that the oceanic boundary layer, depending on the state of SST anomaly, can provide thermodynamic inputs to the lower atmosphere which modify the regional circulation and moisture fluxes. This tendency has been observed when SST-rainfall correlations were analysed in the previous chapter. Realizing the very complex nature of the interactions within the atmosphere-hydrosphere-cryosphere system, on an average there appears to be a sort of 'equilibrium' between convective intensities over land versus central ocean basins. It is implied that teleconnections are, at least partly, associated with the evolution of anomalous atmospheric/oceanic situations, and are not random.

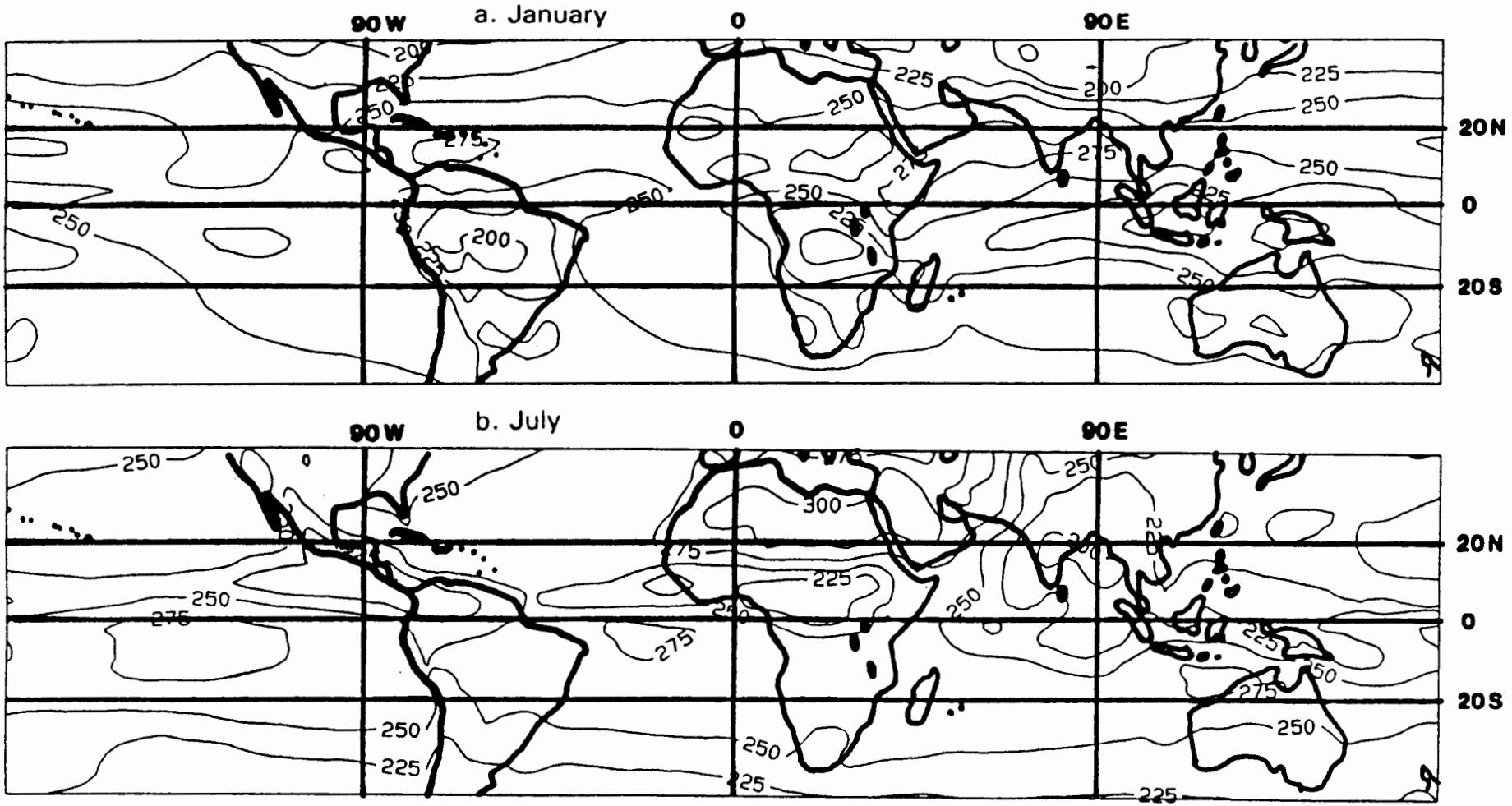

Figure 3.1. Mean OLR distribution (Wm^{-2}). Data not corrected for 1970's relative to 1980's bias.
a. January (based on years 1975 to 1987, excluding 1978).
b. July (based on years 1974 to 1986, excluding 1978).

Figure 3.2. Simultaneous correlation (x100).
January OLR against All-Area rainfall.
Data period: 1974-1986. Bias in OLR data removed.
Shading represents approximate location of rainfall area.

LONG.	-41	-37	-33	-29	-24	-20	-15	-10	-5	0	+5	+10	+15	+20	+24	+29	+33	+37	+41	LONG.
LATITIDE --->																				
180	-10	-20	7	-13	-7	-4	6	23	2	-3	4	17	-12	-7	46	53	47	-20	-29	180
175	-25	-11	3	-9	10	6	4	11	15	3	-3	16	-21	-41	27	46	15	-10	12	175
170	-30	1	-1	8	9	-16	-4	14	22	11	-8	-6	-54	-59	-12	30	13	-5	35	170
165	-19	-5	-8	6	-8	-47	4	16	25	18	3	-5	-30	-29	-3	17	11	-16	-14	165
160	-4	-20	-32	-10	-27	-19	14	19	27	22	9	-4	-14	7	14	18	1	9	9	160
155	-6	-39	-33	-27	-27	25	17	18	28	23	5	-3	-24	9	39	28	-5	-27	-23	155
150	-21	-27	-32	-27	4	27	26	27	30	22	0	-19	-29	-2	36	34	1	-24	-27	150
145	-30	-28	-35	-4	39	32	27	26	24	20	1	-23	-37	-21	20	32	3	-19	-34	145
140	-52	-44	-35	36	46	20	11	23	24	18	10	-35	-37	-29	13	20	13	-9	-25	140
135	-73	-48	5	30	5	-5	3	17	20	15	17	-20	-39	-22	0	8	-4	-12	-21	135
130	-28	-10	0	12	7	-21	-10	8	7	13	26	-7	-50	-18	-18	2	3	-8	-22	130
125	39	18	9	16	11	-31	-8	19	2	13	35	-23	-49	-39	-23	-5	20	11	-6	125
120	35	27	19	29	35	-19	-39	-11	-6	11	30	-32	-51	-37	-19	-1	26	19	16	120
115	12	29	42	42	19	-34	-74	-68	-17	7	15	-42	-43	-18	-10	-8	1	13	19	115
110	32	45	58	47	5	-66	-77	-78	-34	4	6	-32	-35	-2	-5	11	-7	4	8	110
105	53	51	47	38	-5	-68	-81	-84	-68	6	9	-19	-22	16	1	-16	-14	-3	-7	105
100	62	55	37	25	-32	-87	-91	-81	-58	20	14	-10	-3	-22	-2	7	7	4	-9	100
95	54	53	39	11	-63	-86	-86	-78	-57	7	-10	14	-30	20	31	27	15	17	9	95
90	42	40	22	-27	-78	-81	-79	-61	-23	-22	-13	15	41	-20	28	26	0	15	7	90
85	28	13	-18	-51	-68	-69	-78	-58	-25	-42	-8	-3	38	-14	35	34	-11	6	-9	85
80	8	-33	-29	-41	-52	-58	-63	-25	13	16	20	6	-14	13	35	41	29	-1	-23	80
75	-40	-16	-10	-49	-49	-51	-26	26	3	28	28	12	-34	1	37	42	56	25	-30	75
70	-25	14	10	-39	-32	-31	13	22	22	9	13	15	-33	-3	32	44	53	21	-30	70
65	0	31	27	-23	-26	6	53	48	-3	-10	0	33	11	-39	21	31	47	37	-20	65
60	9	1	-29	-49	-28	36	67	65	11	10	-4	6	18	10	1	23	43	62	-5	60
55	-17	-61	-22	36	-27	35	68	60	-6	-1	-22	6	22	-3	3	15	39	58	23	55
50	-22	-41	3	-34	-41	39	62	53	-6	1	-8	-7	11	-13	-7	18	29	65	42	50
45	-45	-37	32	3	38	52	60	59	-1	6	-17	-14	6	16	30	39	24	42	65	45
40	-30	-34	22	22	57	52	45	44	1	3	-35	-33	-6	28	31	29	20	26	44	40
35	-11	-1	8	65	55	44	31	15	7	-8	-44	-51	-36	15	1	2	10	21	41	35
30	7	-1	27	52	51	37	-6	-15	16	-7	-56	-55	-48	-17	-14	17	16	-2	14	30
25	12	0	33	53	46	28	-22	18	25	6	-47	-67	-52	-38	-5	16	26	23	19	25
20	-17	14	40	60	47	24	8	28	22	3	-36	-16	-57	-43	-14	16	30	37	41	20
15	15	54	55	57	43	-3	-5	13	16	12	-22	-19	-56	-58	-30	11	18	26	46	15
10	66	71	50	46	-6	-49	-44	-3	1	8	-14	-30	-36	-64	-52	-19	14	25	36	10
5	52	53	36	16	-40	-61	-49	-5	-9	-18	-21	-28	-29	-57	-63	-51	-16	21	19	5
0	16	37	23	-23	-62	-66	-35	48	-6	-31	-10	-43	-31	-44	-63	-63	-28	25	30	0
-5	20	38	23	-43	-70	-64	-40	12	12	-13	-5	-49	-29	-39	-66	-63	-33	29	33	-5
-10	37	38	-1	-47	-68	-49	10	26	12	-13	-16	-32	-42	-40	-68	-62	-43	28	43	-10
-15	27	32	5	-46	-72	-67	8	22	-25	-20	-17	-24	-32	-44	-69	-73	-34	12	30	-15
-20	5	14	-60	-78	-75	-56	-26	38	-25	-33	-11	-37	-32	-43	-63	-73	-48	-8	5	-20
-25	2	7	-75	-91	-72	-56	-42	40	51	-2	-6	-43	-41	-52	-62	-73	-54	-16	-10	-25
-30	-13	-21	-62	-77	-52	-37	-6	60	77	29	9	-45	-45	-49	-68	-66	-29	-20	-24	-30
-35	-38	-60	-25	-16	-22	-11	21	43	43	43	21	-18	-45	-37	-62	-46	-9	-25	-46	-35
-40	-36	-44	4	12	9	28	36	28	20	11	8	5	4	10	-50	-62	-19	-9	-41	-40
-45	-10	-27	-14	44	33	32	17	7	23	42	-32	-11	-3	-13	-49	-64	-13	20	-10	-45
-50	-22	-42	-3	40	36	49	38	12	7	42	32	-22	5	-20	-41	-42	-19	36	29	-50
-55	-34	-43	11	49	70	61	53	41	4	20	40	38	34	-19	-35	-41	-37	27	32	-55
-60	-33	-8	36	76	80	56	29	57	7	-5	25	34	46	31	-27	-34	-20	15	23	-60
-65	-20	6	47	69	65	46	34	43	6	-14	-3	30	44	24	-29	-42	-25	15	35	-65
-70	-4	26	50	57	31	32	21	38	9	-22	9	27	30	23	-58	-55	-34	6	43	-70
-75	2	19	34	38	25	59	52	44	15	-15	7	11	-19	11	-46	-49	-26	-12	1	-75
-80	-9	6	33	26	27	53	61	57	15	1	16	8	-25	-23	1	-25	-6	-17	-24	-80
-85	-10	-28	9	2	13	45	47	64	13	5	6	3	-2	23	-12	-27	-3	-7	-26	-85
-90	-3	-23	-3	-15	-12	1	27	58	13	0	16	0	-5	-3	-36	-30	-4	7	-23	-90
-95	8	12	-23	-31	-36	-18	21	12	7	24	21	0	-17	-50	-41	-27	7	-18	-16	-95
-100	59	23	-44	-44	-25	-11	0	2	2	41	6	-2	-33	-51	-54	-31	14	-8	-21	-100
-105	5	-3	-39	-15	-38	-51	-24	-3	15	37	26	2	-37	-38	-58	-40	1	-11	-25	-105
-110	15	-20	-45	-37	-61	-39	-25	-1	35	55	16	-13	-26	-14	-20	-35	-4	-7	-21	-110
-115	0	-24	-52	-52	-40	-34	-13	10	44	-12	-16	-23	-35	-16	-10	-13	-16	1	-13	-115
-120	-6	-41	-61	-12	2	-18	5	9	48	-15	-8	-30	-35	-18	-13	7	3	21	0	-120
-125	-33	-40	-38	2	25	2	-1	5	11	-17	-1	-14	-25	-27	-24	16	27	22	-23	-125
-130	-31	-26	-16	-17	-3	12	2	2	16	-27	-5	-12	-17	-14	-17	2	37	37	3	-130
-135	-19	-41	-42	-24	-10	1	3	-2	-11	-20	13	-7	-4	-11	-7	-1	35	27	-1	-135
-140	27	-20	-49	-29	-2	-1	6	2	-8	-4	17	-14	-15	-12	-8	-4	36	36	-5	-140
-145	34	-22	-51	-38	-12	-15	4	-10	-32	-16	9	-17	-29	0	1	-10	15	17	25	-145
-150	30	-12	-20	-12	-3	-11	4	-19	-41	-33	7	-18	-26	15	7	-24	19	24	32	-150
-155	22	4	12	21	35	40	20	-35	-37	-34	7	-9	-25	23	22	-15	2	-29	3	-155
-160	20	2	19	19	30	21	-11	-36	-26	-23	9	-3	-21	14	36	10	-2	-4	-12	-160
-165	18	-3	6	1	-1	-32	-54	-59	-17	-15	13	11	-3	13	49	22	25	-37	-10	-165
-170	-22	-37	-7	-18	-29	-36	-54	-24	-16	-13	18	15	4	1	49	26	12	-19	-2	-170
-175	-32	-37	-22	-19	-17	-11	-19	7	-17	-13	24	13	3	6	47	42	30	-17	-29	-175
-180	-10	-20	7	-13	-7	-4	6	23	2	-3	4	17	-12	-7	46	53	47	-20	-29	-180

Figure 3.3. Lagged correlation (x100).
December OLR against following January All_area rainfall.
Data period: 1974–1986. Bias in OLR data removed.
Shading represents approximate location of rainfall area.

	LATITIDE --->																		
LONG.	-41	-37	-33	-29	-24	-20	-15	-10	-5	0	+5	+10	+15	+20	+24	+29	+33	+37	+41	LONG.
180	-13	-21	0	9	-2	-15	24	58	53	20	-10	-15	0	20	-8	-19	-24	27	8	180
175	5	-15	-22	-29	-11	20	20	47	39	16	-7	-15	7	11	10	-5	-22	26	31	175
170	17	-14	-45	-35	-3	15	14	33	31	16	-3	-14	-5	14	5	2	-20	-5	35	170
165	0	-48	-48	-12	3	14	13	13	19	19	0	-19	-19	8	1	0	-14	-1	5	165
160	-22	-25	-7	3	18	18	7	21	19	24	6	-28	-19	-23	-16	-21	-25	7	9	160
155	-26	-24	3	24	37	10	4	23	21	29	19	-30	-27	-48	-26	-20	-43	-38	-7	155
150	-41	-18	-10	12	24	10	24	28	24	27	21	-12	-29	-26	-25	-2	-3	-34	-50	150
145	-47	-24	2	29	26	12	23	18	24	27	20	-4	-7	-1	-25	-11	8	0	-12	145
140	-35	-18	18	21	10	0	9	18	27	26	27	21	2	14	-4	-16	9	22	31	140
135	-33	-22	4	34	26	0	-1	19	23	25	34	41	5	9	11	1	-5	28	28	135
130	-24	-1	28	60	29	1	-29	-8	17	26	48	62	1	-4	-3	6	4	40	36	130
125	-5	31	63	45	16	-4	-39	-36	3	20	52	69	-11	-13	-18	8	33	52	41	125
120	30	48	72	34	11	-9	-43	-35	-20	6	41	55	-4	-27	-37	-19	28	53	51	120
115	31	53	68	34	15	-6	-56	-46	-21	-11	29	31	-16	-21	-34	-16	12	42	56	115
110	44	59	53	33	14	-15	-70	-42	-35	-23	35	61	-19	-13	-20	-14	12	28	48	110
105	45	55	57	36	21	-42	-76	-53	-39	-23	40	80	45	-3	-28	-34	11	25	43	105
100	38	56	37	29	-3	-56	-72	-53	-53	-31	38	87	63	20	-18	-22	29	33	27	100
95	49	55	22	4	-13	-49	-72	-54	-72	-49	39	80	57	27	12	10	26	43	47	95
90	45	31	10	-8	-32	-47	-75	-62	-85	-26	6	47	24	37	22	24	19	28	26	90
85	36	27	-18	-41	-33	-43	-57	-51	-78	2	17	17	39	28	39	34	7	29	18	85
80	9	-17	-36	-38	-49	-31	-5	8	36	33	51	24	21	31	24	39	22	11	13	80
75	-33	-22	-8	-46	-78	-28	35	19	42	40	41	28	5	-9	-4	24	29	12	11	75
70	-20	-8	31	13	-31	-3	28	53	72	62	37	14	-10	-22	-16	-12	-1	-5	3	70
65	8	18	50	52	72	46	45	51	75	43	22	16	-10	-7	-5	-27	-10	-22	6	65
60	8	34	39	15	28	45	49	19	9	21	12	-4	-8	9	9	-16	-14	-13	-3	60
55	5	33	50	26	25	36	33	-2	-15	2	18	-9	-10	21	16	5	-24	3	-17	55
50	11	40	51	20	13	36	29	9	3	12	37	0	-7	-2	19	30	-22	-61	-28	50
45	18	26	35	6	47	63	52	19	-5	-7	-19	3	-14	-13	-8	17	8	-7	8	45
40	19	30	28	22	59	38	-1	-17	-16	7	30	18	-29	-40	-28	-27	3	29	29	40
35	10	33	21	13	25	11	-21	-13	4	15	60	16	-6	-45	-36	-32	10	55	73	35
30	2	13	14	22	27	20	-6	-9	4	11	53	37	18	-27	-14	-18	-16	32	83	30
25	-7	1	55	31	26	12	-14	10	-6	26	30	49	34	-27	-50	-52	-56	0	49	25
20	-17	35	65	16	-2	-36	-28	-7	-4	28	30	53	44	-18	-56	-65	-54	-12	30	20
15	-20	31	21	8	-40	-43	-33	-19	-7	3	30	37	41	-15	-74	-74	-58	-15	23	15
10	-9	20	18	-24	-44	-46	-30	-31	-20	-11	26	-3	35	-18	-71	-89	-60	-16	30	10
5	-20	22	37	-48	-58	-52	-52	-34	-4	-27	1	-39	27	-12	-71	-88	-72	-29	0	5
0	-7	23	40	-62	-64	-59	-39	-20	-2	-28	-21	-45	6	-13	-66	-86	-73	-11	-4	0
-5	22	36	6	-54	-58	-52	-30	-11	24	-21	-35	-60	-22	-9	-46	-79	-72	4	29	-5
-10	21	23	0	-53	-68	-53	3	-22	23	18	-6	-53	-32	-23	-39	-70	-53	24	49	-10
-15	40	48	4	-42	-40	-14	28	5	-43	41	14	-46	-49	-37	-35	-74	-63	13	38	-15
-20	48	42	-29	-55	20	26	11	-13	-3	11	-1	-54	-62	-48	-49	-68	-54	22	60	-20
-25	42	29	-35	[redacted]	-16	-31	-50	11	49	-2	-13	-66	-67	-63	-56	-70	-46	19	37	-25
-30	37	-1	-50	-4	-54	-42	-39	21	47	50	8	-68	-64	-60	-59	-74	-36	-1	12	-30
-35	16	-22	-41	-59	-40	-27	-12	22	32	48	42	-60	-63	-54	-56	-70	-52	-46	-29	-35
-40	29	-4	-43	-35	1	20	39	51	62	44	32	-26	-35	-28	-56	-87	-76	-60	-25	-40
-45	10	-19	-28	-3	-9	-37	19	68	54	41	-5	-37	-34	-55	-69	-83	-84	-75	-61	-45
-50	6	-8	-27	-24	-3	15	29	28	29	41	40	-22	-15	-16	-53	-62	-69	-56	-38	-50
-55	-3	-12	0	14	25	16	-1	55	35	36	37	49	71	-5	-10	-59	-71	-57	-41	-55
-60	-17	-24	42	53	45	27	19	75	36	44	35	50	55	66	24	-51	-58	-48	-40	-60
-65	-20	16	60	44	41	9	40	69	39	33	21	61	41	52	36	-39	-37	-32	-20	-65
-70	-10	43	55	37	42	24	47	50	43	26	17	47	41	27	-36	-33	-24	-13	-9	-70
-75	-6	54	45	40	25	23	41	52	57	18	30	45	28	2	-34	-33	1	-17	-32	-75
-80	14	67	47	33	19	21	43	59	62	15	38	25	33	-7	-26	-19	25	-31	-55	-80
-85	29	60	51	34	21	14	32	59	49	17	38	33	17	2	-3	-12	18	-29	-58	-85
-90	8	54	39	16	6	36	45	41	35	-10	7	2	14	25	32	-11	0	-26	-64	-90
-95	10	44	15	-7	-1	28	15	-3	18	-7	-30	-23	-17	-9	38	16	18	-53	-59	-95
-100	4	12	0	-3	11	5	-22	-4	-23	6	-17	-24	-48	-34	-2	15	22	-47	-58	-100
-105	2	15	15	18	24	1	-18	2	-44	31	17	-35	-60	-55	-11	15	-15	-65	-64	-105
-110	2	20	33	29	37	4	-9	-7	-17	22	17	-54	-63	-63	-37	36	-8	-52	-47	-110
-115	22	33	61	46	13	-32	-16	-39	-29	8	-24	-41	-71	-75	-64	-30	-35	-56	-46	-115
-120	13	34	38	33	13	-36	-21	-39	-11	-18	-25	-34	-52	-63	-74	-55	-23	-38	-52	-120
-125	6	37	37	36	25	2	-38	-44	-21	-17	-18	-21	-22	-34	-49	-60	-38	-28	-55	-125
-130	3	37	65	46	12	22	-38	-51	-12	-15	-11	-1	-3	-5	-15	-34	-29	-21	-42	-130
-135	24	81	69	12	-37	-44	-59	-57	-30	-7	-17	-1	31	11	9	-17	-45	-25	-14	-135
-140	40	59	39	-32	-59	-71	-58	-30	-2	6	-6	27	56	33	4	-8	-24	-41	1	-140
-145	24	47	17	-43	-83	-82	-49	-25	21	20	30	50	60	40	6	-15	-18	-27	-10	-145
-150	26	29	9	-35	-66	-68	-32	6	42	46	25	27	56	48	12	-13	-18	-9	-9	-150
-155	38	41	19	6	-12	-36	-37	-1	57	49	7	10	57	57	21	7	-21	-17	-19	-155
-160	29	33	13	-8	-12	-40	-48	23	66	45	-13	12	55	-14	10	26	14	4	-50	-160
-165	48	16	0	-3	4	-19	-6	47	70	45	-16	4	26	-52	-48	2	14	6	-38	-165
-170	45	29	13	14	9	-10	33	54	72	36	-5	-2	0	-43	-43	-18	3	9	-25	-170
-175	35	3	10	14	18	3	38	59	61	31	6	-3	-1	0	-21	-21	-15	15	-13	-175
-180	-13	-21	0	9	-2	-15	24	58	53	20	-10	-15	0	20	-8	-19	-24	27	8	-180

Figure 3.4. Lagged correlation (x100).
November OLR against following January All-area rainfall.
Data period: 1974–1986. Bias in OLR data removed.
Shading represents approximale location of rainfall area.

	LATITIDE --->																	
LONG.	-41	-37	-33	-29	-24	-20	-15	-10	-5	0	+5	+10	+15	+20	+24	+29	+33	+37	+41	LONG.
180	41	22	28	24	-8	-34	-23	44	39	34	42	64	41	15	-1	4	48	57	38	180
175	36	0	25	15	-22	-45	-19	45	50	33	46	51	61	30	10	-6	11	64	35	175
170	4	9	16	8	-23	-43	3	51	48	30	56	55	48	19	6	-5	22	49	21	170
165	-24	6	10	-2	-33	-69	23	57	41	34	53	70	15	23	11	-18	-14	54	26	165
160	-12	4	-18	-14	-40	-46	27	49	36	35	49	71	-1	27	-1	-44	-31	-2	17	160
155	-38	-33	-43	-38	-36	-12	14	38	29	28	29	30	-18	-8	-1	-31	-18	2	-27	155
150	-39	-49	-49	-29	-11	16	19	35	25	24	24	43	-17	-33	-8	10	17	29	-11	150
145	-51	-30	-19	-10	23	38	21	29	25	25	31	34	-9	-22	-8	6	24	24	-3	145
140	-29	-1	-8	5	22	32	18	24	25	27	33	43	-34	-52	-36	2	33	39	24	140
135	-15	-10	-34	4	24	24	15	13	16	24	36	45	-10	-33	-51	-8	56	55	20	135
130	-17	-17	-36	-5	16	21	-1	4	3	15	39	18	-2	-6	-32	8	65	72	48	130
125	-8	-20	-22	-5	32	27	-3	-5	-26	11	32	40	14	-20	4	30	60	72	56	125
120	-10	-47	-21	6	46	15	-50	-49	-46	11	31	28	-7	-8	30	36	62	64	46	120
115	-38	-38	-14	29	34	-13	-75	-72	-61	3	35	-11	4	-21	19	31	41	45	32	115
110	-56	-26	20	60	35	-44	-82	-75	-77	-26	31	-43	-2	3	14	42	44	38	23	110
105	-35	1	42	65	19	-42	-67	-70	-75	-25	28	-21	3	22	6	21	37	41	22	105
100	-24	0	33	41	3	-51	-64	-68	-72	-58	34	4	2	4	-5	10	28	30	17	100
95	-32	-1	31	22	-26	-61	-68	-67	-80	-61	37	12	-10	-5	11	22	24	39	41	95
90	-25	2	36	6	-50	-73	-75	-78	-79	-26	48	1	-31	-14	-4	7	22	22	17	90
85	-44	-16	18	-8	-47	-70	-85	-78	-42	-13	63	6	-37	-43	-15	-5	9	33	24	85
80	-57	-23	13	-6	-26	-76	-74	-2	-1	17	57	14	-51	-47	-4	27	57	65	29	80
75	-62	-32	0	3	-51	-83	26	36	45	14	34	-20	-71	-24	-9	28	70	61	32	75
70	-43	-33	3	1	-31	-7	50	66	43	22	-5	-28	-22	8	34	26	53	47	11	70
65	-13	23	34	43	26	22	40	54	-1	50	10	14	15	8	42	31	34	42	10	65
60	-11	26	31	27	20	16	42	32	16	34	13	35	4	4	9	54	43	40	13	60
55	-29	4	40	19	8	9	10	2	12	26	1	-1	1	25	11	45	63	56	22	55
50	-19	19	33	27	7	-1	5	7	8	15	25	2	22	30	24	29	61	47	30	50
45	-14	3	26	14	2	9	17	42	10	18	20	-7	17	26	-6	-11	52	53	46	45
40	-18	20	16	25	39	26	15	11	-30	-11	6	14	16	12	0	4	7	25	50	40
35	-6	24	21	23	35	20	15	-6	-43	-25	-2	23	25	25	6	12	0	-2	22	35
30	-16	14	2	17	17	-15	-4	-12	-29	8	20	41	26	19	-19	-7	-21	-30	11	30
25	-15	-13	-19	16	-22	-29	-9	-5	23	24	16	15	37	5	-21	-27	-11	5	20	25
20	-13	-29	12	12	-53	-30	-27	-15	10	6	42	28	24	17	9	10	8	25	37	20
15	2	5	20	-12	-52	-32	-45	-37	-24	-9	55	33	-1	19	4	50	40	30	25	15
10	-13	-11	-5	-45	-32	-37	-48	-39	-35	-9	22	-1	-15	-23	-13	45	53	38	23	10
5	-16	-11	-40	-45	-21	-40	-42	-43	-34	-40	39	-13	-22	-32	-25	-14	8	27	-4	5
0	-9	13	-20	1	10	-14	-30	-26	-2	-17	45	-36	-35	-44	-45	-54	-17	2	11	0
-5	0	0	14	21	28	1	-11	-25	2	-12	54	-62	-58	-59	-53	-63	-45	-10	-31	-5
-10	-9	-15	-4	9	19	-14	15	-5	-21	-38	-47	-42	-49	-67	-72	-54	-42	-5	-30	-10
-15	-13	-20	-21	-6	-45	45	-22	-15	3	41	-57	2	-27	-62	-81	-50	30	39	-15	-15
-20	-25	-10	-31	-43	-51	23	56	18	33	31	-10	5	-40	-52	-80	-54	56	43	-14	-20
-25	-23	-13	-28	-36	1	49	60	38	13	12	-14	2	-30	-56	-79	-76	41	38	-28	-25
-30	-4	27	-25	-18	1	45	56	35	37	38	23	21	-11	-44	-65	-74	49	35	-7	-30
-35	14	28	-5	17	30	17	13	20	40	45	28	5	-7	-20	-44	-57	48	47	16	-35
-40	22	-9	15	60	78	19	6	21	24	6	8	12	20	19	-8	-41	-8	39	39	-40
-45	9	18	46	67	34	9	51	13	6	17	-4	6	-13	-19	-15	-29	-9	23	30	-45
-50	-24	-2	36	73	36	18	34	-14	-7	19	36	-7	-16	-30	-3	5	-14	-9	-10	-50
-55	-36	13	55	69	56	52	16	-4	14	18	47	13	11	34	9	0	-31	-23	-16	-55
-60	-33	28	70	77	62	37	22	17	31	24	61	37	20	17	-4	-18	-28	-37	-43	-60
-65	-24	41	76	83	51	40	41	14	50	31	56	36	18	25	14	-40	-26	-28	-32	-65
-70	-2	37	71	81	64	58	74	48	72	36	51	47	18	16	10	-30	-21	-26	-21	-70
-75	-24	1	43	79	40	51	50	50	62	42	41	31	14	10	12	6	17	-32	-32	-75
-80	-19	30	66	59	24	8	18	-14	3	24	37	17	3	-17	8	26	25	-39	-54	-80
-85	-18	49	60	55	12	-4	6	5	-3	23	42	39	-20	52	-18	42	51	24	-30	-85
-90	-8	17	41	22	-22	-51	-20	9	9	42	50	42	17	-17	39	26	54	5	-9	-90
-95	-36	-9	28	17	-36	-44	-28	-10	-1	51	36	40	44	21	-15	12	58	-39	-1	-95
-100	-18	11	9	6	-20	-25	-14	1	-4	0	-29	25	40	42	19	15	9	-51	-14	-100
-105	-29	-4	15	35	12	-2	37	10	4	35	13	37	22	25	18	-13	-37	-38	2	-105
-110	-34	-14	34	34	45	38	42	-1	5	46	31	40	22	15	25	9	-31	-38	4	-110
-115	-35	8	61	27	15	43	37	-2	10	-8	6	37	39	21	9	12	-7	-24	13	-115
-120	-25	39	46	6	19	44	30	10	6	10	10	33	37	35	12	8	11	1	12	-120
-125	-41	37	31	23	20	32	23	-6	-15	0	2	16	47	49	39	32	43	28	26	-125
-130	-19	-4	-9	24	33	27	0	-20	-13	-2	-2	23	47	34	36	40	40	11	27	-130
-135	-25	-9	4	7	16	9	-2	-9	-11	12	-9	17	25	10	10	29	44	37	30	-135
-140	-14	33	26	18	18	20	8	-15	19	0	-8	24	30	13	10	21	37	38	39	-140
-145	-15	29	36	49	48	29	12	-45	-8	12	0	-31	-25	-36	-19	9	42	35	26	-145
-150	-31	40	44	38	31	31	10	-23	0	44	-6	-51	-46	-44	-52	-25	29	60	22	-150
-155	-16	39	29	14	19	31	-21	-27	12	38	18	-18	-31	-46	-45	-34	11	37	21	-155
-160	5	25	40	26	14	2	-46	-38	12	31	58	11	11	-32	-41	-33	17	40	23	-160
-165	25	35	28	12	15	-20	-29	-31	21	33	54	36	29	0	-33	-25	23	43	13	-165
-170	24	39	3	12	2	-33	-20	-6	47	34	54	50	34	8	-22	-20	22	48	36	-170
-175	23	7	11	3	-10	-33	-3	54	47	35	56	59	33	5	-6	16	40	59	47	-175
-180	41	22	28	24	-8	-34	-23	44	39	34	42	64	41	15	-1	4	48	57	38	-180

Figure 3.5. Lagged correlation (x100).
October OLR against following January All-Area rainfall.
Data period: 1974-1986. Bias in OLR data removed.
Shading represents approximale location of rainfall area.

	LATITIDE --->																		
LONG.	-41	-37	-33	-29	-24	-20	-15	-10	-5	0	+5	+10	+15	+20	+24	+29	+33	+37	+41	LONG.
180	2	-55	-69	-62	-36	-25	36	60	58	44	55	11	41	26	48	35	21	9	-64	180
175	-29	-65	-74	-60	-36	-31	21	45	48	35	54	17	32	38	53	55	30	4	-45	175
170	-46	-60	-79	-62	-36	24	40	50	43	31	53	-1	13	36	51	47	63	57	3	170
165	-38	-40	-52	-34	15	31	40	40	42	33	29	-43	-13	28	35	26	43	49	30	165
160	-22	-44	-47	17	35	27	22	29	44	33	37	-32	-13	4	17	10	15	19	17	160
155	-51	-43	-28	44	35	7	-5	16	45	37	50	-2	26	-31	-4	16	8	-6	-2	155
150	-42	-34	25	47	32	1	-18	22	45	36	47	1	23	-17	13	28	28	0	-5	150
145	-41	-38	28	44	37	-7	-27	35	36	29	40	-23	20	17	28	33	39	16	-4	145
140	12	31	33	42	23	-4	-24	28	22	25	39	20	12	27	28	36	34	10	5	140
135	32	49	29	36	4	-6	-2	18	9	27	36	49	-3	18	13	20	19	-8	5	135
130	20	3	0	4	-10	-8	5	28	-3	25	34	25	-15	-30	8	22	23	12	20	130
125	-22	-61	-3	22	13	8	-50	4	-17	32	39	1	-47	-44	-29	24	36	34	15	125
120	-47	-40	36	47	33	-5	-53	-20	-45	-3	42	1	-35	-29	-38	-25	51	44	17	120
115	-34	10	50	41	25	-36	-55	-32	-53	-39	28	-31	-40	-18	-13	1	63	60	29	115
110	0	31	43	33	9	-47	-62	-49	-69	-61	11	-12	-26	-13	7	17	42	54	39	110
105	-12	16	39	35	-3	-65	-68	-56	-73	-74	27	17	5	27	12	-2	33	62	63	105
100	-25	8	47	24	-22	-80	-68	-58	-69	-60	21	47	48	17	-12	10	36	68	66	100
95	-13	28	22	-5	-19	-77	-61	-60	-74	-42	35	75	58	16	-30	29	41	61	65	95
90	-7	24	15	-10	-28	-68	-63	-67	-73	25	57	81	21	18	-41	-3	15	53	56	90
85	-16	13	10	-35	-36	-57	-73	-61	-48	44	75	71	-12	13	6	6	-10	11	36	85
80	-15	11	-6	-43	-30	-46	-51	22	28	38	81	41	-25	37	35	33	9	14	38	80
75	0	7	-18	-38	-43	-43	17	38	38	49	76	53	16	42	23	17	18	-15	-2	75
70	14	18	-5	-47	-27	-10	29	31	35	59	51	36	9	22	28	32	18	20	-27	70
65	28	5	-13	-32	-18	4	34	37	48	52	59	29	1	21	57	51	42	-29	-26	65
60	32	4	-3	-44	-42	11	50	27	34	54	25	4	-27	22	26	61	69	49	14	60
55	32	32	19	32	-27	44	57	32	45	48	18	-2	-39	-7	73	69	72	80	66	55
50	29	37	10	-33	-22	28	47	30	38	23	36	6	-50	-17	40	64	69	76	72	50
45	29	44	21	-26	-13	36	8	6	11	26	26	18	-7	1	33	56	69	50	53	45
40	44	44	23	-21	-12	2	-25	-10	-23	20	35	36	30	9	2	18	31	13	33	40
35	38	45	44	-18	-29	-21	-5	15	21	25	34	52	24	47	14	7	24	-8	1	35
30	66	79	48	-45	-45	-17	9	45	45	26	35	58	53	53	30	7	-3	-14	2	30
25	58	79	-64	-77	-48	-1	20	43	44	25	31	49	53	58	32	5	-27	-24	6	25
20	44	21	-69	-79	-42	11	20	40	39	5	41	49	55	58	56	-3	-11	-32	-34	20
15	7	8	-56	-65	-29	3	8	17	33	36	56	42	28	58	53	46	30	-17	-38	15
10	-35	-7	-33	-48	-30	-26	-21	-56	-3	40	31	-2	15	30	47	48	42	7	-1	10
5	30	7	-41	-33	-29	-26	-35	-57	-17	8	35	-7	8	16	27	26	37	10	-1	5
0	9	-43	-42	-27	-27	-38	-39	-50	-6	-11	19	-21	5	5	14	0	14	11	5	0
-5	-9	-29	-39	-34	-29	-49	-41	-33	17	11	-16	-37	-10	-9	14	-9	8	23	13	-5
-10	-38	-36	-30	-17	-13	-50	-83	-22	17	6	-19	-20	-13	-22	14	-10	4	23	17	-10
-15	-51	-43	-11	3	-26	-11	-3	3	16	15	33	-10	-12	-27	-10	3	22	22	7	-15
-20	-41	-34	-24	-16	-14	11	45	33	27	36	60	2	-8	-30	-34	-5	25	15	2	-20
-25	-39	-39	14	-7	-1	44	65	67	46	73	0	2	-6	-52	-48	-31	18	-5	-28	-25
-30	19	21	7	-21	29	56	44	69	67	64	31	-22	16	-42	-46	-33	25	10	-14	-30
-35	26	3	-13	9	50	39	41	55	33	29	21	32	20	12	15	-2	28	16	-10	-35
-40	2	-16	-20	28	35	26	45	15	40	47	23	8	13	34	34	-3	-1	34	-1	-40
-45	0	-22	-20	48	33	48	44	37	46	33	25	22	-24	-15	16	12	17	40	-12	-45
-50	-7	-45	1	45	50	51	32	45	55	33	27	-6	-35	-56	-12	28	28	5	-17	-50
-55	11	1	30	42	50	45	28	42	42	29	31	24	-22	52	10	20	11	3	-7	-55
-60	18	-2	-31	3	20	27	27	58	47	30	31	20	-24	-44	2	6	7	0	-9	-60
-65	34	-26	-23	0	0	33	50	55	53	57	17	3	-40	-47	-22	2	9	2	-8	-65
-70	36	-30	-21	-30	-22	22	16	33	63	67	8	-25	-29	-20	-39	4	25	2	3	-70
-75	14	-15	-6	-19	5	-3	-19	-1	46	72	17	-42	-77	21	5	-14	57	45	9	-75
-80	38	3	-9	18	28	-63	-62	-28	38	60	22	-39	-56	-43	-23	7	32	28	-27	-80
-85	14	-20	-1	29	14	-43	-48	-14	24	38	26	-21	-52	28	-15	29	49	49	-16	-85
-90	16	-22	-19	12	-25	-14	-9	-19	24	29	-4	-36	-31	-27	-4	8	31	43	-2	-90
-95	6	-41	-21	-12	-34	10	-6	-40	-5	35	5	-24	-12	22	-18	-17	19	6	-2	-95
-100	37	13	-15	-39	-22	-21	-34	-46	-24	61	-8	-21	-20	25	-8	-27	-2	24	-13	-100
-105	44	45	-15	-32	-14	-43	-58	-49	-19	43	1	-13	5	28	3	-37	-59	-12	-10	-105
-110	57	37	-17	-48	-47	-63	-72	-55	-34	-4	7	-10	2	2	-5	3	-23	-20	-23	-110
-115	55	21	-63	-78	-79	-59	-65	-53	-27	-28	-15	-1	5	-22	-39	-13	-26	-26	-17	-115
-120	28	-21	-62	-59	-68	-60	-47	-41	-34	-19	-12	-6	-5	-31	-44	-28	-27	-28	-29	-120
-125	-4	-21	-35	-67	-78	-66	-62	-43	-43	-30	-4	14	-11	-33	-35	-16	-24	-22	-31	-125
-130	-14	-30	-46	-77	-80	-60	-38	-41	-45	-4	10	15	-15	-46	-41	-19	-42	-33	-34	-130
-135	-70	-51	-72	-71	-64	-39	-27	-47	-58	-6	32	6	-9	10	28	31	-24	-28	-15	-135
-140	-69	-76	-62	-50	-45	-40	-27	-39	-20	14	42	20	14	44	49	42	-6	-33	-17	-140
-145	-56	-26	-23	-32	-53	-46	-23	12	23	31	15	22	28	39	48	22	12	-28	-34	-145
-150	-48	0	6	-32	-47	-43	34	35	43	49	34	9	25	16	-4	13	13	-27	-50	-150
-155	-20	3	-15	-49	-42	-16	28	37	60	45	36	-17	12	-5	-50	-40	0	-25	-51	-155
-160	2	12	-14	-20	-13	21	23	71	57	41	16	-15	2	-20	-64	-66	-45	-32	-42	-160
-165	-39	2	-7	-22	3	10	29	68	64	35	13	-49	-2	-33	-52	-59	-60	-42	-46	-165
-170	46	23	-39	-38	-14	12	35	66	69	41	29	-48	-10	-22	-19	-39	-58	-27	-42	-170
-175	35	-27	-68	-53	-23	4	50	82	74	53	50	-16	3	-3	34	22	5	-14	-78	-175
-180	2	-55	-69	-62	-36	-25	36	60	58	44	55	11	41	26	48	35	21	9	-64	-180

Figure 3.6. Simultaneous correlation (x100).
February OLR against February All-Area rainfall.
Data period: 1974-1986. Bias in OLR data removed.
Shading represents approximate location of rainfall area.

LONG.	-41	-37	-33	-29	-24	-20	-15	-10	-5	0	+5	+10	+15	+20	+24	+29	+33	+37	+41	LONG.
180	23	-2	-24	-48	-58	-59	-51	12	28	8	-36	-37	-43	-81	-61	-25	2	31	20	180
175	-1	-5	-45	-59	-57	-48	-13	33	35	29	-5	-21	-43	-81	-71	-47	-18	10	14	175
170	-1	39	-26	-43	-42	-25	26	37	41	35	-1	-2	-22	-76	-63	-35	24	-14	26	170
165	-26	11	-43	-41	-27	11	21	27	43	41	13	-1	-28	-41	-45	4	49	2	-30	165
160	16	-18	-46	-26	-6	4	13	28	43	41	24	-23	-50	-53	-40	8	72	37	-32	160
155	-17	-45	-32	0	16	24	17	34	43	37	29	-36	-55	-50	-39	2	55	39	-32	155
150	-16	-26	4	21	42	40	38	41	41	37	10	-48	-56	-46	-42	4	45	19	-33	150
145	-2	13	40	47	50	54	49	47	43	38	1	-50	-57	-46	-38	4	56	42	19	145
140	29	33	43	57	51	45	45	53	41	37	8	-44	-46	-40	-31	9	39	44	24	140
135	35	26	61	67	41	21	24	44	33	43	18	-41	-39	-30	-39	-2	40	51	43	135
130	45	65	61	53	44	7	9	42	33	45	10	-16	-33	-23	-36	-5	42	49	48	130
125	52	45	44	46	19	-36	16	29	35	42	9	4	-35	-41	-41	-21	41	50	44	125
120	26	24	39	40	-2	-23	4	16	22	37	25	-5	-32	-46	-52	-37	42	33	31	120
115	-11	24	54	57	3	17	23	-1	8	27	25	-8	-20	-40	-49	-39	-7	0	17	115
110	-2	50	76	54	25	19	25	7	25	34	28	-4	-2	-6	-50	-49	-26	7	-6	110
105	-8	49	60	41	18	3	32	27	23	47	31	23	22	4	-40	-35	-26	4	-22	105
100	-1	38	45	33	20	11	22	46	44	48	46	48	42	-4	-25	-17	-7	7	5	100
95	5	23	30	27	11	-35	-24	41	48	41	51	60	34	17	26	28	20	29	21	95
90	4	20	23	20	1	-51	-49	4	49	50	63	57	22	25	41	54	42	23	8	90
85	11	45	34	15	0	-35	-48	-1	35	38	71	52	26	38	52	60	47	38	-7	85
80	19	34	11	2	-8	-37	-40	14	51	51	58	50	43	43	39	42	38	47	13	80
75	21	9	-11	-17	-33	-47	-22	21	30	49	49	51	48	33	41	38	41	50	30	75
70	-2	-20	-36	-38	-50	-38	5	47	48	39	33	9	32	24	39	41	36	42	36	70
65	-21	-21	-20	-13	-29	-9	41	47	45	20	19	13	-14	19	34	33	15	27	60	65
60	-6	-2	30	11	18	28	30	32	9	1	4	-4	-47	7	44	45	29	19	15	60
55	23	19	49	50	34	2	4	5	-17	-31	-19	-6	-61	-23	29	50	24	24	16	55
50	44	32	49	37	-1	-36	-11	-14	-19	-21	-42	-3	-58	-22	31	58	46	15	8	50
45	4	33	35	-6	-26	-21	-1	1	-17	-28	-45	-9	-25	-9	37	49	46	18	0	45
40	20	25	-2	-37	-22	11	14	5	-16	-25	-45	-25	-29	16	37	39	51	32	-11	40
35	7	17	-22	-26	-6	11	1	3	-5	-17	-27	-37	-46	1	37	42	43	45	13	35
30	13	12	-17	-2	17	17	-18	-6	2	-26	-12	-30	-47	-15	33	34	33	35	25	30
25	10	9	2	22	24	-7	-20	-2	1	-24	-16	-29	-25	-29	24	31	19	18	0	25
20	6	13	11	40	48	-6	-7	5	39	-26	-11	-10	-20	-40	9	34	26	22	-2	20
15	-7	-4	8	19	-8	-11	12	12	38	6	-23	-9	-26	-48	-46	17	18	24	7	15
10	-24	-23	-5	-15	-29	-17	16	31	2	7	-24	-25	-22	-36	-59	-40	-1	8	4	10
5	-18	-26	-9	-13	-34	-39	-12	25	1	-18	-37	-18	-25	-31	-41	-54	-41	-11	-2	5
0	-5	-25	-11	-36	-47	-33	0	3	5	-17	-31	-38	-31	-38	-38	-61	-43	-2	25	0
-5	-21	-7	-26	-45	-48	-5	18	24	13	-4	-26	-44	-34	-43	-39	-58	-52	11	36	-5
-10	2	-8	-22	-40	-33	-13	16	47	-9	-13	-33	-50	-45	-47	-43	-59	-58	11	44	-10
-15	11	2	-4	-54	-51	-36	-22	28	3	-6	-26	-50	-52	-53	-55	-54	-18	32	47	-15
-20	12	-8	-78	-80	-49	-46	-40	25	-9	-24	-24	-57	-60	-58	-61	-53	-11	51	49	-20
-25	30	4	-76	-77	-54	-44	-32	31	-6	-26	-24	-62	-62	-54	-62	-55	-9	15	33	-25
-30	45	9	-59	-60	-59	-58	-40	39	22	-13	-24	-49	-57	-49	-59	-55	-5	8	35	-30
-35	76	-18	-36	-30	-36	-10	-5	21	-18	-7	12	-40	-45	-42	-52	-54	-15	-24	3	-35
-40	33	-18	25	29	0	44	36	6	-32	-34	8	2	-12	4	-45	-60	-35	-35	-13	-40
-45	-15	-40	-9	7	21	13	-14	-16	-40	-27	-56	-4	-2	-11	-35	-55	-38	-29	-43	-45
-50	-40	-33	-29	17	38	7	-11	10	-61	-37	-40	-36	22	-1	-28	-44	-34	-38	-56	-50
-55	-47	-33	-3	30	17	-20	-2	41	-17	-42	-39	-6	45	15	-7	-35	-35	-49	-69	-55
-60	-38	-20	27	24	18	10	9	37	5	-43	-27	-13	4	41	21	-26	-28	-42	-71	-60
-65	-40	-30	9	8	19	26	17	43	-17	-28	7	2	-5	48	34	-8	-18	-47	-67	-65
-70	-41	-41	17	36	47	47	32	43	-4	-16	6	17	-4	43	10	-4	-16	-40	-63	-70
-75	-44	-34	53	61	61	53	43	50	-2	-17	-3	29	-13	12	4	-4	-5	-22	-57	-75
-80	-47	-22	60	59	58	59	55	61	5	4	5	27	38	27	28	7	24	-21	-48	-80
-85	-34	-17	44	54	56	67	49	53	10	21	21	22	41	76	43	15	41	-11	-46	-85
-90	-40	-22	55	51	42	62	49	44	4	3	19	18	30	80	16	0	29	-4	-43	-90
-95	-42	0	55	32	11	48	48	38	12	16	1	11	24	17	-22	-28	18	-26	-32	-95
-100	-20	31	40	16	1	13	27	26	16	14	-2	10	-12	3	-7	-7	8	-27	-25	-100
-105	-25	20	32	26	44	10	19	29	11	8	3	3	-42	-3	11	4	-25	-26	-26	-105
-110	-6	31	49	52	49	27	37	15	19	0	-15	-4	-5	18	42	27	-32	-20	-14	-110
-115	16	51	50	34	10	-6	-1	17	0	-6	-8	7	12	26	47	12	-41	-43	-16	-115
-120	29	49	0	20	25	-25	-14	36	14	0	6	11	6	19	46	38	-33	-50	-36	-120
-125	31	22	2	3	24	-27	-27	18	1	-15	-10	8	-3	11	44	43	-3	-18	-26	-125
-130	31	16	-4	-10	8	-32	-48	10	43	-21	-21	8	15	24	59	49	-15	-33	-23	-130
-135	39	10	-45	-19	-25	-50	-50	7	15	-18	-10	13	16	15	57	56	-26	-6	-11	-135
-140	40	-27	-64	-38	-46	-50	-34	-10	-8	-22	-16	-12	-1	1	50	61	-5	-14	4	-140
-145	46	-19	-64	-59	-63	-44	-28	-48	-46	-27	-22	-19	-13	-20	25	60	45	17	-42	-145
-150	24	-29	-60	-75	-65	-10	-10	-43	-42	-31	-32	-27	-16	-23	-9	53	49	42	-60	-150
-155	-3	-23	-61	-78	-35	22	14	-44	-14	-43	-27	-10	-25	-23	-38	43	36	30	-51	-155
-160	-33	-40	-74	-74	-12	17	13	-22	-11	-33	-26	-4	-28	-28	-22	16	26	26	16	-160
-165	-26	-27	-55	-45	17	17	-1	14	6	-29	-33	-14	-29	-47	-24	2	20	20	43	-165
-170	-11	-9	-27	-26	12	11	-7	-8	3	-28	-37	-35	-32	-50	-19	10	25	21	7	-170
-175	7	6	-20	-28	-14	-36	-47	-14	19	-7	-38	-49	-42	-64	-50	-12	-8	34	2	-175
-180	23	-2	-24	-48	-58	-59	-51	12	28	8	-36	-37	-43	-81	-61	-25	2	31	20	-180

LATITIDE --->

Figure 3.7. Lagged correlation (x100).
December OLR against following February All-Area rainfall.
Data period: 1974–1986. Bias in OLR data removed.
Shading represents approximate location of rainfall area.

LONG.	-41	-37	-33	-29	-24	-20	-15	-10	-5	0	+5	+10	+15	+20	+24	+29	+33	+37	+41	LONG.
LATITIDE --->																				
180	-1	-21	4	34	13	-7	-5	23	43	34	-9	-29	-17	-13	-43	-39	0	58	24	180
175	12	-12	-3	-1	-1	18	-9	21	48	32	5	-33	-19	-21	-32	-39	-35	25	42	175
170	16	-1	-30	-25	-9	3	-20	17	50	35	10	-32	-22	-9	-29	-33	-48	-25	30	170
165	12	-37	-47	-12	-18	-16	-27	7	45	40	8	-40	-34	-1	-12	-17	-48	-25	-11	165
160	-15	-22	7	2	1	-16	-32	21	46	43	13	-39	-35	-29	-19	-18	-31	-8	-2	160
155	-18	-17	29	17	14	-17	-26	39	46	42	23	-24	-27	-46	-30	-24	-41	-48	-11	155
150	-41	-5	21	17	-4	-20	-6	36	45	40	28	-7	-24	-26	-26	-12	-12	-23	-21	150
145	-32	5	26	27	1	-20	7	34	43	41	28	1	-3	-5	-34	-23	-8	-11	-9	145
140	3	21	45	27	-11	-27	17	40	43	41	35	23	13	13	-3	-16	9	28	21	140
135	10	14	30	34	0	-1	25	43	42	41	38	49	9	23	24	4	-8	26	25	135
130	8	30	50	41	14	12	6	22	40	43	44	66	-7	-1	18	23	5	32	34	130
125	25	58	65	21	9	27	0	6	35	39	49	74	-24	-26	-1	29	38	52	46	125
120	66	74	65	13	0	9	-14	0	17	29	44	59	-32	-55	-45	-6	42	55	56	120
115	53	65	52	20	19	5	-26	-12	9	13	35	29	-40	-53	-58	-22	15	33	68	115
110	53	43	24	16	25	0	-46	-15	-7	-1	35	46	-28	-37	-55	-40	-3	17	61	110
105	47	30	33	37	49	-15	-50	-31	-15	-3	34	72	74	-11	-42	-62	-13	20	62	105
100	34	36	31	40	36	-13	-45	-36	-27	-9	33	84	84	30	-25	-41	-2	24	39	100
95	31	46	32	41	30	-11	-48	-39	-56	-27	23	82	76	45	21	0	16	46	61	95
90	26	34	27	38	10	-16	-50	-40	-58	-2	0	65	47	53	38	27	21	53	58	90
85	21	36	6	2	9	-16	-23	-22	-43	15	15	24	39	42	49	49	20	59	56	85
80	5	-16	-30	-14	-22	-10	6	18	52	45	56	28	26	42	28	55	34	30	40	80
75	-41	-38	-34	-32	-56	-17	25	10	22	22	30	34	15	7	3	46	49	28	31	75
70	-50	-46	-1	2	-46	-6	13	41	58	53	20	8	-4	-19	-27	21	28	29	39	70
65	-19	-2	33	34	54	21	38	40	68	32	2	10	-10	-10	-19	-13	12	9	43	65
60	-10	29	27	6	-11	-1	29	47	42	28	-6	-25	-24	2	-9	-22	2	8	26	60
55	-23	17	34	-3	-13	-7	3	21	23	20	-9	-37	-37	7	2	-16	-9	13	3	55
50	-28	15	23	-24	-15	-1	8	28	34	30	40	-31	-43	-33	-3	-1	-26	-42	-31	50
45	-17	0	16	-8	35	28	31	31	20	23	0	-13	-45	-41	-33	-20	-18	-8	22	45
40	-14	-1	30	38	61	26	26	22	18	23	14	11	-46	-57	-41	-43	5	28	22	40
35	-22	2	26	38	26	30	25	27	31	12	38	19	-15	-58	-38	-15	39	59	55	35
30	-26	-7	29	34	27	36	34	25	24	15	53	62	24	-31	-13	-3	-3	39	77	30
25	-26	-11	72	29	21	28	13	44	19	21	27	77	55	-27	-42	-27	-23	20	56	25
20	-28	8	69	3	-20	-38	-7	25	18	12	28	70	58	-11	-57	-64	-33	-6	28	20
15	-34	4	5	-15	-53	-48	-21	4	12	0	28	38	43	-13	-65	-70	-45	-14	13	15
10	-31	-2	-3	-41	-55	-60	-31	-22	-11	8	18	-21	23	-23	-65	-77	-45	-10	26	10
5	-20	4	6	-52	-66	-71	-56	-32	-1	-2	2	-64	4	-29	-61	-74	-62	-27	4	5
0	-15	2	36	-62	-73	-71	-50	-33	-2	-6	-3	-53	-23	-22	-56	-66	-61	-24	-9	0
-5	12	20	11	-54	-60	-59	-52	-55	6	-7	6	-51	-46	-21	-37	-56	-55	-16	10	-5
-10	14	18	-8	-47	-62	-58	-33	-64	15	35	41	-36	-57	-38	-29	-45	-41	-4	13	-10
-15	29	30	8	-31	-33	-18	-7	-42	-37	66	55	-15	-62	-52	-32	-53	-38	-10	13	-15
-20	19	22	-6	-44	27	41	-18	-29	12	25	13	-33	-54	-60	-52	-46	-35	-2	40	-20
-25	10	21	-13	-17	[redacted]	-8	-51	8	50	13	3	-54	-64	-65	-63	-54	-18	5	30	-25
-30	0	-3	-22	-7	-19	-30	-21	37	53	48	26	-57	-66	-58	-69	-67	0	3	10	-30
-35	-20	-15	-37	-57	-48	-33	-4	22	32	46	27	-54	-64	-51	-53	-69	-31	-38	-24	-35
-40	-5	-31	-60	-57	-19	-3	47	47	51	35	26	-30	-34	-27	-46	-82	-70	-54	-24	-40
-45	-19	-36	-44	-33	-34	-41	25	59	53	55	-4	-47	-55	-65	-60	-65	-75	-68	-56	-45
-50	-22	-23	-26	-33	-14	20	27	26	42	69	41	-13	-30	-40	-53	-47	-56	-50	-38	-50
-55	-18	-16	10	5	15	17	21	65	59	69	48	55	79	-30	-32	-58	-62	-44	-40	-55
-60	-23	-15	40	49	43	31	43	81	59	81	60	52	62	42	-7	-55	-48	-46	-41	-60
-65	-15	6	48	45	46	42	66	84	63	71	59	64	44	50	4	-50	-41	-22	-19	-65
-70	-27	22	57	45	61	52	77	77	72	65	52	50	35	12	-55	-46	-22	25	1	-70
-75	-18	58	62	59	57	49	76	71	70	59	59	54	28	-12	-53	-45	2	-7	-24	-75
-80	12	74	76	58	46	45	75	67	53	51	62	28	26	-1	-25	-33	6	-33	-54	-80
-85	15	70	85	58	39	32	45	54	30	36	61	24	-17	-15	-11	-35	1	-31	-63	-85
-90	6	78	74	33	16	28	21	21	5	-3	20	-8	-28	-7	15	-19	-8	-28	-62	-90
-95	17	76	48	16	16	6	-28	-43	-18	1	-20	-33	-39	-39	-5	4	12	-48	-64	-95
-100	17	40	24	27	22	-20	-52	-32	-43	14	-14	-24	-50	-40	-19	4	4	-49	-67	-100
-105	-1	25	38	52	35	-16	-48	-19	-40	41	20	-39	-57	-29	-12	-16	-33	-68	-67	-105
-110	-9	32	40	42	32	5	-10	-3	-24	33	25	-56	-56	-38	-28	15	-26	-62	-52	-110
-115	17	39	44	36	-3	-43	-21	-39	-48	-8	-27	-41	-68	-51	-36	-27	-49	-62	-44	-115
-120	-8	33	44	36	5	-56	-38	-59	-30	-27	-32	-41	-47	-42	-33	-32	-32	-38	-49	-120
-125	-6	26	51	35	14	-19	-60	-63	-43	-35	-42	-37	-19	-9	-7	-25	-27	-27	-43	-125
-130	-20	25	73	34	-1	10	-47	-56	-29	-25	-29	-8	-15	-11	20	9	-19	-23	-29	-130
-135	1	67	76	3	-22	-15	-52	-58	-42	-13	-20	-2	14	3	21	14	-20	-11	-11	-135
-140	34	58	32	-39	-43	-58	-62	-38	-25	1	-1	21	42	27	11	12	9	-29	8	-140
-145	19	58	15	-56	-68	-77	-53	-34	-11	-2	24	32	49	20	6	4	12	4	-23	-145
-150	25	38	16	-16	-65	-70	-36	-16	15	19	9	-8	28	28	1	3	6	22	-16	-150
-155	35	55	57	21	-14	-49	-44	-25	32	23	-11	-29	20	24	2	5	3	15	4	-155
-160	32	42	41	6	7	-44	-54	8	40	20	-39	-30	20	-34	-11	23	42	24	-41	-160
-165	56	39	25	10	28	-22	-19	30	39	22	-34	-15	31	-52	-64	-7	39	12	-37	-165
-170	26	23	17	22	21	-13	10	30	47	24	-23	3	14	-35	-60	-24	30	29	-37	-170
-175	23	5	20	29	23	1	15	31	43	32	-6	-9	4	-6	-49	-33	19	50	-20	-175
-180	-1	-21	4	34	13	-7	-5	23	43	34	-9	-29	-17	-13	-43	-39	0	58	24	-180

Figure 3.8. Lagged correlation (x100).
October OLR against following February All-Area rainfall.
Data period: 1974-1986. Bias in OLR data removed.
Shading represents approximate location of rainfall area.

	LATITIDE --->																		
LONG.	-41	-37	-33	-29	-24	-20	-15	-10	-5	0	+5	+10	+15	+20	+24	+29	+33	+37	+41	LONG.
180	7	-38	-65	-59	-29	-12	64	55	49	45	42	43	62	34	67	53	22	-14	-80	180
175	-11	-48	-73	-56	-30	-29	20	37	42	41	40	46	51	50	59	61	35	-12	-58	175
170	-25	-38	-73	-50	-31	16	30	25	45	37	46	27	10	52	74	61	62	40	-6	170
165	-40	-59	-66	-29	10	11	29	25	43	42	29	-26	-6	49	54	42	36	24	13	165
160	-45	-55	-55	9	15	9	-5	27	46	42	26	-30	-8	21	32	12	-3	-19	-8	160
155	-45	-42	-35	19	16	-11	-24	20	45	45	32	5	19	-17	23	30	-12	-41	-33	155
150	-30	-33	-17	22	13	-16	-30	12	46	43	33	13	24	-23	36	53	26	-33	-42	150
145	-48	-39	-11	19	21	-13	-29	25	49	38	35	-3	28	25	43	68	54	3	-35	145
140	25	40	-4	15	20	3	-21	22	38	32	34	22	19	37	55	68	62	23	9	140
135	29	30	-5	17	26	13	-5	16	28	36	37	52	21	41	46	60	48	7	14	135
130	-8	-23	-30	6	17	5	-16	32	37	43	39	24	8	15	47	57	48	23	9	130
125	-29	-61	-12	31	33	14	-44	27	26	52	49	11	-20	8	1	50	56	25	-1	125
120	-32	-30	24	51	51	14	-36	4	-12	31	51	18	-7	14	0	-7	68	18	-4	120
115	-33	2	42	54	49	-3	-25	-4	-26	1	33	-3	-7	-1	2	20	45	31	2	115
110	10	28	44	45	28	-34	-43	-30	-48	-26	21	7	10	8	7	14	29	27	20	110
105	-2	16	46	42	11	-49	-59	-42	-54	-35	52	26	26	54	17	-5	24	33	32	105
100	-28	21	53	32	5	-60	-65	-48	-46	-17	34	47	65	30	-3	10	29	47	30	100
95	-13	42	31	13	15	-63	-57	-54	-44	-5	48	68	69	23	6	36	41	49	44	95
90	-8	27	17	23	-14	-66	-61	-55	-34	51	63	57	15	2	2	25	25	35	35	90
85	-17	13	13	2	-22	-64	-73	-46	-22	45	69	46	-17	9	35	42	11	9	17	85
80	-15	8	4	-17	-30	-54	-62	-16	17	25	67	61	-5	33	37	55	40	27	21	80
75	-1	11	9	-18	-46	-58	-4	30	36	39	57	38	14	55	30	13	14	8	-20	75
70	20	30	9	-37	-58	-37	13	16	19	41	40	39	22	36	40	26	27	9	-11	70
65	37	25	-10	-51	-46	-12	25	32	31	30	43	41	13	31	45	33	43	-5	-33	65
60	43	29	-7	-64	-41	-3	44	14	10	28	9	14	-11	12	7	32	52	68	14	60
55	45	47	10	-43	-17	53	62	26	24	19	16	15	-25	-22	37	34	47	80	70	55
50	47	43	0	-49	-23	37	53	28	18	-9	35	27	-40	-18	39	65	53	52	73	50
45	54	64	6	-48	-20	44	16	21	4	-5	17	33	3	2	43	70	76	39	53	45
40	68	56	22	-12	-11	3	-6	6	-34	1	30	45	37	8	24	59	41	17	39	40
35	54	60	36	2	-23	-20	13	9	-9	16	37	44	20	41	14	25	43	17	15	35
30	77	88	46	-17	-36	-13	19	24	20	18	38	45	38	41	28	35	26	21	22	30
25	76	88	-70	-72	-45	7	6	7	31	24	22	38	40	34	43	29	8	4	7	25
20	61	26	-62	-72	-32	12	-14	26	43	12	35	30	37	32	48	22	5	-15	-35	20
15	23	-3	-59	-48	-11	-4	-1	15	47	34	51	29	-7	33	42	62	29	-21	-48	15
10	-13	-13	-31	-24	-6	-26	-24	-29	23	43	15	-27	-20	-6	24	45	35	-16	-32	10
5	50	10	-31	-17	-12	-24	-35	-28	9	16	1	-32	-30	-14	12	22	23	-17	-29	5
0	40	-42	-47	-22	-26	-47	-29	-27	13	-1	-3	-39	-21	-30	-1	1	-5	-9	-18	0
-5	27	-29	-46	-47	-39	-39	-21	-5	51	40	-3	-40	-32	-37	-6	-5	-15	0	-10	-5
-10	-9	-44	-50	-35	-15	-23	-54	9	50	38	-19	-38	-40	-33	-12	-21	-17	-1	-3	-10
-15	-48	-56	-27	0	-22	-11	-14	22	57	44	15	-32	-38	-34	-22	-4	3	4	-11	-15
-20	-59	-56	-33	-16	-26	-13	8	17	61	70	48	-6	-21	-43	-40	-2	14	-4	-20	-20
-25	-47	-62	8	[redacted]	-31	11	27	48	66	77	-22	-16	-25	-45	-49	-29	14	-15	-44	-25
-30	-1	-14	4	-32	-20	19	22	47	63	52	36	-22	3	-53	-48	-33	28	8	-18	-30
-35	-7	-13	8	-9	2	16	38	54	41	44	44	27	19	-24	-29	-37	26	25	-7	-35
-40	-19	-17	3	32	24	23	53	34	57	58	57	32	30	15	-9	-43	-20	17	4	-40
-45	-19	-24	-6	35	19	39	32	42	59	57	63	48	-5	-25	-5	-4	3	12	-23	-45
-50	-14	-35	-7	25	32	33	39	52	63	40	63	32	-9	-54	-18	34	28	4	-18	-50
-55	15	12	13	21	38	43	45	50	63	37	42	44	4	-44	8	17	18	5	-10	-55
-60	24	7	-38	0	24	40	40	60	68	42	39	37	5	-34	-11	-8	12	10	-9	-60
-65	32	-17	-22	-1	5	33	39	53	80	76	38	15	-28	-49	-42	-14	10	15	0	-65
-70	19	-21	-20	-17	0	23	-1	59	87	89	44	-9	-31	-24	-57	-22	23	18	14	-70
-75	-3	-13	-11	-8	18	0	-17	41	79	88	61	-17	-58	30	13	-12	55	53	24	-75
-80	34	17	3	38	47	-42	-47	-2	73	80	66	-1	-37	-33	5	40	34	33	-5	-80
-85	27	2	12	45	40	-25	-33	-7	44	62	63	15	-37	23	4	52	56	52	-6	-85
-90	47	16	-5	27	8	-2	-1	-11	39	46	16	-9	-20	-20	-3	19	45	51	-1	-90
-95	14	-22	-2	16	-11	14	0	-28	3	43	24	-4	7	4	-5	-8	33	28	7	-95
-100	34	1	-2	1	-4	-3	-15	-41	-28	30	-10	-2	4	30	-6	-31	-2	53	2	-100
-105	60	41	5	7	12	-26	-50	-49	-33	11	-24	-5	8	40	13	-41	-52	17	9	-105
-110	40	46	13	-11	-9	-44	-73	-61	-47	-10	-19	-24	-14	7	7	17	-6	8	-12	-110
-115	43	35	-35	-60	-65	-45	-57	-56	-41	-29	-29	-20	-15	-14	-23	6	1	8	-5	-115
-120	14	-14	-38	-40	-49	-57	-42	-48	-48	-39	-35	-19	-11	-21	-31	-9	2	8	-15	-120
-125	5	3	-9	-42	-56	-63	-64	-44	-36	-41	-17	-1	-32	-31	-27	-13	-1	5	-24	-125
-130	15	1	-15	-56	-58	-53	-44	-33	-33	-25	-5	-1	-26	-49	-49	-28	-37	-17	-33	-130
-135	-61	-27	-45	-48	-51	-42	-29	-38	-48	-23	4	-6	-14	2	13	6	-43	-32	-18	-135
-140	-65	-47	-52	-39	-44	-37	-32	-40	-19	5	11	6	7	37	20	23	-15	-40	-25	-140
-145	-77	-35	-33	-33	-55	-41	-31	3	4	19	-12	2	29	37	7	5	15	-15	-31	-145
-150	-69	-4	-13	-45	-51	-38	22	19	26	29	1	-10	26	12	-14	11	23	0	-30	-150
-155	-19	3	-24	-64	-48	-14	8	27	48	24	5	-28	13	-2	-40	-29	15	-5	-38	-155
-160	-16	8	-29	-40	-23	0	2	61	46	22	-17	-15	5	-16	-48	-59	-35	-12	-29	-160
-165	-50	-19	-36	-45	-13	-12	18	55	47	17	-25	-22	-1	-35	-43	-35	-52	-24	-30	-165
-170	15	-1	-60	-49	-26	-9	28	52	54	22	-1	-18	15	-26	-12	-17	-48	-23	-26	-170
-175	16	-30	-68	-55	-24	1	63	70	61	45	38	11	34	4	45	31	-3	-22	-71	-175
-180	7	-38	-65	-59	-29	-12	64	55	49	45	42	43	62	34	67	53	22	-14	-80	-180

Figure 3.9. Simultaneous correlation (x100).
Seasonal (October to March) OLR against All-Area rainfall.
Data period: 1974–1986. Bias in OLR data removed.
Shading represents approximate location of rainfall area.

	LATITIDE --->																		
LONG.	-41	-37	-33	-29	-24	-20	-15	-10	-5	0	+5	+10	+15	+20	+24	+29	+33	+37	+41	LONG.
180	-3	-56	-3	-27	-34	-45	-31	57	59	50	38	35	11	3	10	36	49	56	28	180
175	-39	-73	-39	-35	-35	-50	-12	50	56	46	46	39	20	-17	9	26	19	46	38	175
170	-53	-50	-43	-55	-47	-36	12	74	52	44	49	33	0	-15	-8	32	37	22	49	170
165	-63	-43	-53	-56	-42	-37	22	64	48	43	47	26	-14	5	19	20	12	14	18	165
160	-45	-47	-62	-37	-38	-24	27	56	48	41	55	27	-24	-3	6	1	-2	7	7	160
155	-57	-64	-60	-27	-24	-2	27	44	41	37	53	15	-17	-24	-1	-2	-16	-44	-48	155
150	-64	-64	-39	-19	-2	17	45	47	39	33	38	11	-20	-26	-8	7	5	-24	-55	150
145	-57	-53	-12	13	35	41	43	43	35	33	36	4	-26	-17	-12	-5	11	-3	-26	145
140	-55	-15	4	49	50	43	27	37	30	31	39	23	-14	-15	-9	-10	17	15	4	140
135	-68	-29	7	56	54	24	19	25	23	29	45	42	-7	-8	-16	-5	27	30	15	135
130	-60	-22	11	71	61	26	8	15	11	26	45	40	-12	0	-6	16	47	61	50	130
125	-46	-10	46	63	62	1	-7	2	-3	26	45	54	-24	-12	-9	19	62	73	58	125
120	-4	5	54	51	63	-6	-35	-42	-22	18	42	17	-31	-17	-4	-1	66	80	70	120
115	-7	17	58	61	48	-11	-61	-63	-22	7	35	-21	-33	-19	7	25	64	78	70	115
110	9	45	68	49	31	-31	-60	-58	-30	0	38	-8	-29	-12	12	36	58	75	64	110
105	12	41	65	58	12	-46	-55	-52	-44	-4	35	15	17	10	3	18	45	67	55	105
100	11	34	60	48	-10	-55	-62	-55	-41	-5	31	20	22	2	2	27	59	80	54	100
95	-1	29	47	22	-27	-60	-64	-67	-54	-5	28	24	12	8	28	52	64	72	62	95
90	-10	19	34	1	-46	-72	-58	-75	-57	10	34	11	3	11	23	47	57	67	53	90
85	-16	8	9	-23	-56	-66	-60	-72	-46	8	43	21	4	17	35	41	33	69	44	85
80	-38	-28	-12	-26	-48	-61	-50	17	23	25	49	26	-5	34	42	50	55	54	30	80
75	-53	-50	-4	-30	-51	-58	17	43	47	43	53	15	-13	31	34	46	57	53	28	75
70	-31	-2	7	-27	-30	-22	34	56	58	36	12	-8	-14	41	53	34	35	22	14	70
65	14	29	31	12	5	38	59	56	41	20	-1	6	14	23	67	42	13	13	32	65
60	22	17	2	-13	9	55	56	44	21	11	-9	-10	-12	47	70	69	52	29	11	60
55	-8	-25	-5	-24	-7	54	65	31	-13	-9	-11	-21	-59	22	62	74	62	39	-1	55
50	8	-15	-3	-14	-17	5	63	33	-8	-2	2	-31	-66	-6	62	79	60	55	-1	50
45	-21	-14	15	-10	13	61	74	50	-21	-10	-3	-35	-57	-3	50	82	60	52	30	45
40	-13	-2	1	2	55	74	52	14	-41	-10	8	-31	-47	-28	28	55	76	55	28	40
35	2	20	30	54	60	53	32	18	-17	-14	26	-20	-55	-24	20	42	61	66	50	35
30	10	38	66	60	56	51	25	21	-2	-22	39	1	-37	-32	15	39	30	31	46	30
25	11	48	55	56	49	48	21	47	5	-18	41	-2	-14	-35	4	19	10	7	21	25
20	-1	55	58	46	33	22	23	34	8	-21	55	67	4	-26	0	24	25	21	25	20
15	-1	54	26	26	-3	5	14	16	-15	-14	32	34	1	-35	-20	35	45	23	27	15
10	-5	25	10	-20	-30	-21	2	-7	-38	-13	-7	-17	6	-34	-26	5	47	37	33	10
5	9	13	-8	-52	-54	-37	-13	-18	-42	-30	-37	-28	-7	-27	-35	-18	2	21	14	5
0	-12	-12	-15	-46	-55	-33	-24	-11	-15	-24	-34	-45	-12	-20	-46	-40	-31	20	19	0
-5	-12	-7	-9	-53	-60	-45	-44	-43	-4	-25	-52	-62	-21	-22	-37	-48	-47	23	41	-5
-10	-2	15	-22	-48	-50	-57	-38	-20	-18	-29	-55	-50	-26	-31	-47	-48	-44	31	44	-10
-15	5	24	12	-70	-81	-75	1	29	-12	11	-35	-17	-30	-43	-60	-58	-27	28	34	-15
-20	12	30	-67	-83	-74	-45	20	48	32	2	-41	-31	-35	-43	-64	-66	-1	40	34	-20
-25	23	15	-72	-84	-57	-34	-16	62	62	0	-34	-27	-33	-46	-63	-69	-10	2	-22	-25
-30	43	14	-84	-55	-37	-23	-10	63	67	56	11	-25	-22	-38	-56	-60	8	1	-22	-30
-35	38	-31	-42	-19	-8	-8	-1	61	50	59	51	-11	-17	-23	-42	-45	12	-12	-29	-35
-40	2	-39	-18	7	11	16	35	55	57	48	37	16	8	23	-24	-49	-13	3	-7	-40
-45	19	-6	-20	16	10	-8	14	47	47	49	3	12	2	-16	-37	-46	-29	9	-30	-45
-50	5	-27	-23	23	24	27	18	35	34	52	63	-3	8	-21	-33	-30	-35	-7	-32	-50
-55	-26	-40	-15	18	42	30	16	67	48	34	65	53	53	-9	-10	-25	-41	-17	-28	-55
-60	-36	-38	-1	35	77	42	40	90	71	23	57	49	53	37	2	-25	-28	-25	-35	-60
-65	-36	-24	28	64	74	57	65	83	70	32	32	26	49	42	11	-20	-8	-13	-14	-65
-70	-16	13	42	71	67	69	56	63	69	34	33	19	35	51	-28	-10	10	-23	1	-70
-75	-24	10	43	63	54	64	39	59	67	44	14	-2	-36	-7	-15	-10	53	2	-38	-75
-80	-14	24	48	56	52	37	31	52	44	26	7	-32	-43	-35	-4	10	58	-28	-65	-80
-85	-7	12	45	51	50	31	9	52	11	0	10	-17	-41	-48	-7	42	77	25	-49	-85
-90	-5	8	47	48	34	17	14	51	-5	-6	1	-24	-27	-8	-19	36	66	39	-34	-90
-95	-31	3	38	40	22	22	12	-10	-17	17	-19	-22	-28	-36	-28	4	72	-7	-20	-95
-100	16	25	24	24	24	19	-4	-17	-18	23	-26	-29	-51	-30	-15	15	45	-10	-28	-100
-105	-19	23	30	33	26	-21	-27	-20	-26	21	-9	-27	-58	-33	-22	-28	-48	-57	-40	-105
-110	-15	24	40	32	9	-43	-39	-36	-10	13	-7	-28	-49	-21	3	2	-41	-59	-31	-110
-115	-8	35	35	-14	-31	-58	-60	-55	-21	-33	-35	-30	-39	-31	-10	-12	-42	-58	-21	-115
-120	-5	24	-19	-16	-12	-45	-36	-43	-17	-28	-29	-35	-45	-38	-12	-10	-25	-47	-24	-120
-125	-20	24	-4	-22	2	-9	-41	-50	-37	-35	-32	-30	-39	-37	-13	31	-10	-20	-25	-125
-130	-16	15	-4	-31	-16	-9	-51	-52	-26	-36	-34	-24	-25	-37	-12	25	-10	-20	-28	-130
-135	-19	29	-36	-42	-52	-42	-55	-52	-31	-29	-32	-25	-6	-28	15	32	-10	-25	-28	-135
-140	60	7	-61	-63	-51	-36	-44	-46	-22	-18	-22	-17	-1	2	20	35	-9	-29	-5	-140
-145	18	-26	-68	-66	-54	-47	-39	-46	-4	0	-14	-21	-6	0	-6	10	2	-33	-19	-145
-150	-15	-39	-48	-69	-50	-24	-16	-33	9	19	-7	-25	9	-6	-38	-12	8	7	-12	-150
-155	-39	-23	-39	-68	-16	13	-10	-22	44	28	-9	-14	22	-5	-60	-12	13	-28	-32	-155
-160	-39	-32	-38	-62	-9	-1	-20	12	60	32	3	10	25	-27	-66	-26	8	-5	-35	-160
-165	14	-8	-42	-44	7	-14	-20	37	69	39	10	17	31	-31	-68	-43	10	-15	-10	-165
-170	38	2	-29	-13	-8	-21	-20	38	69	42	32	20	11	-28	-36	-38	17	21	-15	-170
-175	23	-17	-34	-23	-20	-20	-15	50	65	48	44	18	4	-14	-9	18	37	47	8	-175
-180	-3	-56	-3	-27	-34	-45	-31	57	59	50	38	35	11	3	10	36	49	56	28	-180

CHAPTER 4

ATMOSPHERIC CIRCULATION AND SOUTH AFRICAN RAINFALL

4.1. INTRODUCTION

Studies dealing with long-period variability in the tropical troposphere (especially in the upper levels) were infrequent prior to 1970 due to the lack of data. However, earlier studies (Riehl, 1954) had already noted the unsteadiness in the wind flow within the upper tropospheric layers and had recognized the importance of the intrusion of extratropical waves and disturbances into the tropics. In addition to regions of mean easterly winds, the tropical atmosphere contains substantial areas of mean westerlies in both the upper and lower troposphere, as for example in the eastern Pacific Ocean. Their existence is thought to be related to the large-scale atmospheric response to regional convective heating and, ultimately, to the latent heating and sea surface temperature distribution in the tropics. On the other hand, seasonal modulation of the lower tropospheric winds across the tropical Indian Ocean are associated with the Asian monsoon.

Variations in boundary forcing and circulation features within the tropics are believed to be a key component in the functioning of the global climate system (Arkin, 1982). From theoretical investigations, Webster and Holton (1982) suggested that, where the equatorial upper tropospheric flow was westerly (or even weak easterly), interhemispheric propagation of waves (e.g., Rossby type) could occur through equatorial wave ducts.

Extensive work has been done towards understanding the functioning of the global circulation system through the study of large-scale circulation. Research on large-scale

dynamics (Krishnamurti, 1971; Kanamitsu and Krishnamurti, 1978) and studies of interannual cloudiness fluctuations (Heddinghaus and Krueger, 1981; Liebmann and Hartmann, 1982; Lau and Chan, 1983a, b) have demonstrated the importance of equatorial convective activity maxima over broad areas. Tropical Africa, tropical Americas, and southeast Asia-Indonesia regions appear to represent three main large-scale mean energy sources, with the southeast Asia-Indonesia region being the dominant convective source, a feature resembling an equatorial wave number one.

Using 11 years of upper tropospheric wind data, Arkin (1982) showed that a substantial portion of the interannual variability in the 200 hPa circulation was related to the Southern Oscillation. The anomalous circulation in the Pacific was characterised by a pair of anticyclonic (cyclonic) anomalies straddling the equator during periods of low (high) Southern Oscillation Index. Zonal wind differences of 8 to 11 ms^{-1} between low-Index and high-Index phases of the Southern Oscillation were found in the region of 25°N, near the equator, and around 25°S in the central Pacific Ocean longitudes. Moreover, composites relative to El Niño events during different seasons reveal that anomalous anticyclonic circulations in the Pacific are associated with the presence of a positive sea surface temperature anomaly in the eastern and central equatorial Pacific.

As generally recognized, the tropical part of the global atmosphere receives energy (in various forms) in excess of what is lost to space. Some of the known circulations via which exchanges in energy and mass occur within the atmosphere between the lower and higher latitudes are, in the average sense, the tropical temperate troughs and the Hadley and Walker types of circulation cells. Significant exchanges also occur via ocean currents and circulations.

Harrison (1986) has provided a detailed study concerning the manner in which tropical and temperate circulation systems maintain major cloud bands and act as transfer mechanisms for momentum and energy across Southern Africa. Cloud bands linking the tropical and temperate circulations supply a high proportion of the summer rainfall over the interior of South Africa (Harrison 1984, 1986; Tyson, 1986). These bands are thought to have preferred locations within two major zones, one across South Africa and the other over the western Indian Ocean/Madagascar area. Tropical-temperate troughs are most likely to form across South Africa when moisture concentrations are highest and the Inter-Tropical Convergence Zone (ITCZ) is furthest south over the subcontinent; this situation facilitates tropical-temperate links via interaction with troughs embedded in the upper-level westerlies of the mid latitudes. It was also observed (Harrison, 1983) that upper-level near-tropical easterly flow and heat release at 20°S over the central African continent provide suitable conditions for tropical-temperate trough formation and rainfall over Southern Africa.

Quasi-stationary long waves, induced either orographically (Palmen and Newton, 1969) or by large-scale latent heat release in the tropics (Kidson, 1975; Heddinghaus and Krueger, 1981; Webster, 1983; Harrison, 1986) or by a combination of both, play a major role in fixing the location of mid- to high-tropospheric troughs (Tyson, 1986). The long-wave systems are closely associated with the northwest-southeast oriented cloud bands which link perturbations in the westerlies to the tropical circulation. It is the composite system linking the tropical and higher-latitude circulations that forms the tropical-temperate trough. This trough represents channels for large-scale transfer of momentum and energy in the form of heat and moisture from the tropics to higher latitudes; cloud bands associated with such troughs usually provide large amounts of precipitation (Streten, 1973; Harrison, 1983, 1986; Tyson, 1986).

There is a longitudinal displacement of the quasi-standing wave-trough embedded within the 200 hPa westerly flow in the African region. This shift is believed to be modulated in sympathy with a similar wave across the South American land mass; the latter wave is closely linked to the Amazon Basin region heat source (Harrison, 1986; Tyson, 1986).

The various circulations implied so far in relation to the dynamics of the tropical atmosphere, especially over the Africa-Indian Ocean areas, have been generally speculative and based on fairly limited wind data. With the intention of furthering the understanding of atmospheric dynamics, this chapter investigates circulation patterns through analyses of gridded wind data and derived parameters. Even though the data is meagre, it is believed that whatever is available can be used to supplement and confirm results obtained from previous investigations. It should, however, be noted that the wind data are constrained within a period when summer rainfall across South Africa shows a relatively dry phase, especially during the later part of the season (see Figure 1.8). Chapter 1 contains a description of the data set utilized in the present study as well as the methods employed to obtain the relevant parameters. The following section outlines the objectives. Results of the analyses are discussed in Section 4.3. Summary and discussions are presented in Section 4.4.

4.2. OBJECTIVES

SST appears to be one of the key factors influencing the generation and maintenance of large-scale deep convection and cloudiness over the tropical oceans. The relationship between convection and SST is, however, not uniform, but shows regional and seasonal dependence. The immediate effect of a SST anomaly is to alter the sensible heat flux

and evaporation across the air-sea boundary over the region of the SST anomaly. Subsequently, the temperature and moisture contents of the overlying air may be modified. This does not necessarily imply a change in the atmospheric circulation. In order to alter the circulation, the sensible heating of the air must produce horizontal surface atmospheric pressure gradients. In such cases, the heating can change the convergence of the moist air (and precipitation) in the region of the SST anomaly. Under suitable conditions, the convergence of warmer and more moist surface air might lead to further enhancement of the pressure gradients, and in turn increasing moisture convergence within the boundary layer, thus developing a CISK type of feedback. Depending on the basic climatological SST structure upon which the SST anomaly is superimposed as well as the anomaly structure itself, the feedback process can lead to heating in the vertical column and transform the surface anomaly into a three-dimensional heating anomaly, which in turn can produce changes in the large-scale atmospheric circulation via thermodynamical processes.

In Chapter 2, key SST regions were identified with respect to South African rainfall variations. The intention here is to show, from an almost-global circulation perspective, that the Pacific has an important impact on Southern African climate system via the circulation across the Indian Ocean. It is conjectured that the western branch of the Indonesian Walker cell (Bjerknes, 1969), instead of behaving like one huge circulation cell with descending motion over the western equatorial Indian Ocean (as during southern hemisphere winter months), displays a rather complicated structure during the southern summer months. The cells are, however, not independent of the circulations involving the Indonesian heat source; they are geared with each other. The climatology of the vertical circulations in the zonal and meridional planes are explored with the aim of justifying results observed in the previous investigations. It will be shown that the

dipole-like behaviour of the circulation in the Africa-equatorial Indian Ocean area, implied by the OLR-rainfall and SST-rainfall variations, is consistent with tropical atmospheric dynamics of the region.

Shannon et al. (1990) have suggested that variations in the trade winds to the east of Madagascar force changes in the Agulhas Current to the South of Africa with a possible feedback to climate variability. Jury et al. (1991) have observed that an anomaly in the surface wind (anti-clockwise sense) across the western equatorial and tropical Indian Ocean is conducive to wet summers over South Africa. In a study relating to the Southern Oscillation, Harrison (1983) has proposed a zonal circulation model which implies wetter conditions over Southern Africa when low-level westerly winds prevail across the equatorial Indian Ocean, and vice versa. On the other hand, Walker (1989) found that tropical and trade wind easterlies in the southwest Indian Ocean increased significantly during wetter summer months over South Africa. The aim here is to further explore the tropical circulation dynamics in view of understanding the climate regulations.

4.3. RESULTS

4.3.1. LONG-TERM MEAN WINDS

The aim in this section is to briefly discuss those aspects of long-term circulation distributions that are relevant in developing a background against which anomalous situations may be compared. The monthly mean variations of wind have been described in many previous studies and atlases. A brief description of the salient features is included here in order to provide the large-scale context for the subsequent discussions. Only January and July circulations will be considered. November, December,

February, March, April showed similar patterns as January, while June and August were similar to July mean conditions; sudden shifts occur from May to June and during the months of October and November. Long-term mean monthly wind distributions were computed using all the available Climate Analysis Center (USA) gridded products for the 850, 500, and 200 hPa levels; the other levels were also examined, but are not presented here. The averaging periods are different for the various levels (see Chapter 1 for a description of the data set). In some cases the number of years used for long-term representation is insufficient from a climatological perspective, but the results may still be used for comparison purposes.

Figures 4.1 and 4.2 show the mean vector wind distributions for January and July, respectively. The 200 hPa mean flow showed very similar patterns to the mean statistics in Arkin et al. (1986) who used five to seven years of data to summarize the average state of circulation at this level. The lower level mean wind distributions resembled those in Halpert and Ropelewski (1989) who used COADS surface wind data. Tropical winds at 500 hPa are generally slack, but the anticyclonic pattern over Southern Africa should be noted. The winds generally follow the annual cycle in solar declination together with longitudinal and hemispheric asymmetries associated with differing distributions of continents and oceans. The main features in the lowest level are the subtropical highs with the trade-wind belts on their equatorward sides, and the zone where the trades meet, corresponding to a low-pressure belt. This low-pressure belt is not continuous around the globe and represents the ITCZ (sometimes referred to as the trade-wind confluence, the equatorial trough, or the thermal equator).

The oceans have a much greater thermal inertia than land masses. Hence the ITCZ in the oceanic latitudes should be close to the equator and show only slight seasonal variance, whereas, along the longitudes of tropical continents, the ITCZ should

undergo a strong seasonal migration, thus permitting an appreciable heat transfer across the equator. The wave number three structure may be visualized within the tropics. Over continents, a large meridional flux of moisture takes place from the winter to the summer hemisphere in the low-level monsoon-type of flow via the trade-wind system. The corresponding latent heat release within the rising branch of the mean meridional cell (Hadley type), together with sensible and latent heat gained in the summer hemisphere, is realized and carried upward, wherefrom it is exported (not necessarily within the same longitudes) towards the polar latitudes, mainly of the winter hemisphere. This feature is comparable to the variation of the OLR field (with respect to South African summer rainfall), discussed in Chapter 3.

Generally, the winds are more westerly at latitudes poleward of 20° than equatorward; however, the flow also exhibits substantial longitudinal variability. Ridges and closed anticyclonic circulations are observed in most months in the longitudes of Africa, the Americas, and the western Pacific and southeast Asian regions. Westerly jets occur along the poleward flanks of the upper-level anticyclones and ridges, with circulation in the winter hemisphere being stronger.

4.3.2. MEAN CIRCULATION VIA THE VELOCITY POTENTIAL FIELD

The velocity potential field is analysed in order to gain more insight into the circulation structure. Figures 4.3, 4.4, and 4.5 display the mean velocity potential field for December, February, and July for the 850, 500, and 200 hPa levels. The averaging period is from 1979 to 1987 for February and from 1979 to 1986 for December and July.

In the diagrams, it should be noted that the patterns of velocity potential do not directly represent those of the divergence field; rather, the divergence is the Laplacian of the velocity potential, and, additionally, the velocity potential is characterized by larger spatial scales. The sign convention used here is such that the divergent part of the total horizontal wind flows from negative to positive values; the flow is perpendicular to the contours with divergent speed of flow proportional to the gradient of the contours. Although the method employed here may somewhat underestimate the small-scale features of the convergent/divergent flow, the large-scale patterns can be clearly depicted. Regions of large divergence are related to the curvature and shear of the velocity potential Krishnamurti (1973). Given the nature of the original data, emphasis will be placed on the geometry of the systems. It should be noted that isopleths of velocity potential parallel to latitude circles indicate lack of zonal circulations. On the other hand, Hadley-type of circulations (vertical-meridional) would be absent if the isopleths are parallel to longitude lines.

In general, the three 'centres of action' (wave number three pattern) can be located around the maritime continent of southeast Asia, tropical Americas, and tropical Africa. The correspondence of these large-scale features to those obtained with the OLR field should be noted. The centres of action show significant longitudinal and latitudinal displacements during the course of the year. The most conspicuous system of the southeast Asia-west Pacific region is readily seen throughout the year, particularly at upper levels, where the values are negative throughout the year. The negative values at 200 hPa are larger during the northern hemisphere summer season, the location of the centre of action being biased towards the northern latitudes. Some interesting features are observed in the oscillation of this system in sympathy with solar declination. On an average, the centre of minimum values always lies just to the east of

the maritime continent. At 200 hPa the centre of minimum velocity potential values displaces from its southeast-most location (to the northeast of Australia) in March to a northwest-most position (Philippines area) in June to September months (not shown). A lag of the order of about three months in the southern location with respect to solar declination is noteworthy. The difference in the delay is associated with the difference in heating due to the diverse nature of land mass distributions.

Compared to the upper level pattern, the positive 850 hPa centre of the Indonesian system shows more complicated displacements; but the general southeast to northwest translations are evident. Apart from a sudden jump observed in May-June (maps not shown) of the aggregate system during its general northwestward movement, the translation seems rather regular. The sudden shift reflects a manifestation of the onset of the northern summer monsoon season.

One of the descending branches associated with the rising Indonesian system overlies the usually dry southeast Pacific zone. The associated 200 hPa centre of positive values within this region does not show significant translocations during the course of the year, although its lower-level counterpart negative centre does show meridional displacements.

The patterns in the African region are not well defined during the southern hemisphere summer months, but the velocity potential values in the area are relatively small at 200 hPa. On the other hand, at 850 hPa a positive centre appears over the central African region, where OLR shows a minimum during this time of the year (Figure 3.1). It is suggested that the average large-scale outflow resulting from the low level convergence is not clearly resolved here due to masking in the presence of (and interaction with) the vigorous Indonesian system. Possibly the mean outflow occurs at

levels lower than the 200 hPa. Examination of the 500 hPa velocity potential field (Figures 4.3b and 4.4b) indicates a negative centre across the African region and almost overlying the 850 hPa positive centre; whereas values over the Indonesian areas at this level remain positive (Figures 4.3 and 4.4). In the mean, the implied convection over Africa appears to be shallow; since summer rain over this area is mostly of convective nature, the outflow from individual weather systems may penetrate to higher levels, but the divergent signal is blurred, probably due to the strong upper-level outflow from the Indonesian region. Climatological zonal and meridional indices are discussed in the next section in order to further explore the mean atmospheric dynamics.

Unlike during southern summer, during southern winter the geometry of the velocity potential fields shows much clearer patterns over the African region. A marked centre of positive values at 200 hPa becomes established over the southern subcontinent. This 200 hPa centre overlies a well-defined cell of negative (divergent) values at 850 hPa (Figure 4.5). At the intermediate level, the magnitudes of the velocity potential are negative and show slack gradient, but the divergent component shows outflow from the area. The circular nature of the 200 hPa cell over southeastern Africa should be noted as well as the tight gradient between the Indonesian and Southern African centres. These features are associated with the winter dryness over the interior of Southern Africa. During this time, the strong minimum in velocity potential within the west Pacific region has moved northwestward from its January location to assume a position centred around the Philippines area. Its 850 hPa counterpart of minimum potential shows a sympathetic northwestward shift.

4.3.3. MEAN MERIDIONAL AND ZONAL CIRCULATION INDICES

It has been stressed earlier that vertical atmospheric circulations form important integral parts of the tropics. The two most known and most studied features in this respect are the meridional (Hadley-type) and zonal (Walker-type) large-scale mass overturnings. It should be mentioned that the vertical circulations referred to here are manifested in a climatological sense, they may not necessarily imply real material exchanges.

A convenient way to locate vertical circulation cells is through the analysis of circulation indices derived from the velocity potential field at various levels of the troposphere. The Zonal (east-west) Circulation Index (ZCI) and the Meridional (north-south) Circulation Index (MCI) have been defined in Chapter 1. These indices, which are obtained through integrations of the gradients of the velocity potential within a domain and along the required plane, give a measure of the intensities of the circulations and are also useful in determining large-scale energy sources and sinks. The indices are used here in order to investigate mass overturnings along the zonal and meridional planes. The meridional circulation index distributions for December, January, February and July along the north-south plane are displayed Figure 4.6. Computations of the MCIs are based on the limited 0°-90°E longitudinal domain. In these diagrams, positive values of the MCI at a particular pressure level indicate a southerly (south to north) divergent component of the total wind. The results for areas poleward of about 35 degrees latitude may not be interpreted as they are contaminated by the boundary conditions imposed during the velocity potential calculations. Figure 4.7 shows the zonal distributions of the ZCIs for December, January, and February. The latitude belt considered in the computation of this index spans from the equator to 28.7°S. The ZCI averages for the southern hemisphere winter months are not shown because during this period the nodes reflecting the major heat sources shift

over to the northern hemisphere. Positive ZCI values represent divergent westerly (west to east) component and negative values represent divergent easterly component of the total wind. Indices for three levels, 850, 500, and 200 hPa, superposed on the diagrams should facilitate interpretation of circulation pattern distributions. Results for other levels were also examined during the investigations, but are not shown here.

Plots of the indices indicate large-scale circulation features. One simple way of interpreting the curves is to consider negative values as flow from north to south and positive values as flow from south to north. It is then deduced that, during the southern hemisphere summer months, there is low-level (850 hPa) convergence and upper-level (200 hPa) divergence within the 10 to 15°S belt, with counterpart motion at about 20°S; This represents the major meridional (Hadley) cell (Figure 4.6a, b, and c). The reverse occurs in southern winter during which period the intensity of the circulation increases significantly (Figure 4.6d); the large scale rising branch at this time of the year occurs at about 20°N and the sinking around 20°S.

The diagrams in Figure 4.7 visually depict the mean zonal, vertical circulations implied by the velocity potential field. It is observed that the zonal and meridional circulation indices are of the same order of magnitude in the regions of interest in this study. Like the MCI, the ZCI distributions also show similar patterns during the three summer months. However, there are certain subtle differences which may prove to be important in tropical climate dynamics. Attention will be focused particularly on the African, the Indian Ocean, and the Atlantic ocean sectors. The zonal circulations along most of the other longitude lines are more pronounced further to the north than the African-Indian Ocean region. So the signal is not captured in the latitude belt considered in the computations of the indices.

The most notable feature of the region seems to be the 850-500 hPa anticlockwise (viewed from the south) zonal cell which implies mean rising motion over southeastern parts of Africa and mean sinking over central south Atlantic. This zonal vertical circulation will hereafter be referred to as the African cell or system. The African cell shows a slight westward shift from December through January to February. This trend is consistent with the observations of Taljaard (1986) who found a westward expansion of the heavy precipitation over southeast Africa during these months.

In February, an adjacent 850-500 hPa clockwise cell (hereafter referred to as the Indian Ocean cell or system) is evident to the east; this cell connects the rising limb of the African system to a sinking branch over the Indian Ocean. During December and January the Indian Ocean cell displays complex features, with a tendency towards gradual development from December through February. The 200 hPa ZCI to the east of the African subcontinent shows a slight eastward shift as well as development (smoother geometrical trough in February than in December). The behaviour of the average circulations may be attributed to the gradual warming of the sea surface during these months. As the SSTs rise, the outflow becomes more defined at higher levels; the inflow pattern likewise indicates a lifting. No attempt is made here to investigate the thermodynamical links involved. However, it is believed that higher equivalent potential temperatures in the lower levels over these regions are conducive to taller clouds, and hence the associated elevated outflow. In other words, there should be a general deepening of the systems eastward across the Indian Ocean where the SSTs are relatively higher.

A rising limb in the regions of tropical South America is linked to two sinking branches, one over the eastern parts of the Atlantic Ocean and the other over the

eastern parts of the Pacific Ocean. In these latter areas, the climate is relatively dry with suppressed convective activity, and the SSTs are cooler.

4.4. CIRCULATIONS DURING WET VERSUS DRY COMPOSITES

Compared to the long-term rainfall distribution, the period for which wind data are available are biased towards a drier regime. Even though the data are restricted, an attempt is made to group them into composites corresponding to relatively wet and dry periods across South Africa. January and February of 1981 and 1985 are found to be relatively wet compared to January and February of 1983 and 1984 (see Figure 1.8). Meridional circulation index distributions for the two ensembles as well as for the anomaly (wet composite minus dry composite) are displayed in Figure 4.8, while Figure 4.9 shows the corresponding zonal circulation index distributions.

The MCI patterns for the wet case generally resemble the mean MCI distributions for January and February (compare Figures 4.6b, c and 4.8a, b). But a striking departure is observed at the 200 hPa level in the dry scenario with a much weaker signal at this level within the equatorial belt. In addition, Figure 4.8c indicates an anomalous (wet minus dry) 500-200 hPa circulation cell with rising air near the fifteenth parallel south and sinking at a similar latitude in the north. The difference in the 850 hPa MCI does not seem to be significant.

The ZCI signals are noisier in the dry scenario than in the wet. The 850-500 hPa cells (Atlantic Ocean and Indian Ocean cells, viewed from the south) can be noticed with rising motion around 30° to 40°E in both the wet and the dry cases (Figure 4.9). However, in the wet scenario, the 200 hPa circulation appears to enhance the rising branch, especially in the Atlantic sector. Within the belt extending from the equator to

28.7°S, the zonal circulations indicate generally stronger cells around the globe in the wet years than in the dry years.

The anomaly diagram (Figure 4.9c) indicates a clockwise (viewed from the south) cell with rising motion around 30°E and sinking at about 40 to 50°E. Across the southwest Indian Ocean, the structure involves divergent easterlies at the 500 hPa level (also at 850 hPa, but to a lesser extent) and divergent westerlies at 200 hPa. This cell reflects the dipole connection between southern Africa and the Indian Ocean, as observed earlier.

4.5. SUMMARY AND DISCUSSION

Compared to the higher latitude areas, tropical regions represent a surplus of energy and momentum. Exchanges occur in interactions between the regions. The interactions are manifested in the meridional (Hadley-type) and zonal (Walker-type) circulations as well as the tropical-temperate troughs. These features display spatial and temporal dependence as well as preference in locations. SST has been recognized as one of the major factors affecting tropical atmospheric circulations. The effect, however, displays temporal and spatial dependence. No attempt has been made to study tropical thermodynamics; rather, the dynamics of large-scale tropospheric circulations have been investigated through the use of gridded wind data. Velocity potential fields, as well as indices derived to represent zonal and meridional circulation intensities, have been examined in this chapter.

Correlations between variations of South African summer rainfall and wind distributions at various levels were also examined. These results are not presented here because of data limitations (quality and quantity) and hence lack of confidence. It

should be noted that the correlations computed with different data periods gave inconsistent results. However, an attempt is made to distinguish between circulations associated with relatively wet and dry periods over South Africa. The results supplement the findings of investigations with respect to longer term means.

Since the patterns of the velocity potential field display larger spatial scales than the actual divergence field, the former are more useful for the broad scale description of the thermally forced direct circulations which participate in, for example, the east-west overturnings within the tropical troposphere. The overturnings generate eddy kinetic energy through baroclinic processes and the energy is closely linked to the surface thermal boundary conditions across the tropics, particularly over the oceans. For example, the Walker circulation can be easily located by an upper level (200 hPa) divergent area in the velocity potential field over the highly convective region of the maritime continent (Indonesia and Borneo regions). In this area, high sea surface temperatures are associated with the ascending branch of the Walker cell. An upper-level convergent area is located over the cooler equatorial waters of the eastern Pacific, coincident with the descending branch of the cell (Figures 4.3, 4.4, and 4.5). The opposite divergent-convergent pattern can be depicted in the velocity potential field within the lower troposphere, such as at the 850 hPa level. This type of atmospheric response appears to be phase-locked with pools of warmer waters. When a warmer SST anomaly builds up in a region of the descending branch of the cell, for instance in an El Niño type of situation, the descending motion is arrested by the release of latent heat of condensation (Webster, 1981).

The locking of the high values of the divergent part of the total horizontal wind to the western Pacific and the Indonesia-Borneo region is evident throughout the year. The mass overturnings implied in the distribution of the velocity potential field form part of

the remote responses involved in atmospheric teleconnections. This field clearly locates three major centres of action around the maritime continent of southeast Asia, tropical Americas, and tropical Africa. These areas represent heat sources associated with tropospheric circulations which oscillate in sympathy with solar declination. They also show longitudinal shifts during the course of the year; the shifts appear to be phase-locked to areas of warmest waters and to continentality factors. Over Africa the systems display well-defined features during southern hemisphere winter. But they are more complex during the summer months.

The meridional and zonal circulation indices (MCIs and ZCIs) derived from the velocity potential field have been used as a convenient means of describing vertical circulations in the meridional and zonal vertical planes, respectively. The region of integration for the MCIs extends from 0° to 90°E and for the ZCIs from equator to 28.7°S. The MCIs clearly indicate rising motion around 10°S to 15°S and sinking at about 25°N during the southern hemisphere summer season.

The ZCI plots indicate an 850-500 hPa anticlockwise (viewed from the south), zonal, vertical cell (the African cell) with mean rising motion across Southern Africa and mean sinking over the Atlantic Ocean. A westward shift in the position of the cell from December through February is consistent with the observation of a sympathetic westward expansion of the heavy rains during these months, thus indicating a deeper layer of moisture flux inland. An adjacent 850-500 hPa clockwise cell (the Indian Ocean cell) connects the rising branch of the African system to a sinking branch over the Indian Ocean; this feature develops from December through February. The 200 hPa ZCI pattern also shows a gradual change from December through February when the Indian Ocean cell tends to deepen. It is suggested that these features are associated with the gradual warming of the sea surface from December (about 28°C) through February

(about 28.5°C), an increase in temperature of the order of one standard deviation for the area. Since the SSTs across the Indian Ocean are relatively high, a slight increase in the temperature can be expected to significantly increase the surface vapour pressure, and hence causing a circulation anomaly through related thermodynamic processes. A SST anomaly of about +0.5°C imposed in such areas can increase the surface vapour pressure by over 1 hPa. In other words, the higher low-level equivalent potential temperatures in these areas are conducive to taller clouds (via convective available potential energy), and thus elevated outflow signatures are more readily observed.

a. 850 hPa

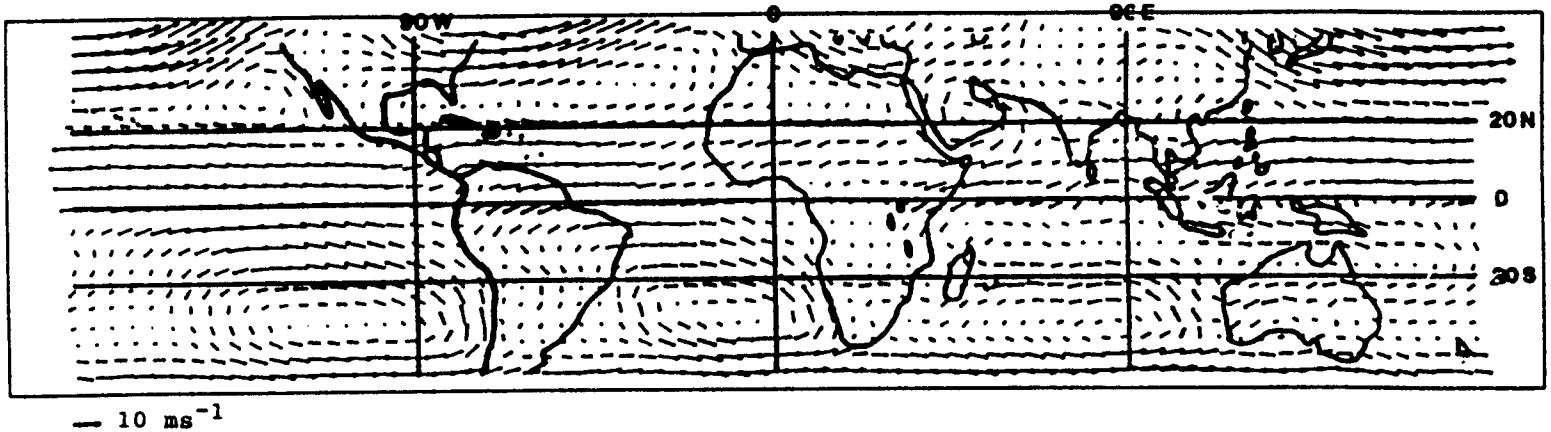

Figure 4.1
January mean winds, see text for data period.
a. 850 hPa
b. 500 hPa
c. 200 hPa

b. 500 hPa

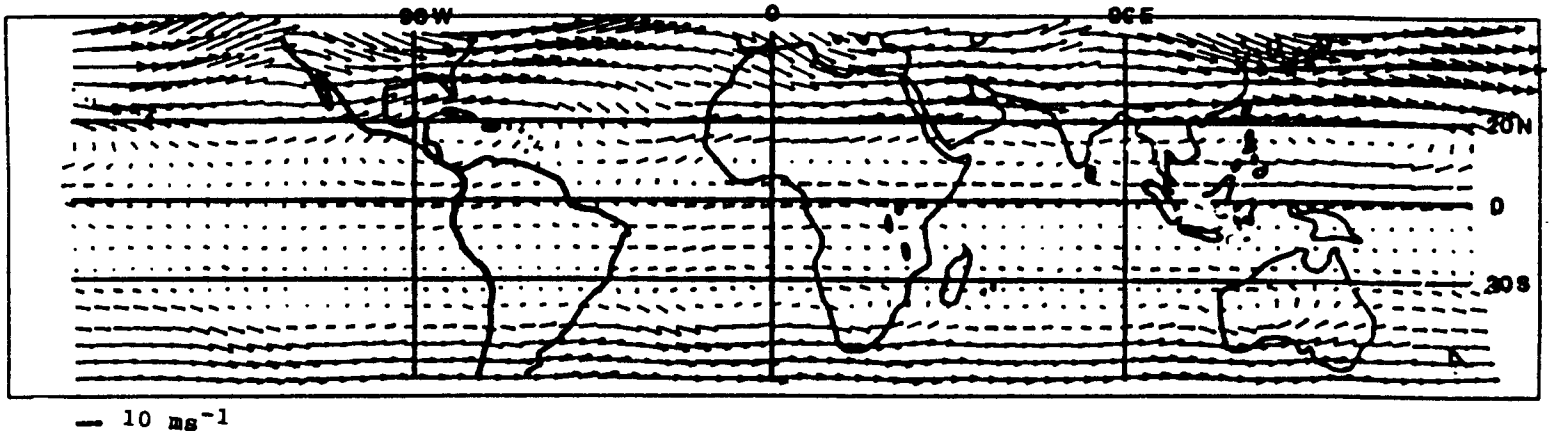

c. 200 hPa

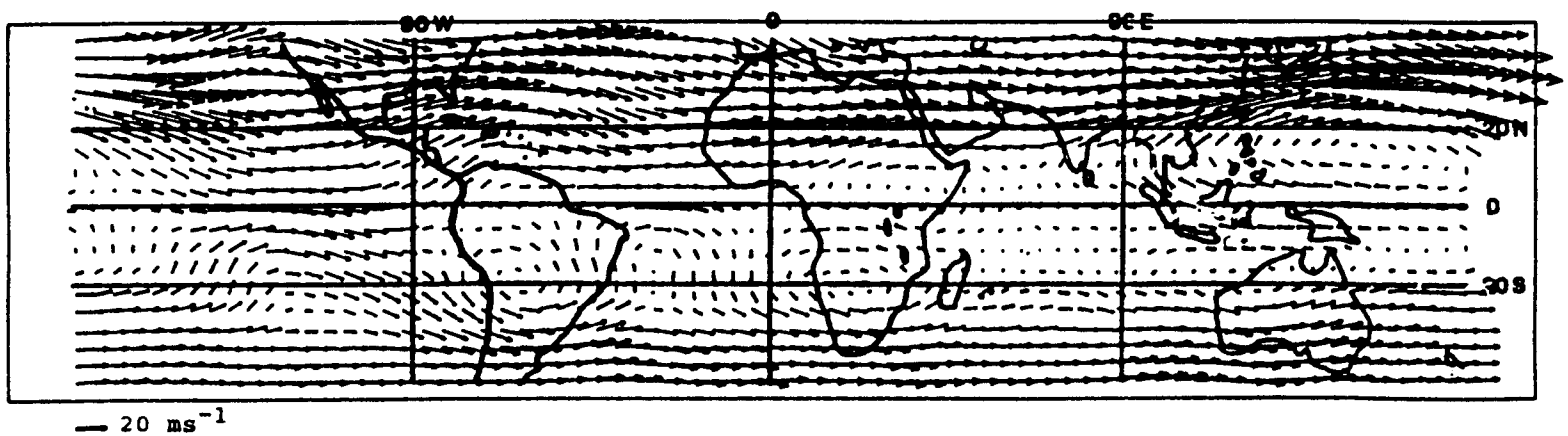

a. 850 hPa

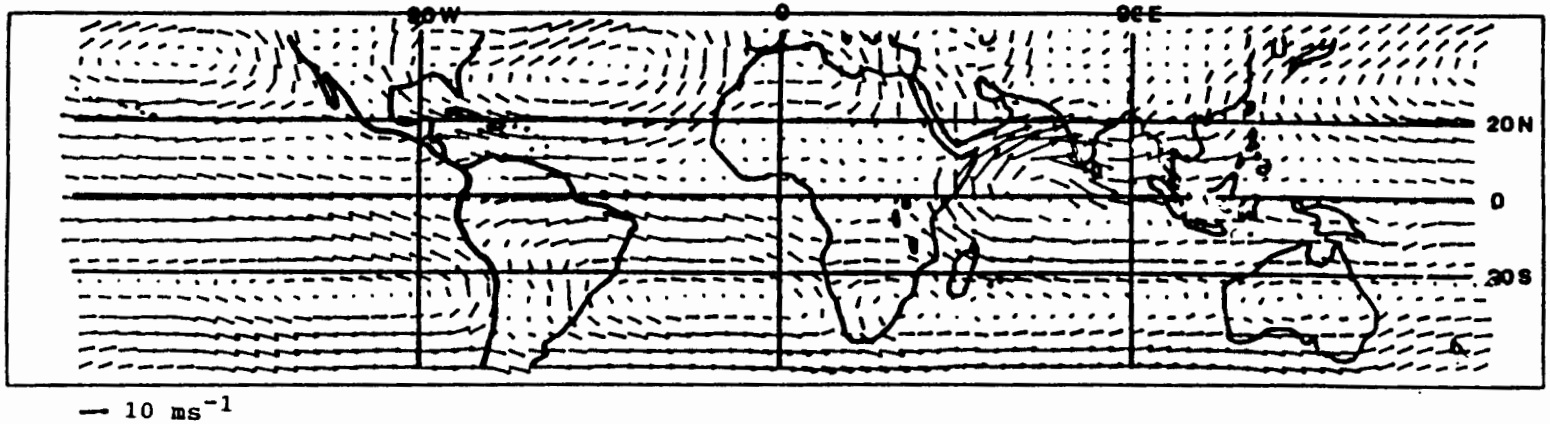

Figure 4.2
July mean winds,
see text for data period.
a. 850 hPa.
b. 500 hPa.
c. 200 hPa.

b. 500 hPa

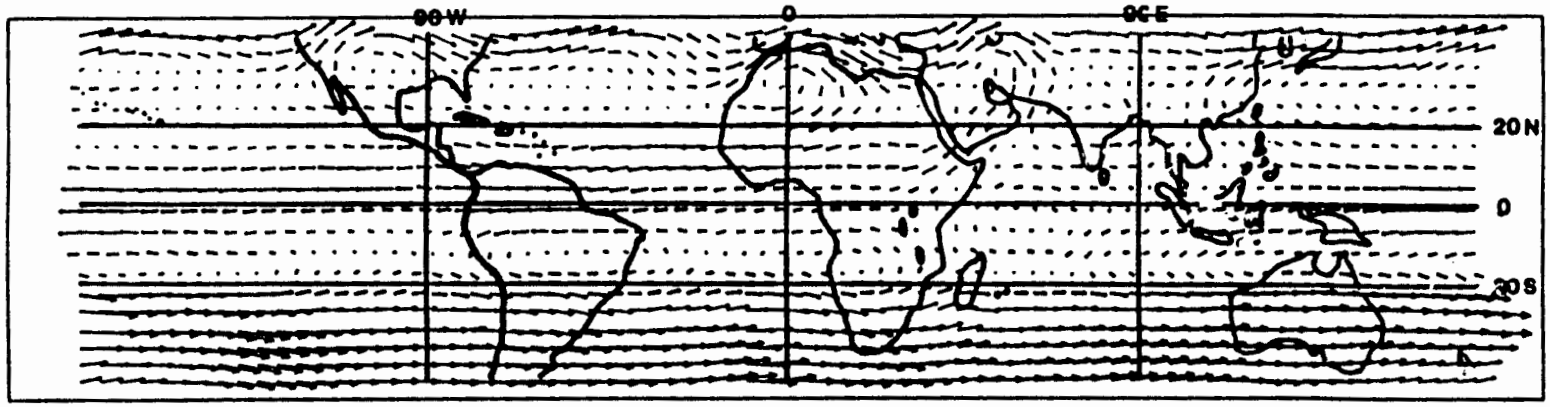

c. 200 hPa

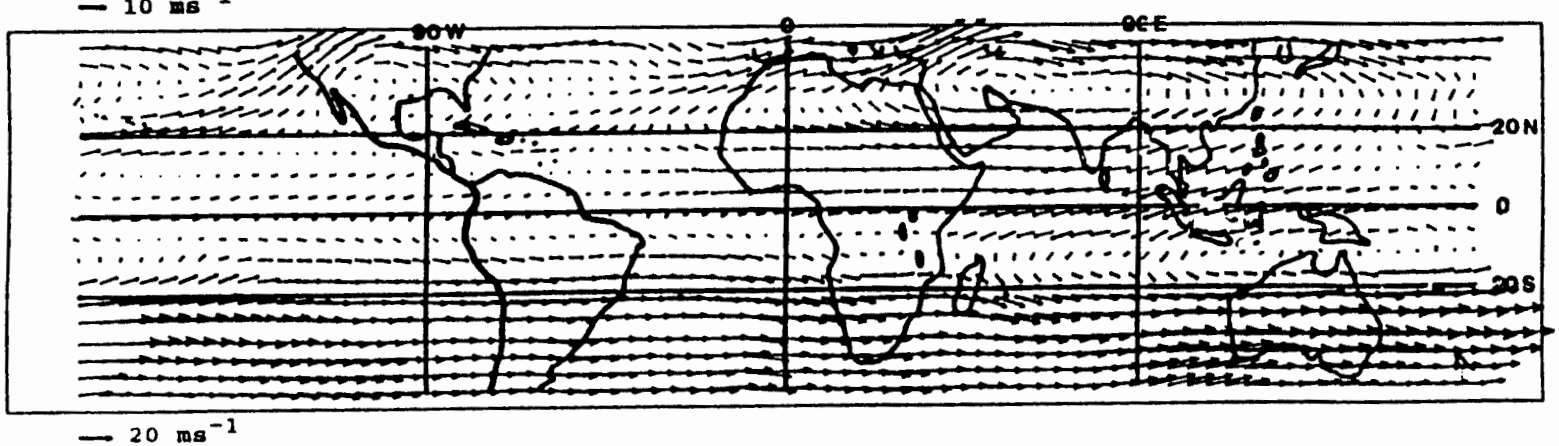

a. 850 hPa

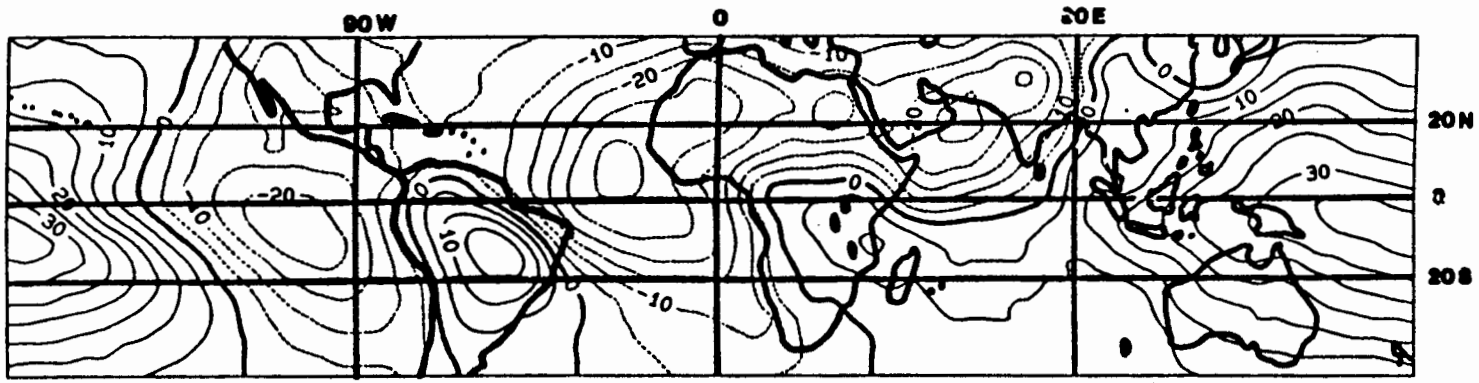

Figure 4.3
December mean velocity potential (m^2s^{-1}), based on years 1979-1986.
a. 850 hPa.
b. 500 hPa.
c. 200 hPa.

b. 500 hPa

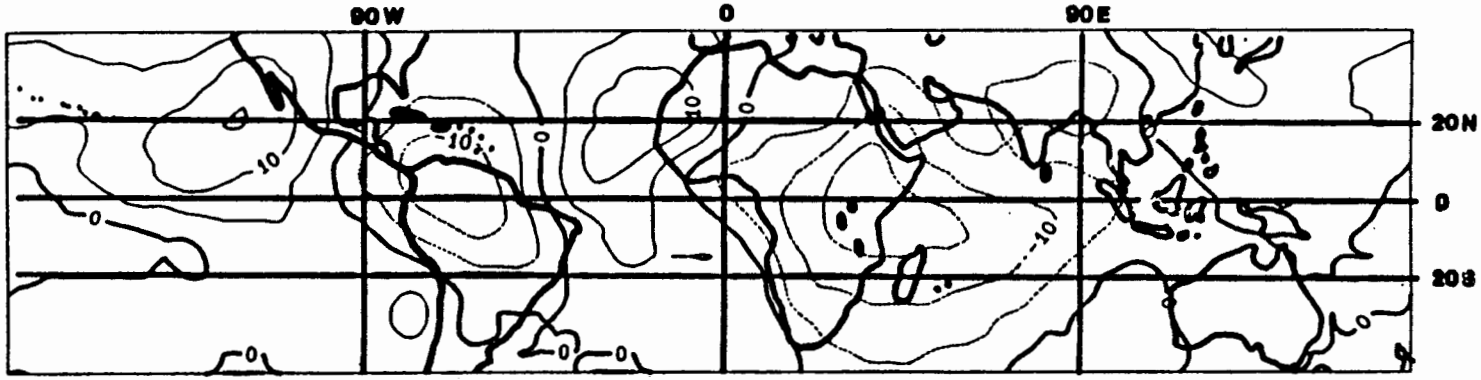

c. 200 hPa

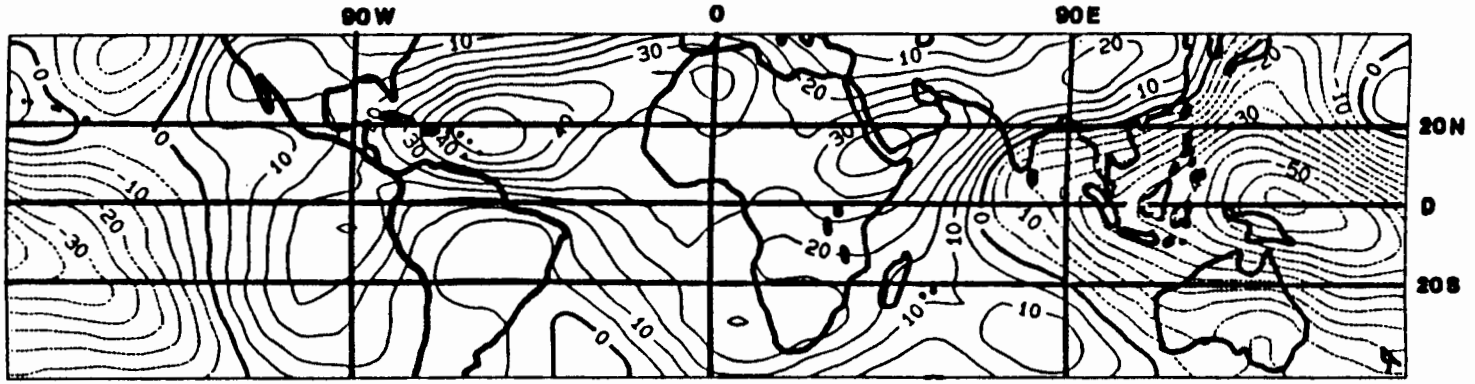

a. 850 hPa

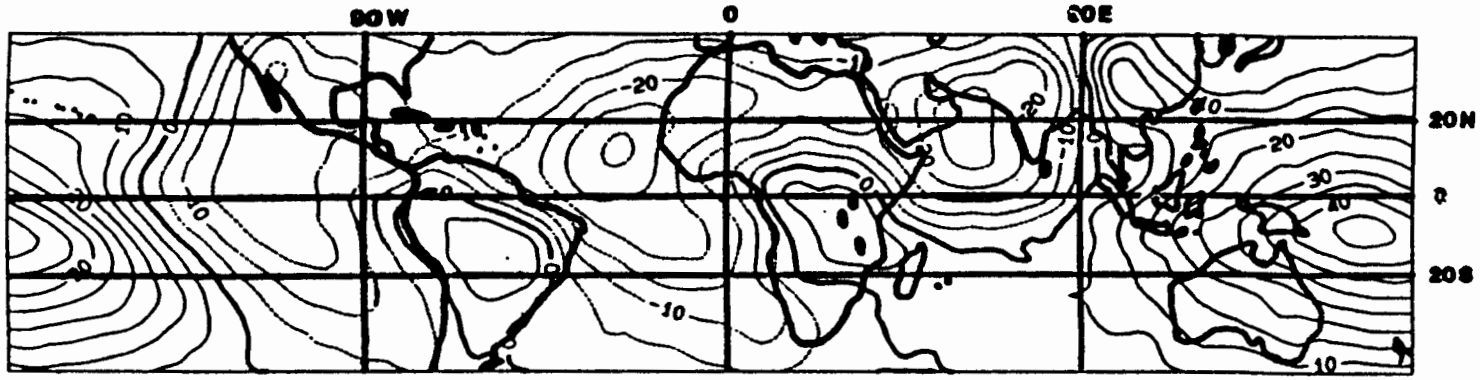

Figure 4.4
February mean velocity potential (m^2s^{-1}), based on years 1979-1987.
a. 850 hPa.
b. 500 hPa.
c. 200 hPa.

b. 500 hPa

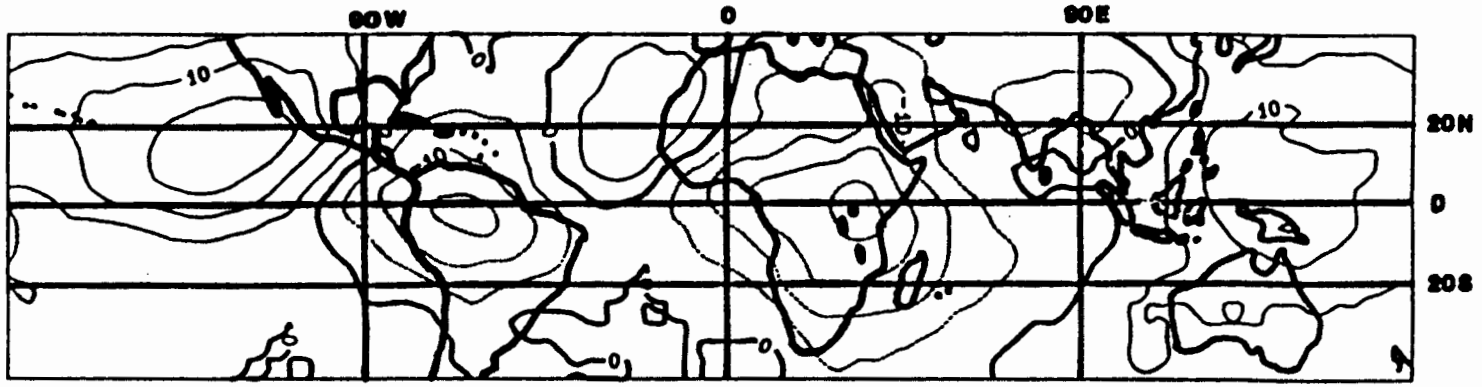

c. 200 hPa

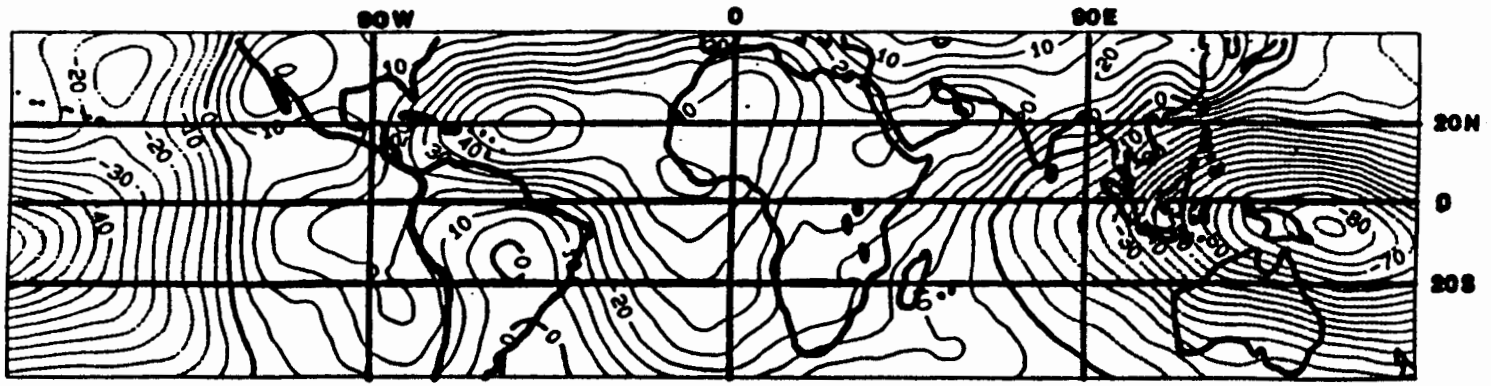

a. 850 hPa

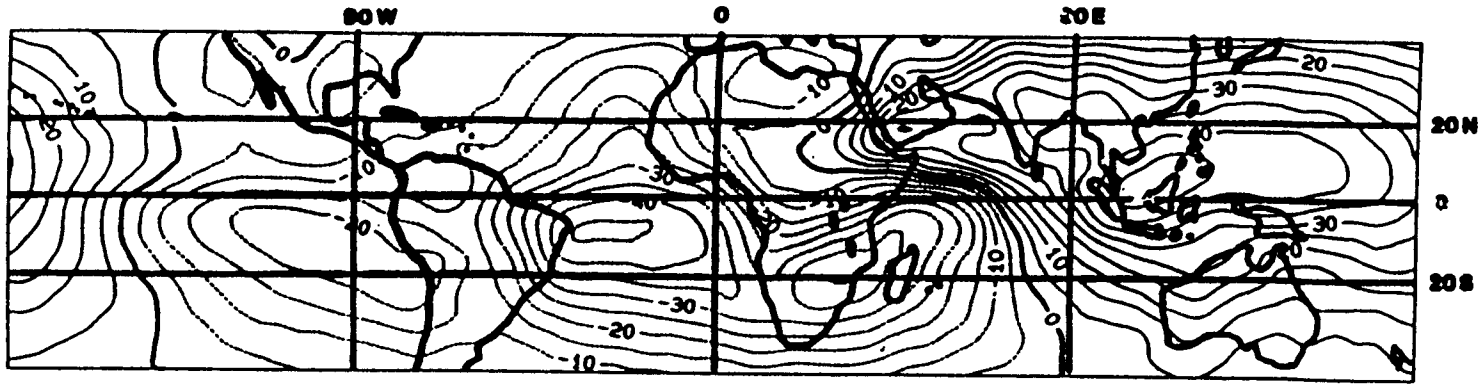

Figure 4.5
July mean
velocity potential (m^2s^{-1}),
based on years 1979-1986.
a. 850 hPa.
b. 500 hPa.
c. 200 hPa.

b. 500 hPa

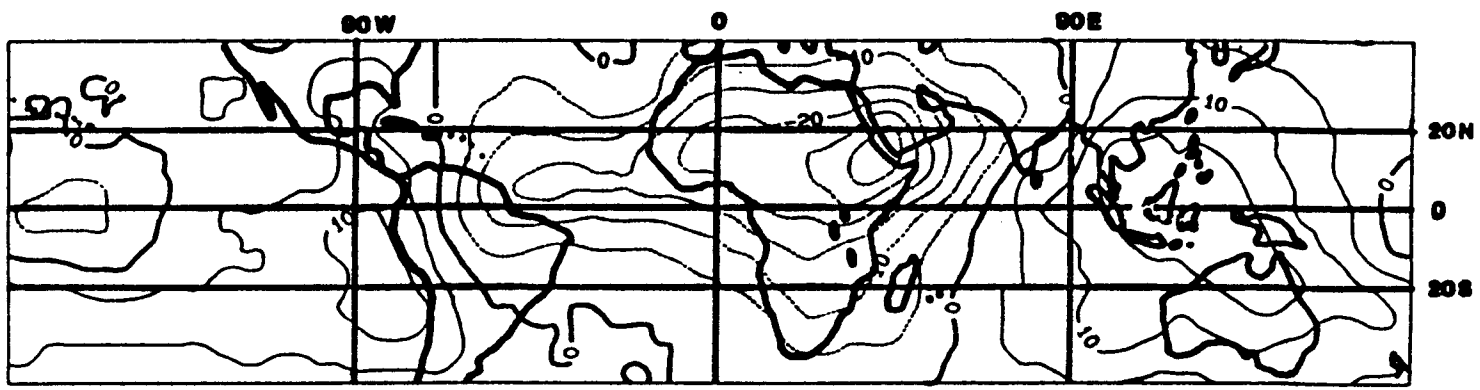

c. 200 hPa

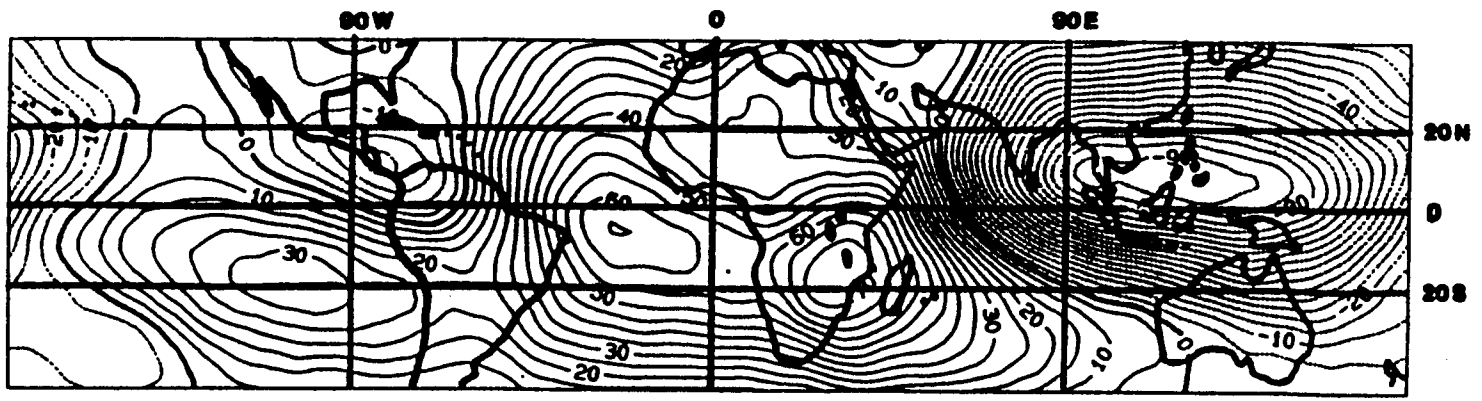

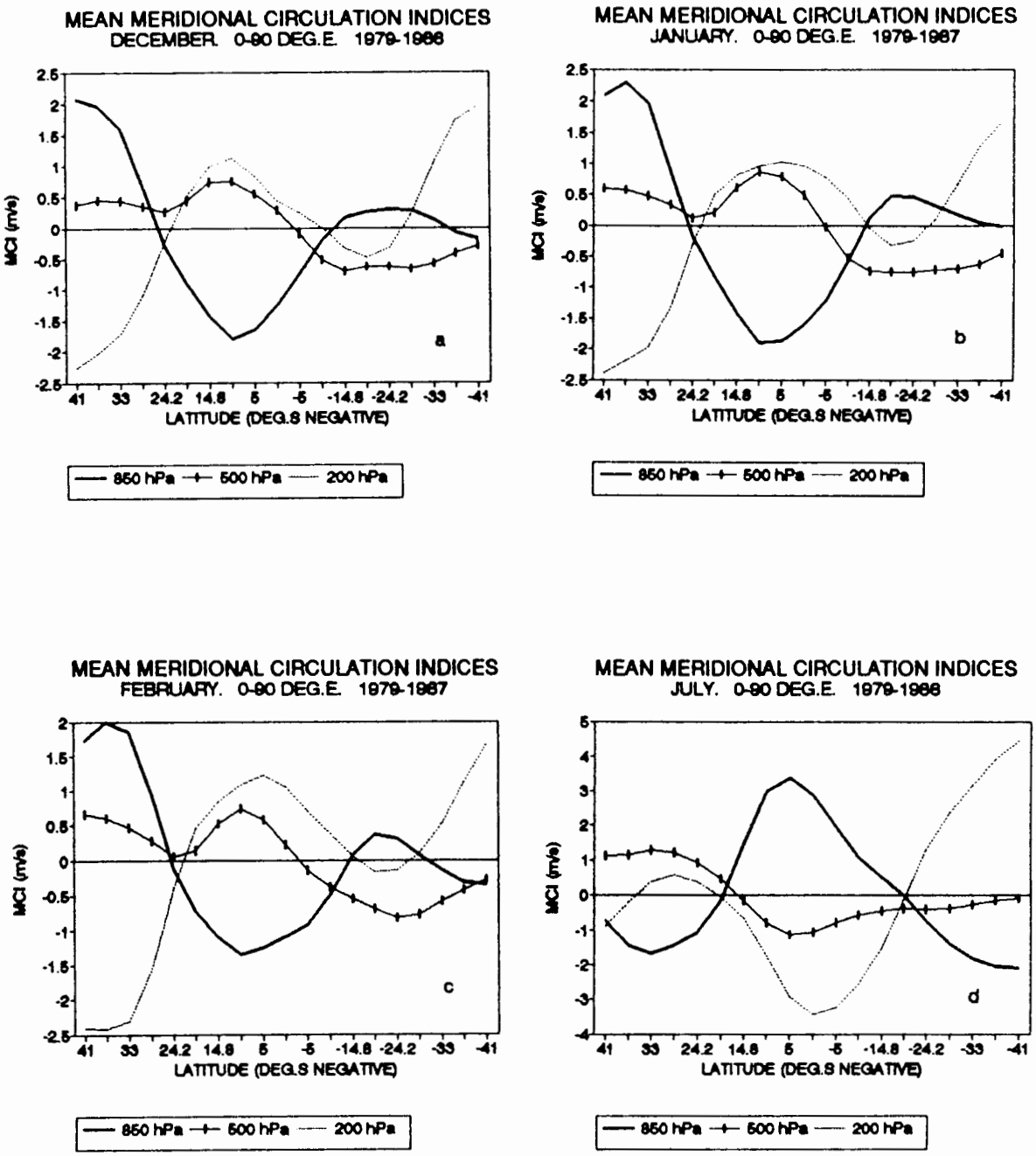

Figure 4.6

Mean meridional circulation indices. Integration belt: 0 to 90 deg. E.

a. December. b. January.

c. February. d. July.

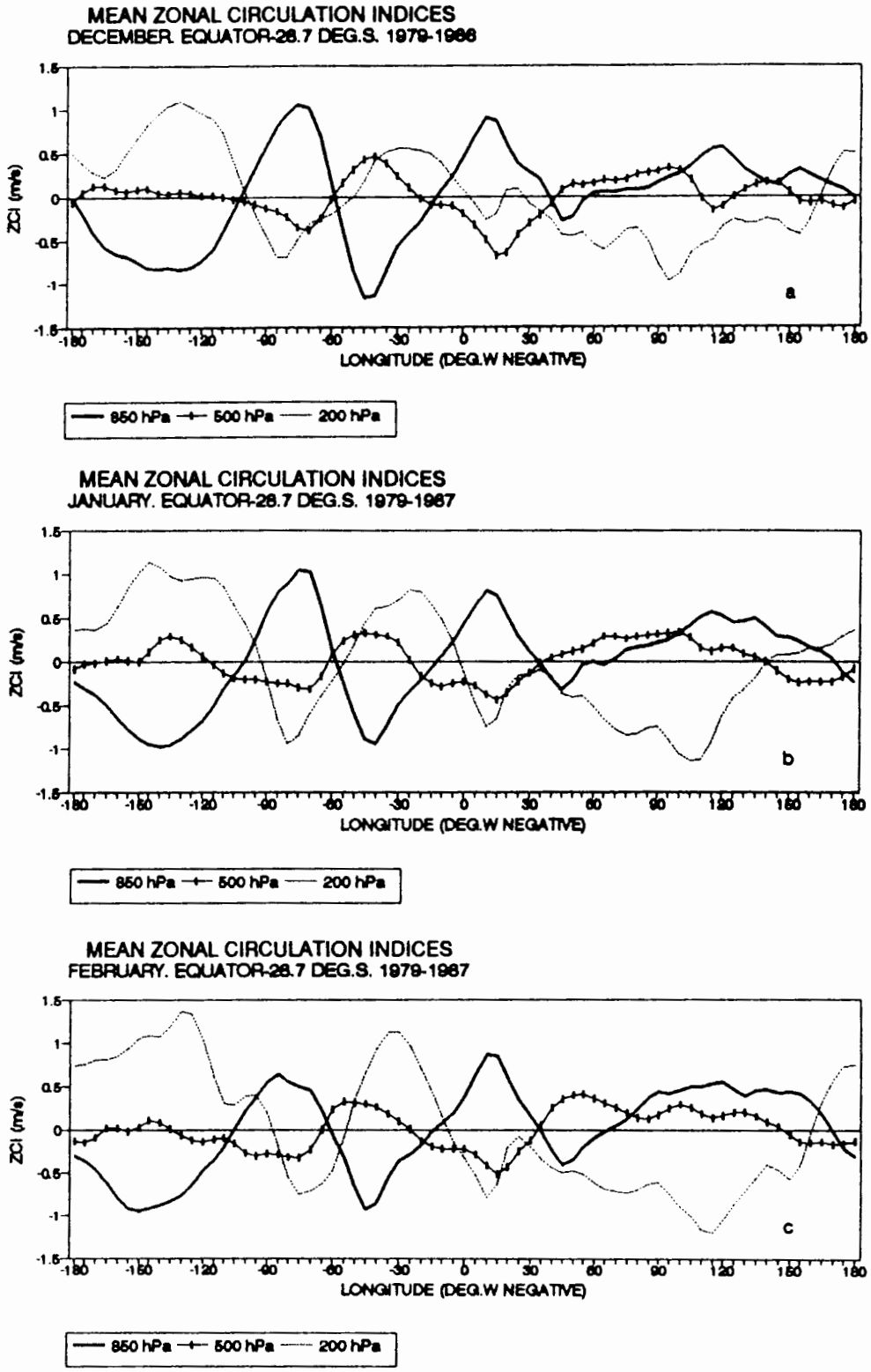

Figure 4.7

Mean zonal circulation indices.
Integration belt: Equator to 28.7 deg. S.
a. December. b. January.
c. February.

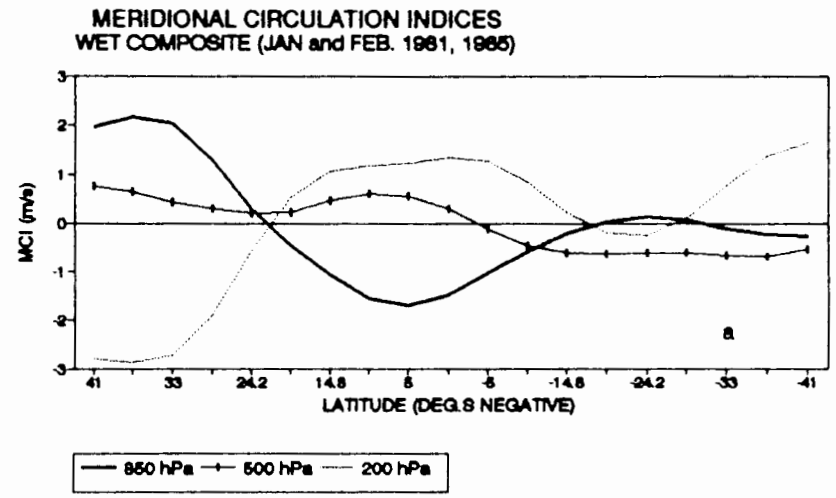

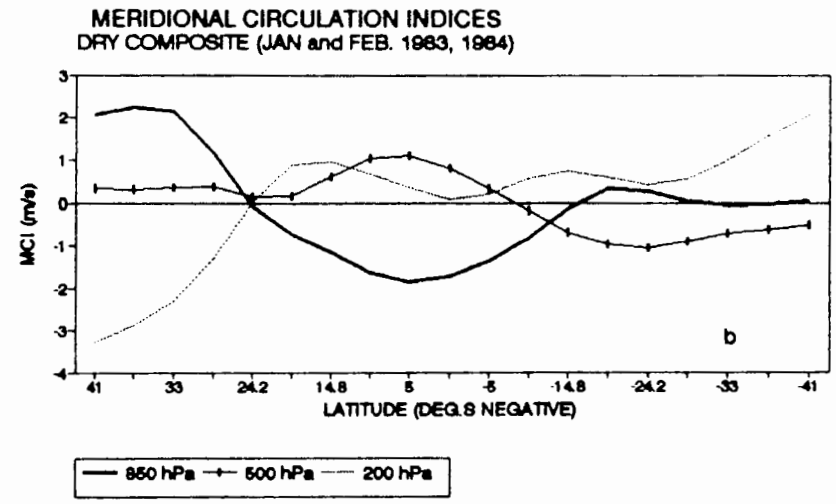

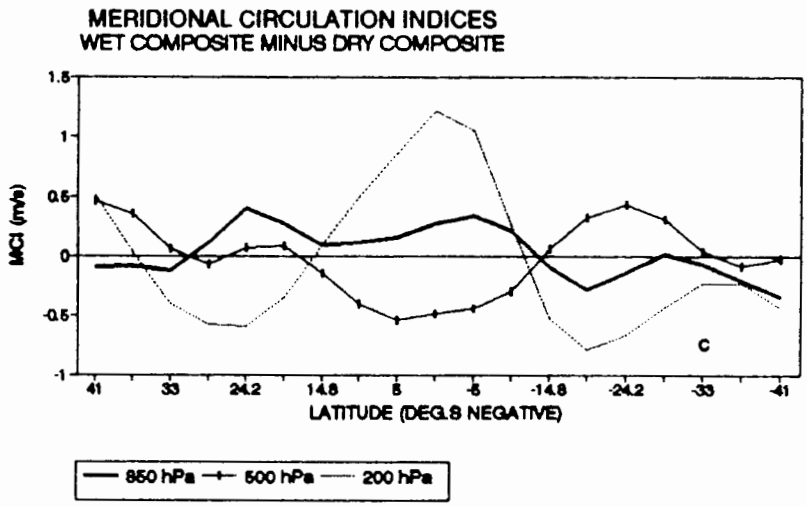

Figure 4.8

Meridional circulation index distributions.
Integration belt: 0 to 90 deg. E.

a. Wet composite. January and February, 1981 and 1985.
b. Dry composite. January and February, 1983 and 1984.
c. Wet composite minus dry composite.

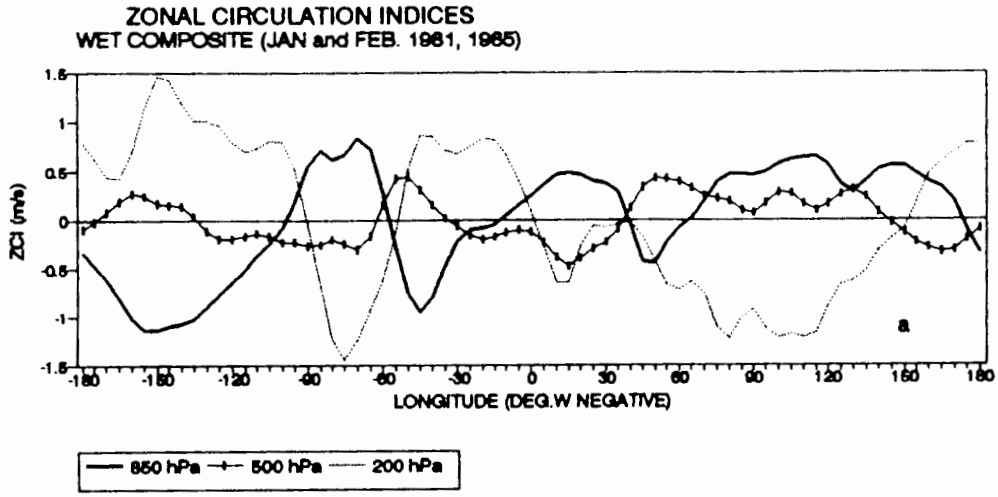

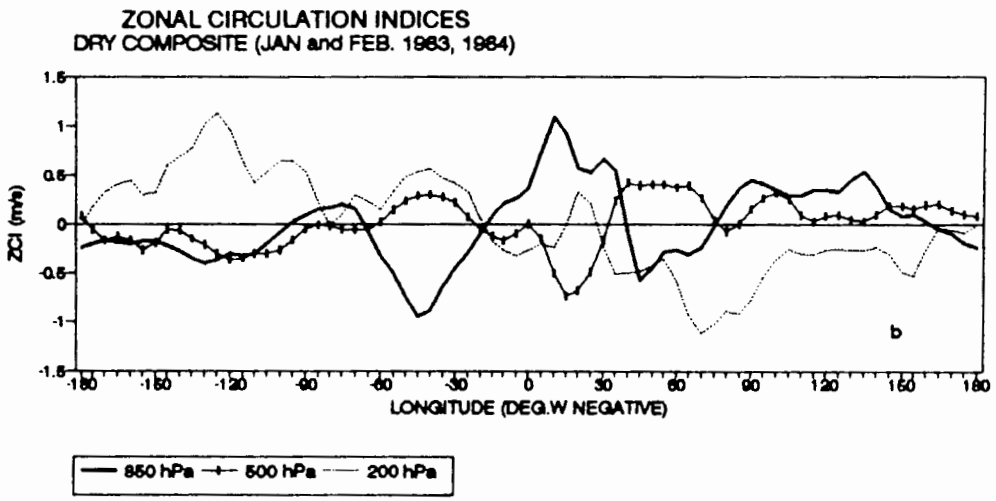

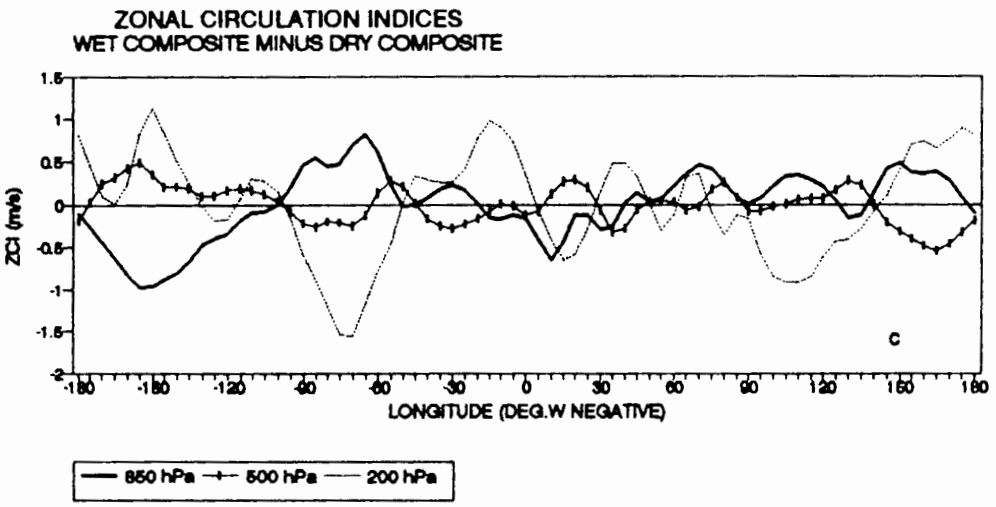

Figure 4.9

Zonal circulation index distributions.
Integration belt: Equator to 28.7 deg. S.

a. Wet composite. January and February, 1981 and 1985.
b. Dry composite. January and February, 1983 and 1984.
c. Wet composite minus dry composite.

CHAPTER 5

CONCLUSION AND SUGGESTIONS

5.1 CONCLUSION

Rainfall is one of the most important parameters reflecting climate variability and one of the most useful to forecast. The main bulk of summer rain over tropical and near-tropical regions of Africa, including South Africa, precipitates from convective systems. An understanding of the factors that control deep convection is essential to many aspects of ocean-atmosphere interaction research. Since realistic Coupled General Circulation Models tailored for use in the prediction of South African rainfall are yet to come, an alternative approach is to investigate the possibility of developing empirical models through statistical associations. Moreover, results from statistical studies are of value in testing the performance of numerical models; a sound empirical understanding is believed to be a prerequisite for the design of realistic numerical models (Hastenrath, 1986).

The principal goal of this study is to provide an objective, statistical basis for the prediction of South African summer rainfall anomalies on monthly to seasonal time scales. In order to achieve the goal, South African rainfall variations are analysed with respect to the fluctuations of SST and OLR. It is recognized that SST is one of the key factors influencing the generation and sustenance of large-scale deep convection. The relationship between convection and SST is, however, not uniform, but shows regional and seasonal dependence. Tropical circulation patterns are examined in order to confirm and complement observed and/or expected relationships. Part of the results presented in this study may be compared to those compiled in a correlation atlas (Jury et al., 1993) where various indices of rainfall and climatic determinants are employed.

Precursors of October and November All-Area rainfall are not evident in the SST and OLR fields. Of particular note is the change in sign of association from the October/November rainfall regime to the December through March regime, a feature indicative of a shift from advective processes to more of a teleconnection type of behaviour. December rainfall shows consistent positive correlations with the Western and Eastern Equatorial Pacific (WEP and EEP) SST and OLR variations up to lags of several months.

January, February and March All-Area rainfall variations tend to behave rather similarly with respect to OLR fluctuations within the four equatorial boxes (WEI, CEI, WEP, and EEP). December OLR in WEI can explain a large portion (about 50%) of the variance in rainfall of the following January, February and March. This link is probably related to the evolution of the Indian monsoon. The positive association implies that reduced cloudiness off the eastern coast of Africa in the November-December period precedes above normal mid- and late- summer rainfall over South Africa.

It has been observed that the All-Area rainfall variations during the months December to March are significantly (and negatively) correlated with SST variations over the equatorial belt of the Pacific and Indian Oceans. The rainfall relationships with convective activity across these areas confirm, and are consistent with, results obtained in analyses with respect to SST fluctuations. SST and OLR variations over the equatorial band represent tentative variables which could be utilized in the prediction of summer rainfall anomaly patterns across the central interior of South Africa. The contrasting nature of the correlation patterns with respect to December and January rainfall regimes appears intriguing. Independent checks show that December rainfall is uncorrelated with January rainfall. This aspect deserves further investigations.

Warmer than normal SSTs in the Central Equatorial Indian Ocean are conducive to deep cumulus/cumulonimbus convection and intense tropical cyclogenesis. These organized

systems then tend to be steered more poleward while exporting energy and momentum from the tropics. When the equatorial waters are cooler than normal, depressions in the Southwest Indian Ocean remain relatively shallow and are steered in the easterlies to eventually affect the Southern African subcontinent. Through subjective analyses of satellite image composites for the mid-summer months of January and February, Jury and Pathack (1991) have shown the existence of a wide variety of transient convective waves in the Southwest Indian Ocean. Complex feedback effects from (to) higher latitude westerlies could also influence (be influenced by) the processes.

Concentration of high values of the divergent part of the total horizontal wind over the warmer oceanic pools is evident throughout the year. The mass overturnings implied in the distributions of the velocity potential field form part of the responses involved in atmospheric responses at remote places. The wave number three pattern observed in the analyses is found to be a common feature of large-scale atmospheric circulation. The three areas represent heat sources associated with tropospheric circulations which oscillate in sympathy with solar declination. The circulations also show longitudinal shifts during the course of the year; the shifts are phase-locked to areas of warmest waters and are influenced by continentality factors. Over Africa the systems display well-defined features during southern hemisphere winter, but more complex patterns appear during the southern summer months.

Results of the investigations suggest that the vertical tropospheric systems (including the African and Indian Ocean cells) are among the important components which modulate South African climate. The large-scale circulations have an impact upon regional circulation cells. Of interest in this regard is the influence of the upper-level broad scale flow which affect the mean rising (and sinking) motion over the African areas.

Although the actual circulations are complex, Figure 5.1 schematically summarizes the implied, relative, zonal circulation anomalies corresponding to wet and dry summer conditions across southern African longitudes. The idealized cells exist only in a climatological sense and they reflect those features which are believed to be of importance to southern African summer climate variability. The 'coupled' African and Indian Ocean cells involve mean mass ascent over the southern African subcontinent and mean mass descents over the Indian and Atlantic Oceans in wet summers over South Africa (Figure 5.1a), while a relative reversal corresponds to drier conditions across the central interior of the country (Figure 5.1b). The Indian Ocean connection reflects a dipole-like behaviour between the two areas from a dynamic point of view, thus confirming results obtained from investigations involving SST and OLR variations with respect to rainfall. These east-west cells develop after November, and gradually intensify to attain peak amplitude about February or March. The upper-level (200 hPa) ZCI pattern also indicates a gradual change from December through February while the Indian Ocean cell tends to deepen. It is conjectured that, to a large extent, the anomalies are regulated by the evolution of the equatorial/tropical SSTs. The node over the Indian Ocean separates low-level easterlies to its west from low-level westerlies to its east (wet over South Africa). This feature is consistent with the findings of both Harrison (1983) and Walker (1989). The ZCI distributions are indicative of a westward tilt with altitude (at least over southern Africa).

The reason why near-equatorial SST anomalies exert a significant impact on atmospheric circulations in the equatorial and tropical areas is understandable. Since SST is relatively uniform in the equatorial band, anomalies of limited amplitude occurring there are able to produce considerable displacements of convective areas, which are the major atmospheric energy source regions; the associated divergent Hadley and Walker circulations are altered accordingly. This is true not only in regions within the maritime continent of Indonesia,

but also in the tropical areas of the Indian Ocean and probably in the Western parts of the Atlantic Ocean. In these areas, which are generally characterized by 'critical' thermal conditions, cumulus activity is very sensitive to even a slight additional heating in the lower troposphere.

Evidence has been provided on the possibility of formulating empirical models for the long-range prediction of summer rainfall anomalies over the central interior of South Africa. The statistically significant predictors could be utilized in new statistical forecasting techniques designed to make regional and broad scale circulation forecasts. Techniques involving partial and canonical correlations, cluster and linear discriminant analyses are being envisaged in the design of models to make probability forecasts of circulation and precipitation patterns on time scales of months and seasons.

Continued work is needed to establish long time series of high-quality data and to ensure their availability to research workers. Likewise, the rapid and regular analysis and dissemination of data in near-real time is necessary if they are to be successfully incorporated into operational long-range prediction schemes.

5.2 SUGGESTIONS

As far as long-range forecasting is concerned, it can be said that, given the equatorial SST field, the displacement of convective areas over equatorial oceans appears to be predictable to a considerable extent because they tend to follow the shifts of SST maxima and anomalies; consequently, the resulting alteration of the divergent Hadley and Walker types of circulation should be reasonably well determined from variations in the SST field. It is therefore believed that monitoring SST across the tropical ocean areas should form a crucial part of operational monthly and seasonal forecast system. Other oceanic and atmospheric variables will assist in the preparation of long-range forecasts. Such

monitoring activities and diagnostical as well as theoretical and numerical studies should help understand and improve the physical basis of long-range forecast techniques.

Of particular importance to practical long-range forecasting is the displacement of convective areas over the continents on a regional scale. Therefore, the additional influence of topography and the character of the ground surface has yet to be fully clarified.

Considering the relative importance of the continentality factor (as related to the vertical sensible heat fluxes and associated convergence), it is hypothesized that the oceanic boundary layer, depending on the state of SST distribution, can provide thermodynamic inputs to the lower atmosphere which in turn modify the regional circulation and moisture fluxes. Such tendency has been observed in the results of analyses of various meteorological parameters. Moreover, it is likely that the low-level trade wind inversion is involved in the processes, that is, teleconnections regulate the inversion level and thus moisture influx (and hence precipitation) across the land.

When moisture in the lower levels is available, enhanced convection is usually associated with a warm boundary layer and increased lapse rate (decreased atmospheric stability). Cooling in the mid-troposphere may further increase the intensity of convection. Here, the latent heat released by convection complicates the evolution. In addition, diabatic cooling due to melting of hydrometeors affect the vertical temperature profile and hence lapse rate. It is, therefore, suggested that further studies employing thermodynamic (including moisture) parameters should be carried out in order to identify the important contributing factors.

The El Niño-Southern Oscillation (ENSO) phenomenon normally occurs when higher than normal SSTs associated with lower than normal sea-level atmospheric pressure develop across the central and eastern Pacific Ocean; reduced trade winds in the area is an additional factor. The influence of such anomalous circulations on South African climate

has not been specifically investigated in this study. It is believed that, during 'strong ENSO' or 'strong anti-ENSO' periods, the Pacific SST dominates tropospheric circulations on a global scale. Hence, incorporation of variables related to ENSO should improve long-range prediction schemes.

Although the tropics are the major regions from the standpoint of air-sea interaction, the extratropical oceans should not be neglected. It has long been known that mean SSTs in mid-latitudes contribute appreciably to the intensity of evaporation and to changes in the thermal field along storm tracks at middle and high latitudes, thus modulating the degree of baroclinic instability.

More research, using more and better data sets, is required in order to further the understanding of the dynamics and thermodynamics of atmospheric circulation systems. Testing of the observed results through the use of General Circulation Models (GCMs) should not be neglected. Meanwhile, in light of the present study, empirical formulations could be designed for the prediction of South African summer rainfall anomalies through the use of tropical SST and OLR as predictors.

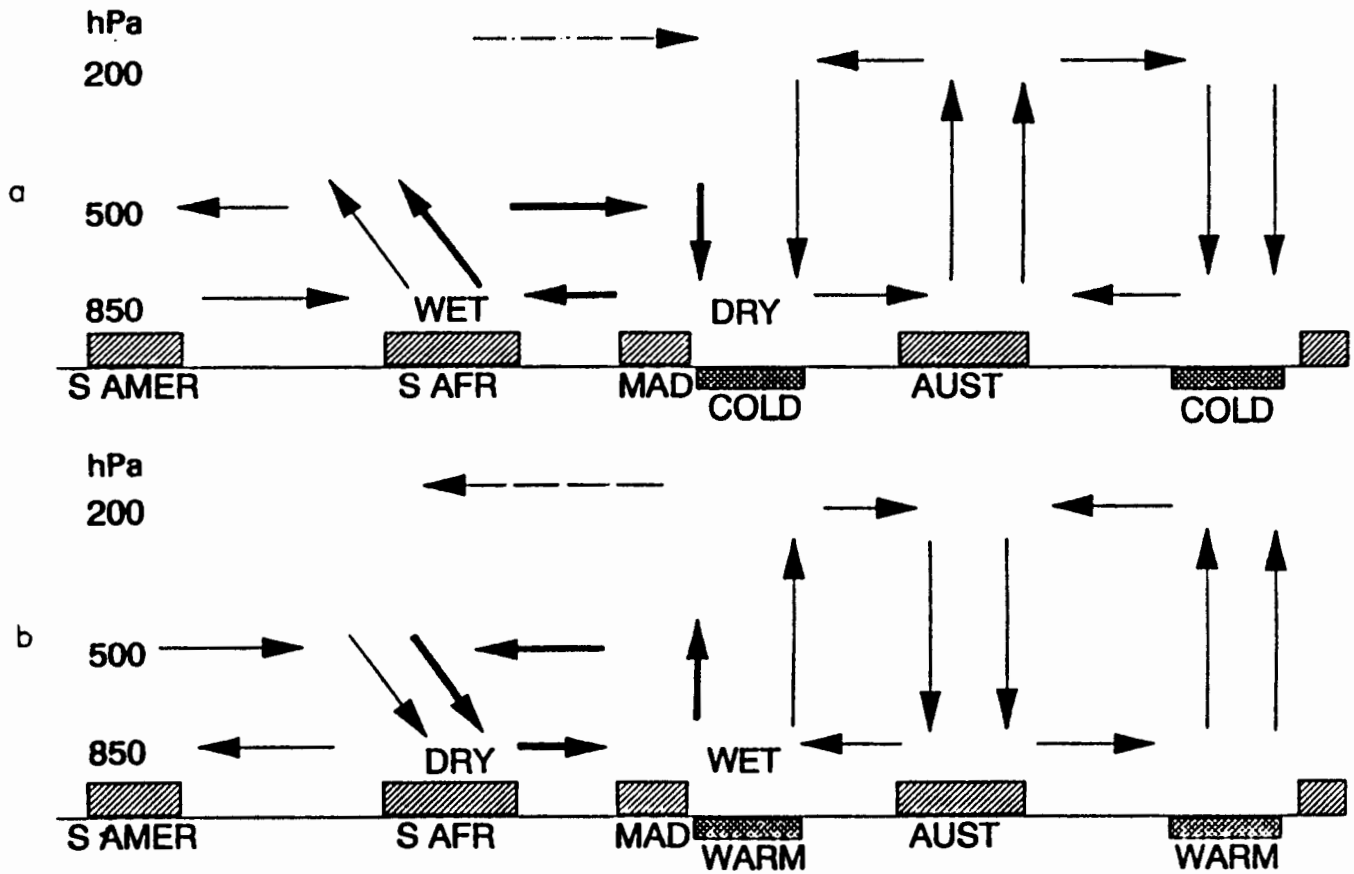

Figure 5.1. Idealized schematic of zonal–vertical circulations. Believed important with respect to southern African climate.
S AFR: South Africa. MAD: Malagasy. AUST: Australia.
S AMER: South America.
a. Relatively wet over South African summer rainfall area.
b. Relatively dry over South African summer rainfall area.

REFERENCES

Angell, J.K., 1981: Comparison of variations in atmospheric quantities with sea surface temperature variations in the equatorial eastern Pacific, *Monthly Weather review*, 109, 230-243.

Arkin, P.A., 1982: The relationship between interannual variability in the 200 mb tropical wind field and the Southern Oscillation. *Monthly Weather review*, 110, 1394-1404.

Arkin, P. A. and P. E. Ardunay, 1989: Estimating climatic-scale precipitation from space: A review, *Journal of Climatology*, 2, 1229-1238.

Arkin, P. A., V. E. Kousky, J. E. Janowiak and E. A. O'Lenic,1986: Atlas of the tropical and subtropical circulation derived from National Meteorological Center operational analyses. *NOAA Atlas No. 6*, United States Department of Commerce.

Barnett, T. P., 1977: An attempt to verify some theories of El Niño, *Journal of Physical Oceanography*, 7, 633-647.

Barnett, T.P., 1983: Interaction of the monsoon and Pacific trade wind systems at interannual time scales. Part I: The equatorial zone, *Monthly Weather review*, 111, 756-773.

Barnett, T.P., 1984 a: Interaction of the monsoon and Pacific trade wind systems at interannual time scales. Part II: The tropical band, *Monthly Weather review*, 112, 2380-2387.

Barnett, T.P., 1984 b: Interaction of the monsoon and Pacific trade wind systems at interannual time scales. Part III: A partial anatomy of the Southern Oscillation, *Monthly Weather review*, 112, 2388-2400.

Barnett, T.P., 1984 c: Long-term trends in surface temperature over the oceans, *Monthly Weather review*, 112, 303-312.

Barnett, T.P., 1985: Variations in mean-global sea level pressure, *Journal of Atmospheric Sciences*, 42, 478-501.

Barnett, T.P. and R.C.J. Somerville, 1983: Advances in short-term climate predictions, *Reviews in Geophysics and Space Physics*, 21, 1096-1102.

Bedient, H.A., W.G. Collins and G. Dent, 1967: An operational tropical analysis system, *Monthly Weather review*, 95, 942-949.

Bergman, K.H., 1979: Multivariate analysis of temperature and winds using optimum interpolation, *Monthly Weather review*, 107, 1423-1444.

Berlage, H. P., 1957: Fluctuations of the general atmospheric circulation of more than one year, their nature and prognostic value. *Meded. Verh. Koninklijk Netherlands Meteorologisch Instituut*, No. 69, 152 pp. (Available from Royal Netherlands Meteorological Institute, De Bilt, 3730 AE, Netherlands).

Berlage, H. P., 1966: The Southern Oscillation and world weather. *Meded. Verh. Koninklijk Netherlands Meteorologisch Instituut*, No. 88, 152 pp. (Available from Royal Netherlands Meteorological Institute, De Bilt, 3730 AE, Netherlands).

Bjerknes, J., 1966: A possible response of the atmospheric Hadley circulation to equatorial anomalies of ocean temperature, *Tellus*, 18, 820-829.

Bjerknes, J., 1969: Atmospheric teleconnections from the equatorial Pacific, *Monthly Weather Review*, 97, 163-172.

Buchmann, J., L.E. Buja, J. Paegle, C.D. Zhan and D.P. Baumhefner, 1986: FGGE forecast experiements for Amazon Basin rainfall, *Monthly Weather review*, 114, 1625-1641.

Buchmann, J., J. Paegle, L. E. Buja and R.E. Dickinson, 1989: Further FGGE forecast experiments for the Amazon Basin rainfall, *Monthly Weather review*, 117, 1093-1102.

Buchmann, J., J. Paegle, L. E. Buja and R.E. Dickinson, 1990: The effect of tropical Atlantic heating anomalies upon GCM rain forecasts over the Americas, *Journal of Climate*, 3, 189-208.

Cane, M.A., 1986: El Niño, *Annual review of Earth and Planetary Sciences*, 14, 43-70.

Chelliah, M., J.E. Chemm and H.M. van Den Dool, 1988: The impact of low-latitude anomalous forcing on local and remote circulation: Winters 1978/79-1986/87, *Journal of Climate*, 1, 1138-1152.

Chiu, W.-C. and A. Lo, 1979: A preliminary study of the possible statistical relationship between the tropical Pacific sea surface temperature and the atmospheric circulation, *Monthly Weather Review*, 107, 18-25.

Chu, P.S. and S.U. Park, 1984: Regional circulation characteristics associated with a cold surge event over east Asia during winter MONEX, *Monthly Weather Review*, 112, 955-965.

Cressman, G. P. and B. W. Helmick, 1989: Origins of the winter dryness of Southern Africa. *Third International Conference on Southern Hehisphere Meteorology and Oceanography*, American Meteorological Society, 238, 239.

Danard, M., 1986: On the sensitivity of predictions of maritime cyclogenesis to convective precipitation and sea temperature, *Atmosphere-Ocean*, 24, 52-72.

Dyer, T.G.J., 1979: Rainfall along the east coast of Southern Africa, the Southern Oscillation and the latitude of the subtropica high pressure belt, *Quarterly Journal of the Royal Meteorological Society*, 105, 445-452.

Ferranti, L. T. N. Palmer, F. Molteni and E. Klinder, 1990: Tropical-extratropical interaction associated with teh 30-60 day oscillation and its impact on medium and extended range prediction, *Journal of Atmospheric Sciences*, 18, 2177-2199.

Fletcher, J., R. J. Slutz, S. J. Lubker, J. D. Hiscox, S. D. Woodruff, R. L. Jenne, D. H. Joseph, P. M. Steurer and J. D. Elms, 1985: Comprehensive Ocean Atmosphere Data Set, Release I. *NOAA, Environmental Research Laboratories*, Climate Research Program, Boulder, Colorado, 268 pp.

Gadgil S., A. Guruprasad and J. Srinivasan, 1992: Systematic bias in the NOAA longwave radiation dataset ?, *Journal of Climate*, 8, 867-875.

Gandin, L.S., 1963: Objective analysis of Meteorological fields. Gidrometeor, Leningrad. *Israel Program for Scientific Translations*, Jerusalem, 1965, 242 pp.

Godfrey, J.S. and T.J. Golding, 1981: The Sverdrup relation in the Pacific-Indian Ocean throughflow on the Indian Ocean circulation and on the East Australian Current, *Journal of Physical Oceanography*, 11, 771-779.

Gorven, J., 1988: User guide (CCWR Data). Available from *Computing Centre for Water Research*, Pietermaritzburg, South Africa.

Gorven, J. and M.C. Dent, 1988: CCWR Data products and applications guide. Available from *Computing Centre for Water Research*, Pietermaritzburg, South Africa.

Gutzler, D. S. and T. M. Wood, 1990: Structure of large-scale convective anomalies over tropical oceans, *Journal of Climate*, 3, 483-496.

Halpert, M. S. and C. F. Ropelewski, 1989: Atlas of tropical sea surface temperatures and surface winds. *NOAA Atlas No. 8, National Meteorological Center, National Weather Service*, Silver Spring, MD, U. S. Department od Commerce.

Harrison, M.S.J., 1983: The Southern Oscillation, zonal equatorial circulation cells and South African rainfall. *Reprints of the 1st International Conference on Southern Hemisphere Meteorology*, American Meteorological Society, 302-305.

Harrison, M.S.J., 1984: A generalized classification of South African summer rain-bearing synoptic systems, *Journal of Climatology*, 4, 547-560.

Harrison, M.S.J., 1986: A synoptic climatology of South African rainfall variations. *Unpublished Ph.D. thesis*, University of the Witwatersrand, 341pp.

Harrison, M.S.J., J.A. Lindesay and G.F. Theron, 1985: Progress towards long-term rainfall forecasting over South Africa. R*eprints from proceedings of the Second South African National Hydrology Symposium*, Pietermaritzburg, 16-18 September 1985, South African National Committee for the International Association of Hydrological Sciences.

Hastenrath, S., 1984: Interannual variability and annual cycle: Mechanisms of circulation and climate in the tropical Atlantic sector, *Monthly Weather Review*, 112, 1097-1197.

Hastenrath, S., 1985: Climate and Circulation of the Tropics. D. Reidel, *Dordrecht*, 455 pp.

Hastenrath, S., 1986: On climate prediction in the tropics, *Bulletin of American Meteorological Society*, 67, No.6, 696-702.

Hastenrath, S., 1990: Tropical climate prediction: A progress report, 1985-90, *Bulletin of American Meteorological Society*, 71, 819-825.

Hastenrath, S., 1990: The relationship of highly reflective clouds to tropical climate anomalies, *Journal of Climate*, 3, 353-365.

Heddinghaus, T.R. and A.F. Krueger, 1981: Annual and interannual variations in outgoing longwave radiation over the tropics, *Monthly Weather review*, 109, 1208-1218.

Hildebrandsson, H. H., 1897: Quelques recherches sur les centres d'action de l'atmosphere, *Konglica Svenska Ventenskapsa Kademiens Handlingar*,29, 33pp.

Hirst, A.C. and S. Hastenrath, 1983: Atmosphere-ocean mechansism of climate anomalies in the Angola-tropical Atlantic sector, *Journal of Physical Oceanography*, 13, 1146-1157.

Höflich, O., 1984: Climate of the South Atlantic Ocean, in *World Survey of Climatology*, 15, edited by H. van Loon, 1-132, Elsevier, New York.

Hofmeyr, W.L. and V. Gouws, 1964: A statistical and synoptic analysis of wet and dry conditions in northwestern Transvaal, *Notos*, 13, 37-48.

Holton, J.R., 1973: An introduction to dynamic meteorology. *Academic Press*, 319pp.

Holton, J.R., 1979: An introduction to dynamic meteorology. *Academic Press*, 391pp.

Horel, J.D. and J.M.Wallace, 1981: Planetary scale atmospheric phenomena associated with the Southern Oscillation, *Monthly Weather review*, 109, 813-829.

James, I.N. and L.T. Anderson, 1984: The seasonal mean flow and distribution of large-scale weather systems in the Southern Hemisphere: effects of moisture transports, *Quarterly Journal of the Royal Meteorological Society*, 110, 943-966.

Janowiak, J.E., 1988: An investigation of interannual rainfall variability in Africa, *Journal of Climate*, 1, 240-255.

Janowiak, J. E., 1992: Tropical rainfall: A comparison of satellite-derived rainfall estimates with model precipitation forecasts, climatologies and observations, *Monthly Weather review*, 120, 448-462.

Julian, P.R. and R.M. Chervin, 1978: A study of the Southern Oscillation and Walker Circulation phenomena, *Monthly Weather Review*, 106, 1433-1451.

Jury, M.R. and N.D. Walker, 1988: Marine boundary layer modification across the edge of the Agulhas Current, *Journal of Geophysical Research*, 93, 647-654.

Jury, M. R. and B. Pathack, 1991: A study of climate and weather variability over the tropical southwest Indian Ocean, *Meteorology and Atmospheric Physics*, 47, 37-48.

Jury, M.R., B. Pathack and D.M. Legler, 1991: Structure and variability of surface atmospheric circulation anomalies over the tropical south-west Indian Ocean in the Austral summer, *South African Journal of Marine Science*, 11, 1-14.

Jury, M. R., B. Pathack, G. Campbell, B. Wang and W. Landman, 1991: Transient convective waves in the tropical SW Indian Ocean, *Meteorology and Atmospheric Physics*, 47, 27-36.

Jury, M. R., K. Levey, C. Mc Queen, B. Parker, A. Lee-Thorpe, A. Makarau and B Pathack, 1993: Correlation atlas of climatic determinants for sub-tropical southern Africa and the SW Indian Ocean. *Prepared under the auspices of the Water Research Commission Project: Mechanisms of rainfall variability. Supervised by M. R. Jury, Oceanography Department, University of Cape Town, South Africa.*

Kanamitsu, M. and T.N. Krishnamurti, 1978: Northern Summer Tropical circulations during drought and normal rainfall months, *Monthly Weather Review*, 106, 331-347.

Kidson, J. W., 1975: Tropical eigenvector analysis and the Southern Oscliiation, *Monthly Weather review*, 103, 197-216.

Kistler, R.E. and D.F. Parrish, 1982: Evolution of the NMC data assimilation system: September 1978 - January 1982, *Monthly Weather review*, 110, 1335-1346.

Kraus, E. B., 1977: Subtropical droughts and cross-equatorial energy transports, 105, *Monthly Weather review*, 1009-1018.

Krishnamurti, T. N., 1971: Tropical east-west circulations during the northern summer, *Journal of Atmospheric Sciences*, 28, 1342-1347.

Krishnamurti, T.N., M. Kanamitsu, W.J. Koss and J.D. Lee, 1973: Tropical East-West Circulations during the Northern Winter, *Journal of Atmospheric Sciences*, 30, 780-787.

Kung, E.C. and T.A. Sharif, 1982: Long-range forecasting of the Indian Summer monsoon onset and rainfall with upper air parameters and sea surface temperature, *Journal of the Meteorological Society of Japan*, 60, 672-681.

Lau, K.-M. and P.H. Chan, 1983 a: Short-term climate variability and atmospheric teleconnections from satellite-observed outgoing longwave radiation. Part I: Simultaneous relationships, *Journal of Atmospheric Sciences*, 40, 2735-2750

Lau, K.-M. and P.H. Chan, 1983 b: Short-term climate variability and atmospheric teleconnections from satellite-observed outgoing longwave radiation. Part II: Lagged correlations, *Journal of Atmospheric Sciences*, 40, 2751-2767.

Lau, N.-C. and A.H. Oort, 1981: A comparative study of observed Northern hemisphere circulation statistics based on GFDL and NMC analyses. Part I: The time-mean fields, *Monthly Weather review*, 109, 1380-1403.

Liebmann, B. and D. L. Hartmann, 1982: Interannual variation of outgoing IR associated with tropical circulation changes during 1974-78, *Journal of Atmospheric Sciences*, 39, 1153-1162.

Lindesay, J.A., 1988: The Southern Oscillation and atmospheric circulation changes over Southern Africa. *Unpublished Ph.D. thesis*, University of the Witwatersrand, Johannesburg, 284 pp.

Lindesay, J.A., Harrison, M.S.J. and M.P. Haffner, 1986: The Southern Oscillation and South African rainfall, *South African Journal of Science*, 82, 196-198.

Livezey, R.E. and W.Y. Chen, 1983: Statistical field significance and its determination by Monte Carlo techniques, *Monthly Weather Review*, 111, 46-59.

Lockyer, N. and W. J. S. Lockyer, 1902: On the similarity of the short-period pressure variation over large areas, *Proceedings of the Royal Society of London*, 73, 459-470.

Machado, L. A. T., M. Desbois and J. P. H. Duvel, 1992: Structural characteristics of deep convective systems over tropical Africa and the Atlantic Ocean, *Monthly Weather review*, 120, 392-406.

Markham, C.G. and D.R.McLain, 1977: Sea surface temperature related to rain in Ceara, noth-eastern Brazil, *Nature*, 265, 320-323.

Mey, R.D., N.D. Walker and M.R. Jury, 1989: Surface heat fluxes and marine boundary layer modification in the Agulhas Retroflection region, *Journal of Geophysical Research*, submitted.

Mitchell, J.M., B. Dzerdzeevski, H.F. Flohn, W.L. Hofmeyr, H.H. Lamb, K.N. Rao and C.C. Wallén, 1966: Climatic Change, *Technical Note* No. 79, World Meteorological Organization, 79pp.

Mobley, C.D. and R.W. Preisendorfer, 1985: Statistical analysis of historical climate data set, *Journal of Climate and Applied Meteorology*, 24, 555-567.

Molinari J. and M. Durek, 1992: Parameterization of convective precipitation in mesoscale numerical models: A critical review, *Monthly Weather review*, 120, 326-344.

Montgomery, R.B., 1940: Report on the work of G.T. Walker, *Monthly Weather review*, 39 (Supplement), 1-22.

Moura, A.D. and J. Shukla, 1981: On the dynamics of droughts in northeast Brazil: Observations, theory and numerical experiments with a general circulation model, *Journal of Atmospheric Sciences*, 38, 2653-2675.

Namias, J., 1968: Long-range weasther forecasting: history, current status and outlook, *Bulletin of American Meteorological Society*, 49, 438-470.

Namias, J., 1972: Influence of northern hemisphere general circulation on drought in northeast Brazil, *Tellus*, 24, 334-343.

Namias, J., 1973: Thermal communication between the sea surface and the lower trophosphere, *Journal of Physical Oceanography*, 3, 373-378.

Namias, J. and R. M. Born, 1974: Further studies of temporal coherence in north Pacific sea surface temperatures, *Journal of Geophysical Research*, 79, 797-798.

Namias, J. and D.R. Cayan, 1981: Large-scale air-sea interactions and short-period climate fluctuations, *Science*, 214, 869-876.

Nicholls, N., 1980: Long-range weather forecasting: Value, status and prospects. *Reviews in Geophysics and Space Physics*, 18, 771-788.

Nicholls, N., 1984: The Southern Oscillation, sea surface temperature and interannual fluctuations in Australian tropical cyclone activity, *Journal of Climate*, 4, 661-670.

Nicholson, S.E., 1986 a: The spatial coherence of African rainfall anomalies: Interhemispheric teleconnections, *Journal of Climate and Applied Meteorology*, 25, 1365-1381.

Nicholson, S.E., 1986 b: The nature of rainfall variability in Africa south of the equator, *Journal of Climatology*, 6, 515-530.

Nicholson, S.E. and D. Entekhabi, 1987: Rainfall variability in equatorial and Southern Africa: Relationships with sea surface temperatures along the southwestern coast of Africa, *Journal of Climate and Applied Meteorology*, 26, 561-578.

Nicholson, S.E and B.S. Nyenzi, 1990: Temporal and spatial variability in the Tropical Atlantic and Indian Oceans, *Meteorology and Atmospheric Physics*, 41, 1-17.

Nuss, W.A. and R.A. Anthes, 1987: A numerical investigation of low-level processes in rapid cyclogenesis, *Monthly Weather review*, 115, 2728-2743.

Oort, A.H., Y.H. Pan, R.W. Reynolds and C.F. Ropelewski, 1987: Historical trends in the surface temperature over the oceans based on the COADS, *Climate Dynamics*, 21, 29-38.

Padya, B.M., 1989: Weather and Climate of Mauritius. *Mahatma Gandhi Institute*, Moka, Mauritius, 283 pp.

Paegle, J., C.D. Zhan and D.P. Baumhefner, 1987: Atmospheric response to tropical thermal forcing in real data integrations, *Monthly Weather review*, 115, 2975-2995.

Palmen, E. and C. W. Newton, 1969: Atmospheric Circulation Systems. *Academic Press*, 603 pp.

Panofsky, H.A. and G.W. Brier, 1968: Some Applications of Statistics to Meteorology. *The Pennsylvania State University*, 224 pp.

Parthasarathy, B. and G.B. Pant, 1984: The spatial and temporal relationships between the Indian summer monsoon rainfall and the Southern Oscillation, *Tellus*, 36A, 269-277.

Philander, S.G.H., 1983: El Niño-Southern Oscillation Phenomena, *Nature*, 302, 295-301.

Quenouille, M.H., 1952: Associated Measurements. *Butterworths*, 242 pp.

Quiroz, R.S., 1983: The climate of the El Niño winter of 1982-83: A season of extraordinary climate anomalies, *Monthly Weather review*, 111, 1685-1706.

Ramage, C. S., 1968: Role of a tropical maritime continent in the atmospheric circulation, *Monthly Weather review*, 96, 365-370.

Ramage, C. S., 1977: Sea surface temperature and local weather, *Monthly Weather review*, 105, 540-544.

Ramage, C.S., 1984: Can shipboard measurements reveal secular air-sea heat flux?, *Journal of Climatology and Applied Meteorology*, 2, 187-193.

Rasmusson, E.M. and T.H. Carpenter, 1982: Variations in Tropical sea surface temperature and surface wind fields associated with the Southern Oscillation/El Niño, *Monthly Weather review*, 110, 354-384.

Rasmusson, E.M. and J.M. Wallace, 1983: Meteorological aspects of the El Niño/Southern Oscillation, *Science*, 222, 1195-1202.

Reed, R.J. and M.D. Albright, 1986: A case study of explosive cyclongenesis in the Eastern Pacific, *Monthly Weather review*, 114, 2297-2319.

Riehl, H., 1954: Tropical Meteorology. *McGraw-Hill*, New York, 392 pp.

Rodhe, H. and H. Virji, 1976: Trends and periodicities in East African rainfall data, *Monthly Weather review*, 104, 307-315.

Ropelewski, C.F. and M.S. Halpert, 1987: Global and regional scale precipitation and temperature patterns associated with El Niño/Southern Oscillation, *Monthly Weather Review*, 115, 1606-1626.

Rosen, R.D. and D.A. Salstein, 1980: A comparison between circulation statistics computed from conventional data and NMC Hough analyses, *Monthly Weather review*, 108, 1226-1247.

Rosen, R.D. and D.A. Salstein, 1985: Effect of initialization on diagnoses of NMC large-scale circulation statistics, *Monthly Weather review*, 113, 1321-1337.

Rowntree, P. R., 1972: The influence of tropical east Pacific Ocean temperature on the atmosphere, *Quarterly Journal of the Royal Meteorological Society*, 98, 290-321.

Rowntree, P. R., 1976: Tropical forcing of atmospheric motions in a numerical model, *Quarterly Journal of the Royal Meteorological Society*, 102, 583-605.

Sanders, F. and J.R. Gyakum, 1980: Synoptic-dynamic climatology of the "bomb", *Monthly Weather review*, 108, 1589-1606.

Sawyer, J. S., 1965: Note on the possible physical causes of long-term weather anomalies. Technical Note No. 66, *World Meteorological Organization*, 227-237.

Schulze, G. C., 1986: South African rainfall related to cold and warm events. Preprints of the Second International Conference on Southern Hemisphere Meteorology, *American Meteorological Society,* 465-467.

Shannon, L.V., J.J. Agenbag, N.D. Walker and J.R.E. Lutjeharms, 1990: A major perturbation in the Agulhas retroflection area in 1986, *Deep-Sea Research*, 37, 493-512.

Shukla, J., 1975: Effect of Arabian sea surface temperature anomaly on Indian summer monsoon: A numerical experiment with the GFDL model, *Journal of Atmospheric Sciences*, 32, 503-511.

Shukla, J., 1986: SST anomalies and blocking, *Advances in Geophysics*, 29, 443-452.

Spiegel, M.R., 1961: Schaum's outline of theory and problems of statistics, *Schaum Publishing Company*, New York, 359pp.

Stoeckenius, T., 1981: Interannual variations of tropical precipitation patterns, *Monthly Weather Review*, 109, 1233-1247.

Stone, P.H. and R.M. Chervin, 1984: The influence of ocean surface temperature on the Walker Circulation: Part II: prescribed global changes, *Monthly Weather review*, 112, 1524-1534.

Streten, N. A., 1973: Some characteristics of satellite-observed bands of persistent cloudiness over the southern hemisphere, *Monthly Weather review*, 101, 486-496.

Streten, N.A., 1983: Extreme distributions of Australian annual rainfall in relation to sea surface temperatures, *Journal of Climatology*, 3, 143-153.

Sui, C. -H. and K. -M. Lau, 1992: Multiscale phenomena in the tropical atmosphere over the western Pacific, *Monthly Weather review*, 120, 407-430.

Taljaard, J. J., 1986: Change of rainfall distribution and circulation patterns over southern Africa in summer, *Journal of Climatology*, 6, 579-592.

Trenberth,, K. E., 1976: Spatial and temporal variations of the Southern Oscillation, *Quarterly Journal of the Royal Meteorological Society*, 102, 639-653.

Troup, A. J., 1965: The 'Southern Oscillation', *Quarterly Journal of the Royal Meteorological Society*, 91, 490-506.

Tyson, P. D., 1980: Temporal and spatial variation of rainfall anomalies in Africa south of latitude 22° during the period of meteorological record, *Climatic Change*, 2, 363-371.

Tyson, P.D., 1984 a:The atmospheric modulation of extended wet and dry spells in the summer rainfall of South Africa, *South African Geographical Journal*, 57, 104-110.

Tyson, P.D., 1984 b: The atmospheric modulation of extended wet and dry spells over South Africa, 1958-1978, *Journal of Climatology*, 4, 621-635.

Tyson, P. D., 1986: Climatic change and variability in Southern Africa, University of the Witwatersrand, Johannesburg. *Oxford University Press*, Cape Town, 220 pp.

Tyson, P. D., T. G. J. Dyer and M. N. Mametse, 1975: Secular changes in South African rainfall: 1880 to 1972, *Quarterly Journal of the Royal Meteorological Society*, 817-833.

Tyson, P.D. and T.G.J. Dyer, 1975: Mean annual fluctuations of precipitation in the summer rainfall of South Africa, *South African Geographical Journal*, 57, 104-110.

Tyson, P.D. and T.G.J. Dyer, 1978: The predicted above-normal rainfall of the seventies and the likelihood of droughts in the eighties in South Africa, *South African Journal of Science*, 74, 372-377.

van Heerden, J., D.E. Terblanche and G.C. Schulze, 1988: The Southern Oscillation and South African summer rainfall, *Journal of Climatology*, 8, 577-597.

Walker, G. T., 1923: Correlation in seasonal variations of weather, VIII. A preliminary study of world weather (World weather I), *Memoirs of the Indian Meteorological Department*, 24, 75-131.

Walker, G. T., 1924: Correlation in seasonal variations of weather, IX. A further study of world weather (World weather II), *Memoirs of the Indian Meteorological Department*, 24, 275-332.

Walker, G. T., 1928: World weather III, *Memoirs of the Royal Meteorological Society*, 2, 97-106.

Walker, G. T. and E. W. Bliss, 1930: World weather IV - Some applications to seasonal forecasting, *Memoirs of the Royal Meteorological Society*, 3, 81-95.

Walker, G. T. and E. W. Bliss, 1932: World weather V, *Memoirs of the Royal Meteorological Society*, 4, 53-84.

Walker, G. T. and E. W. Bliss, 1937: World weather VI, *Memoirs of the Royal Meteorological Society*, 4, 119-139.

Walker, N.D., 1989: Sea Surface temperature-rainfall relationships and associated ocean-atmosphere coupling mechanisms in the Southern African Region. *Unpublished Ph.D. Thesis*, University of Cape Town, 173 pp.

Walker, N. D., 1990: Links between South African summer rainfall and temperature variability of the Agulhas and Benguela Current systems, *Journal of Geophysical Research*, 95, 3297-3319.

Weare, B.C., 1979: A statistical study of the relationships between ocean surface temperatures and the Indian monsoon. *Journal of Atmospheric Sciences*, 36, 2279-2291.

Webster, P. J., 1972: Response of the tropical atmosphere to local steady forcing, *Monthly Weather review*, 100, 518-541.

Webster, P. J., 1981: Mechanisms determining the atmospheric response to sea surface temperature anomalies, *Journal of Atmospheric Sciences*, 38, 554-571.

Webster, P. J., 1982: Seasonality in the local and remote atmospheric response to sea surface temperature anomalies, *Journal of Atmospheric Sciences*, 39, 41-52.

Webster, P. J., 1983: Large-scale structure of the tropical atmosphere, in Large-scale Dynamical Processes in the Atmosphere. Edited by B.J. Hoskins and R.P. Pearce. *Academic Press inc.*, 397pp.

Webster, P. J. and J. R. Holton, 1982: Cross-equatorial response to middle-latitude forcing in a zonally varying basic state, *Journal of Atmospheric Sciences*, 39, 722-733.

Winston, J.S. and A.F. Krueger, 1977: Diagnosis of the satellite observed radiative heating in relation to the summer monsoon, *Pure and Applied Geophysics*, 115, 1131-1144.

Wright, P.B., 1986: Problems in the use of ship observations for the study of interdecadal climate changes, *Monthly Weather review*, 114, 1028-1034.

Wright, P.B., J.M. Wallace, T.P. Mitchell and C. Deser, 1988: Correlation structure of the El Nino/Southern Oscillation phenomenon, *Journal of Climate*, 1, 609-625.

Xu, K. -M. and K. A. Emanuel, 1989: Is the tropical atmosphere conditionally unstable ?, *Monthly Weather review*, 117, 1471-1479.

Yarnal, B. and G. Kiladis, 1985: Tropical teleconnections associated with El Niño/Southern Oscillation (ENSO) events, *Progress in Physical Geography*, 9, 524-558.

Yarnal, B., 1985: Extratropical teleconnections with El Niño/Southern Oscillation (ENSO) events, *Progress in Physical Geography*, 9, 315-352.

ACKNOWLEDGMENTS

This research was funded by the Water Research Commission of South Africa under the project: Research on the prediction of South African summer rainfall variability from ocean surface temperatures. The author is very grateful to Dr Mark R. Jury, not only for his supervision and guidance, but also for his encouragement, interest and unfailingly available advice. Valuable and constructive comments and suggestions were available at different stages of the project from Dr Frank A. Shillington (co-leader of the project), Professor G. Brundrit (Head of the Oceanography Department, University of Cape Town), and Professor J.R.E. Lutjeharms (Oceanography Department, University of Cape Town). Mr Shaun Courtney's expertise in matters concerning computers and programs is deeply appreciated. Thanks are extended to Mrs Lesley Elley and Mrs Shirley Hutchings who helped in the typing.

Interesting and encouraging discussions were held with Dr J.A Lindesay (University of Witwatersrand), Professor L.V. Shannon (Sea Fisheries Research Institute, Cape Town), Professor J. Field (Marine Zoology Department, University of Cape Town), Professor P.D. Tyson (University of Witwatersrand), Professor J. van Heerden (University of Pretoria), Professor R. Diab (University of Durban), Mr S.J. Mason (University of Witwatersrand), Dr N.D. Walker (who submitted the initial proposal of the project to the Water Research Commission) and Dr G.C. Schulze (South African Weather Bureau).

Trips to the United States and various parts of South Africa to attend meetings, conferences and seminars (also financed by the Water Research Commission) provided opportunities for useful interactions with other scientists in related fields. Data, ideas and programs were exchanged with Professor T.N. Krishnamurti and Professor S.E. Nicholson (both of Florida State University, USA); their cooperation

is gratefully acknowledged. The author is indebted to Dr G. Green (Water Research Commission) for his overall support of the project, and also to colleagues at the Computing Center for Water Research, particularly J. Gorven and M.C. Dent who offered help in transferring large volumes of rainfall data.

The valuable and constructive comments, criticisms and suggestions of anonymous examiners and reviewers are acknowledged. Their reviews have helped clarify and improve the thesis. Thanks are also due to the Director and staff of the Meteorological Service, Vacoas, Mauritius, for providing facilities and encouragement.

The author wishes to thank those who, either directly or indirectly, contributed towards the project, namely, Roy van Ballegooyen, Jenny Barclay-Godfrey, Simon Childs, Jackie Cooper, Paul Hanekom, Peter Hughes, John Josepth, Penny Krohn, Kevin Levey, Craig Mc Arthur, Brahmanund M. Padya, Bhawoodien Parker, Richard Phillips, Trevor Probyn, Gordon Rigg, Sarah Searson, Lesley Staegemann, Henry Valentine, Howard Waldron, Richard Washington, Scarla Weeks and Koos Williams.

Finally, special thanks are due to the author's family, particularly his wife (Amita) and children (Amrish and Divya), without whose patience and understanding the work could not have materialized.